UMM-134 = RL-2019

Studies in Radar Cross-Sections XIV

Radar Cross-Section of a Ballistic Missile

by K. M. Siegel, M. L. Barasch
J. W. Crispin, I. V. Schensted
W. C. Orthwein, and H. Weil

Contract W-33(038)-ac-14222
UMM-134
September 1954

University of Michigan
Engineering Research Institute
Willow Run Research Center
Willow Run Airport
Ypsilanti, Michigan

STUDIES IN RADAR CROSS-SECTIONS

I Scattering by a Prolate Spheroid, F. V. Schultz, (UMM-42, March 1950) W-33(038)-ac-14222, UNCLASSIFIED.

II The Zeros of the Associated Legendre Functions $P_n^m(\mu')$ of Non-Integral Degree, K. M. Siegel, D. M. Brown, H. E. Hunter, H. A. Alperin, and C. W. Quillen, (UMM-82, April 1951) W-33(038)-ac-14222, UNCLASSIFIED.

III Scattering by a Cone, K. M. Siegel and H. A. Alperin, (UMM-87, January 1952) AF-30(602)-9, UNCLASSIFIED.

IV Comparison Between Theory and Experiment of the Cross-Section of a Cone, K. M. Siegel, H. A. Alperin, J. W. Crispin, H. E. Hunter, R. E. Kleinman, W. C. Orthwein, and C. E. Schensted, (UMM-92, February 1953) AF-30(602)-9, UNCLASSIFIED.

V An Examination of Bistatic Early Warning Radars, K. M. Siegel, (UMM-98, August 1952) W-33(038)-ac-14222, SECRET.

VI Cross-Sections of Corner Reflectors and Other Multiple Scatterers at Microwave Frequencies, R. R. Bonkowski, C. R. Lubitz, and C. E. Schensted, (UMM-106, October 1953) AF-30(602)-9, SECRET. (UNCLASSIFIED when Appendix is removed).

VII Summary of Radar Cross-Section Studies Under Project Wizard, K. M. Siegel, J. W. Crispin, and R. E. Kleinman, (UMM-108, November 1952) W-33(038)-ac-14222, SECRET.

VIII Theoretical Cross-Sections as a Function of Separation Angle Between Transmitter and Receiver at Small Wavelengths, K. M. Siegel, H. A. Alperin, R. R. Bonkowski, J. W. Crispin, A. L. Maffett, C. E. Schensted, and I. V. Schensted, (UMM-115, October 1953) W-33(038)-ac-14222, UNCLASSIFIED.

IX Electromagnetic Scattering by an Oblate Speroid, L. M. Rauch, (UMM-116, October 1953) AF-30(602)-9, UNCLASSIFIED.

X The Radar Cross-Section of a Sphere, H. Weil, (2144-6-T, to be published) DA-36(039)SC-52654.

XI The Numerical Determination of the Radar Cross-Section of a Prolate Spheroid, K. M. Siegel, B. H. Gere, I. Marx, and F. B. Sleator, (UMM-126, December 1953) AF - 30 (602) -9, UNCLASSIFIED

XII Summary of Radar Cross-Section Studies Under Project MIRO, K. M. Siegel, M. E. Anderson, R. R. Bonkowski, and W. C. Orthwein, (UMM-127, December 1953) AF-30(602)-9, SECRET.

XIII Description of a Dynamic Measurement Program, K. M. Siegel and J. M. Wolf, (UMM-128, May 1954) W-33(038)-ac-14222, CONFIDENTIAL.

XIV Radar Cross-Sections of B-47 and B-52 Aircraft, (2260-1-T, August 1954) AF-33(616)-2531, CONFIDENTIAL.

TABLE OF CONTENTS

PREFACE

This paper is the fourteenth in a series of reports growing out of studies of radar cross-sections at the University of Michigan's Willow Run Research Center. The primary aims of this program are:

(1) To show that radar cross-sections can be determined analytically.

(2) To elaborate means for computing cross-sections of objects of military interest.

(3) To demonstrate that these theoretical cross-sections are in agreement with experimentally determined values.

Intermediate objectives are:

(1) To compute the exact theoretical cross-sections of various simple bodies by solution of the appropriate boundary-value problems arising from the electromagnetic vector wave equation.

(2) To examine the various approximations possible in this problem, and determine the limits of their validity and utility.

(3) To find means of combining the simple body solutions in order to determine the cross-sections of composite bodies.

(4) To tabulate various formulas and functions necessary to enable such computations to be done quickly for arbitrary objects.

(5) To collect, summarize, and evaluate existing experimental data.

Titles of the papers already published or presently in process of publication are listed on the pages following the title page.

K. M. Siegel

ACKNOWLEDGEMENTS

This report is a summary of research results obtained by many people, principally members of the University of Michigan Engineering Research Institute, and reported largely in Willow Run Research Center internal memoranda. This research is composed of contributions by:

M. E. Anderson
M. L. Barasch
R. R. Bonkowski
J. W. Crispin
M. J. Ehrlich
R. E. Kleinman
V. C. Liu
C. R. Lubitz
A. L. Maffett
M. H. Nichols
W. C. Orthwein
C. E. Schensted
I. V. Schensted
K. M. Siegel
F. B. Sleator
H. Weil

Others, including A. H. Halpin and H. E. Hunter, working under the direction of D. M. Brown in the Data Reduction and Computation Department of the Willow Run Research Center, made many contributions.

An appendix on static experimental techniques was contributed by M. J. Ehrlich of the Microwave Radiation Company, Inc., and an appendix on the experimental equipment and procedures used by the Signal Corps Engineering Laboratory was prepared with the aid and advice of R. Wagner. Miss C. Carlson and Miss A. Nelson assisted with the preparation of the manuscript.

The authors wish to acknowledge also the benefits received from reports from other organizations and from correspondence and conversations with G. J. Akerland, W. S. Ament, W. W. Balwanz, S. Bertram, J. T. Evers, G. B. Fanning, L. B. Felsen, R. E. Hiatt, J. L. Hult, M. Katzin, M. Kline, R. Kouyoumjian, R. M. Page, R. Rawhouser, V. H. Rumsey, L. I. Schiff, G. W. Schivley, S. Silver, C. J. Sletten, R. C. Spencer, P. Springer, I. Stokes, H. Trigg, R. Wagner, O. Woodyard, and G. A. Woonton.

I

INTRODUCTION AND SUMMARY

Project Wizard, initiated at the University of Michigan in 1946, is concerned with defense of the United States against missiles of the ballistic type. These missiles may be divided into two classes: short-range ballistic rockets of the V-2 type, and long-range intercontinental rockets of the Atlas type. This report deals with the radar cross-sections of both classes of missiles.

For a particular defense system it is possible to specify the maximum range at which each of the system's many radars must function. This range can be related through simple equations to the radar cross-section of the target, and to the requisite power and other factors describing the radar. If the cross-section is known, it is possible to specify accurately the radar requirements of the system in terms of design parameters. Since it is necessary to make such a specification at some time during the system design, the radar cross-sections of targets must either be known or guessed at; the results in this report are presented with the belief that they predict cross-sections within a factor of 10. This maximum error is tolerable because the range varies as the fourth root of the cross-section. In other words, if the radar cross-section is known within a factor of 10, the range performance of the radar system is known within a factor of 1.8.

Contributions to the cross-section of ballistic missiles may come both from reflections from the missile surfaces and from phenomena associated with missile flight. The latter includes reflections from shock fronts, reflections from the ionization clouds produced at high speeds, and reflections from exhaust flames. Since the reflections received from the missile surfaces are small under most conditions, the contributions from these flight phenomena must be investigated because they could conceivably dominate the radar return. Each of the flight phenomena is considered.

The cone angles of the shock fronts to be expected are computed (Sec. II) and it is shown that, even if they were perfect reflectors, the contribution of shock fronts would not be large in comparison with the reflections from the missile surfaces.

Objects traveling at extremely high speeds (notably meteors) form ionic trails which have been observed by radars. It can be stated that ionization will not contribute to the cross-section of V-2 type missiles since V-2 type missiles never reach the velocities required for measurable ionization. Since future Atlas type missiles may travel at speeds equal to those of the slowest meteors, the possibility of detecting these missiles from their ion trails has been investigated (Sec. III). Enough experimental knowledge of this subject does not exist to make precise estimates about Atlas type missiles, but it was found that, even by making the most optimistic of assumptions (from the point of view of the defense) the maximum speed and the size of the Atlas are such that its associated ion cloud either will not be detectable by a radar or will be visible for only a short time, and in any case not above an altitude of 200 kilometers.

Since exhaust flames exist in the very early portion of missile flight, and since the Wizard study did not visualize that an attempt should be made to detect ballistic missiles on their way up, no major effort was made in this field. The little work which has been done is summarized in Section IV. Thus, for the total portion of missile flight of concern to the defense, no flight phenomena will contribute significantly to the radar return from the missile.

Large quantities of information have been gathered in the last several years, at the Willow Run Research Center and elsewhere, on the radar cross-sections due to the surfaces of ballistic missiles. These data include the results of static experiments, dynamic experiments, and theoretical calculations. Because the design of Atlas type missiles has only recently been initiated, much more data are available on V-2 type missiles than on Atlas-type missiles.

The results of static experiments performed by various organizations are compiled in Section V in the form of graphs showing cross-section as

a function of aspect angle for equivalent full-scale missiles. These experiments have been performed for V-2's at equivalent full-scale frequencies between 20 and 2900 Mc and for Atlas between 75 and 1000 Mc.

Dynamic experimental data for ballistic missiles have been obtained to date only for the V-2 type missiles (Sec. VI). These data were obtained by the Willow Run Research Center (using models) for full-scale frequencies at S- and L-bands and by the Naval Research Laboratory (on V-2's) at 100, 1250, and 2825 Mc.

Theoretical computations have been carried out for both Atlas and V-2 type missiles. These computations were carried out by use of various approximation techniques, principally physical optics (Sec. 7.1). Comparisons have been made, where possible, between theoretical calculations and experimental data to determine if the two methods lead to equivalent results.

The agreement among static measurements, dynamic measurements (where they exist) and theoretical calculations is seen in this report to be quite close. Hence, it is believed that a fairly clear picture has been obtained of the radar cross-sections of ballistic missiles over a wide range of operating conditions.

The cross-section picture of the Atlas 7-OC warhead is summarized in Sections 5.2 and 7.2. The data presented indicate that the nose-on cross-section of the 7-OC warhead is approximately 1 square meter for each of the frequencies at which information has been obtained. The total range in the 7-OC nose-on cross-section at frequencies of 75, 100, 225, 333, 600, and 1000 Mc is from 0.15 to 1.5 square meters.

The nose-on V-2 data are summarized in Figure 2-2 and Sections V and VII.

Because of the large quantity of information available on the cross-section of ballistic missiles, certain compromises have had to be made to keep the size of this report within reasonable bounds for publication. All information available to WRRC on missile ionization and results from

many of the known ballistic missile experiments are presented. The presentation of the results of the theoretical work performed by WRRC has been abbreviated because so much of it appears in other, unclassified reports.

II

REFLECTIONS FROM SHOCK FRONTS

The following three claims are frequently advanced in support of the theory that supersonic missiles may be detected by radar reflections from their associated shock fronts:

1. Small meteors have been observed at great altitudes.

2. Although the reflection coefficient of a shock front is small, the extent of the shock front is so large that its cross-section may be significantly greater than that of the missile body.

3. One often hears (although no written references are known to the authors) that, during World War II, radars detected shells at anomalously long ranges.

These three arguments will now be considered in order.

1. It has been established (Ref. 12) that the detection of small meteors at great altitudes is accounted for by the reflections from the associated ionic clouds, and hence proves nothing concerning reflections from shock fronts.

2. The nose-on cross-section of an infinite cone is small.

It is demonstrated in Section 2.1 that the energy returned to the radar by reflection from the shock front is negligible in comparison with that returned from the missile body.

3. Although the vagueness of claim (3) above makes it very difficult to counter with more concrete evidence, two lines of argument do show that such observations are by no means proofs of the radar-reflecting efficacy of a shock front. First, the calculations which are given below

show that nose-on detection of shells is not appreciably enhanced by the presence of a shock cone. Furthermore, results of dynamic experiments at Boston University (Ref. 1) show that when a radar observes a bullet from the rear, the cross-section at speeds above Mach 1 decreases with an increase in Mach number, whereas the intensity and extent of the shock front would be expected to increase with an increase in speed.

2.1 Calculation of Reflections from Shock Fronts

The following considerations are valid for a missile such as the V-2, with fins and conical nose-section, in supersonic flight.

In Figure 2-1, obtained from Reference 2, shock front angles are presented as a function of missile nose-cone angles and Mach numbers. The trends shown in Figure 2-1 are indicative of the results to be anticipated as the missile velocity increases without limit. References 3 and 4 both contain more accurate information than can be obtained from Figure 2-1, and also contain the extension to large Mach numbers. The shock front angle for a typical V-2 (nose cone about 30 degrees, thus θ_s = 15 degrees) can be obtained by interpolation from Figure 2-1. (The dotted curves represent separation of the shock front from the cone.)

The nose-on cross-section of a metallic (reflectivity $\sim$ 1) semi-infinite cone can be represented accurately as: $\sigma = \frac{\lambda^2 \tan^4 \theta_s}{16\pi}$ (Ref. 5). Applying this relation to the cross-section of the V-2 shock front, an upper bound is obtained for the shock front cross-sections for various wavelengths and Mach numbers, as indicated in Table 2-1.

TABLE 2-1

"Metallic" Shock-Front Cross-Sections

	σ(meters)^2			
λ(meters)	M=4(θ_w=22.5 degrees)	M=6(θ_w=20.0 degrees)	M=9(θ_w=18.9 degrees)	M=∞(θ_w=16.5 degrees)
0.1	5.8×10^{-6}	3.5×10^{-6}	2.7×10^{-6}	1.5×10^{-6}
1.0	5.8×10^{-4}	3.5×10^{-4}	2.7×10^{-4}	1.5×10^{-4}
5.0	1.5×10^{-2}	8.7×10^{-3}	6.8×10^{-3}	3.8×10^{-3}
10.0	5.8×10^{-2}	3.5×10^{-2}	2.7×10^{-2}	1.5×10^{-2}
30.0	5.2×10^{-1}	3.1×10^{-1}	2.5×10^{-1}	1.5×10^{-1}

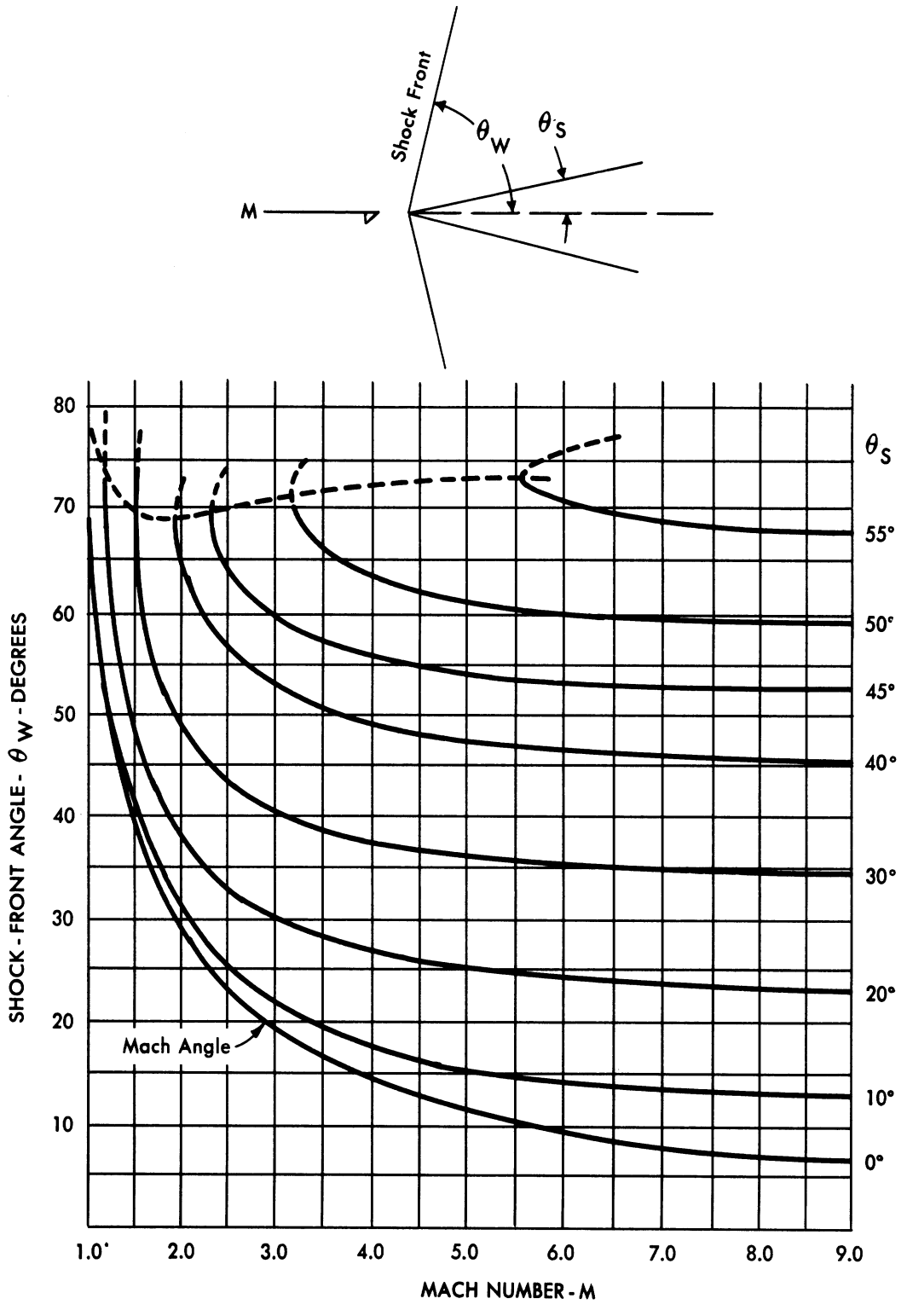

FIG. 2-1 VARIATION OF SHOCK FRONT ANGLE WITH MACH NUMBER FOR VARIOUS CONE ANGLES

Figure 2-2 shows static experimental nose-on cross-sections of a V-2 at various wavelengths. These results (as shown in detail in Sections V-VII) are not radically changed up to aspect angles of about 70 degrees from nose-on.

A comparison between the data of Figure 2-2 and that of Table 2-1 shows that the cross-section of the shock front is negligible in comparison with that of the V-2 itself, even if the shock front is assumed to be a perfect reflector. Only a very small percentage of the energy which strikes a true shock cone is reflected. Ref. 1, Ref. 6, and many others state that typical values for the coefficient of reflectivity of shock fronts vary from 10^{-3} to 10^{-5}.

The conclusion that the reflection from the shock cone is negligible is valid for nose-on and near nose-on aspects, up to approximately the normal to the shock cone. For a V-2 at Mach 9 this is about 70 degrees from nose-on; however, at such large aspect angles, the V-2 itself has a vastly increased cross-section, and the contribution from the shock front would be of less importance.

Although the Boston University results in which bullets were observed from tail-on by radar (Ref. 1) show a decreasing cross-section with increasing supersonic speeds, these same data show a transonic cross-section slightly greater than the subsonic cross-section. This was explained in Reference 1 on the basis that the shock wave is now moving away from the bullet, and presents an almost plane reflecting surface to the radar, contributing to the total cross-section in a measurable fashion; however, even here the increase in cross-section is only about 10 per cent of the subsonic value.

2.2 Effects of Refraction Near a Missile

Since refraction effects were shown to have a measurable effect on the tail-on cross-section of the bullets in the Boston University experiments (Ref. 1), it might be suspected that refraction through the shock cone at nose-on aspect would produce a similar result. Whereas refraction at the tail-on aspect diverges the radar waves away from the

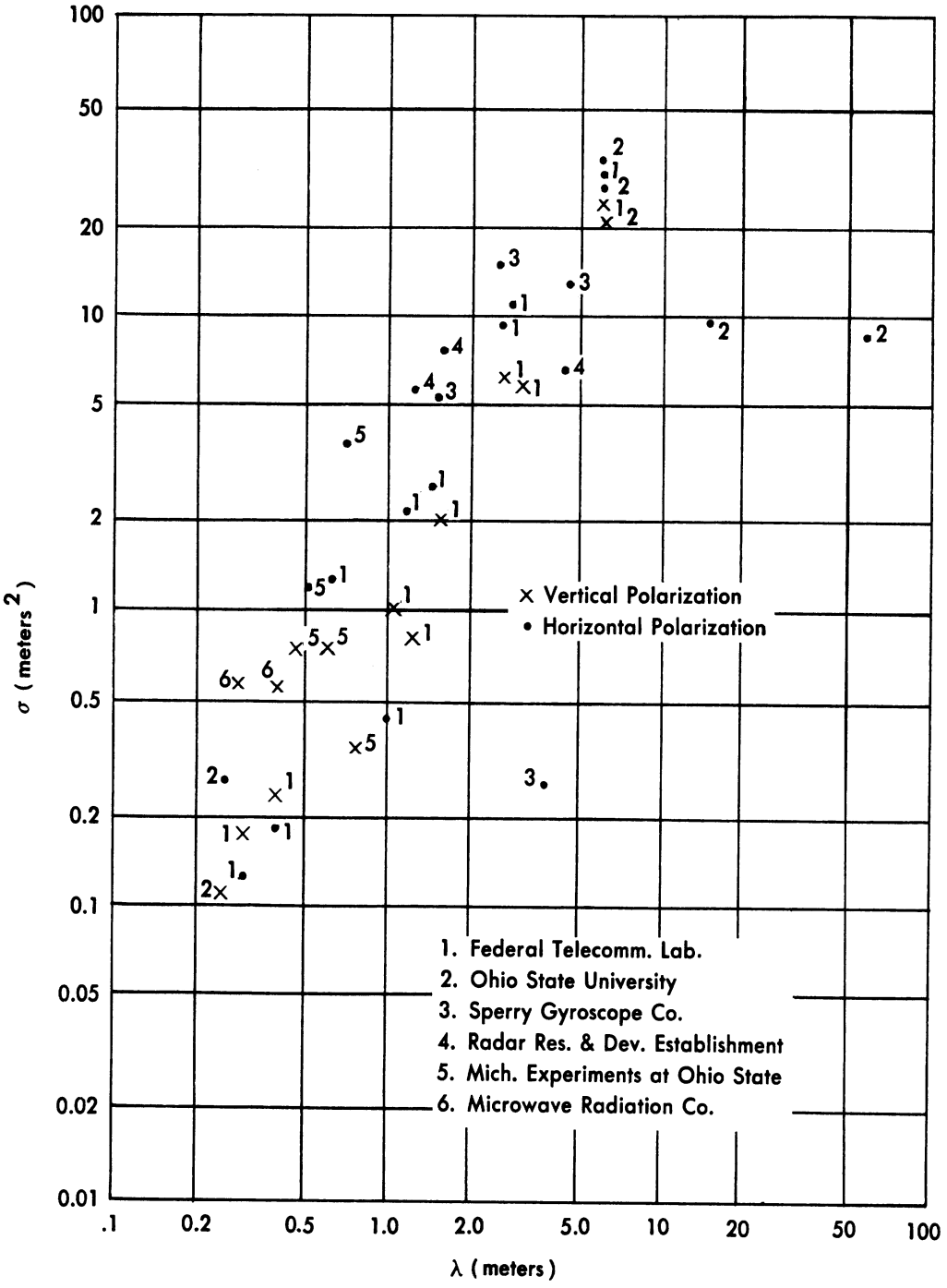

FIG. 2-2 EXPERIMENTAL NOSE-ON V-2 RADAR CROSS-SECTION (IN SQUARE METERS) AS A FUNCTION OF WAVELENGTH (IN METERS).

target, refraction at nose-on converges the waves onto the target. This allows the V-2 to draw energy from an effectively larger area of the incoming waves. However, even this could affect the radar cross-section of a ballistic missile only slightly because of the small changes in index of refraction and the small differences between θ_w and θ_s for Mach numbers of interest, so that it would have only a negligible effect on the radar cross-section of a ballistic missile. Thus for almost all missile cross-section problems of interest the effects of shock fronts may be neglected.

III

REFLECTIONS FROM IONIC CLOUDS

Ionization will appear about a high-speed missile, such as the Atlas missile descending through the atmosphere, and an ionized trail will stream behind it. Hence it is necessary to consider the effect of this ionization on the radar reflections from the missile. Depending on the distribution of ions the radar cross-section of missile plus ion cloud may be greater or less than the radar cross-section of missile alone. (At altitudes of primary interest, i.e. greater than 200 km, there will be no perceptible shock wave because of the low ambient density.)[1]

An analysis of this problem, contained in Appendix 1, shows that no significant increase in radar cross-section of the warhead is to be expected due to this ionization at altitudes above 200 km. No analysis was felt necessary for the separated booster.

Since the relative importance of the possible mechanisms for ionization is affected by body altitude and speed, the fact that meteors are observed by radar reflection from the broadside aspect of their trails does not constitute an objection to our conclusions. The meteor observations by radar[2] are primarily below 120 km (Ref. 12). Most meteor speeds exceed greatly the missile speeds considered here, and the missiles are artificially cooled, so that different mechanisms may be responsible for the bulk of the ionization in the meteor and missile at the altitudes of interest.

The authors do not feel that the ionization question is closed. Some mechanisms of ionization have undoubtedly not been considered in this

1. It is felt that, due to the velocity of intercontinental ballistic missiles, detection must occur at altitudes greater than 200 km to allow sufficient time for defensive action.
2. Reference 17 contains an excellent summary of the theoretical work done on the meteor problem.

paper and it is hoped that further work will be done in connection with this question.

For the trajectories and velocities proposed for Atlas, it appears that ionization is not important before the final minute of missile flight.

IV

RADAR REFLECTIONS FROM EXHAUST FLAMES

There appears to be little definitive information available on the contribution of the combustion products leaving an aircraft or a missile. F. C. MacDonald, for example, has observed much larger echoes before V-2 burnout than after and has attributed this difference to the exhaust flames (Ref. 19).

W. W. Balwanz states that he has not found any reliable experimental data or theoretical reasoning which would indicate that appreciable reflections are obtained from the exhaust stream of a turbojet engine (Ref. 18). The following information is known:

1. F. C. MacDonald has found experimentally that the radar cross-section of a V-2 before fuel cut-off is ten or more times greater than after cut-off (Ref. 19). These results are discussed in more detail in Section 6.2.

2. Considerable work was done in Germany during World War II on the deflection of electromagnetic waves passing through the combustion jet of a V-2 (Ref. 20) and on the physically related problem of the reflection properties of thunderheads (Ref. 21).

3. Many experiments have been performed on the attenuation of radiation passing through V-2 exhausts, but have yielded meager data. In one experiment, for example, a value of attenuation of 16.5 $\pm$ 2 db/m was obtained (Ref. 22).

4. Some experiments have been carried out and others have been proposed on propagation through propellant gases (Ref. 25 to 32). References 31 and 32 are most up-to-date in this field.

5. The physics of the exhaust gas problem are well described in Reference 24.

6. The ionization from flames at altitudes of 30 to 150 km has been investigated (Ref. 6).

7. Some measurements of the conductivity of a jet flame have been made (Ref. 23).

Although little is known about the cross-section of exhaust flames, considerable uncorrelated work has been carried out by various experimenters on increasing or decreasing this cross-section by the introduction of various chemicals into the fuel which change or add to the products of combustion. As far as is known, no success has been obtained by the use of such "additives."

V

REFLECTIONS FROM THE MISSILE SURFACES-- STATIC EXPERIMENTS

5.1 Static Data Available

Many laboratory experiments have been performed on missile models to determine the radar cross-section of ballistic missiles.* The results of these static experiments are summarized graphically in this section. The cross-sections are plotted as functions of aspect angle * * for a variety of wavelengths. In all cases the data presented in this section are scaled up to full missile dimensions.

Static tests on Atlas-type configurations (Fig. 5.1-1) have been conducted by the Microwave Radiation Co., Inc., Venice, Calif., and by the Evans Signal Laboratory, Belmar, N. J., at the instigation of Project Wizard. The results of these experiments are described in Section 5.2.

Static experiments on V-2 type configurations have been carried out by the Microwave Radiation Co., Inc., Ohio State University Antenna Laboratory, Columbus, Ohio, the Sperry Gyroscope Co., Great Neck, N.Y., Federal Telecommunications Laboratory, Nutley, N. J., the Radar Research and Development Establishment, Great Malvern, Worcestershire, England, and the General Electric Co., Schenectady, N. Y. The results obtained from these experiments are described in Sections 5.3 through 5.8 and are summarized in Section 5.9. A typical V-2 configuration is shown in Figure 5.1-2.

The techniques used in the experiments are discussed in detail in Appendix 2. Some of the data (the nose-on data) have been summarized in Reference 37.

*All laboratory tests in which the model is not in flight are classified in this paper under the heading of static tests.

**The aspect angle, referred to on each graph, is measured in the plane determined by the axis of the model and one fin (unless otherwise indicated).

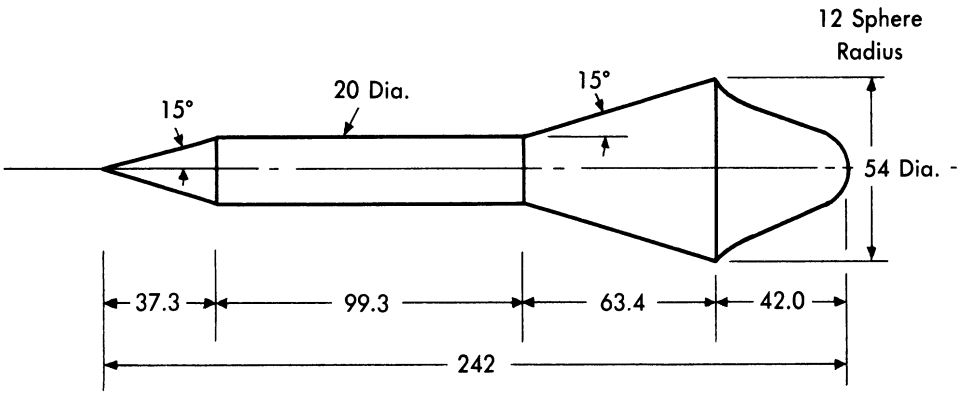

WARHEAD

NOTE: All dimensions in inches.

* This configuration data was obtained in a letter from the Consolidated Vultee Aircraft Company.

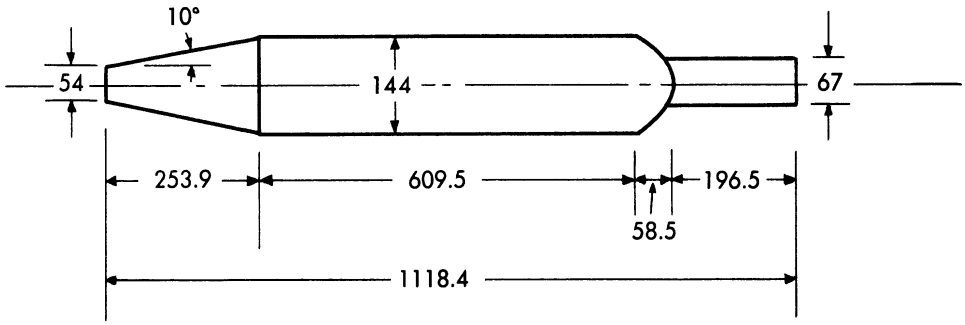

BOOSTER

FIG. 5.1-1 THE ATLAS 7-OC WARHEAD AND BOOSTER.*

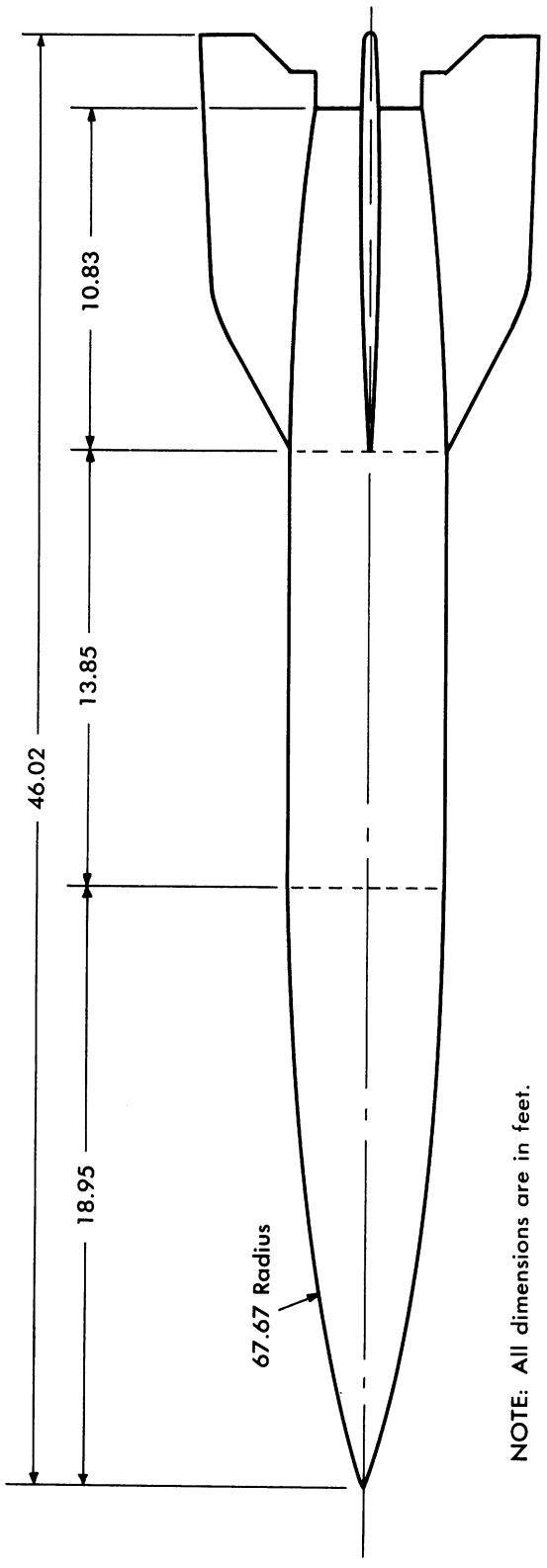

FIG. 5.1-2 A FULL-SCALE V-2 TYPE MISSILE.

NOTE: All dimensions are in feet.

5.2 Atlas-type Missiles*

Static cross-section experiments have been conducted by the Microwave Radiation Co., Inc. (MRC) and the Evans Signal Laboratory (ESL) on Atlas-type configurations. These experiments were performed at the instigation of Project Wizard on models designed by the Willow Run Research Center.

The experiments conducted at MRC were on 1/124 and 1/41.33 scale models at a frequency of 9300 Mc, corresponding to full-scale frequencies of 75 and 225 Mc. The configurations involved were the 7-OC warhead, shown in Figure 5.1-1, and three variations in this warhead, namely a hemispherical stern, a flat stern, and an elongation of the cylindrical portion of the body from 99.3 to 138 inches (Fig. 5.2-1).

The ESL experiments yielded information about the cross-section of:

1. the 7-OC warhead at full-scale frequencies of 75, 225, 333, and 1000 Mc

2. the 7-OC (with hemispherical stern) at full-scale frequencies of 75, 225, 333, and 1000 Mc

3. the 7-OC Booster (see Fig. 5.1-1) at full-scale frequencies of 75 and 225 Mc

4. the "Needle-Nose" warhead** (see Fig. 5.2-2) at full-scale frequencies of 75 and 225 Mc

Figures 5.2-3 and 5.2-4 are photographs of the models used. The ESL experiments were conducted at 3000 Mc and 9000 Mc on 1/9 and 1/40 scale models.

---

*See Appendix 2 for descriptions of the experimental techniques employed. Where possible, theoretical results (Section 7.2-1) are also shown on the figures of this section.

**This warhead configuration was one of the early Atlas configurations.

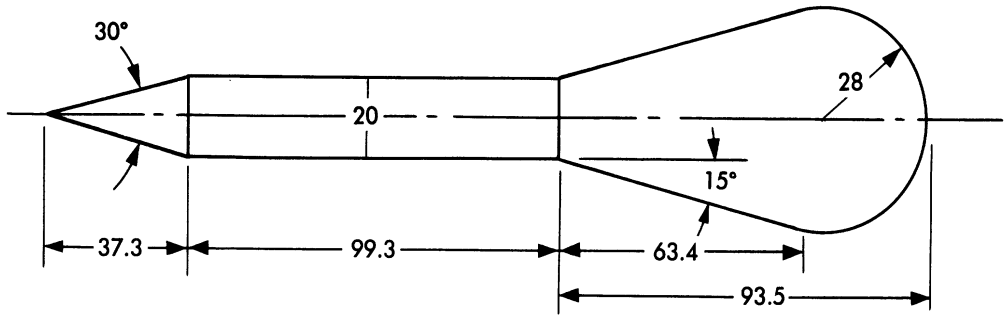

7 - OC Warhead With Hemi - Spherical Stern
(All dimensions in inches)

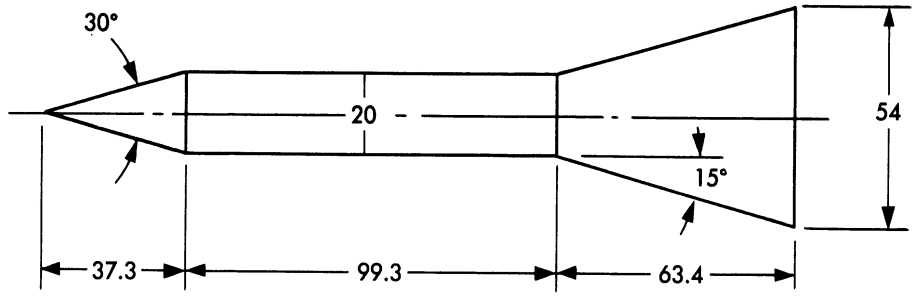

7 - OC Warhead With Flat Stern
(All dimensions in inches)

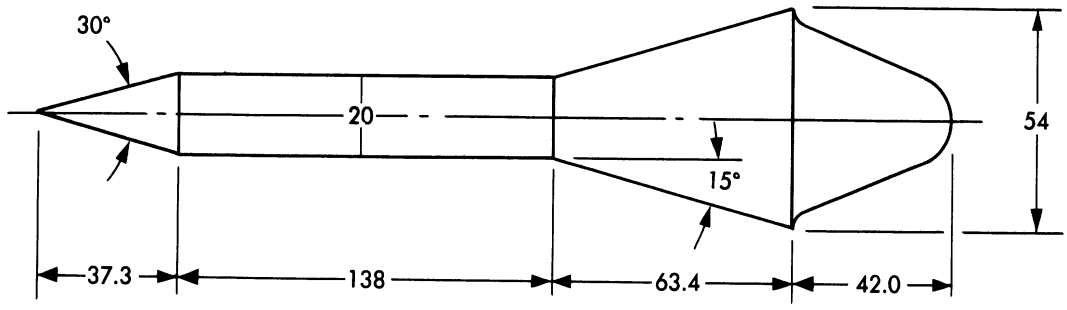

Elongated 7 - OC Warhead
(All dimensions in inches)

FIG. 5.2-1 VARIATIONS IN THE 7-OC WARHEAD USED IN STATIC EXPERIMENTS

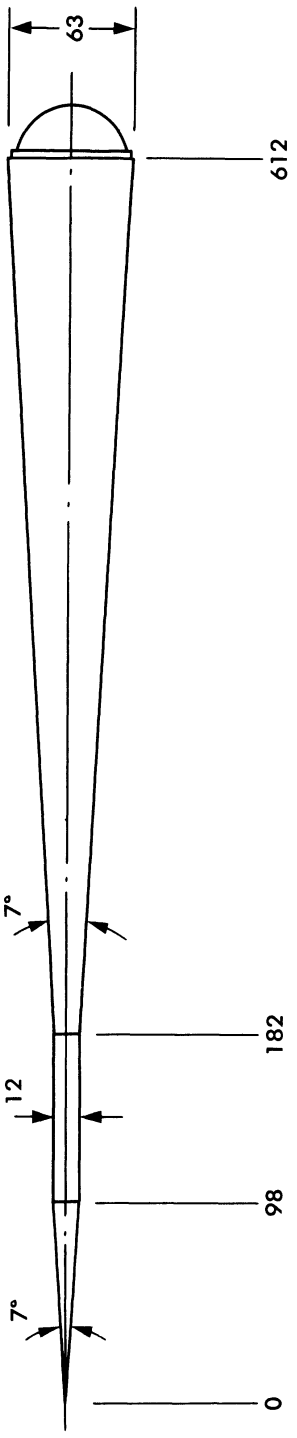

(All dimensions in inches)

FIG. 5.2-2 THE ATLAS "NEEDLE-NOSE" WARHEAD.

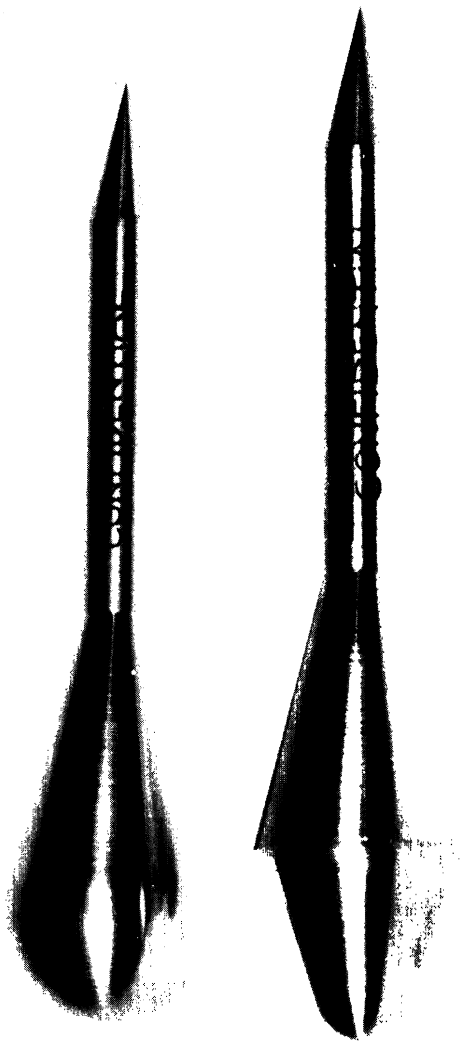

FIG. 5.2-3 PHOTOGRAPHS OF MODELS USED - THE 7-OC WITH HEMI-SPHERICAL STERN AND THE 7-OC

FIG. 5.2-4 PHOTOGRAPH OF THE "NEEDLE NOSE" MODEL USED IN THE TESTS

Figures 5.2-5, 5.2-6, and 5.2-7 contain all the 75 Mc data pertaining to 7-OC type warheads. The theoretical curve (see Section 7.2.1) is included on Figure 5.2-5 for the purpose of comparison.

Figures 5.2-8, 5.2-9, and 5.2-10 contain the 225 Mc data for the 7-OC type warheads. Figure 5.2-8 also contains the theoretically computed curve (see Section 7.2.1).

The 333 Mc data for the 7-OC warhead and the 7-OC with hemispherical stern are shown in Figures 5.2-11 and 5.2-12.

Figures 5.2-13 and 5.2-14 contain the 1000 Mc data for the 7-OC warhead and the 7-OC with hemispherical stern. Except for frequency, their content corresponds to that of Figure 5.2-11 and 5.2-12. Figure 5.2-13 also contains the theoretical curve.

The cross-section of the 7-OC Booster is graphed in Figures 5.2-15 and 5.2-16. Figure 5.2-15 contains the 75 Mc experimental data and Figure 5.2-16 contains the 225 Mc data. The theoretical curve (Section 7.2.1) is included in Figure 5.2-16.

The last two graphs, Figures 5.2-17 and 5.2-18, deal with the cross-section of the "Needle-Nose" warhead. Figure 5.2-17 contains the 75 Mc data and Figure 5.2-18 contains the 225 Mc data with the theoretical result also shown.

The MRC results have been previously published in Reference 33; the ESL results were, until now, unpublished.

It is to be noted that the experimental results of the MRC and the ESL are in good agreement and that in most cases the theoretical curve indicates quite well large-scale trends and average valves over large angular intervals. This was all that was desired from the computations. It should be emphasized that, if they had been needed, more accurate but time consuming computations could have been made within the scope of our present knowledge.

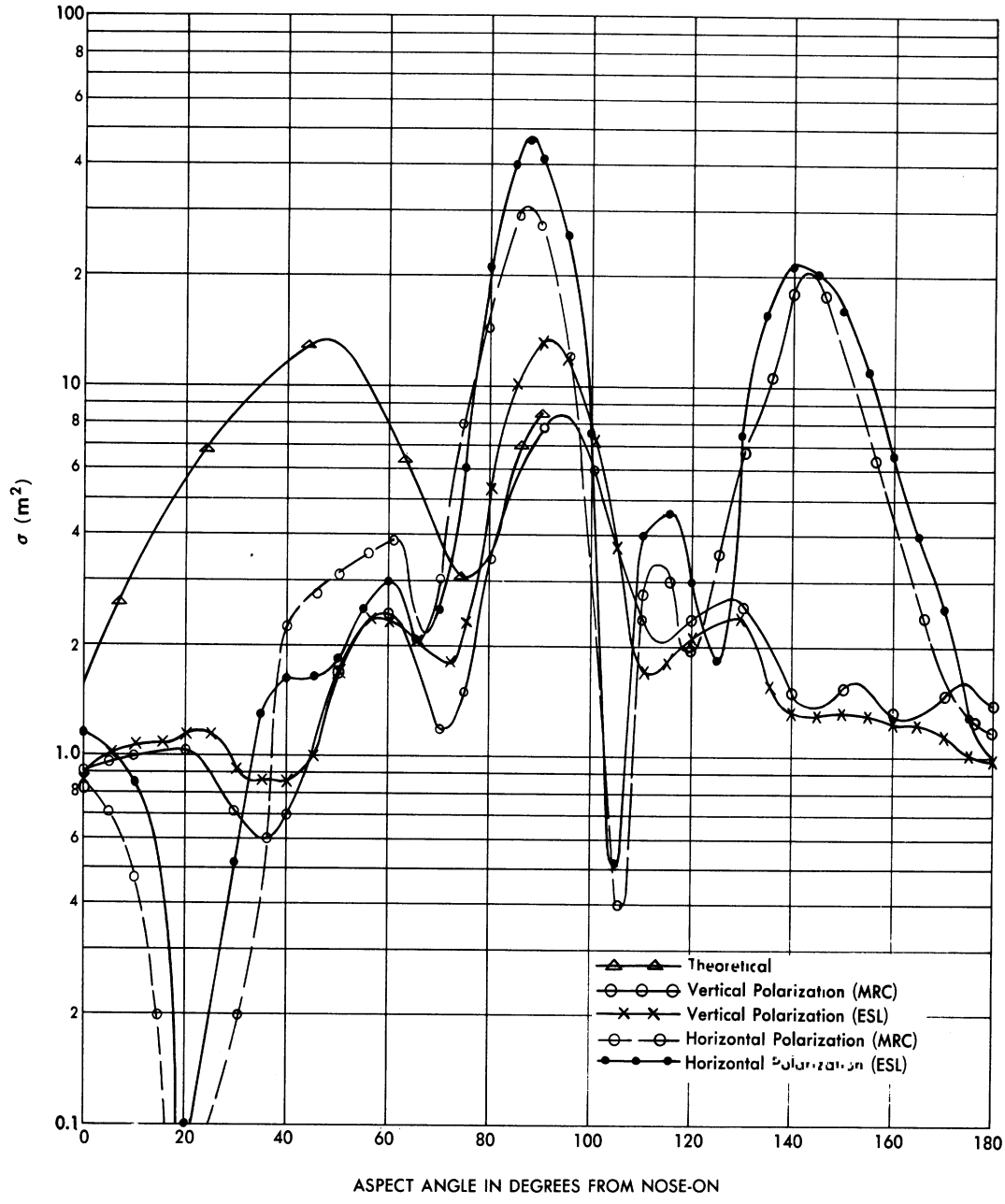

FIG. 5.2-5 CROSS-SECTION OF THE 7-OC WARHEAD AT 75 MC

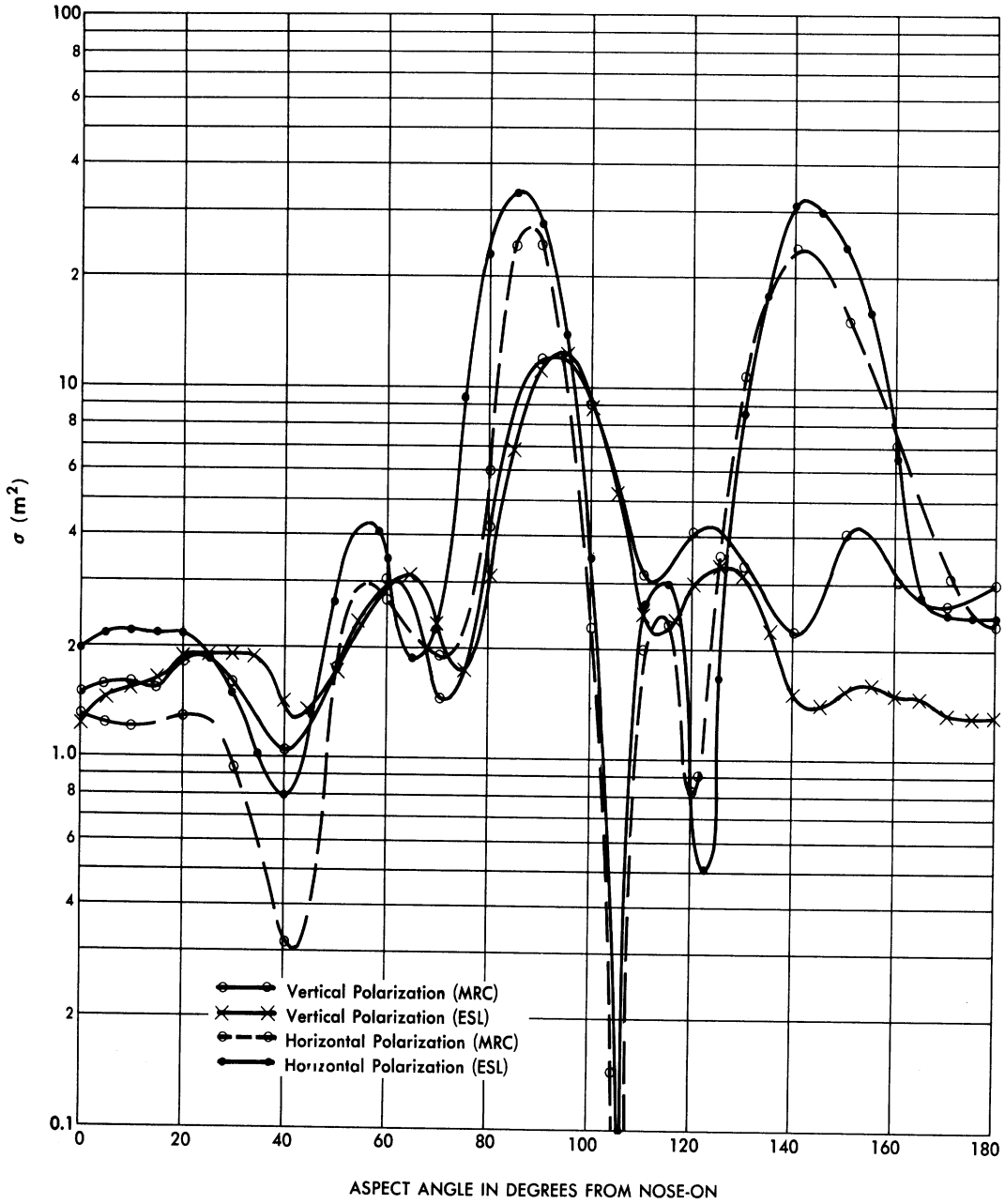

FIG. 5.2-6 CROSS-SECTION OF THE 7-OC WARHEAD WITH A HEMISPHERICAL STERN AT 75 MC

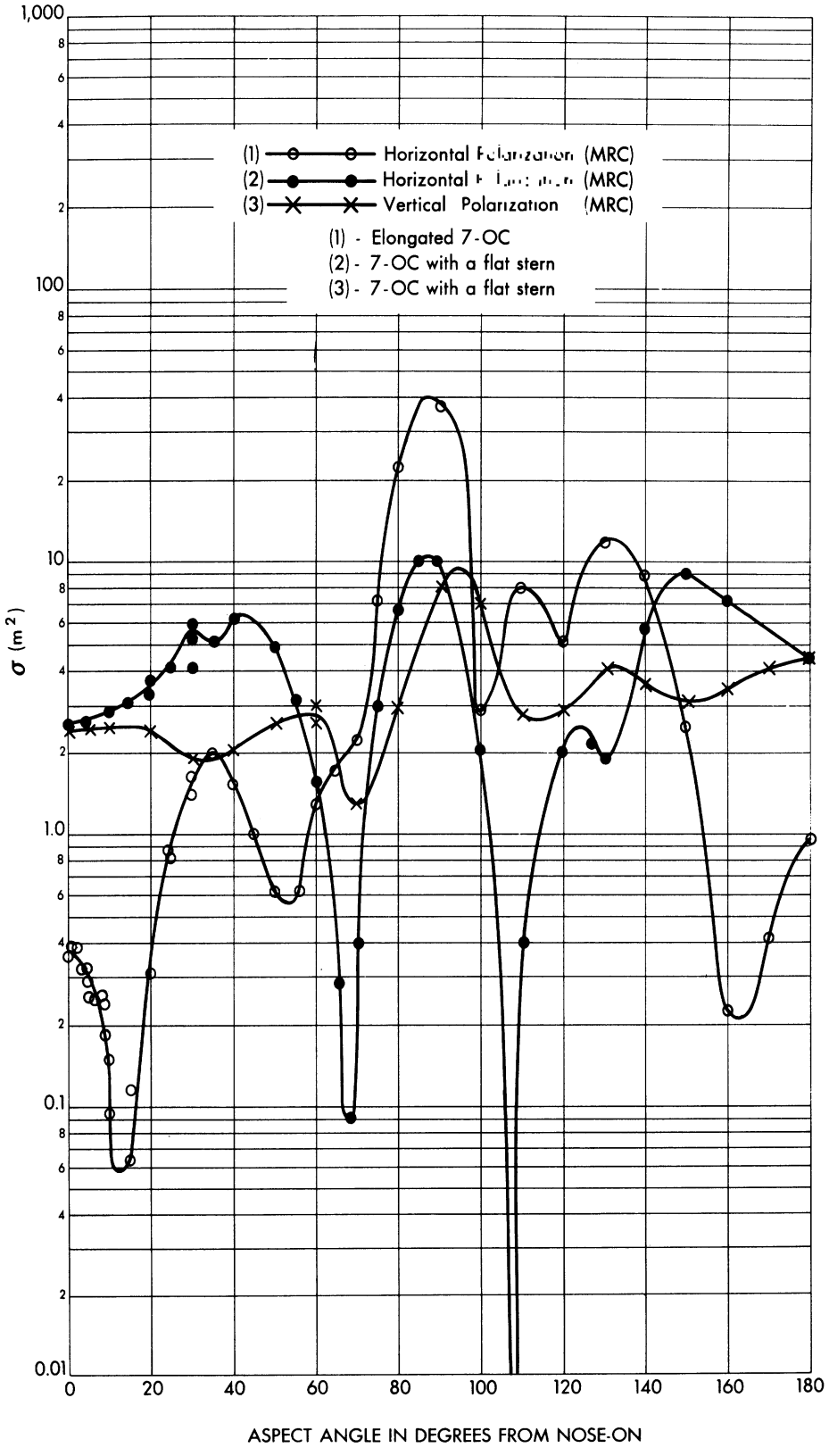

FIG. 5.2-7 CROSS-SECTION OF MODIFIED 7-OC WARHEADS AT 75 MC

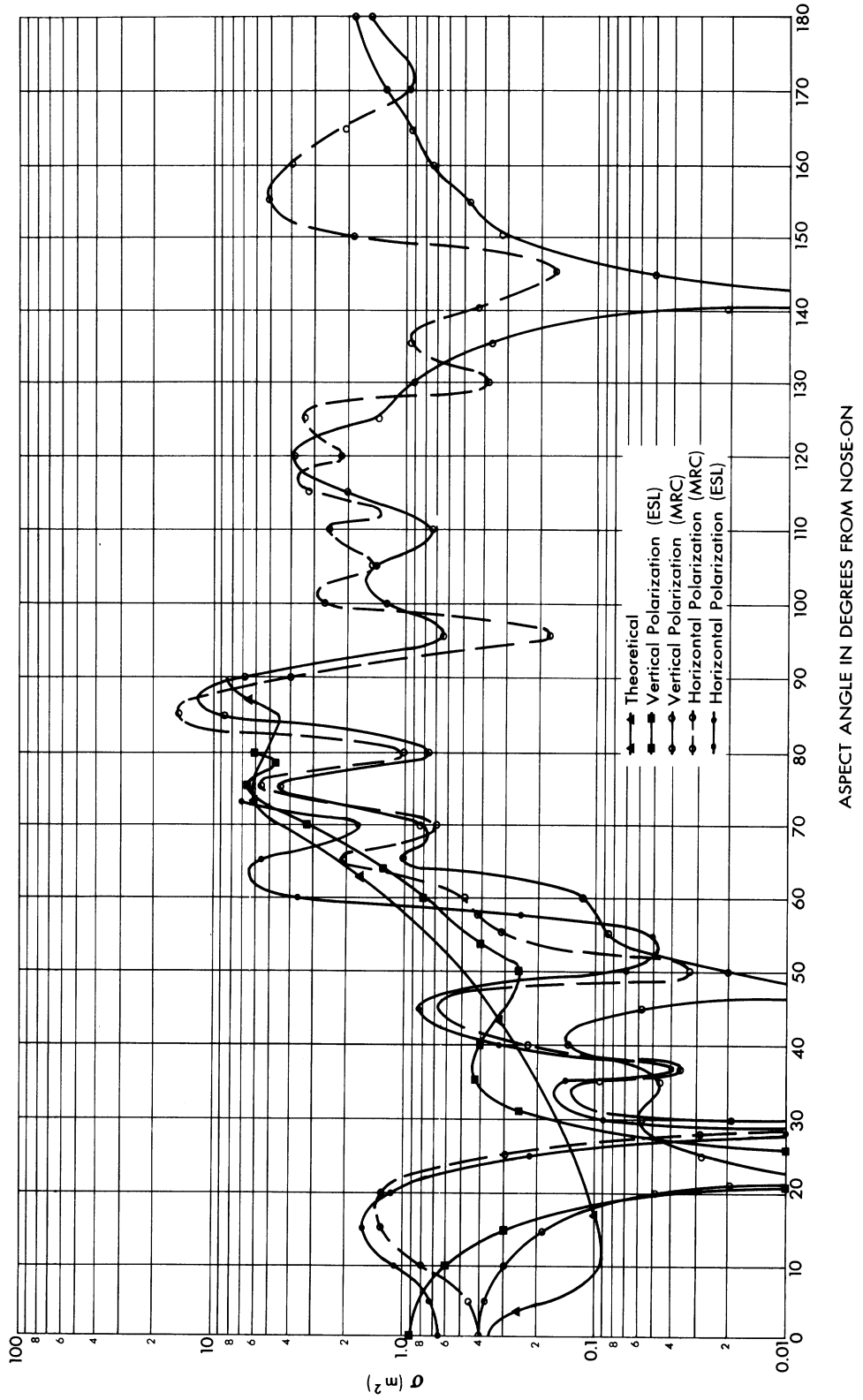

FIG. 5.2-8 CROSS-SECTION OF THE 7-OC WARHEAD AT 225 MC

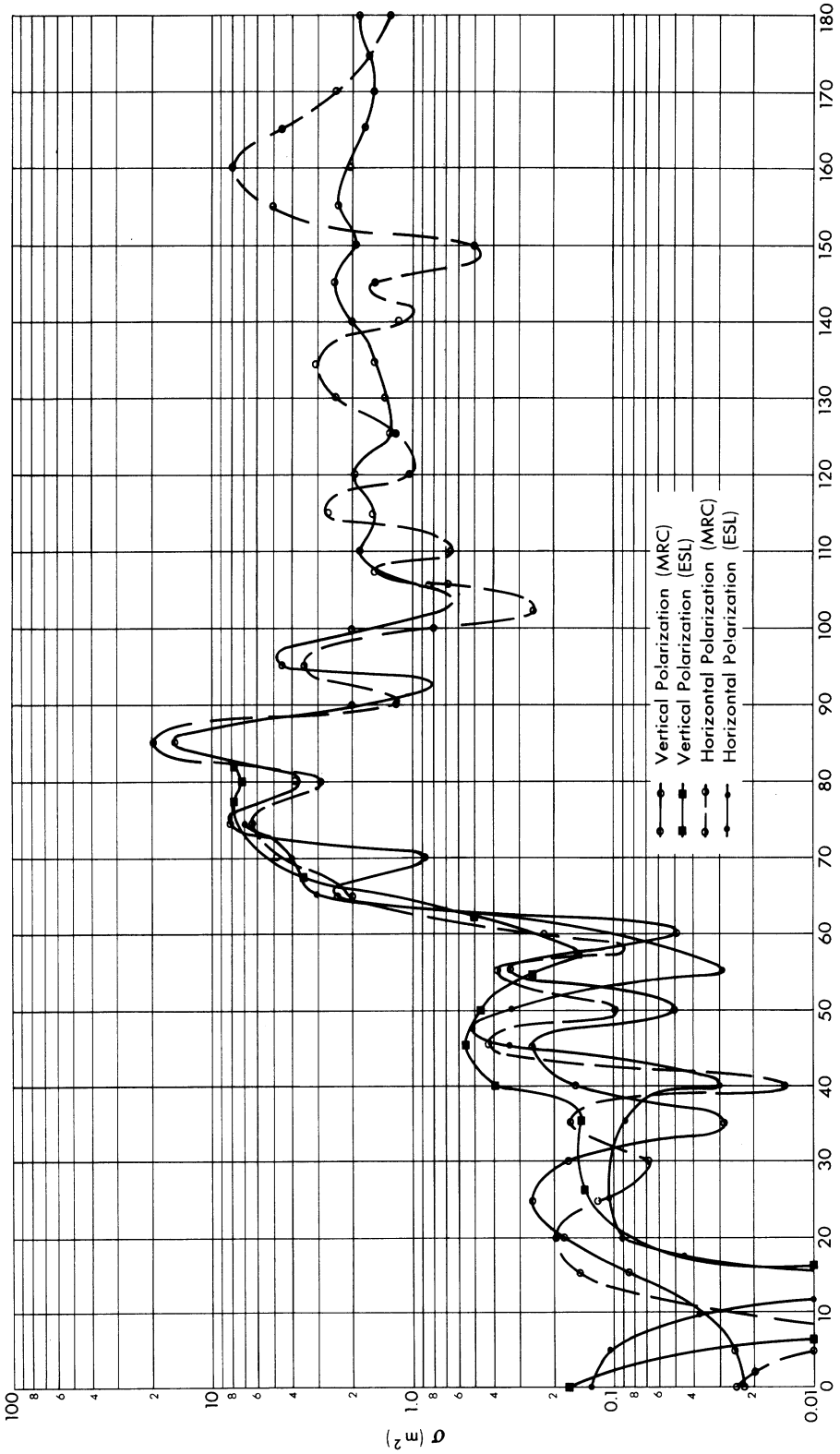

FIG. 5.2-9 CROSS-SECTION OF A 7-OC WARHEAD WITH HEMISPHERICAL STERN AT 225 MC

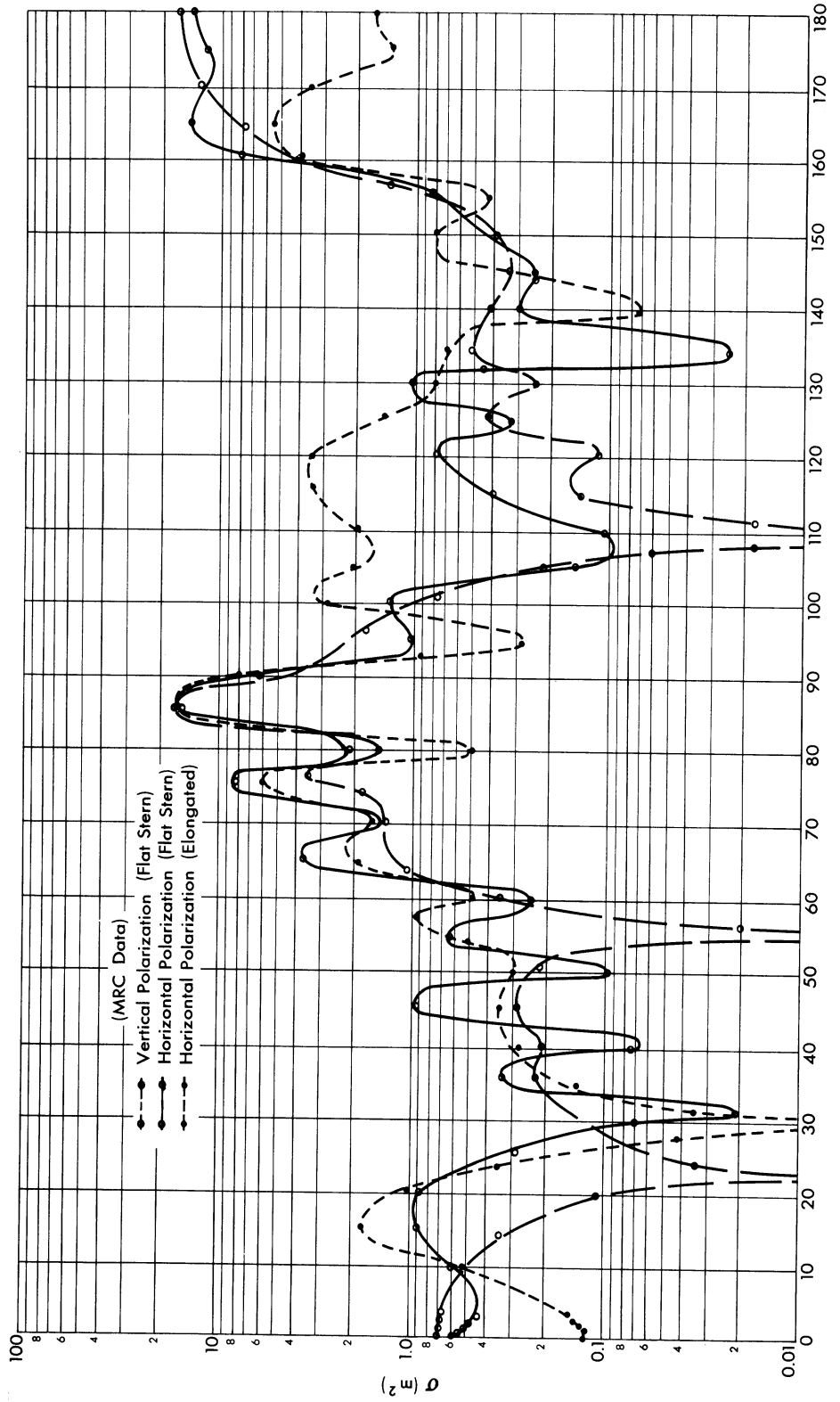

FIG. 5.2-10 CROSS-SECTION OF MODIFIED 7-OC WARHEADS AT 225 MC

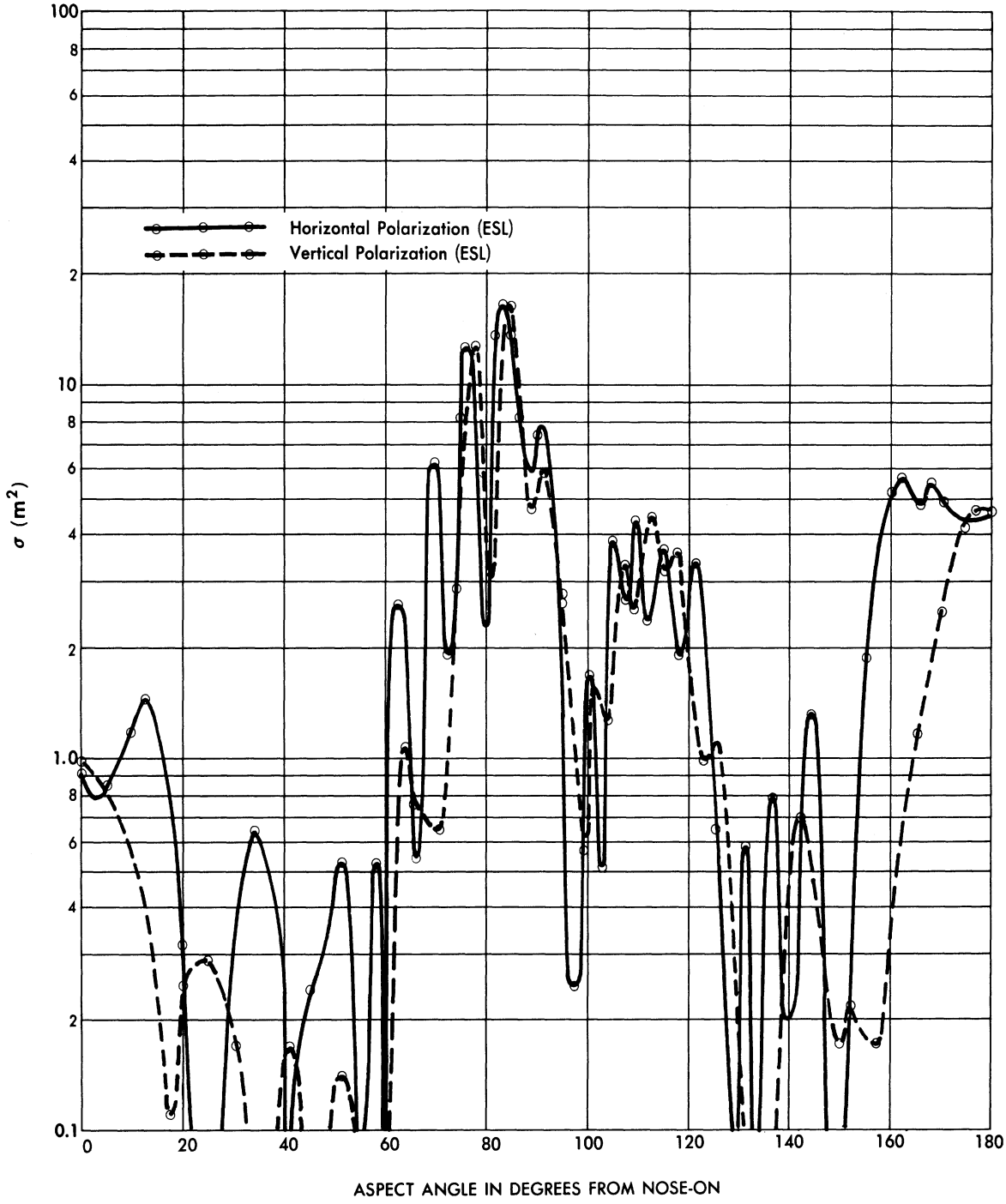

FIG. 5.2-11 CROSS-SECTION OF THE 7-OC WARHEAD AT 333 MC

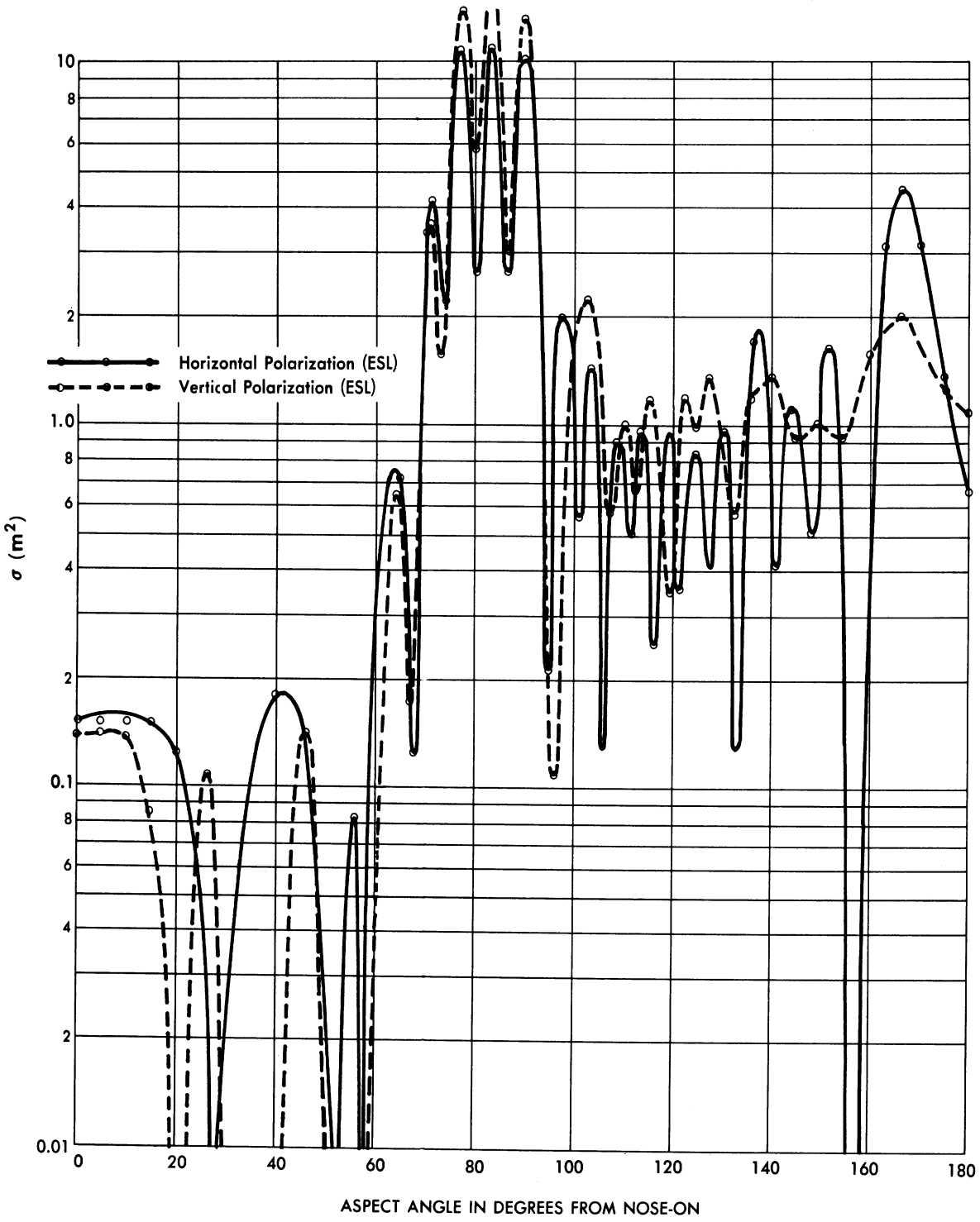

FIG. 5.2-12 CROSS-SECTION OF A MODIFIED (HEMISPHERICAL STERN) 7-OC WARHEAD AT 333 MC

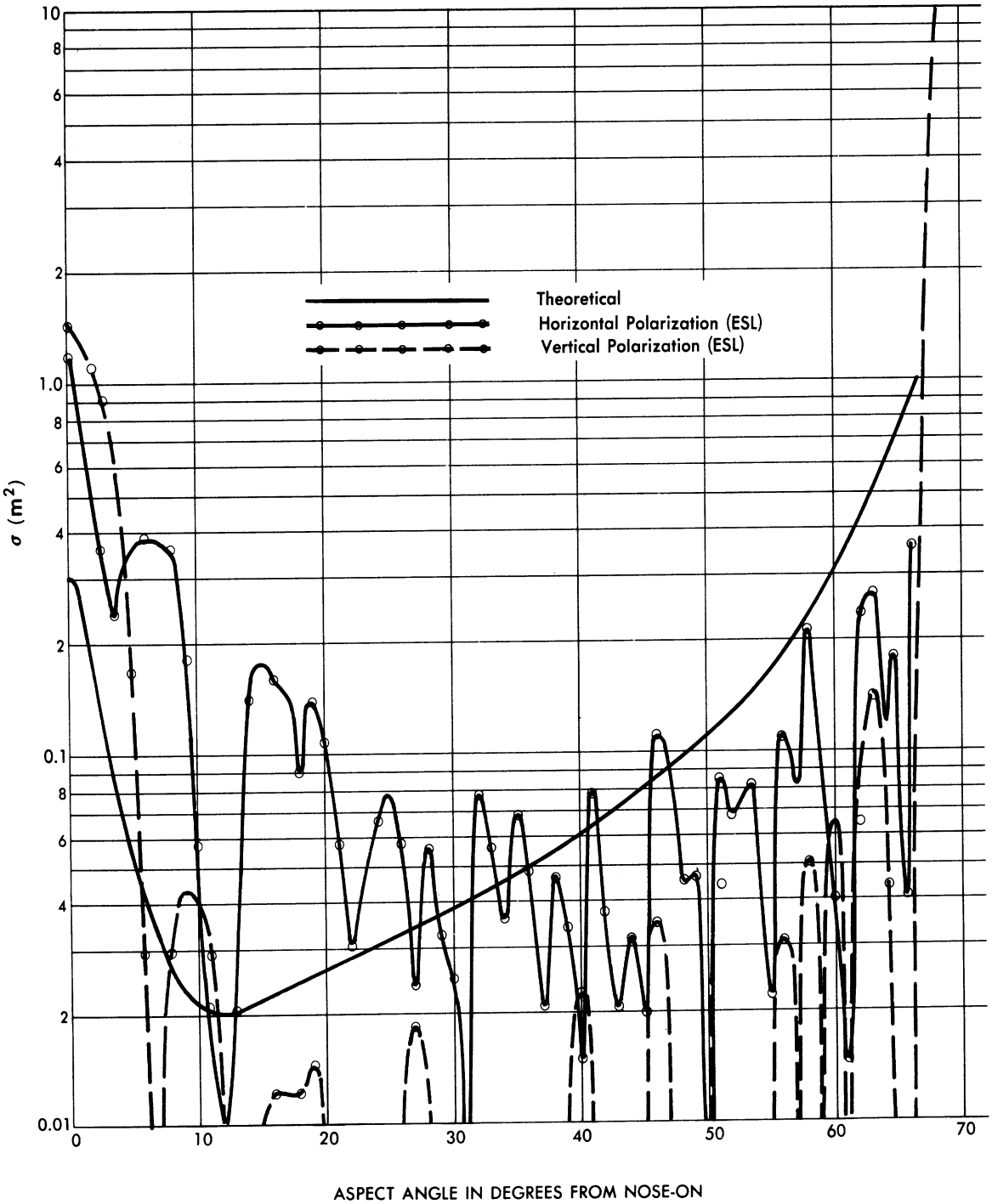

FIG. 5.2-13 CROSS-SECTION OF THE 7-OC WARHEAD AT 1,000 MC

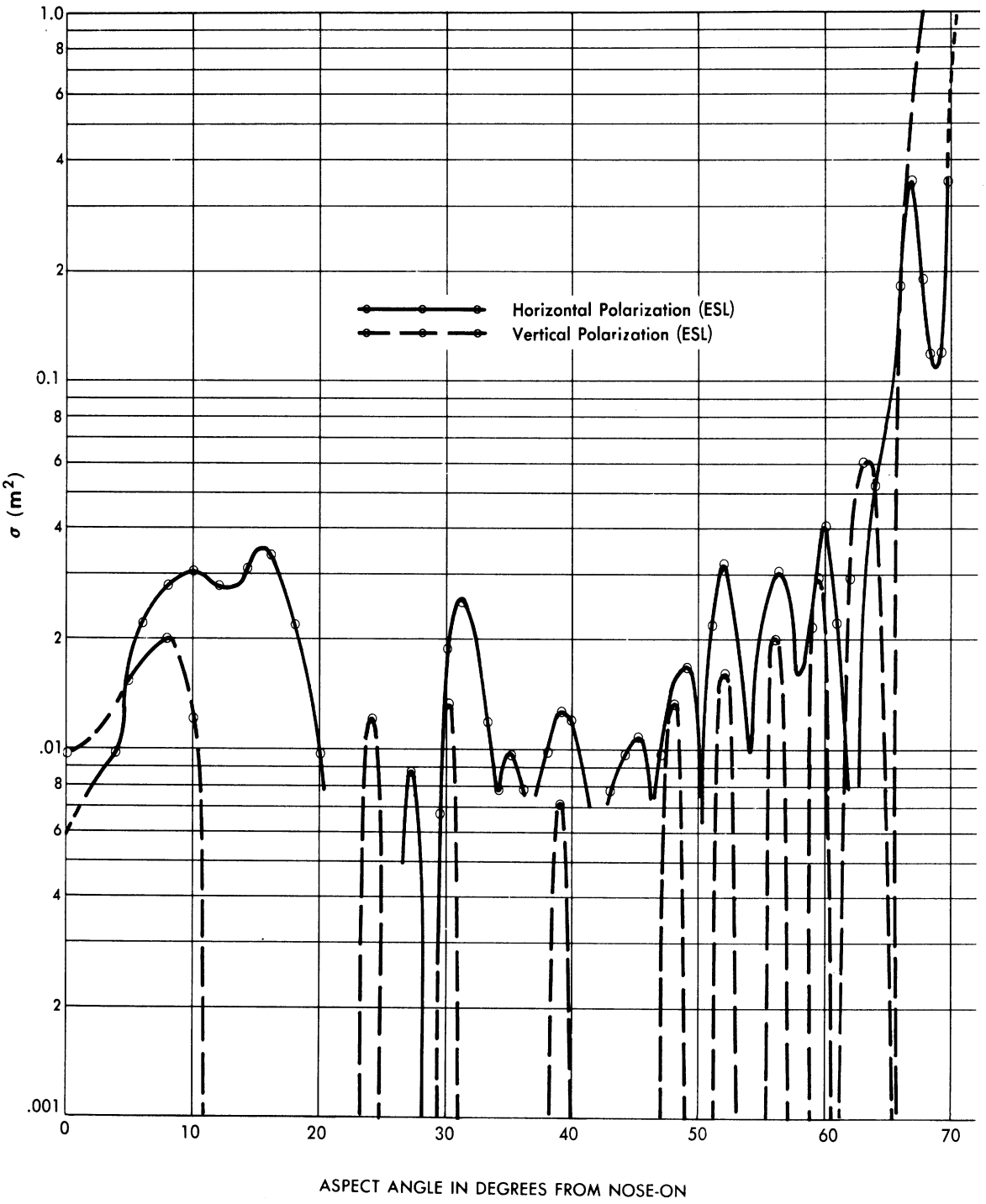

FIG. 5.2-14 CROSS-SECTION OF A MODIFIED (HEMISPHERICAL STERN) 7-OC WARHEAD AT 1,000 MC

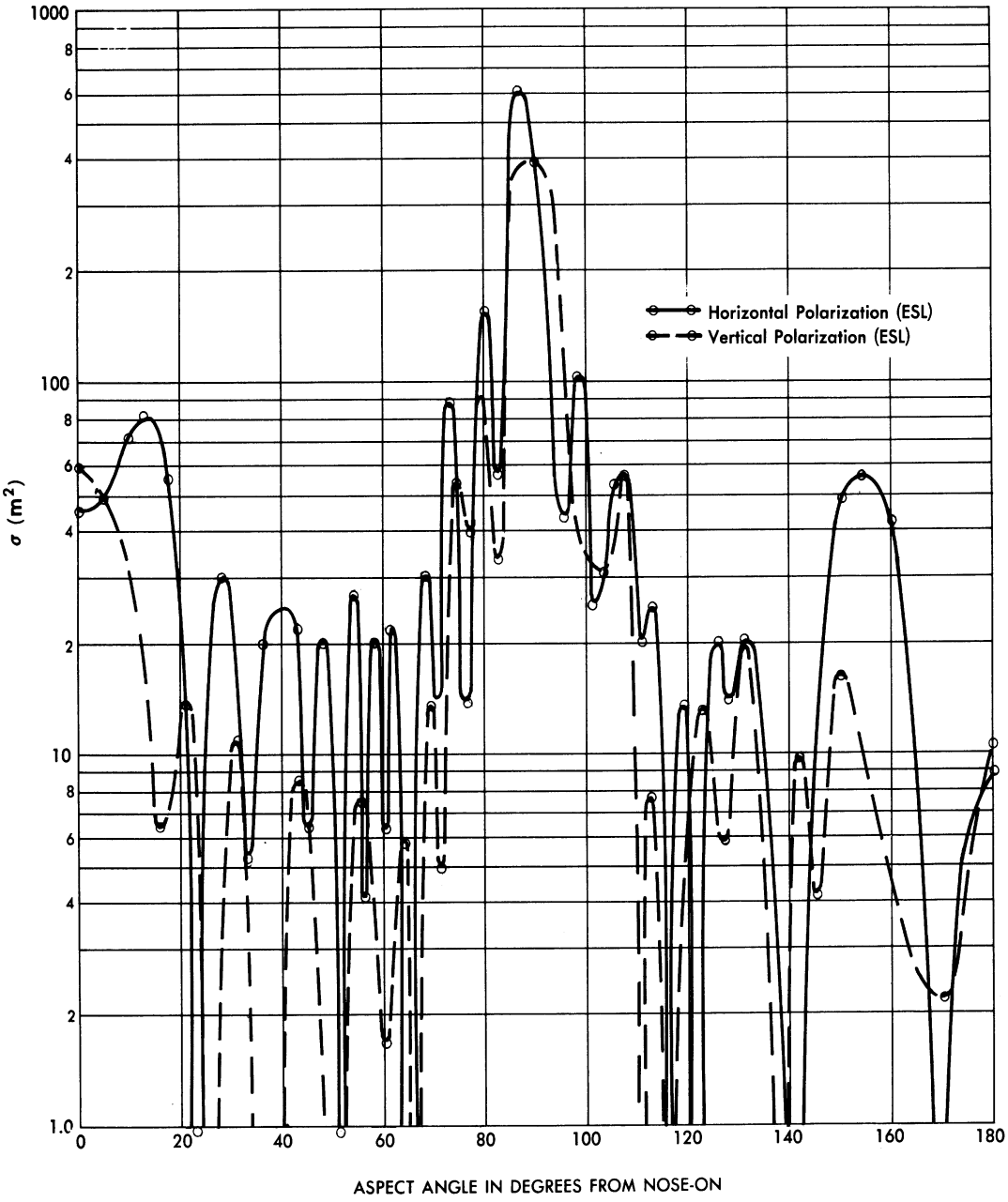

FIG. 5.2-15 CROSS-SECTION OF THE 7-OC BOOSTER AT 75 MC

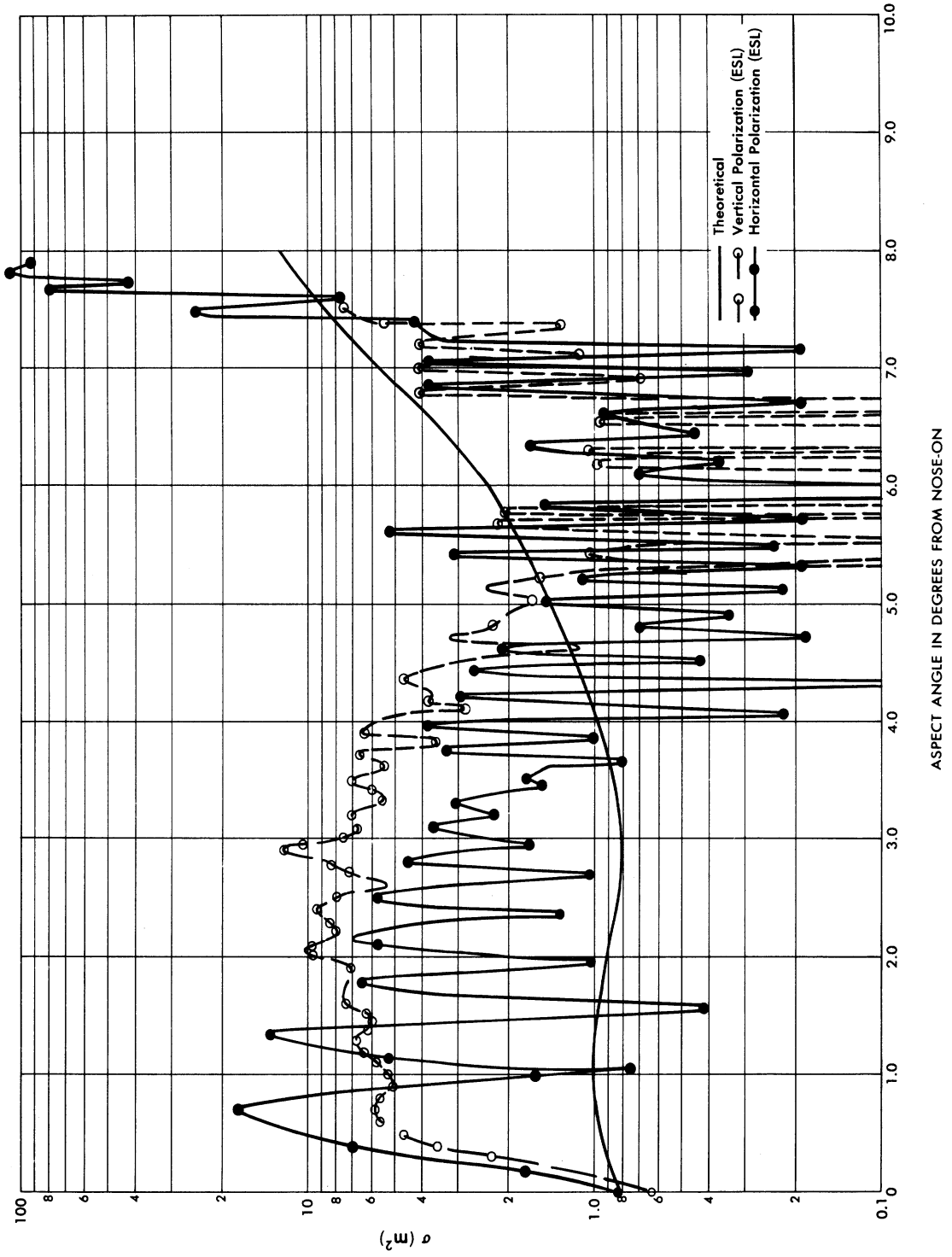

FIG. 5.2-16 CROSS-SECTION OF THE 7-OC BOOSTER AT 225 MC

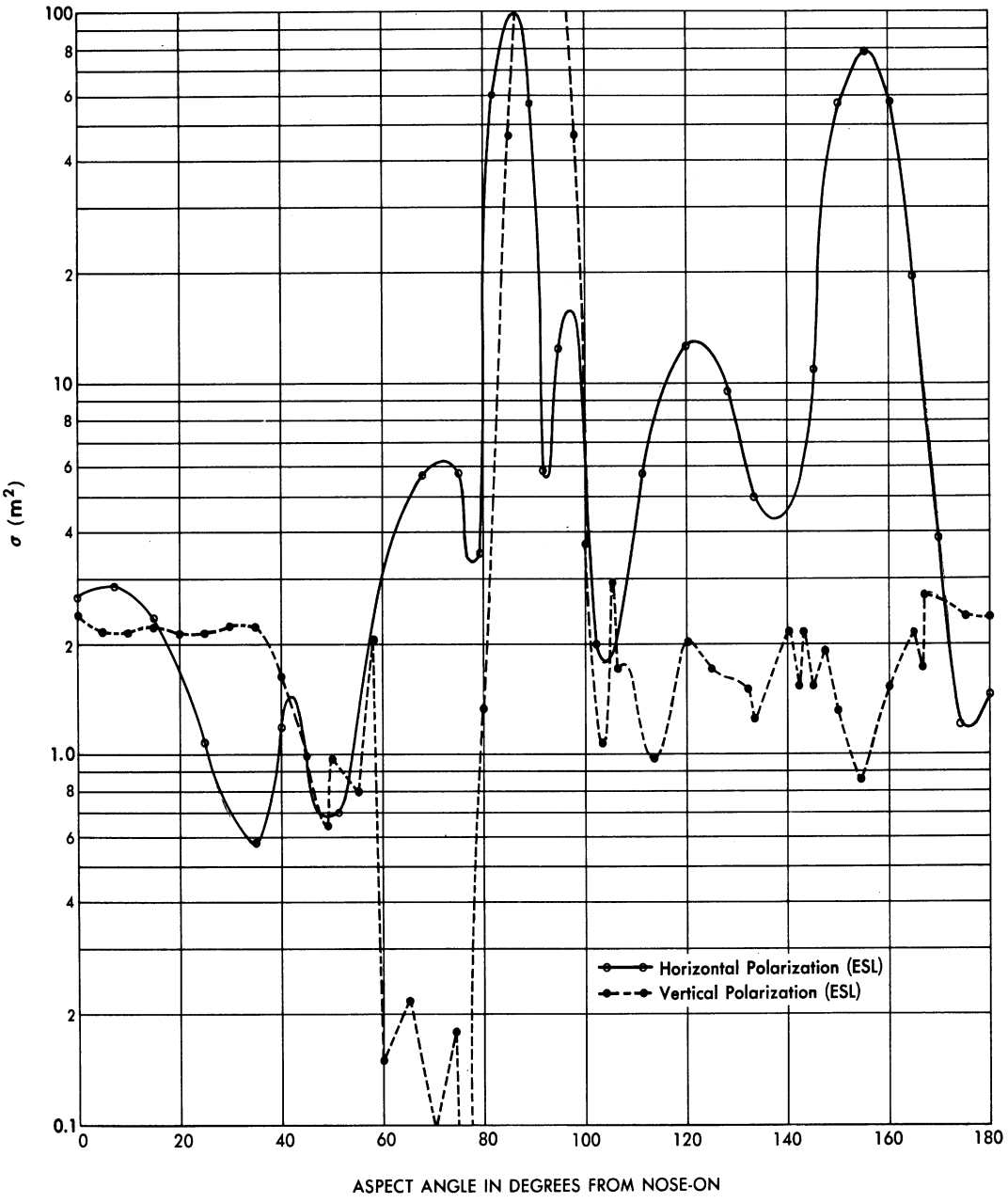

FIG. 5.2-17 CROSS-SECTION OF THE "NEEDLE-NOSE" WARHEAD AT 75 MC

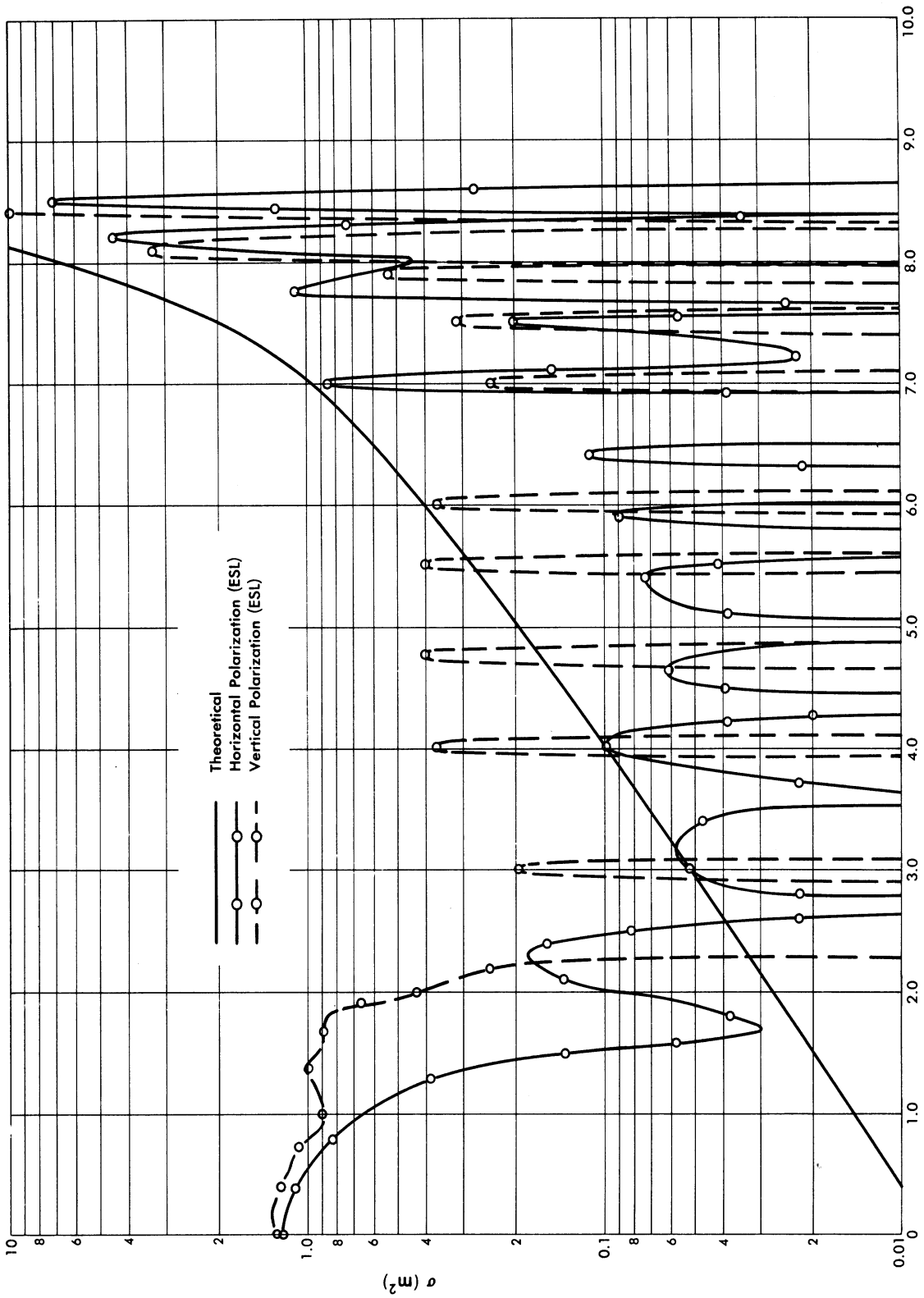

FIG. 5.2-18 CROSS-SECTION OF THE "NEEDLE-NOSE" WARHEAD AT 225 MC

5.3 Static Cross-Section Measurements on V-2 Type Missiles - Microwave Radiation Company, Incorporated.

Static measurements* made by MRC on V-2 models furnished by the Willow Run Research Center were conducted at a frequency of 9200 Mc (Ref. 38) and 9300 Mc (Ref. 39) on a 1/12.9 scale model and at 9300 Mc on an approximately 1/9 scale model (Ref. 33).

All of the tests performed at MRC were designed to serve as a static "check" to be used in connection with the dynamic tests conducted by the Willow Run Research Center (these dynamic tests are discussed in Section VI and in Reference 40).

A sketch of the model used in the experiments reported in Reference 33 is shown in Figure 5.3-1. A photograph of the model mounted in the support structure is shown in Figure 5.3-2.

Figure 5.3-3 shows results reported in Reference 38 for an equivalent full-scale frequency of 710 Mc. Figure 5.3-4 shows the results reported in Reference 39 for an equivalent full-scale frequency of 721 Mc. To obtain information on the effect of the fins on the nose-on cross-section, measurements were made using vertical polarization on:

1. model without fins
2. model with four square fins
3. model with two vertical square fins (no horizontal fins)
4. model with two horizontal square fins (no vertical fins)
5. model with four square fins (one vertical fin displaced longitudinally $\lambda/4$ with respect to the other)
6. model with four V-2 type fins

*The experimental method used is described in Appendix 2.

The results of these six nose-on measurements are shown in Table 5-1, with all cross-sections scaled to full V-2 size at 721 Mc.

Figure 5.3-5 contains the results reported in Reference 33.

TABLE 5-1

Cross-Section of Modified V-2 Models at 721 Mc.

CONFIGURATION	RADAR CROSS SECTION Square Meters
V-2 without fins	0.21
V-2 with swept back fins	0.55
V-2 with four square fins	2.3
V-2 with two vertical square fins: no horizontal fins	1.7
V-2 with two horizontal fins: no vertical fins	0.52
V-2 with four square fins: one vertical fin displaced longitudinally $\lambda/4$ with respect to the other	0.41

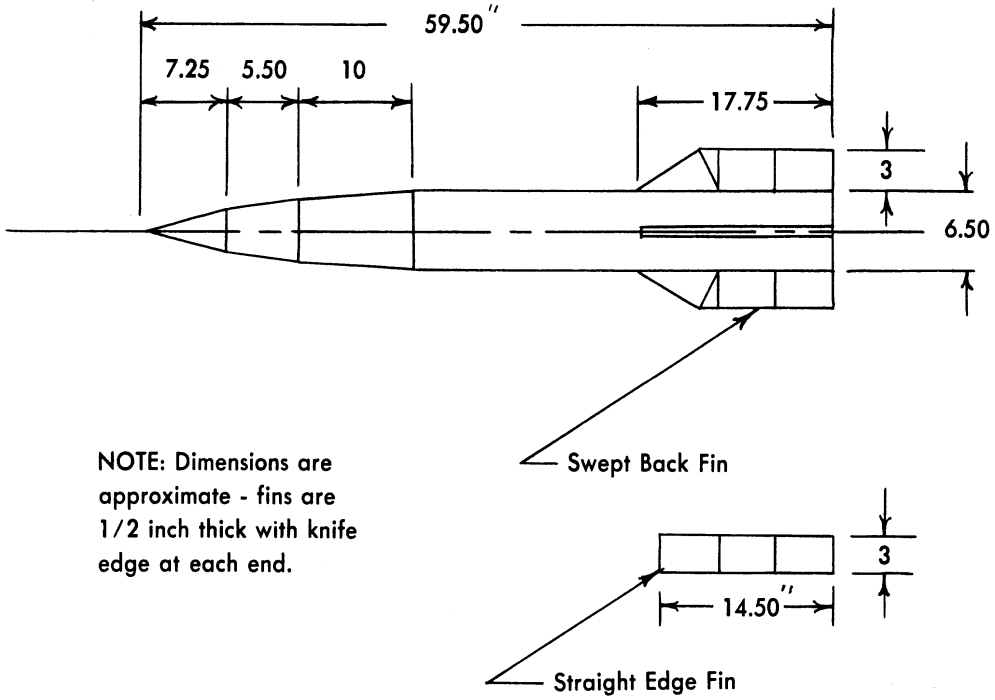

FIG. 5.3-1 V-2 TYPE MODEL USED IN STATIC EXPERIMENTS AT THE MICROWAVE RADIATION COMPANY

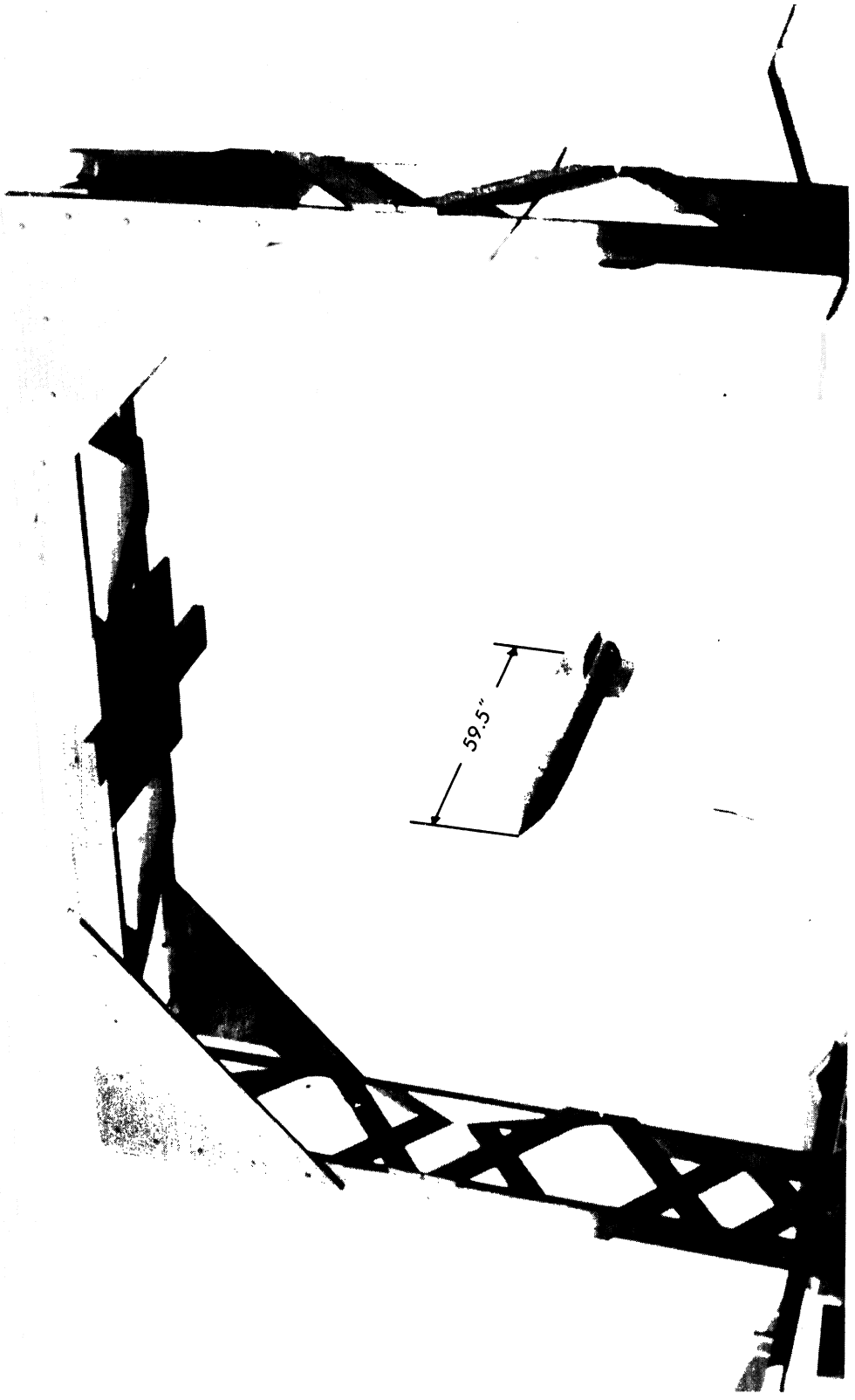

FIG. 5.3-2 MODEL MOUNTED IN THE SUPPORT STRUCTURE

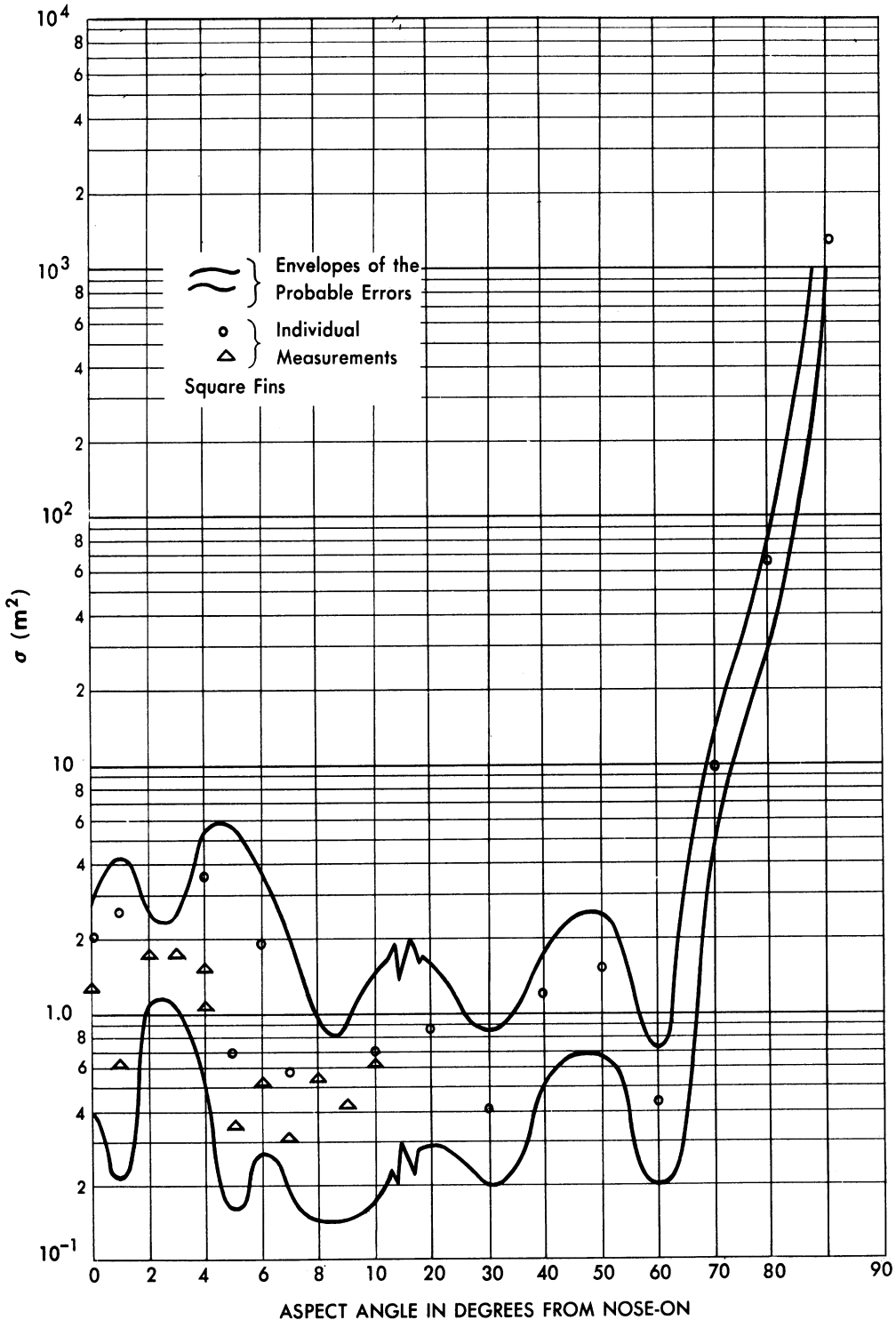

FIG. 5.3-3 CROSS-SECTION OF A V-2 TYPE MISSILE AT 710 MC
(Vertical Polarization)

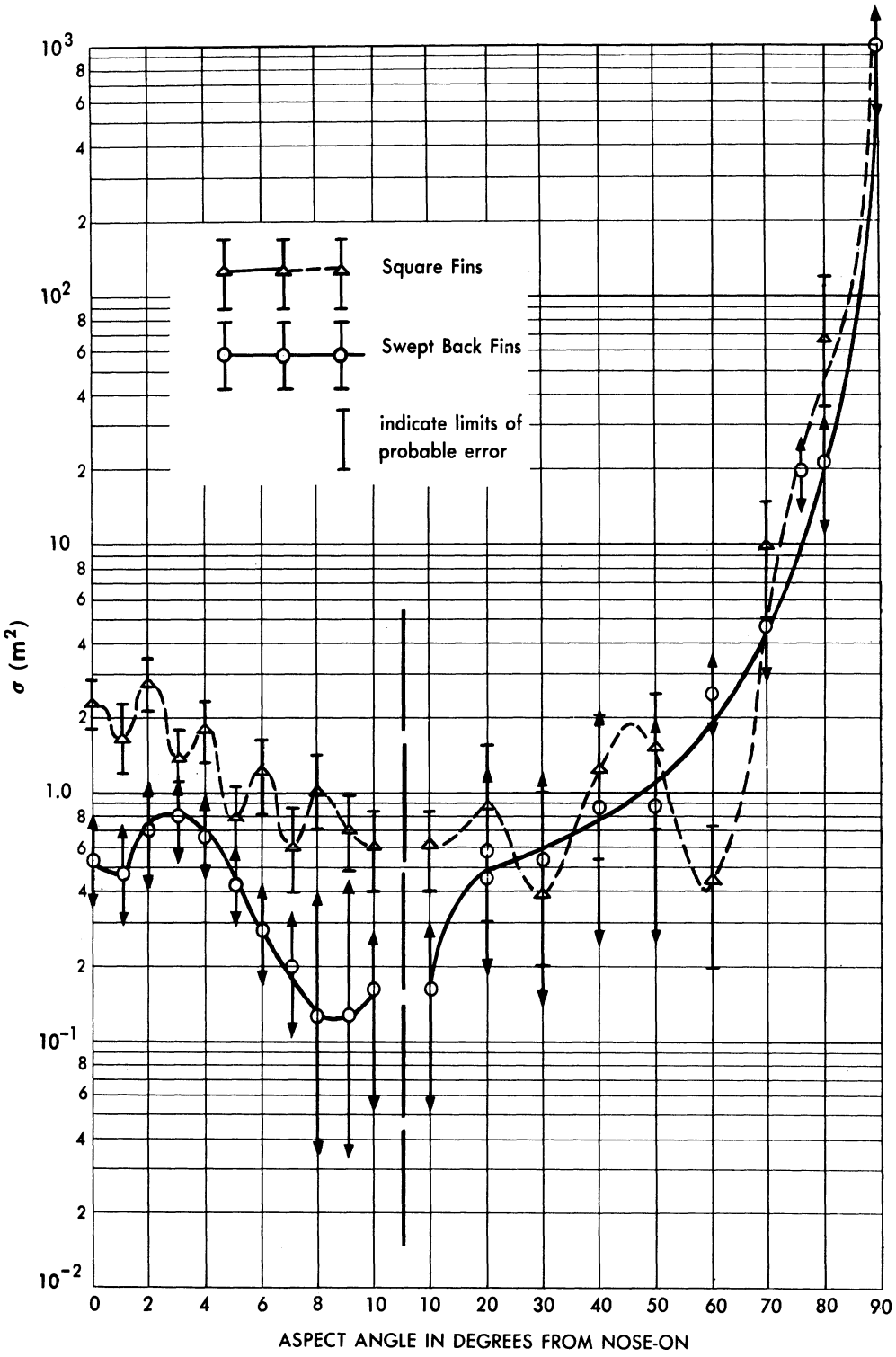

FIG. 5.3-4 CROSS-SECTION OF A V-2 TYPE MISSILE AT 721 MC
(Vertical Polarization)

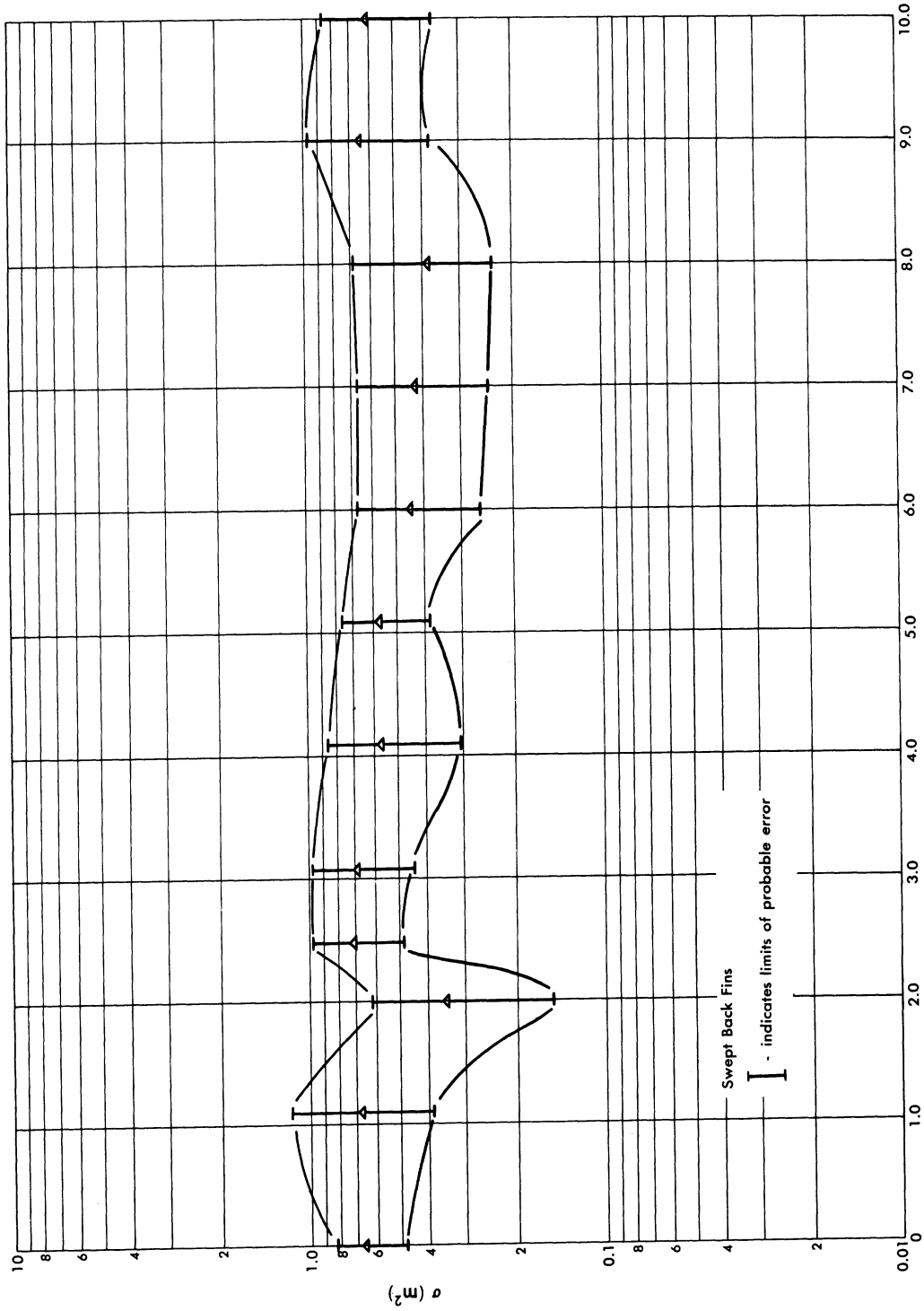

FIG. 5.3-5 CROSS-SECTION OF A V-2 TYPE MISSILE AT 1,000 MC
(Vertical Polarization)

5.4 V-2 Type Missiles - Ohio State University Antenna Laboratory

A large number of static experiments have been conducted on V-2 type missiles by the Antenna Laboratory of the Ohio State University Research Foundation. The results of these experiments are reported in References 41 through 49. The experiments provided data at the full-scale frequencies of 20, 50, 100, 300, 600, and 1200 Mc; the data were obtained by rotating models about a vertical axis for orientations of 0, 15, 30, 45, 60, 75, and 90 degrees from horizontal.

In presenting a summary of these experiments in this section we shall, for each wavelength, present a plot of σ vs aspect angle only for the 0 degree elevation for both horizontal and vertical polarizations. To indicate the effect of increasing elevation angle, the polar plots for a few of the elevation-angle cases are given (for the 20 Mc V-2 case), as well as the calibration curve which permits one to determine σ from the polar diagrams. (The angular variation shown on the polar plots is that of aspect.)*

Since the WAC rocket is a ballistic missile, the data obtained by OSU for this missile is included. The WAC was measured at each of the seven frequencies mentioned above and also at a frequency of 2900 Mc. The results obtained by OSU from measurements made on Willow Run Research Center models of the UMA-I missile are shown in Section 5.4.8. These measurements on this V-2 type missile yielded results corresponding to the full-scale frequencies of 400 and 621 Mc.

Section 5.4.9 contains a summary of the bistatic measurements made at the Antenna Laboratory of the Ohio State University.

*These polar plots, plus the calibration curve also serves to illustrate the method of presentation used by OSU.

5.4.1 - 20 Mc Data

The data obtained by OSU at 20 Mc, (Refs. 41 and 48) are shown in Figures 5.4.1-1 through 5.4.1-4, and the WAC data in Figure 5.4.1-5. The elevation angle * cases of 0, 30, 60, and 90 degrees are used to indicate the effect of increasing elevation angle on the cross-section of a V-2.

The experiments were conducted at a frequency of 3000 Mc on 1/150 scale models.

* The elevation angle is the angle formed at the line between the radar and the model and the plane in which the aspect angle is measured (see page 15).

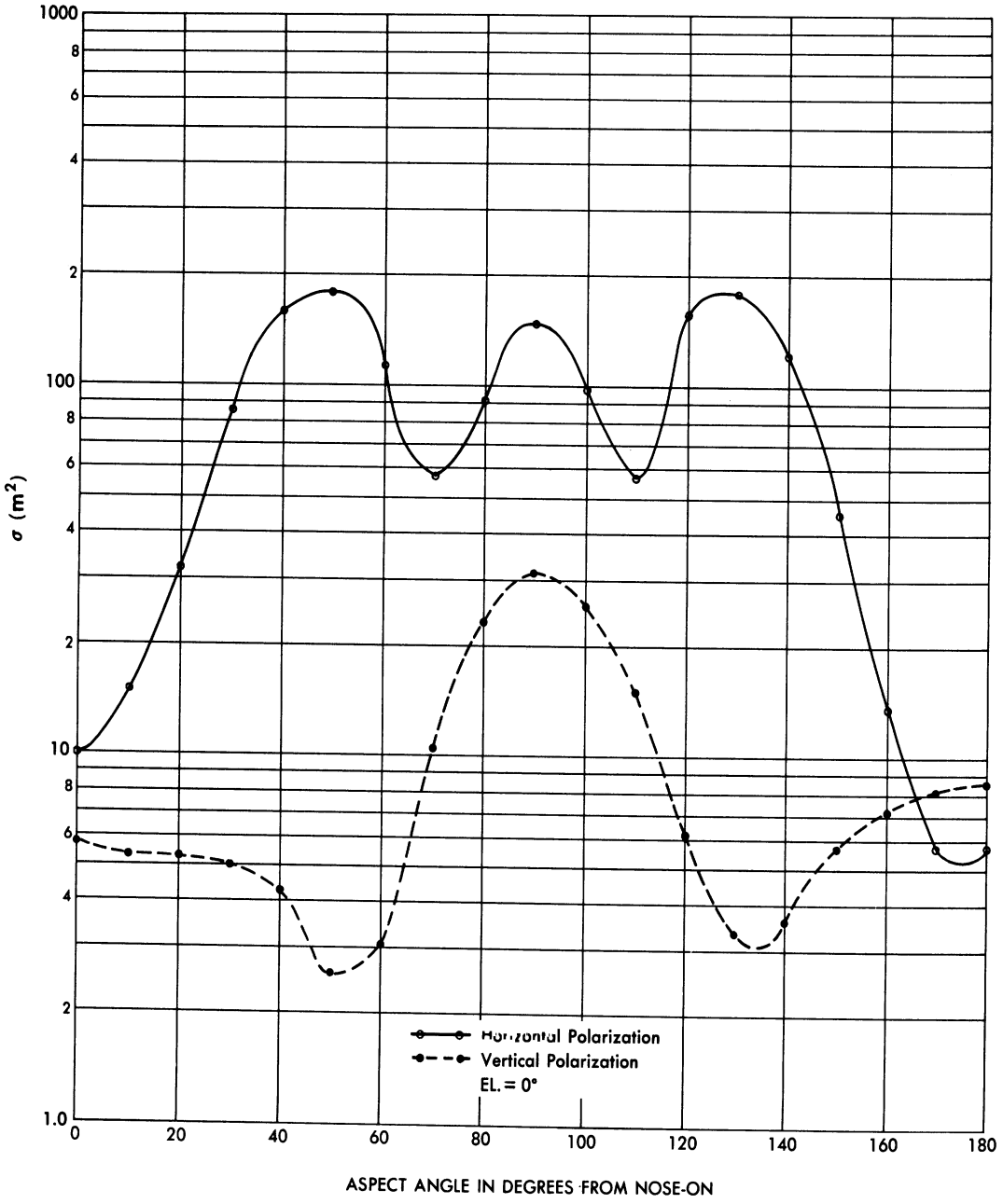

FIG. 5.4.1-1 CROSS-SECTION OF A V-2 TYPE MISSILE AT 20 MC (O.S.U.)

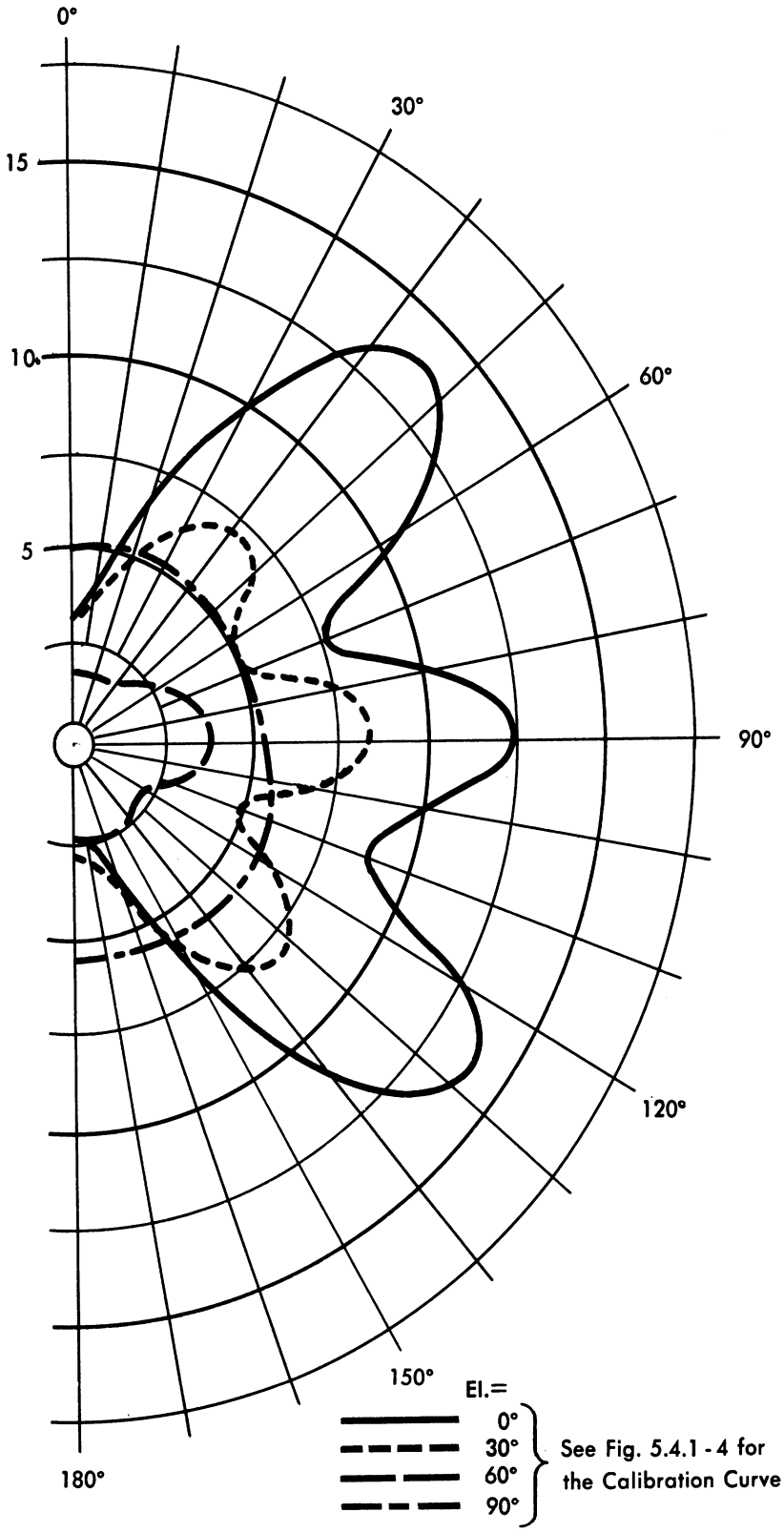

FIG. 5.4.1-2 POLAR PLOT SHOWING EFFECT OF INCREASING ELEVATION ANGLE ON CROSS-SECTION OF A V-2 AT 20 Mc (HORIZONTAL POLARIZATION)

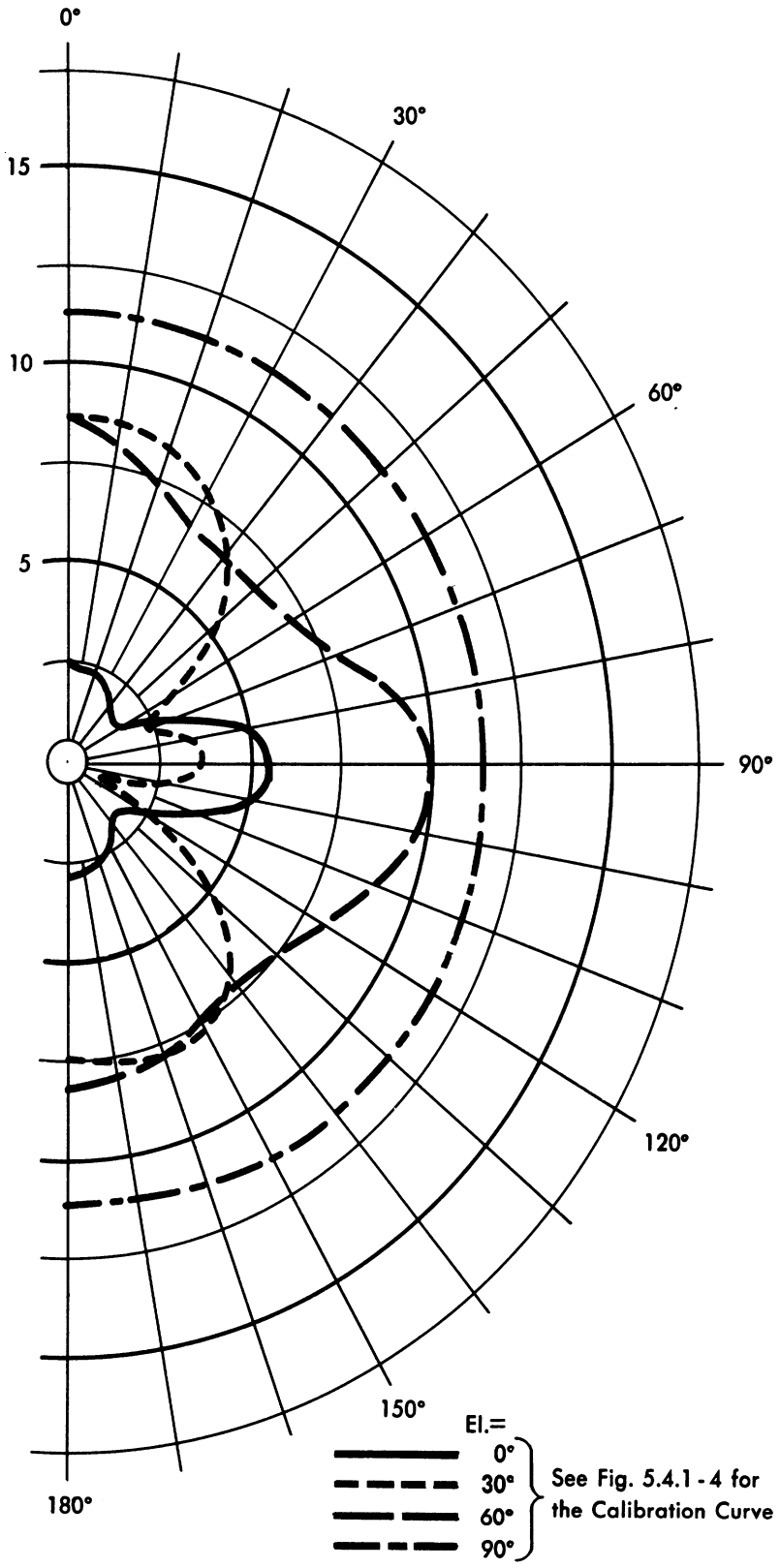

FIG. 5.4.1-3 POLAR PLOT SHOWING EFFECT OF INCREASING ELEVATION ANGLE ON CROSS-SECTION OF A V-2 AT 20 Mc (VERTICAL POLARIZATION)

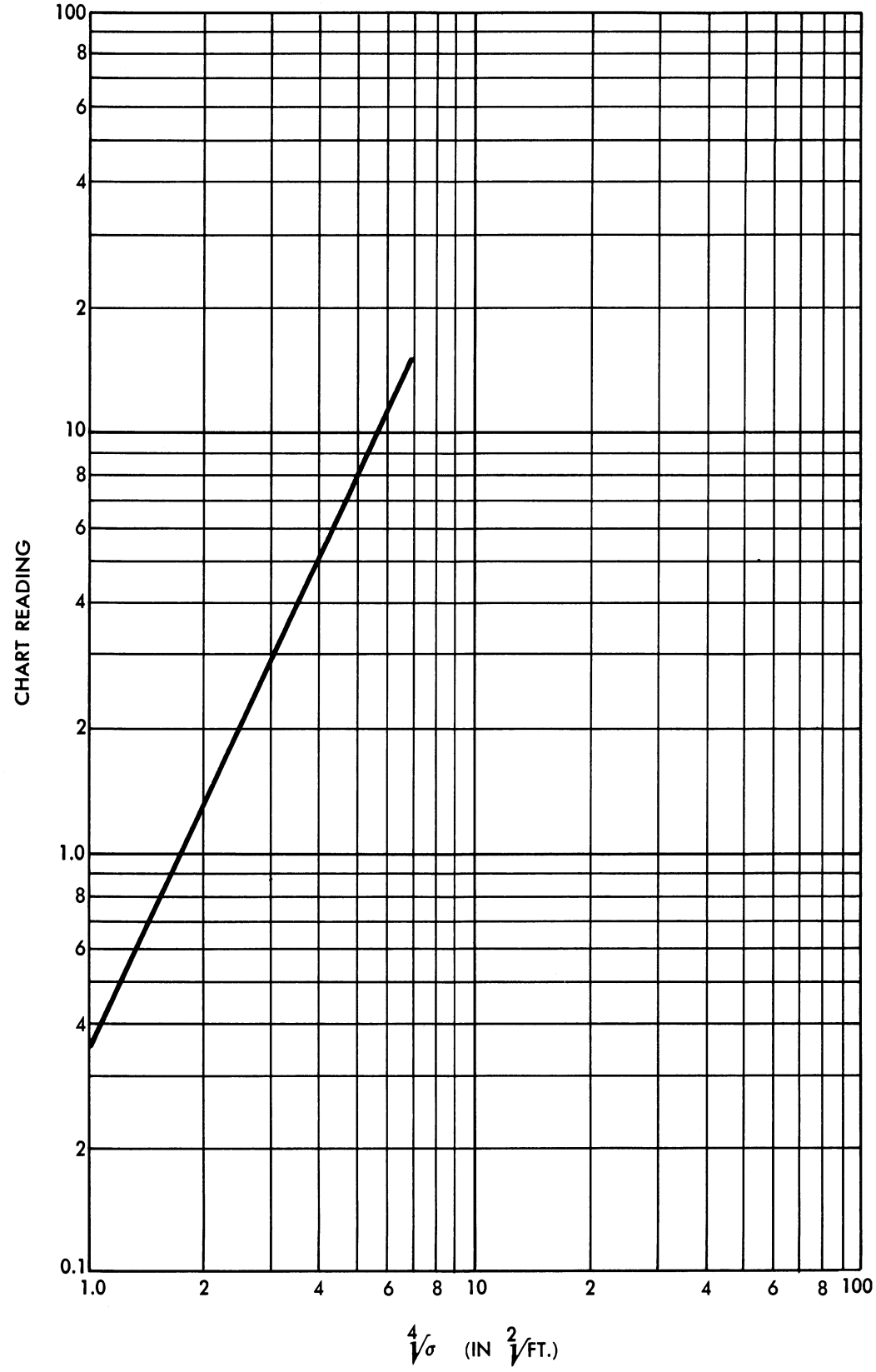

FIG. 5.4.1-4 CALIBRATION CURVE FOR V-2 ROCKET AT 20 MC
(Figs. 5.4.1-2 & 5.4.1-3)

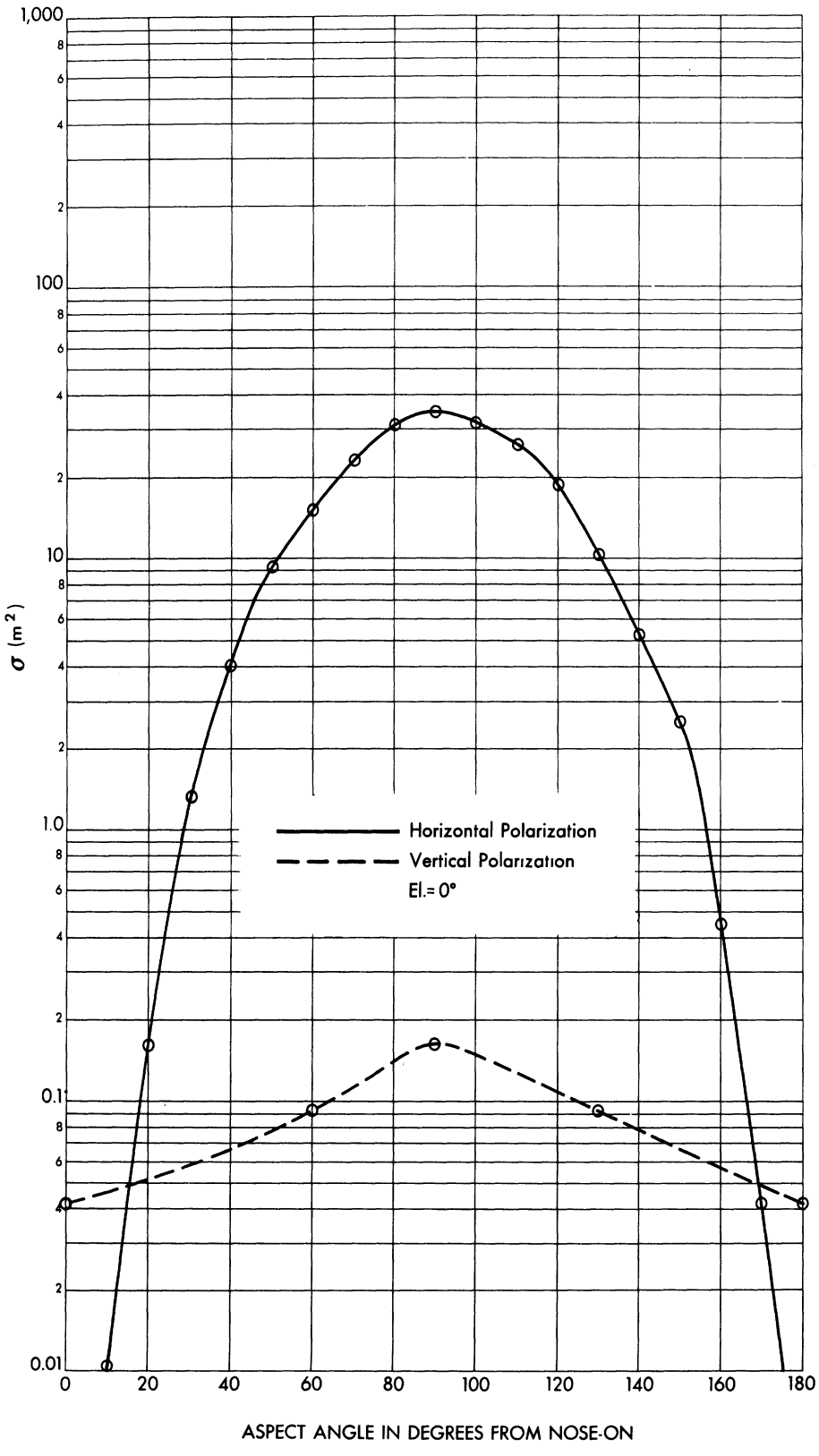

FIG. 5.4.1-5 CROSS-SECTION OF THE WAC MISSILE AT 20 MC (O.S.U.)

5.4.2 - 50 Mc Data

The OSU 50 Mc data (Ref. 42 & 48) are summarized in Figures 5.4.2-1 and 5.4.2-2; the first figure is devoted to the V-2 data, and the second to the WAC data.

The experiments were conducted at a frequency of 3000 Mc on 1/60 scale models.

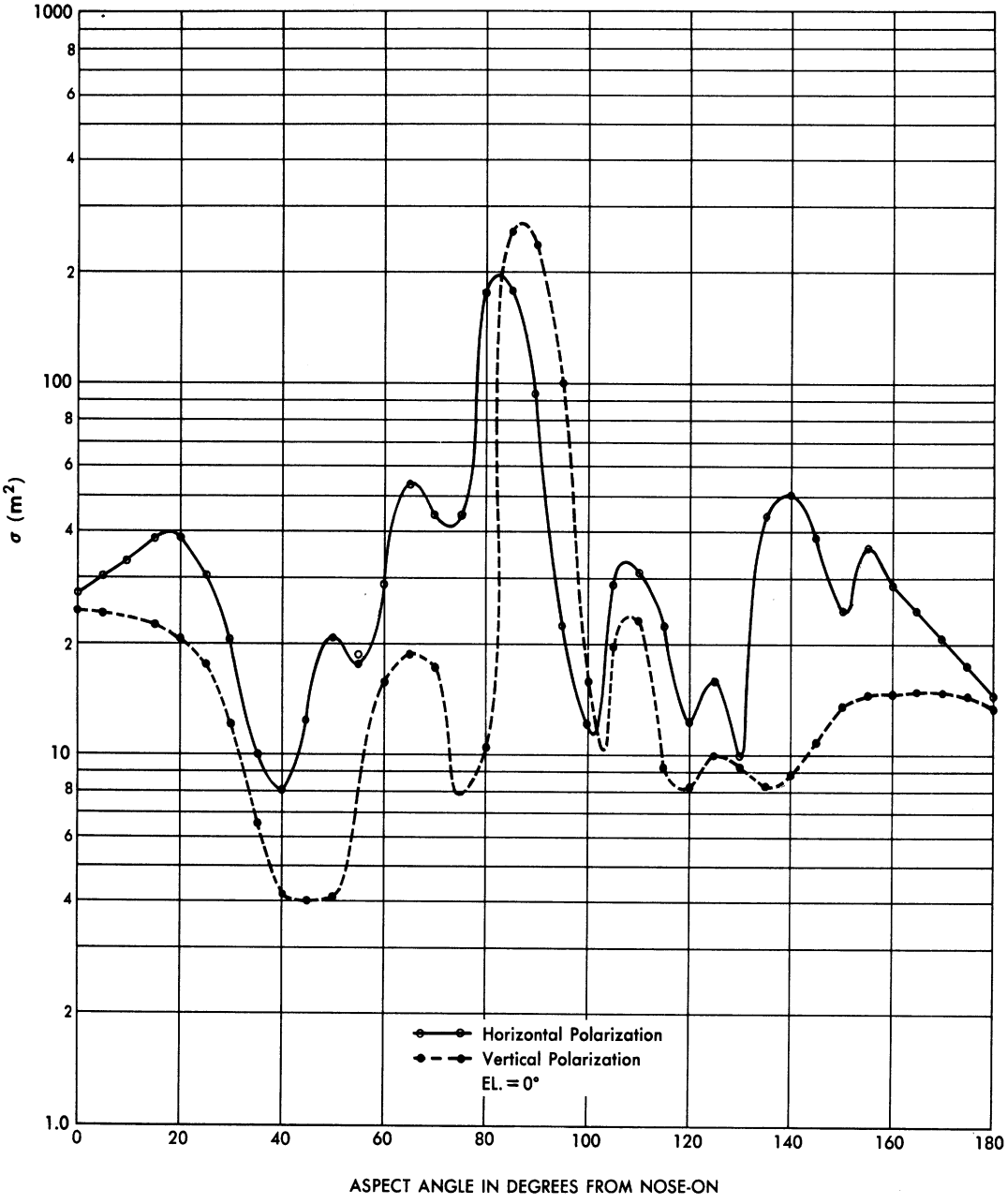

FIG. 5.4.2-1 CROSS-SECTION OF A V-2 TYPE MISSILE AT 50 MC (O.S.U.)

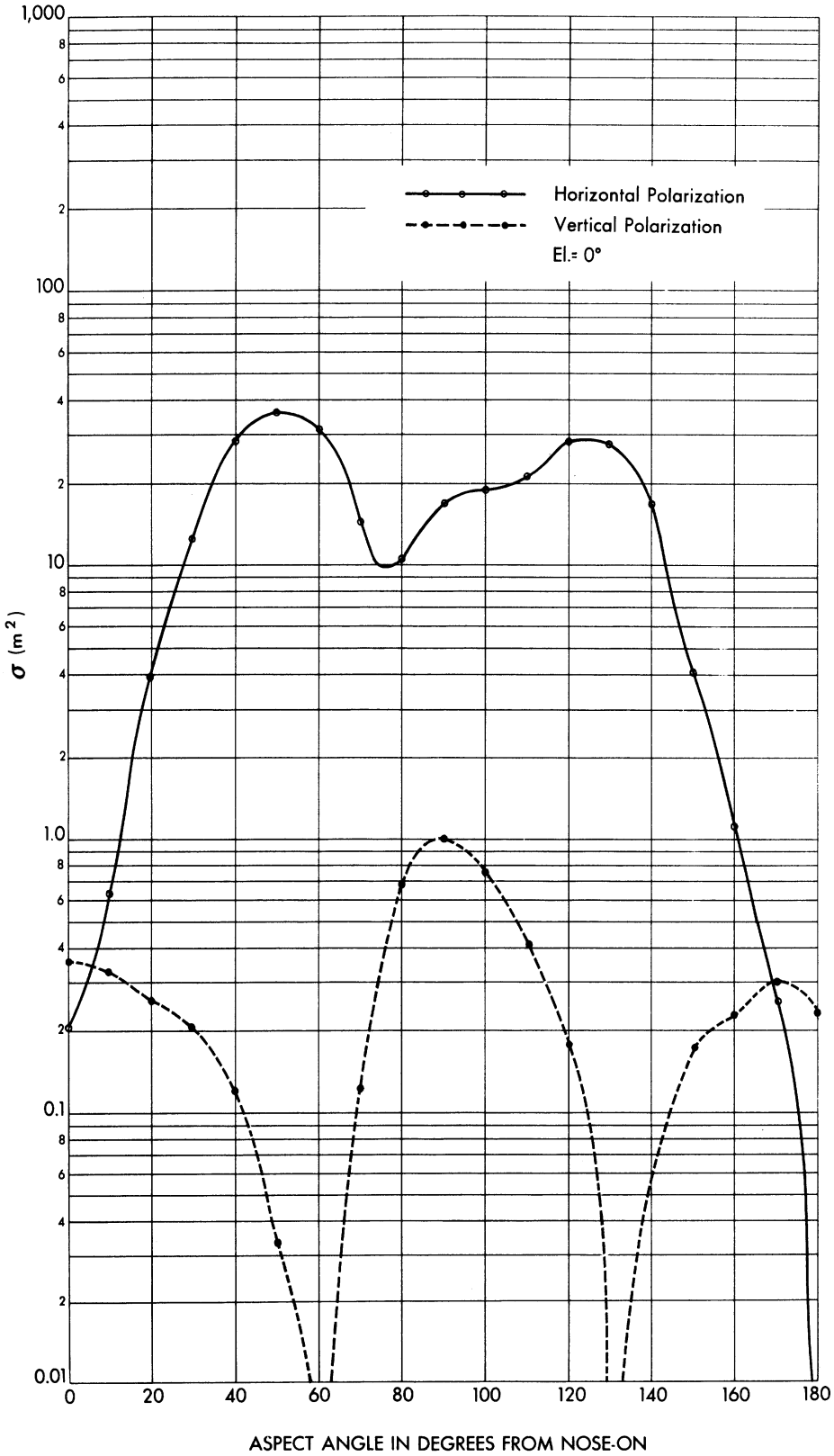

FIG. 5.4.2-2 CROSS-SECTION OF WAC MISSILE AT 50 MC (O.S.U.)

5.4.3 - 100 Mc Data

The OSU 100 Mc data (Ref. 43) appears in Figures 5.4.3-1 and 5.4.3-2. The manner of presentation is the same as for the 50 Mc data in Section 5.4.2.

The experiments were conducted at a frequency of 3000 Mc on 1/30 scale models.

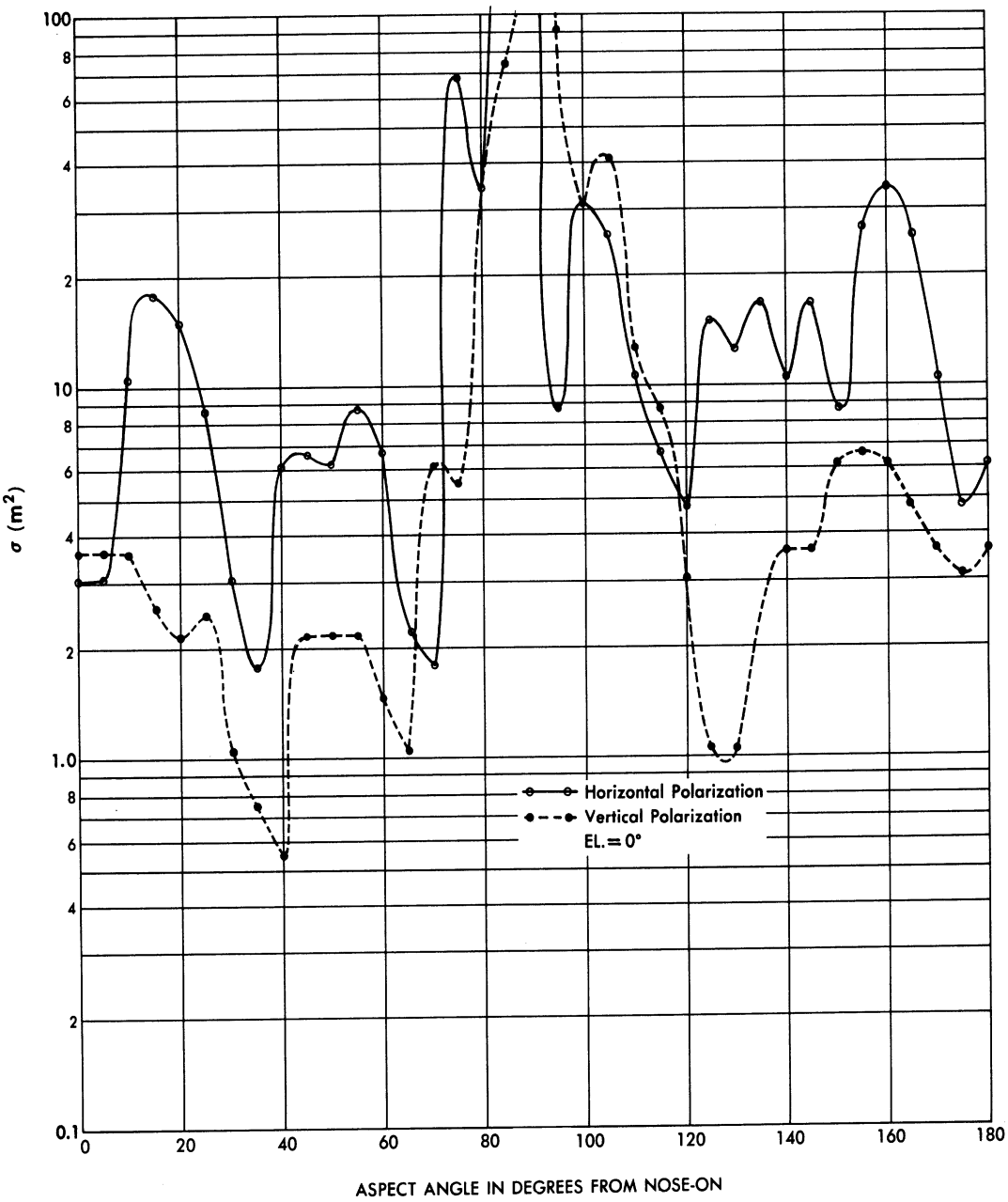

FIG. 5.4.3-1 CROSS-SECTION OF A V-2 TYPE MISSILE AT 100 MC (O.S.U.)

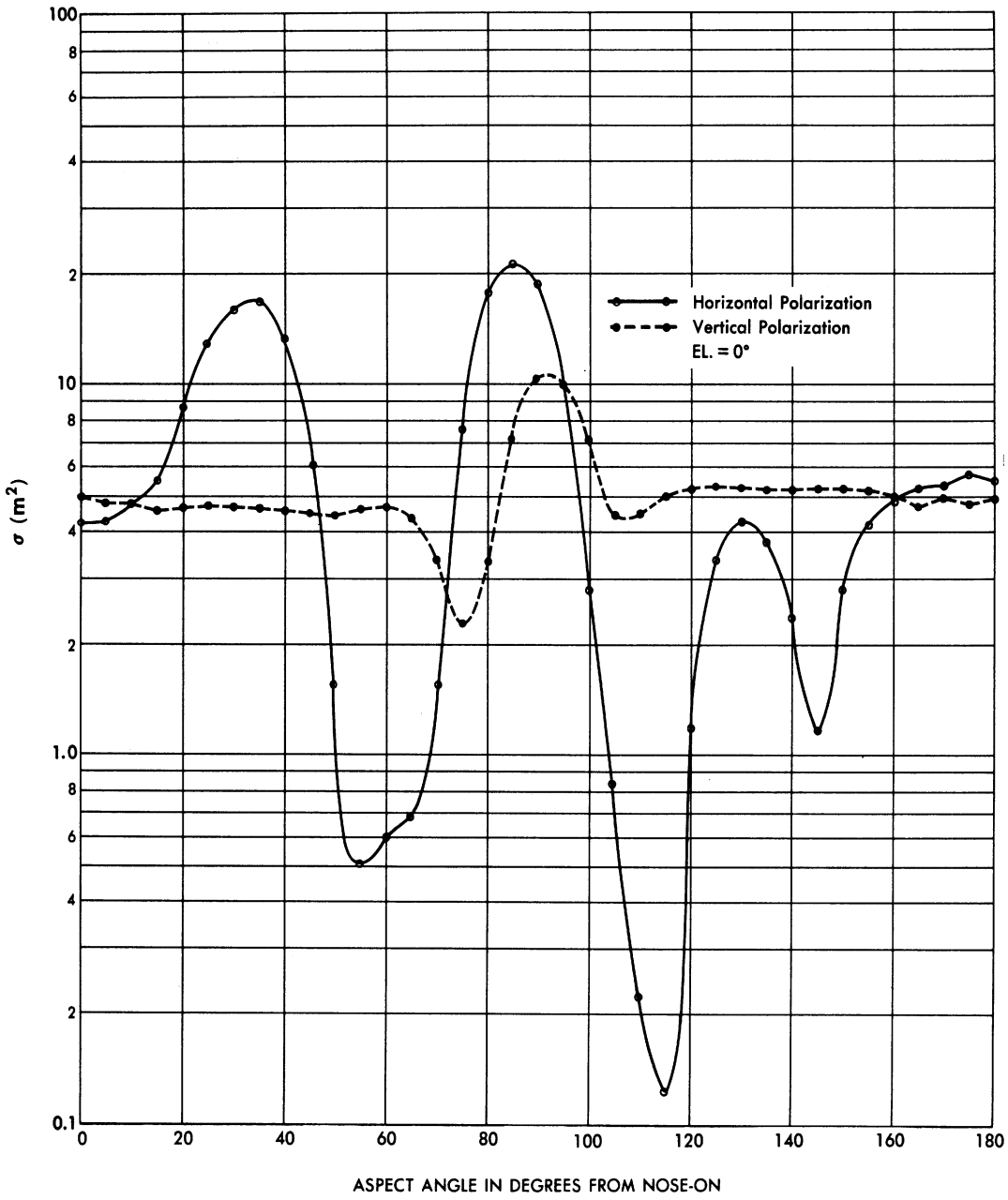

FIG. 5.4.3-2 CROSS-SECTION OF WAC MISSILE AT 100 MC (O.S.U.)

5.4.4 - 300 Mc Data

The OSU 300 Mc data (Ref. 44) are displayed in Figures 5.4.4-1 and 5.4.4-2. The manner of presentation is as used before.

The experiments were conducted at a frequency of 9000 Mc on 1/30 scale models.

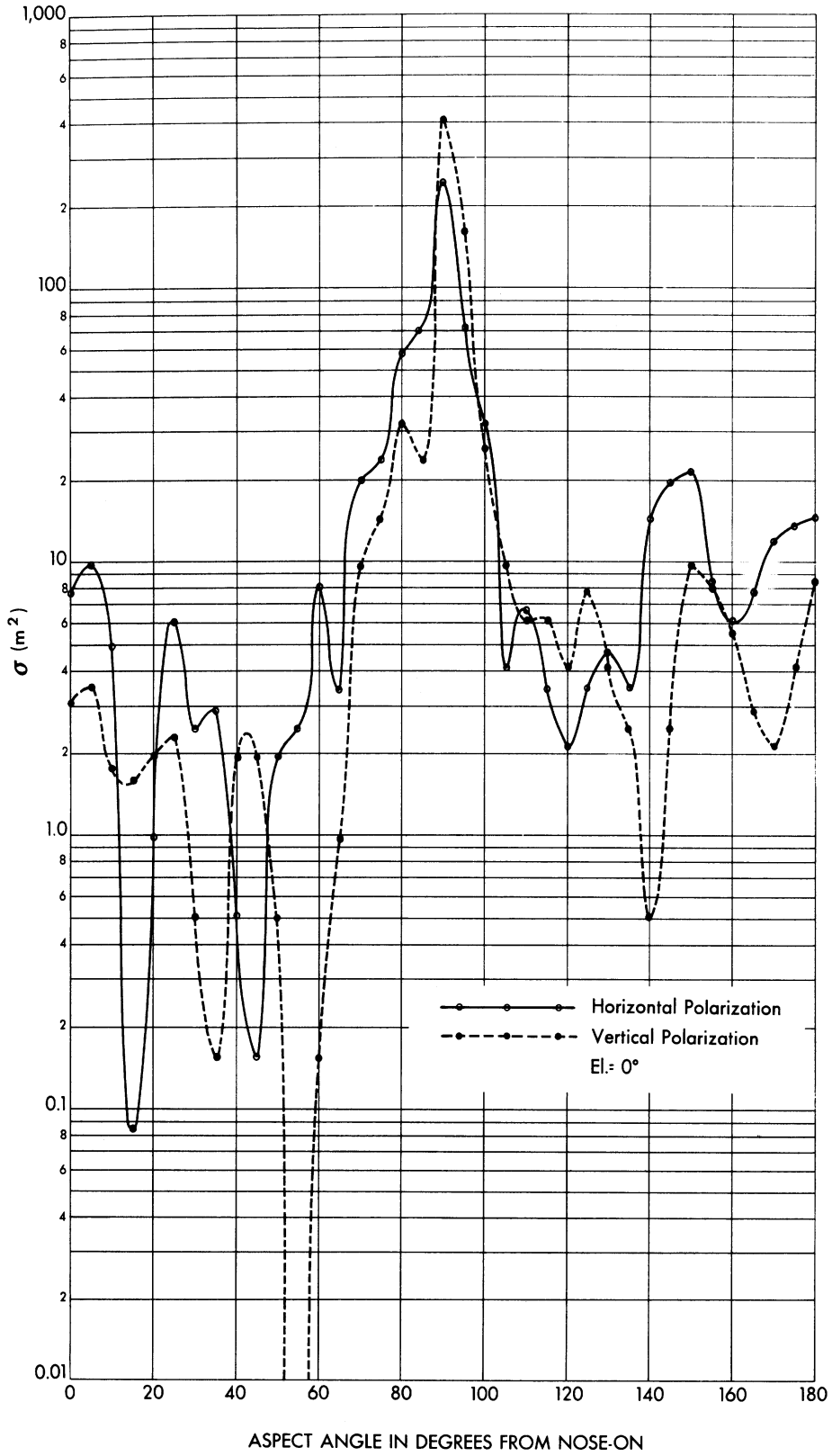

FIG. 5.4.4-1 CROSS-SECTION OF A V-2 TYPE MISSILE AT 300 MC (O.S.U.)

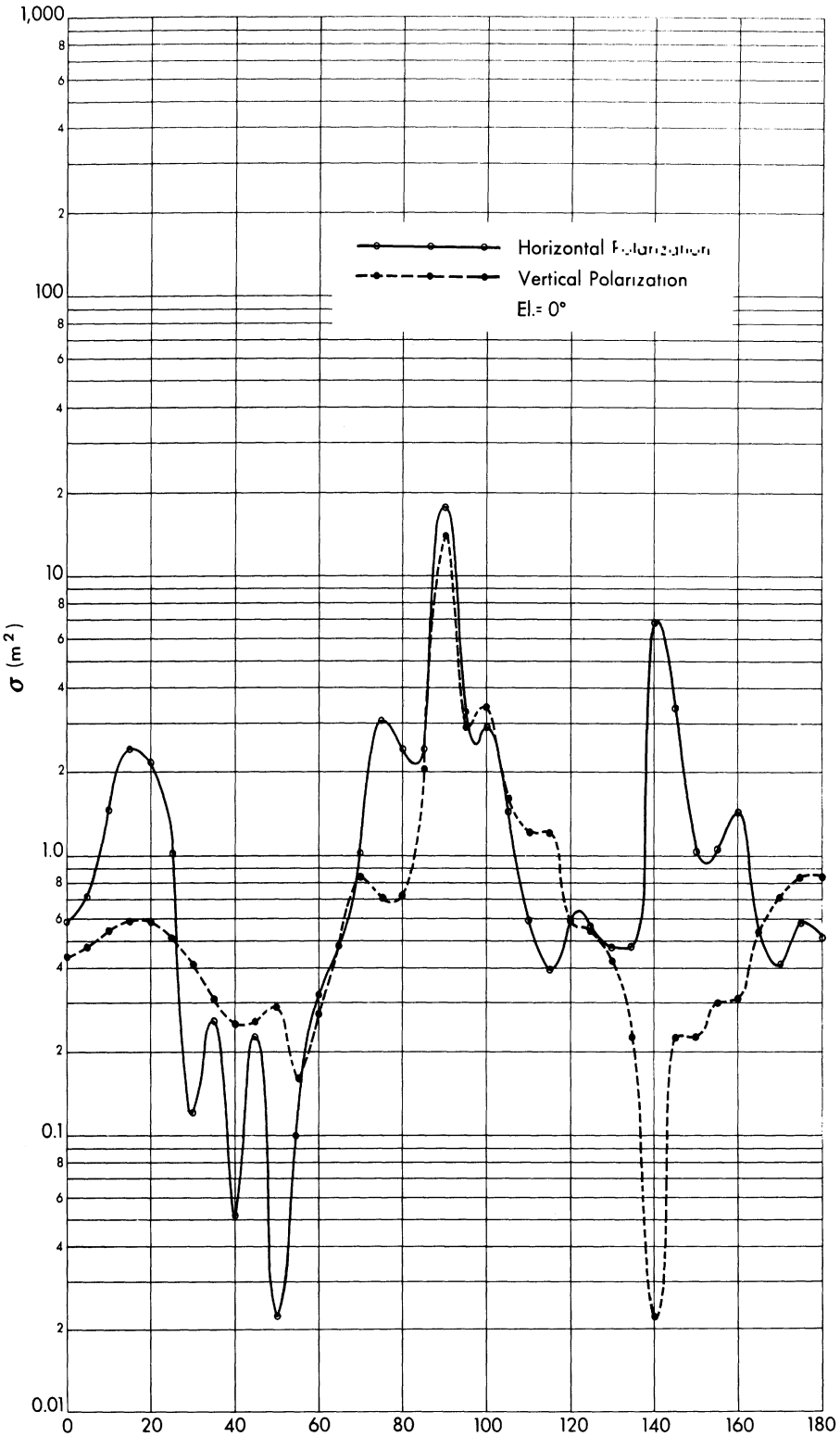

FIG. 5.4.4-2 CROSS-SECTION OF WAC MISSILE AT 300 MC (O.S.U.)

5.4.5 - 600 Mc Data

The 600 Mc data obtained by OSU (Ref. 45) appear in Figures 5.4.5-1 and 5.4.5-2. The content of these figures is the same (except for wavelength) as those used in the preceding sections.

The experiments were conducted at a frequency of 9000 Mc on 1/15 scale models.

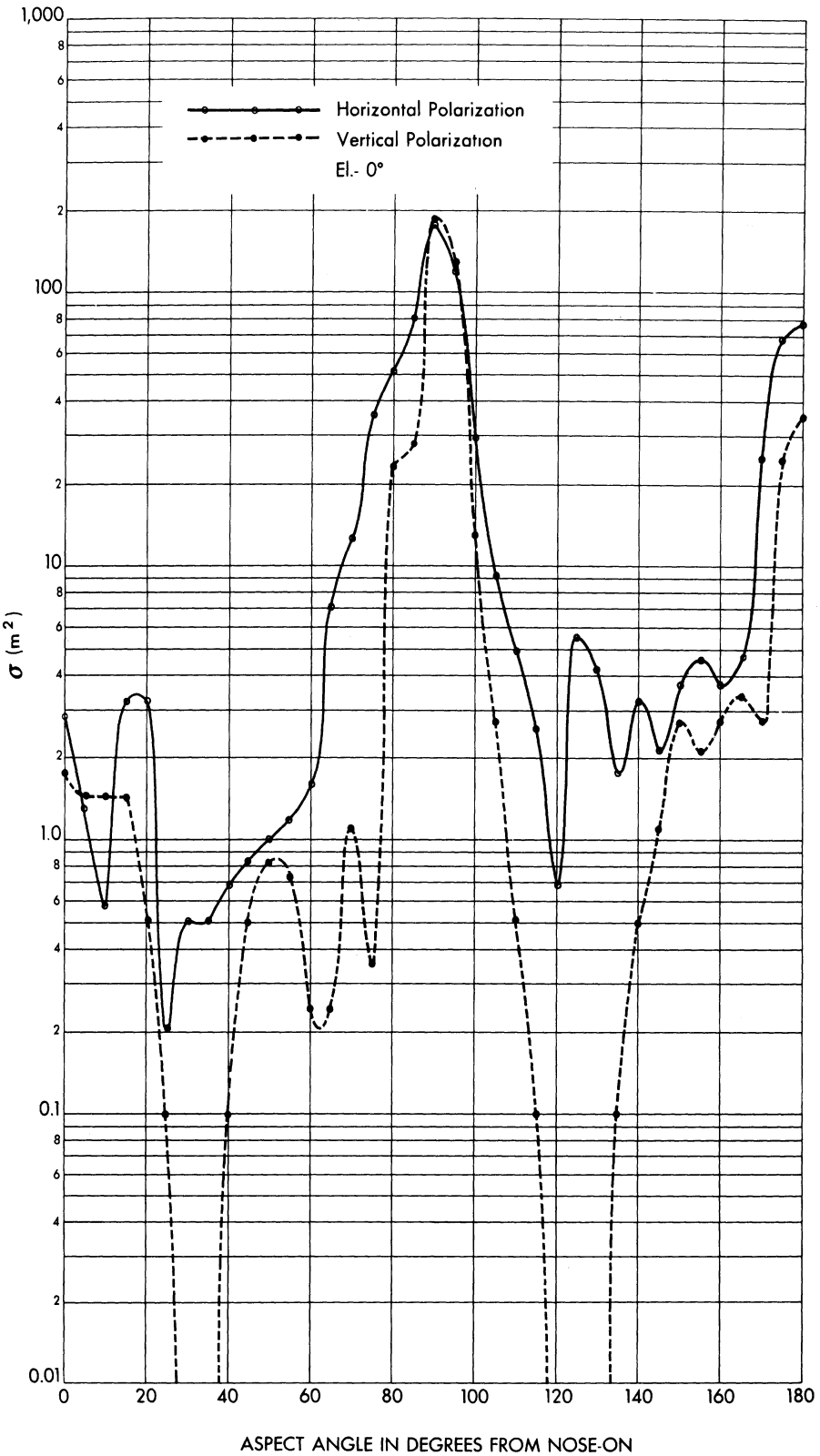

FIG. 5.4.5-1 CROSS-SECTION OF A V-2 TYPE MISSILE AT 600 MC (O.S.U.)

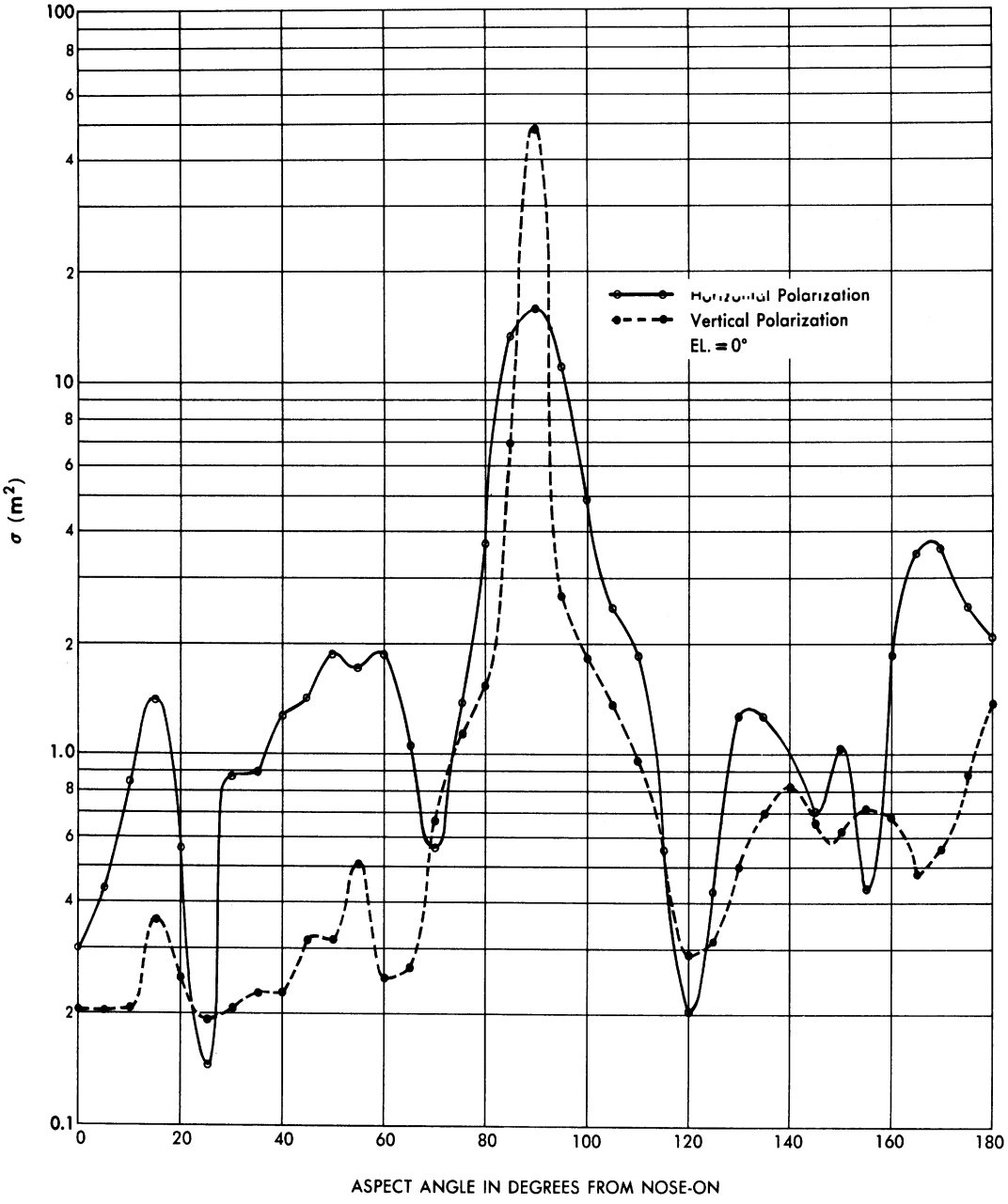

FIG. 5.4.5-2 CROSS-SECTION OF WAC MISSILE AT 600 MC (O.S.U.)

5.4.6 - 1200 Mc Data

The 1200 Mc data obtained by OSU (Ref. 46) appear in Figures 5.4.6-1 and 5.4.6-2. The content of these figures is the same, except for wavelength, as those used in the preceding section.

The experiments were conducted at a frequency of 9000 Mc on 1/7.5 scale models.

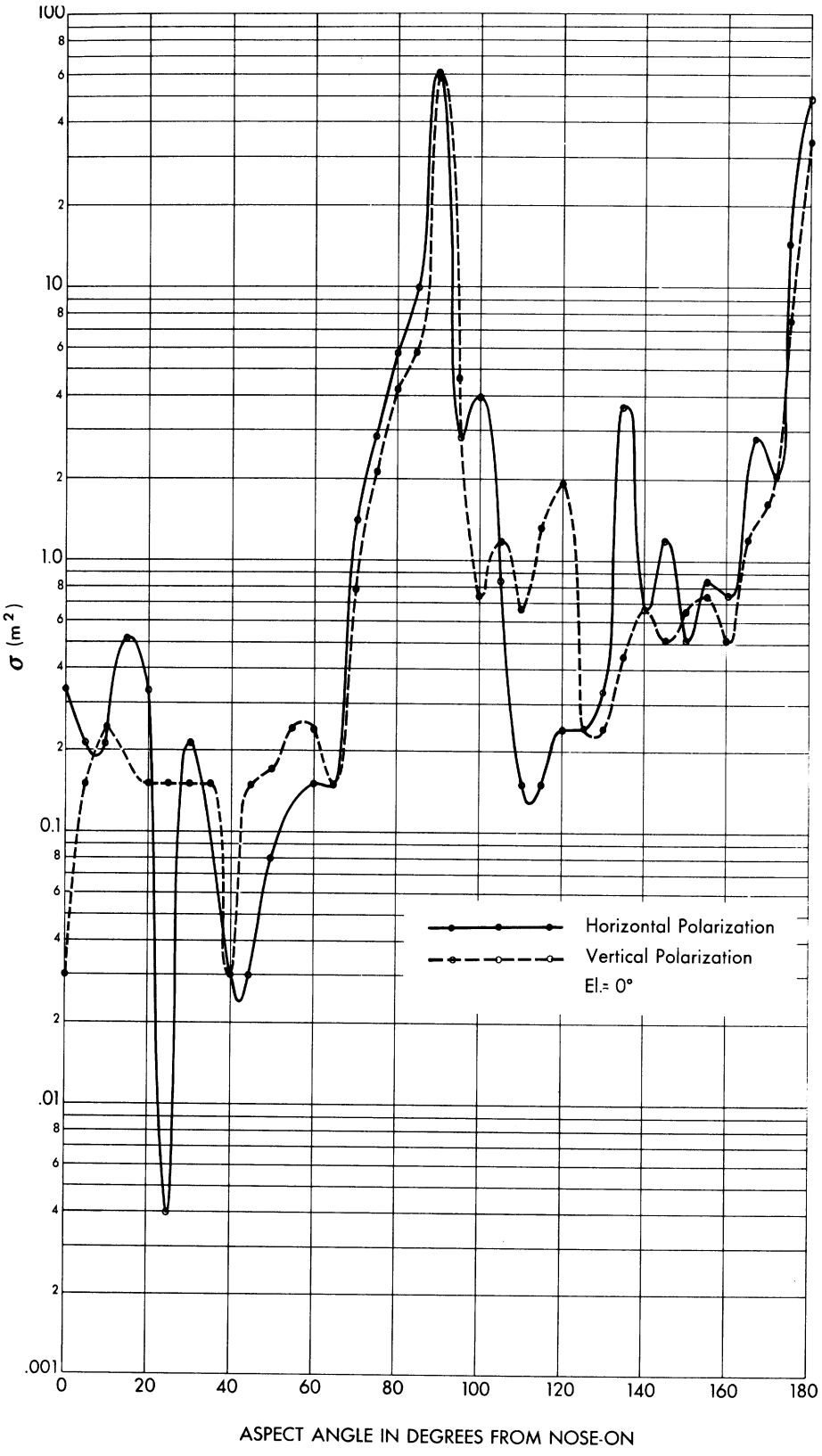

FIG. 5.4.6-1 CROSS-SECTION OF A V-2 TYPE MISSILE AT 1,200 MC (O.S.U.)

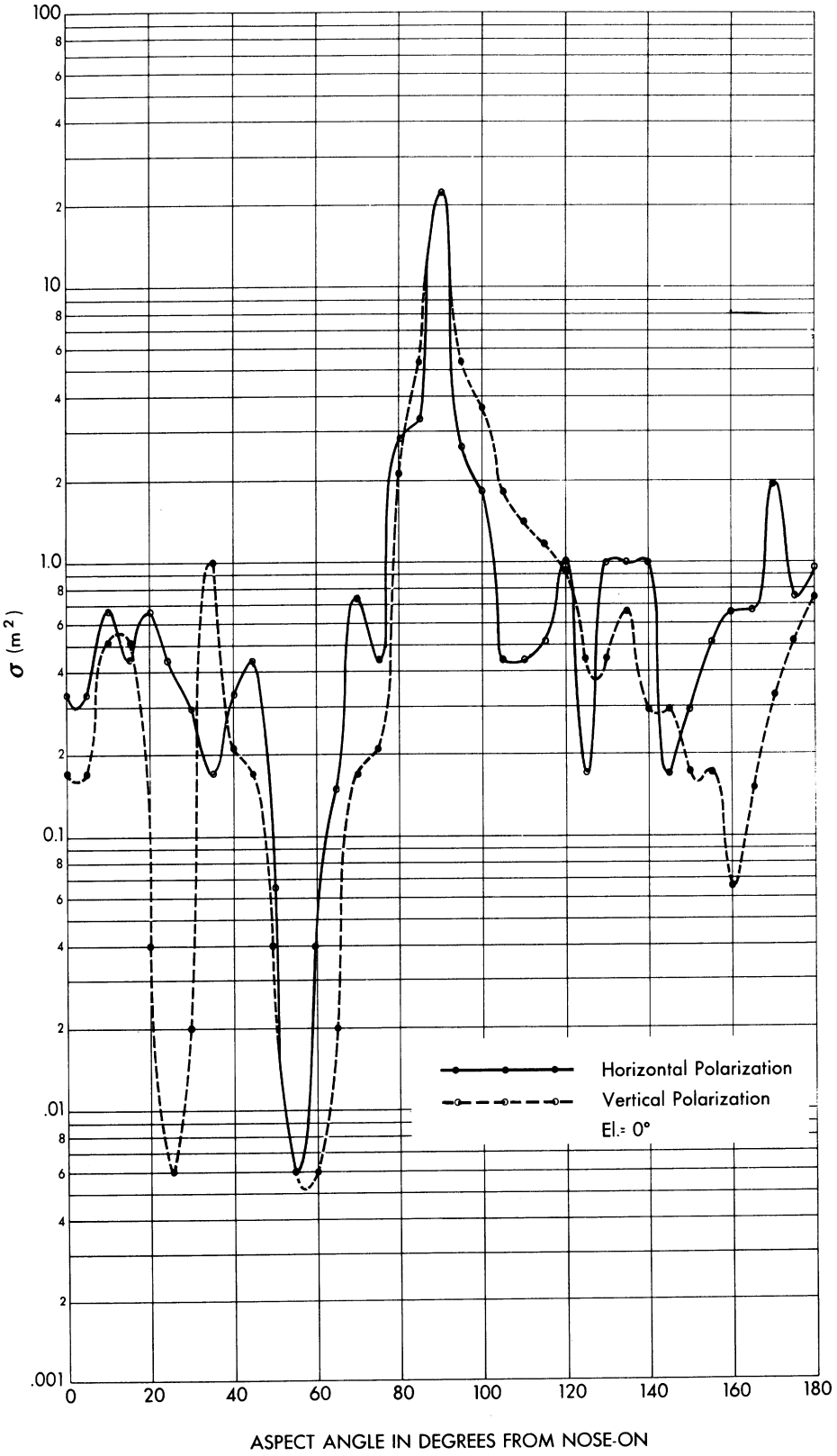

FIG. 5.4.6-2 CROSS-SECTION OF WAC MISSILE AT 1,200 MC (O.S.U.)

5.4.7 - 2900 Mc Data (WAC only)

Reference 49 contains the results obtained by the Antenna Laboratory of the Ohio State University Research Foundation on their measurements of the WAC at the "full-scale" frequency of 2900 Mc. This data are presented in Figures 5.4.7-1 and 5.4.7-2; the 0 degree and 90 degree elevation angle cases are presented.

These experiments were conducted on a 1/3.1 scale model at a model frequency of 9000 Mc.

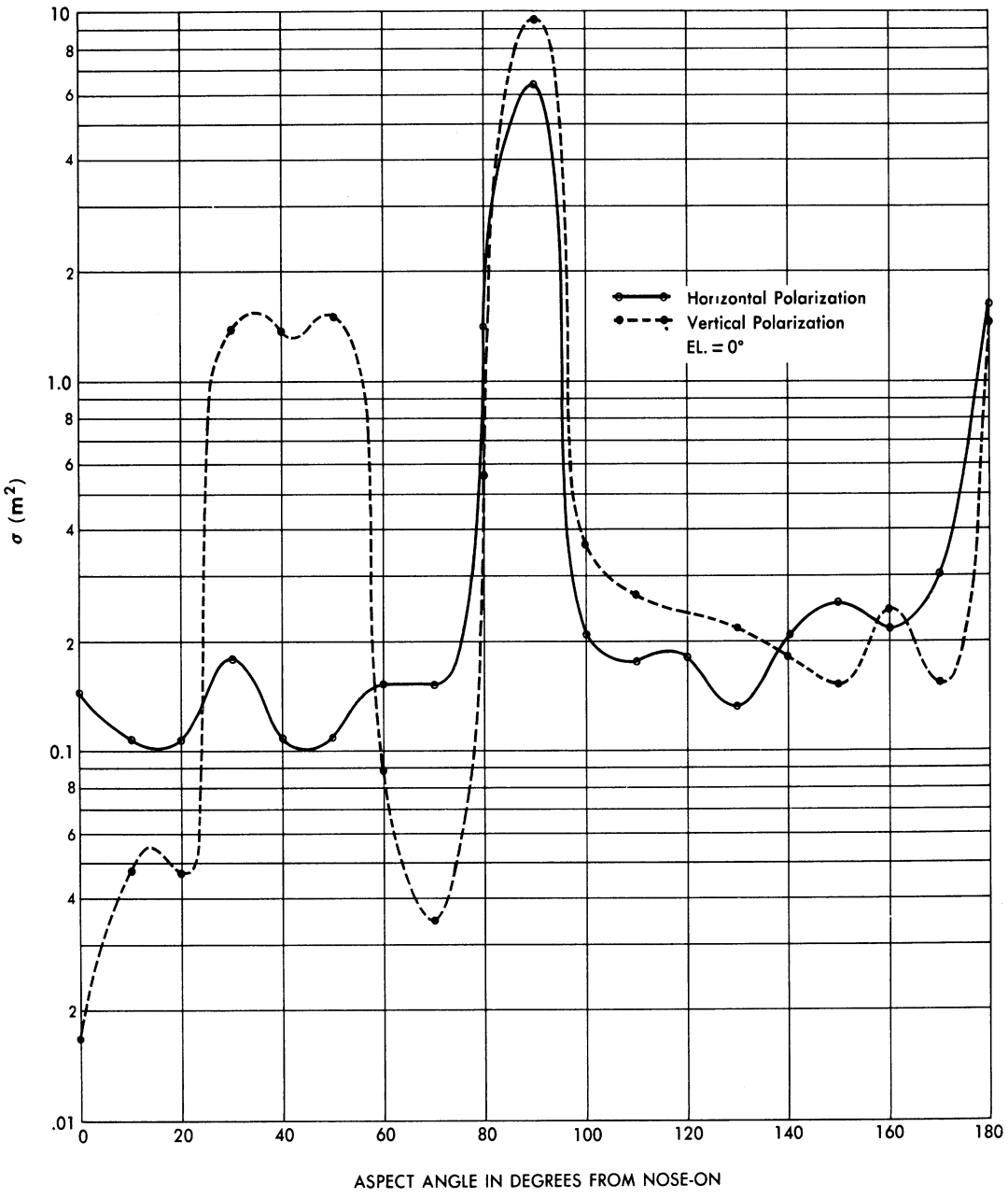

FIG. 5.4.7-1 CROSS-SECTION OF WAC MISSILE AT 2,900 MC (O.S.U.)

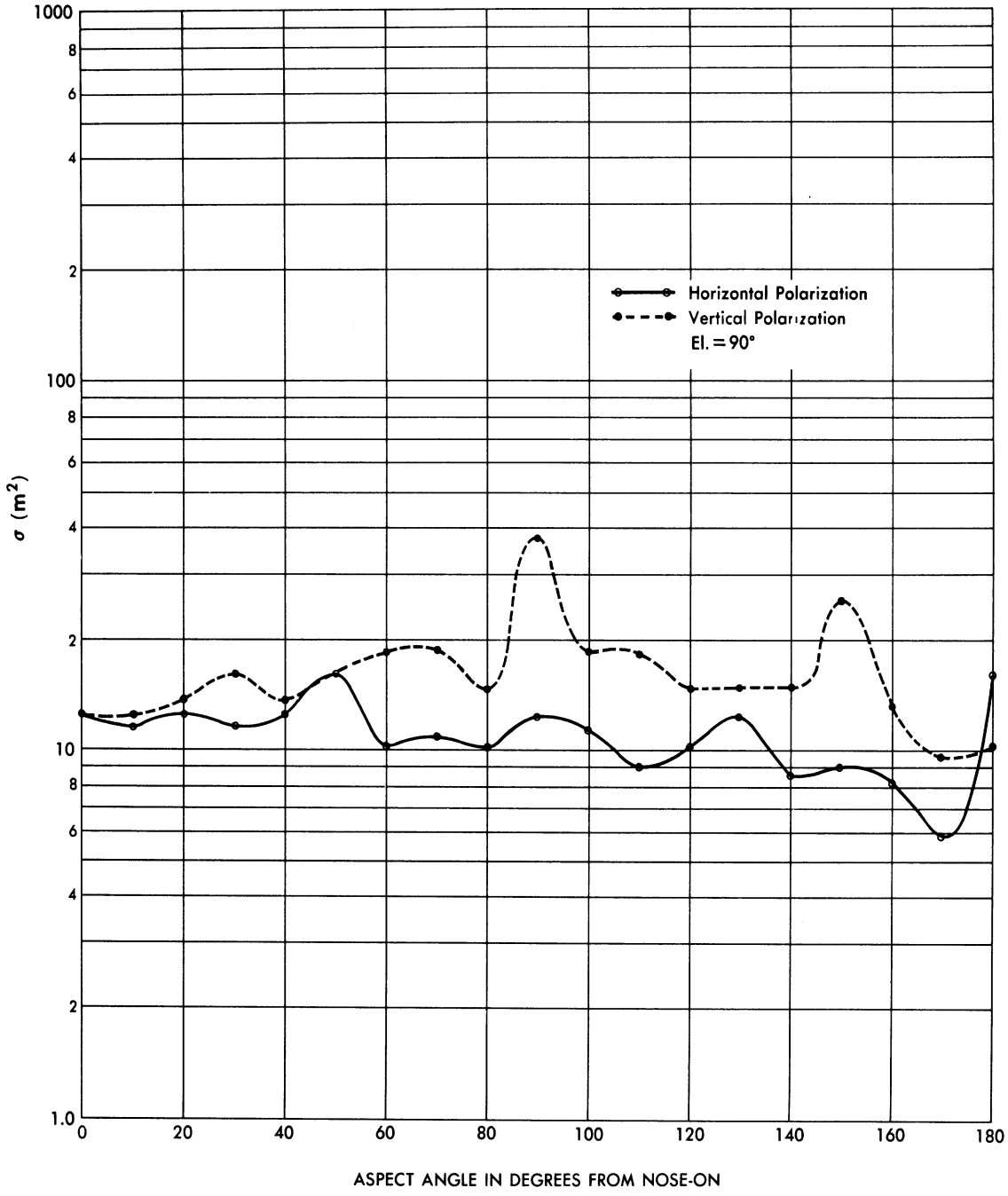

FIG. 5.4.7-2 CROSS-SECTION OF WAC MISSILE AT 2,900 MC (O.S.U.)

5.4.8 - 400 and 600 Mc Measurement on the UMA-1

In May 1950 Ohio State University made some static cross-section measurement on WRRC models of the UMA-1 missile. These models (similar to a V-2) had removable fins; Figure 5.4.8-1 shows the dimensions of these models with the swept back fins removed. The equipment was at X-band and the models were three feet and two feet in length. Thus the data obtained correspond to the full-scale frequencies of 400 and 621 Mc. Figures 5.4.8-2 through 5.4.8-5 show the results of these experiments. The theoretical results (see Section 7.5) are included for comparison.

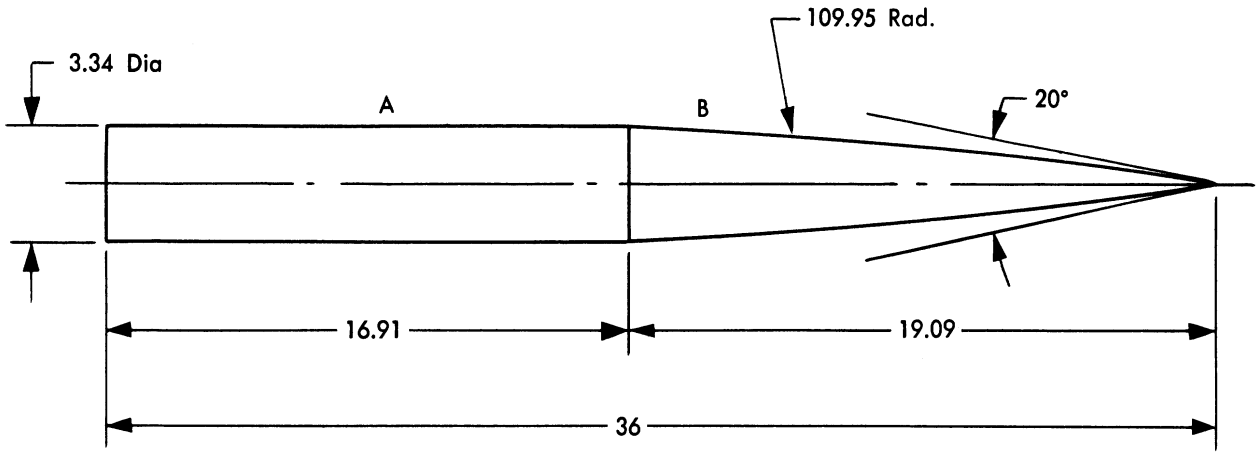

LARGE MODEL
NOTE: All dimensions are in inches.

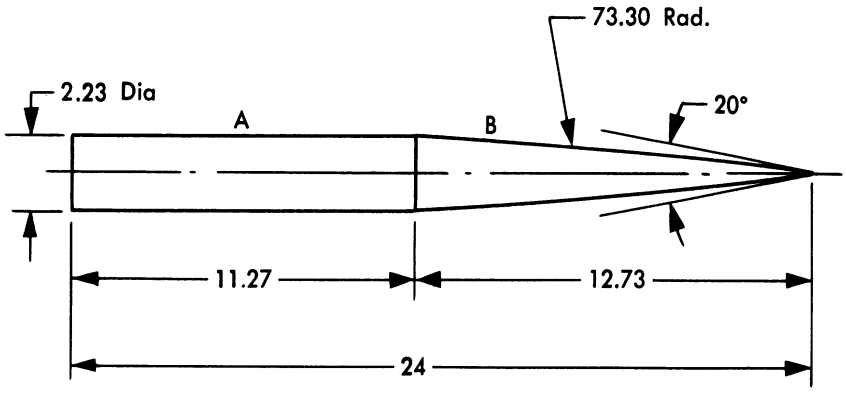

SMALL MODEL
NOTE: All dimensions are in inches.

Section "A" is a Circular Cylinder
Section "B" is an Ogive Joined Smoothly
to Section "A"

FIG. 5.4.8-1 MODELS USED IN OHIO STATE EXPERIMENTS

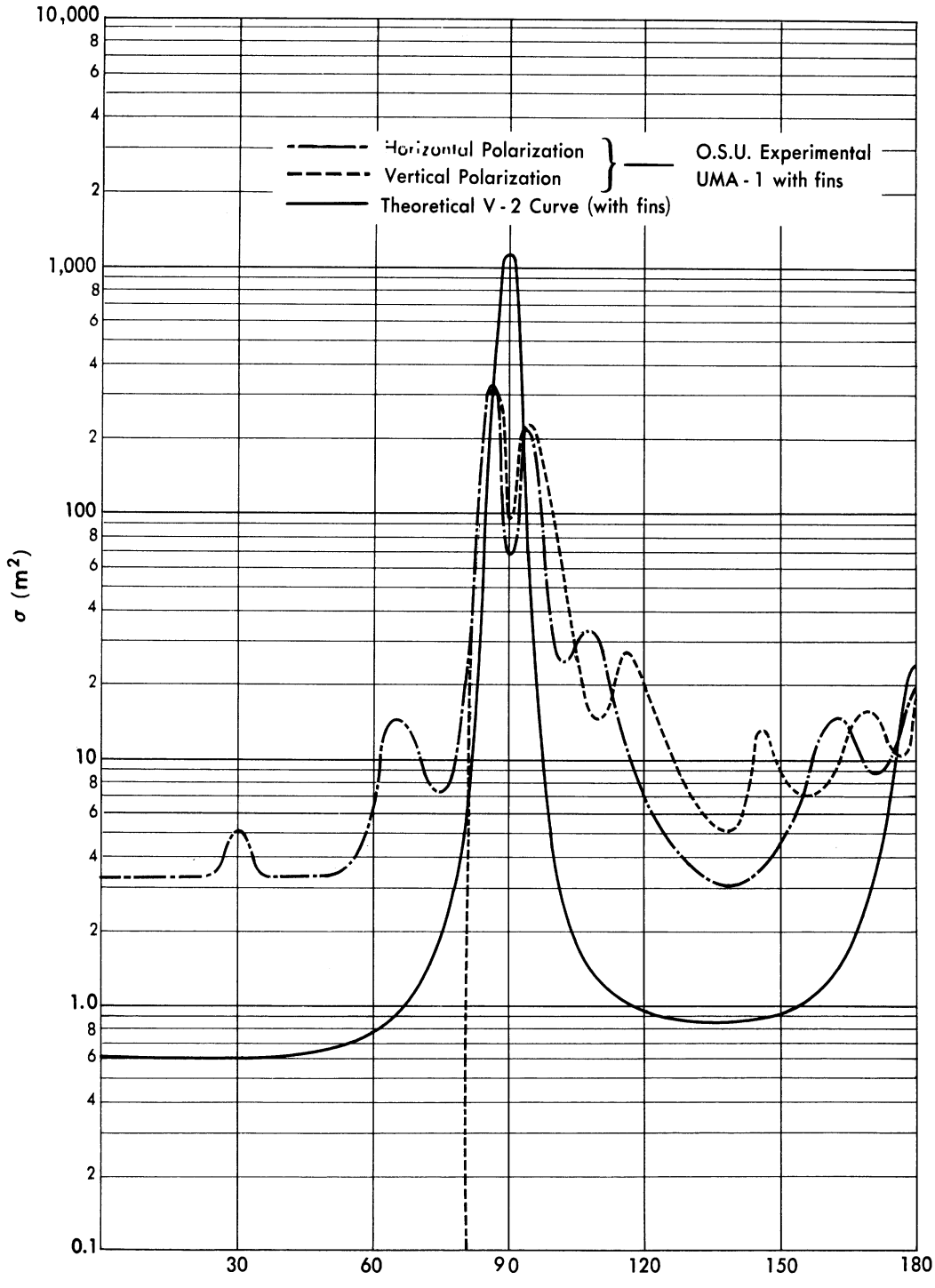

FIG. 5.4.8-2 COMPARISON BETWEEN THE THEORETICAL V-2 CROSS-SECTION AND THE EXPERIMENTAL UMA-1 CROSS-SECTION AS A FUNCTION OF ASPECT ANGLE AT ~400 MC/S-I

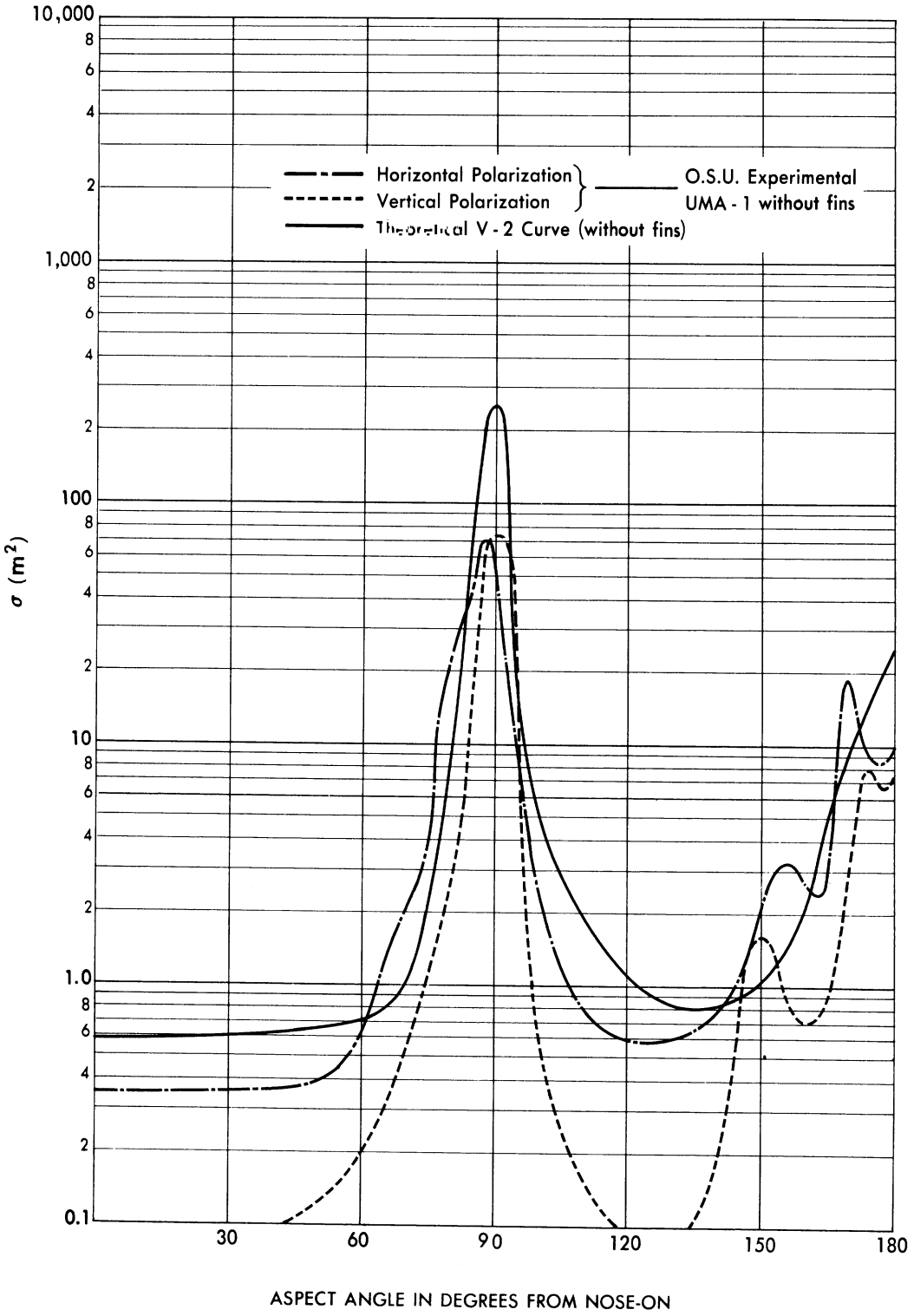

FIG. 5.4.8-3 COMPARISON BETWEEN THE THEORETICAL V-2 CROSS-SECTION AND THE EXPERIMENTAL UMA-1 CROSS-SECTION AS A FUNCTION OF ASPECT ANGLE AT ~400 MC/S - II

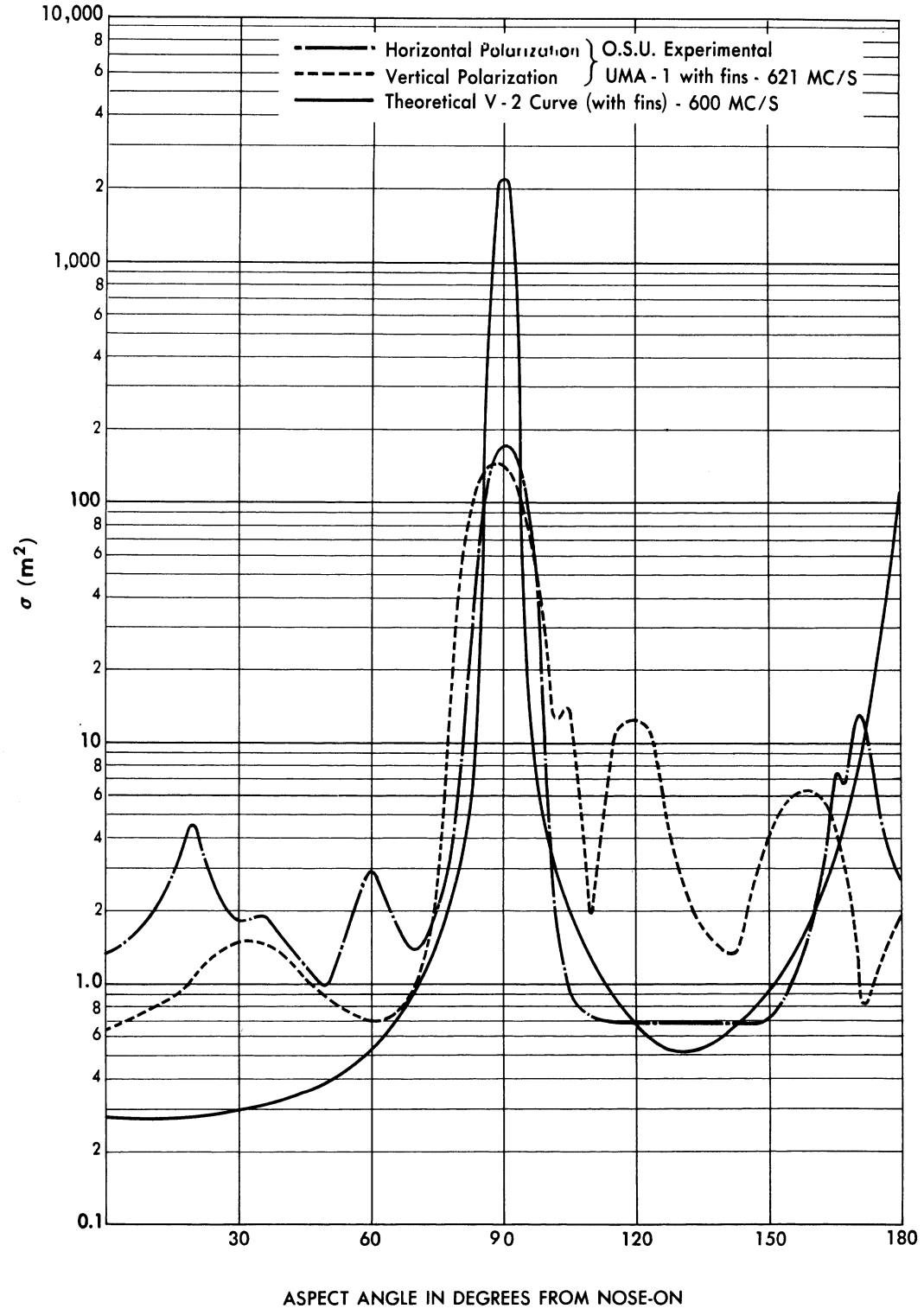

FIG. 5.4.8-4 COMPARISON BETWEEN THE THEORETICAL V-2 CROSS-SECTION AND THE EXPERIMENTAL UMA-1 CROSS-SECTION AS A FUNCTION OF ASPECT ANGLE AT ~ 600 MC/S - 1

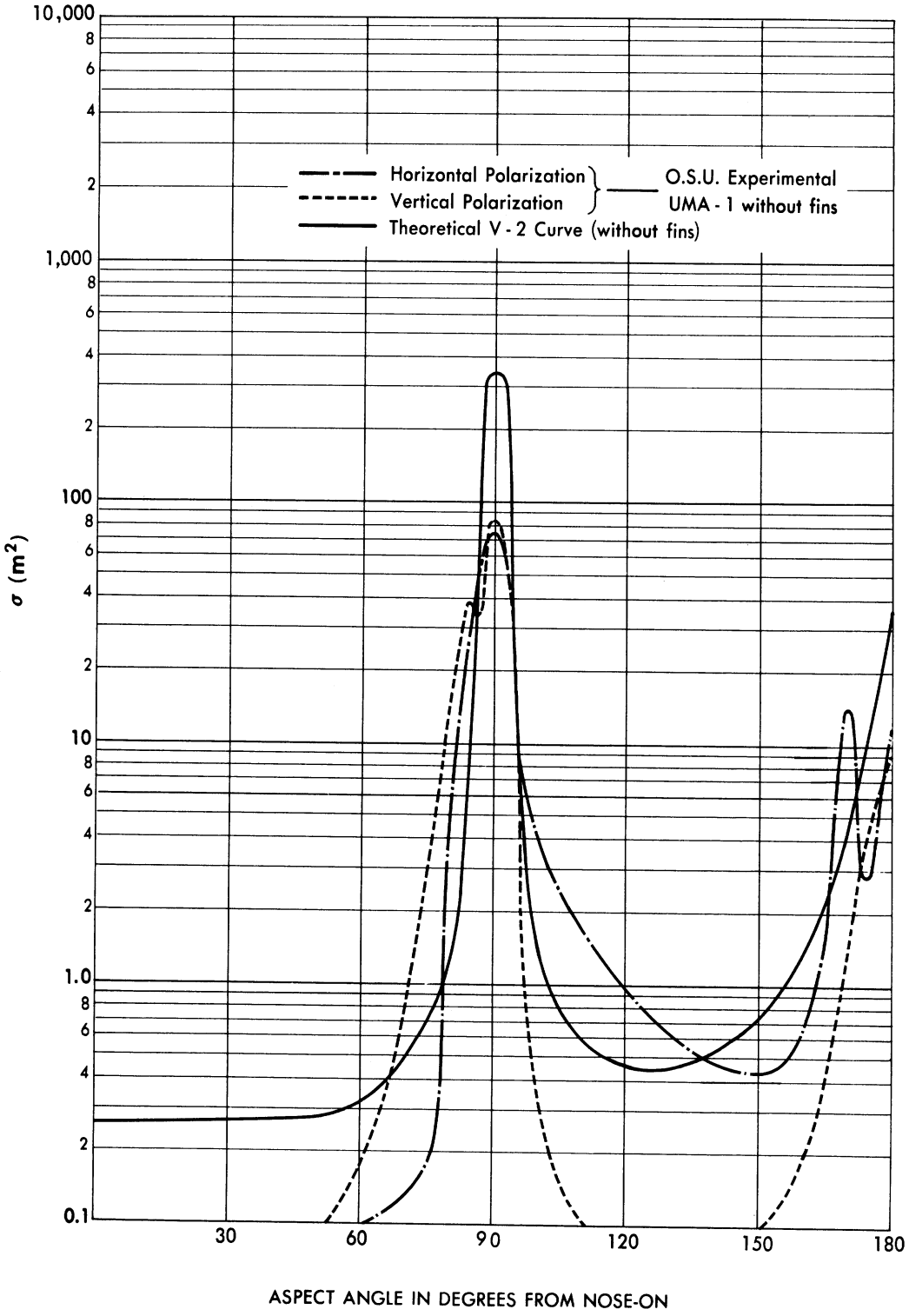

FIG. 5.4.8-5 COMPARISON BETWEEN THE THEORETICAL V-2 CROSS-SECTION AND THE EXPERIMENTAL UMA-1 CROSS-SECTION AS A FUNCTION OF ASPECT ANGLE AT ~ 600 MC/S - II

5.4.9 Bistatic Measurements

Ohio State University conducted some measurements of the echo characteristics of V-2 type missiles for transmitter and receiver at separate locations (Ref. 47). (Such operation is called bistatic.) The full scale frequencies involved were at 20, 50, 100, 300, 600, 1200, and 2900 Mc. As in their other tests, measurements were made for elevation angles of 0, 15, 30, 45, 60, 75, and 90 degrees. Two bistatic cases were investigated: one in which the transmitter and receiver were separated by 30 degrees and the other in which the angular separation was 45 degrees (the 45 degree separation was used for 20 through 100 Mc cases and the 30 degree separation in the 300 through 2900 Mc cases).

Table 5-2 indicates the manner in which the reciprocity rule* held in these experiments. It is felt that this serves as a good measure of the accuracy of the experiment, and in only one instance does the reciprocity rule fail to hold to within an order of magnitude.

Only the 0 degree elevation cases are presented in the figures of this section. In Figures 5.4.9-1 through 5.4.9-7, the cross-section is plotted as a function of the azimuth angle to the receiver; thus, the transmitter is located either 30 or 45 degrees from the plotted azimuth angle.

*This rule states that for smooth finite surfaces, the effective radar cross-section remains the same if the transmitter and receiver are interchanged (Ref. 57).

TABLE 5-2

Missile	Frequency (Mc)	Polarization	Angle between Transmitter & Receiver	Radar Cross-Section in Square Meters	
				Receiver nose-on	Transmitter nose-on
V-2	20	Horizontal	45^0	0.38	7.0
V-2	20	Vertical	45^0	5.0	4.6
V-2	50	Horizontal	45^0	3.0	3.6
V-2	50	Vertical	45^0	15.0	13.
V-2	100	Horizontal	45^0	.12	.21
V-2	100	Vertical	45^0	.041	.10
V-2	300	Horizontal	30^0	2.4	2.1
V-2	300	Vertical	30^0	2.9	1.8
V-2	600	Horizontal	30^0	0.94	1.0
V-2	600	Vertical	30^0	0.51	0.15
WAC	1200	Horizontal	30^0	0.031	.0092
WAC	1200	Vertical	30^0	0.11	.33
WAC	2900	Horizontal	30^0	.10	.065
WAC	2900	Vertical	30^0	0.02	.02

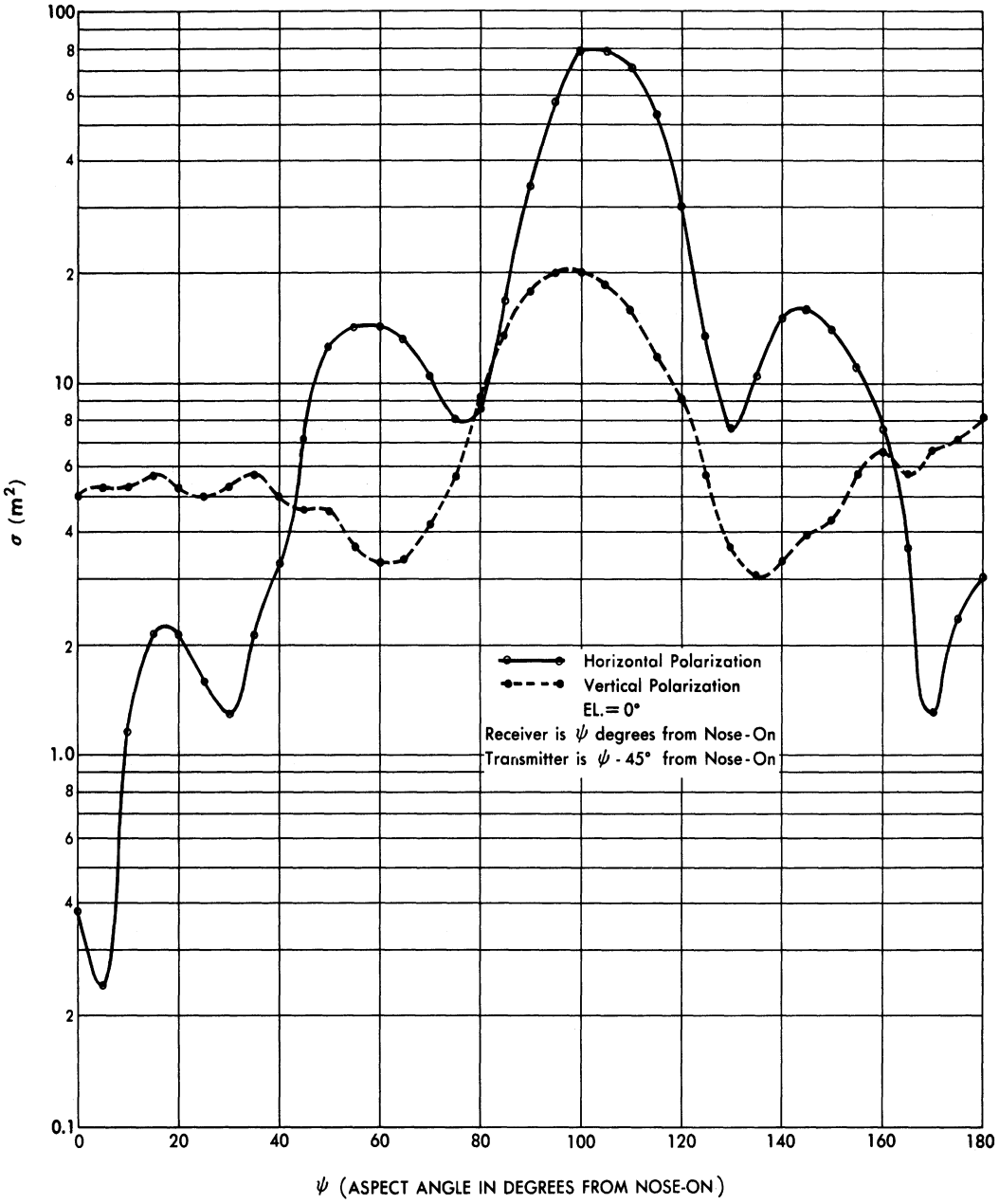

FIG. 5.4.9-1 BISTATIC CROSS-SECTION OF A V-2 AT 20 MC (O.S.U.)

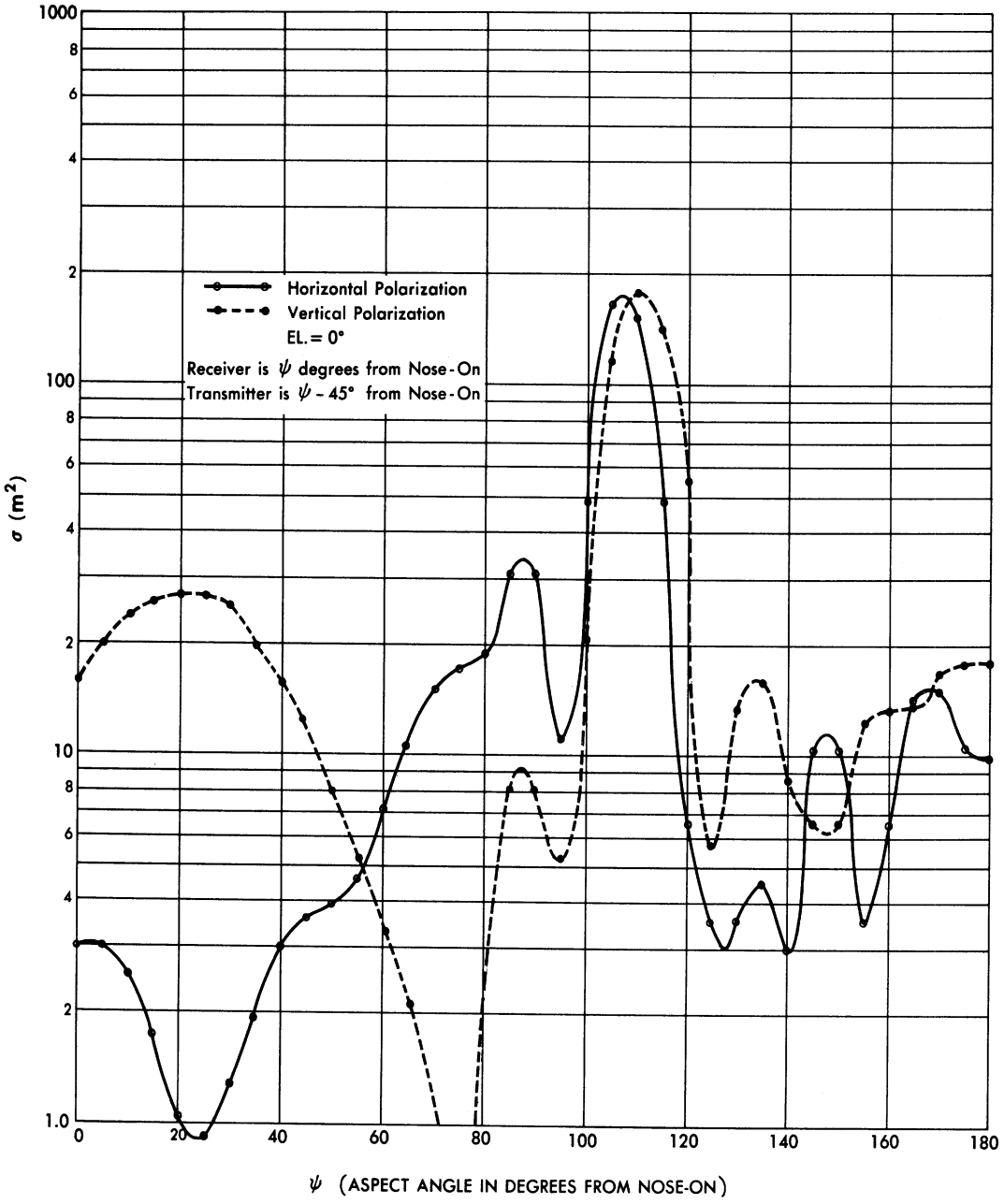

FIG. 5.4.9-2 BISTATIC CROSS-SECTION OF A V-2 AT 50 MC (O.S.U.)

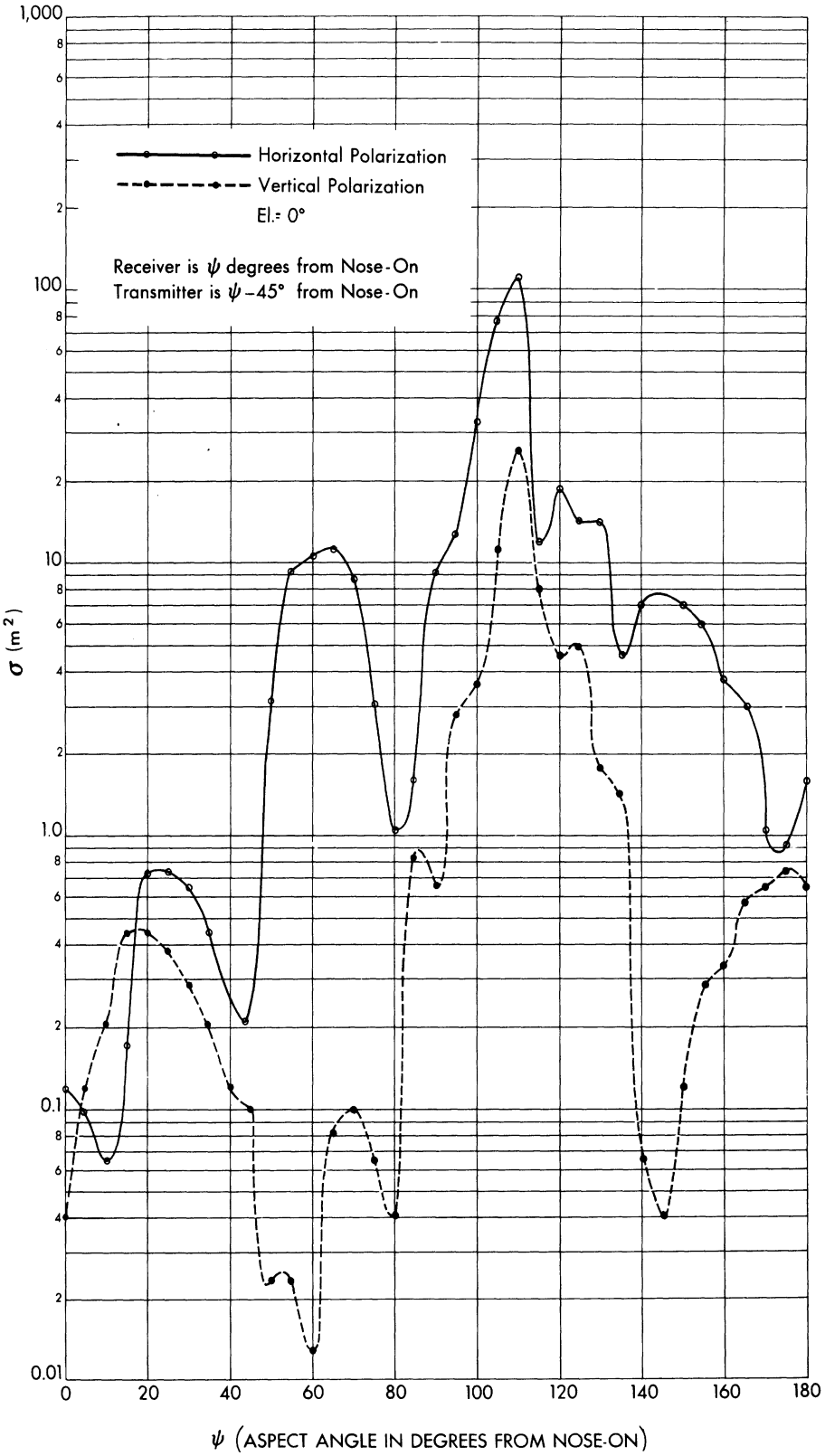

FIG. 5.4.9-3 BISTATIC CROSS-SECTION OF A V-2 AT 100 MC (O.S.U.)

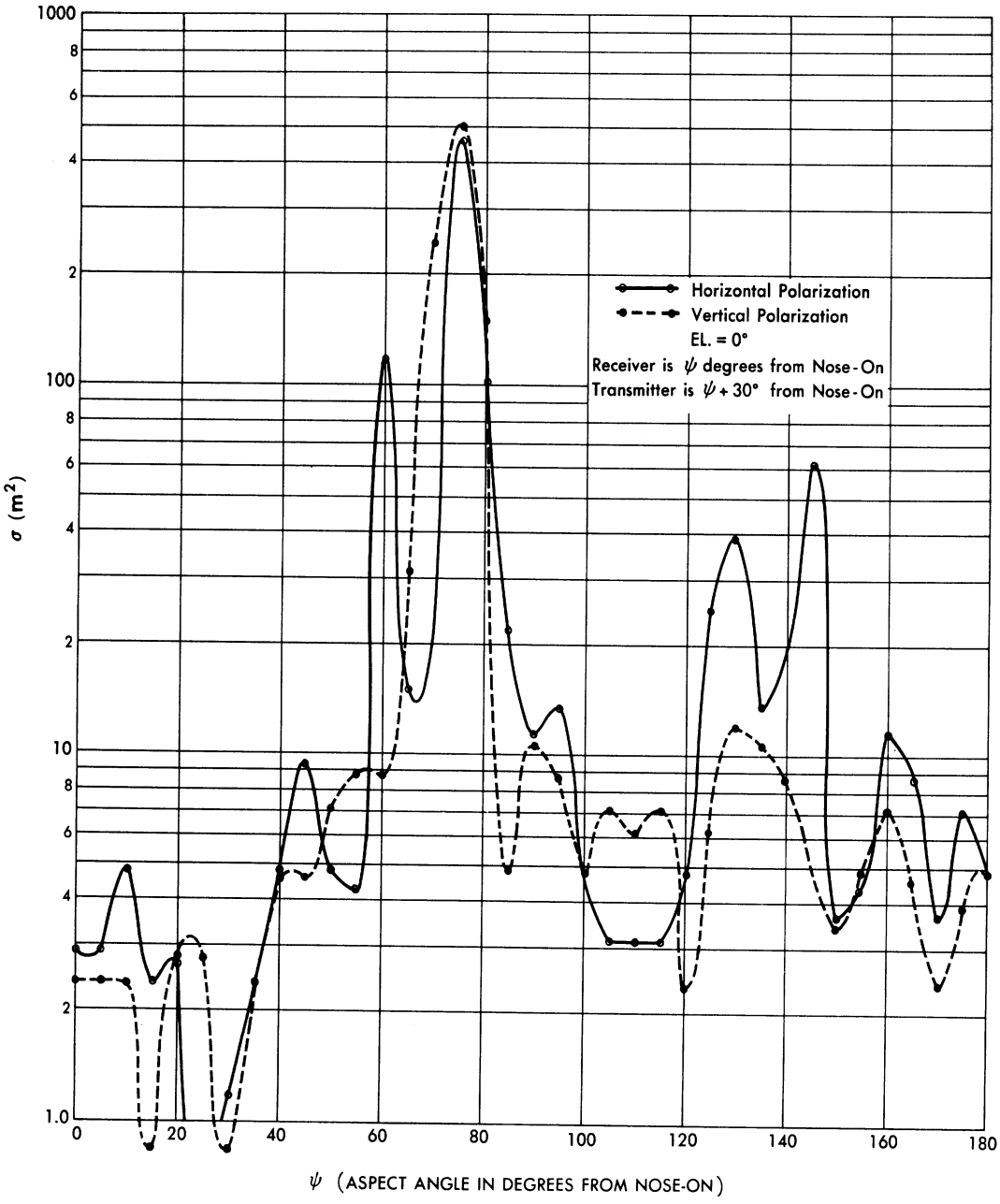

FIG. 5.4.9-4 BISTATIC CROSS-SECTION OF A V-2 AT 300 MC (O.S.U.)

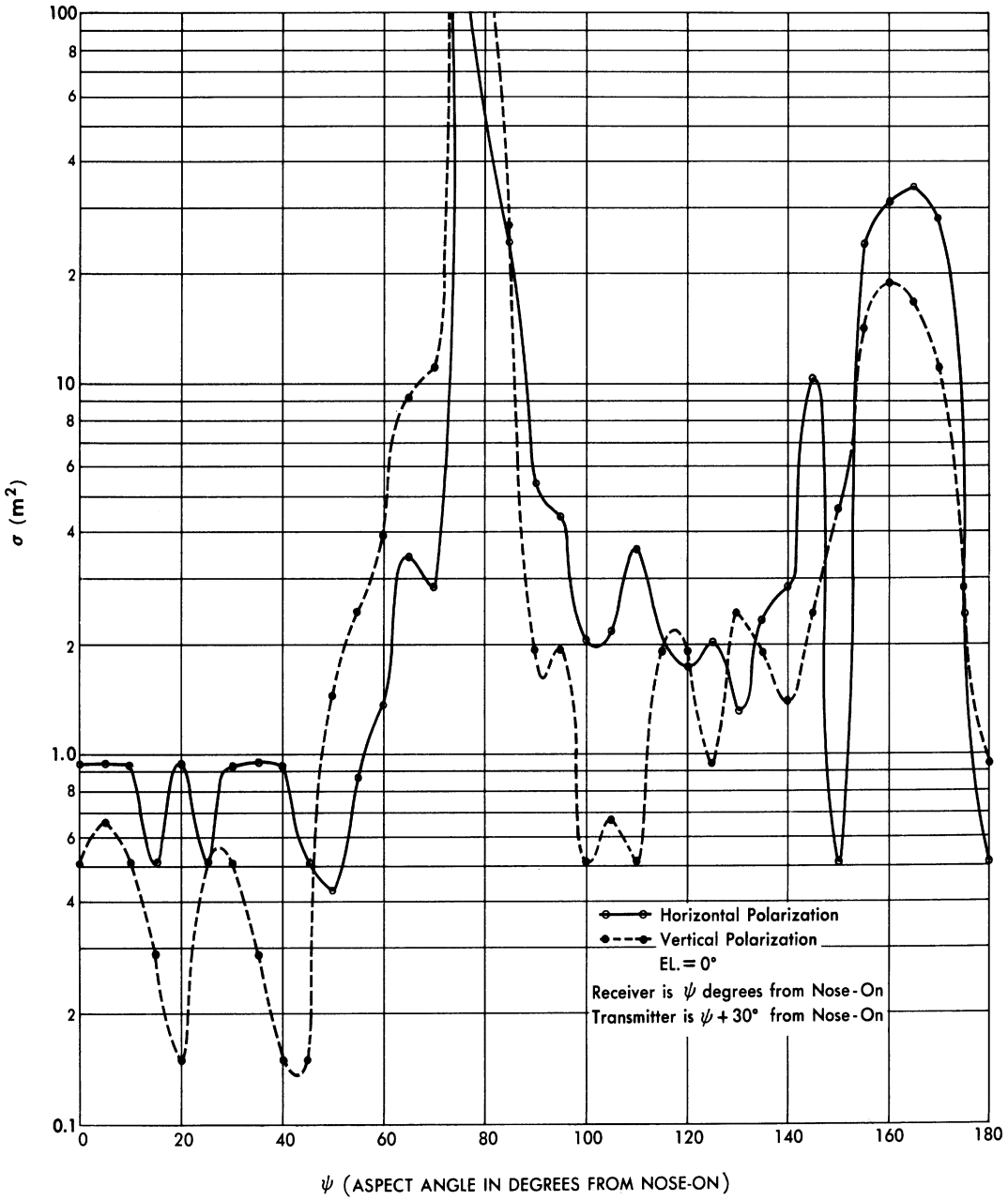

FIG. 5.4.9-5 BISTATIC CROSS-SECTION OF A V-2 AT 600 MC (O.S.U.)

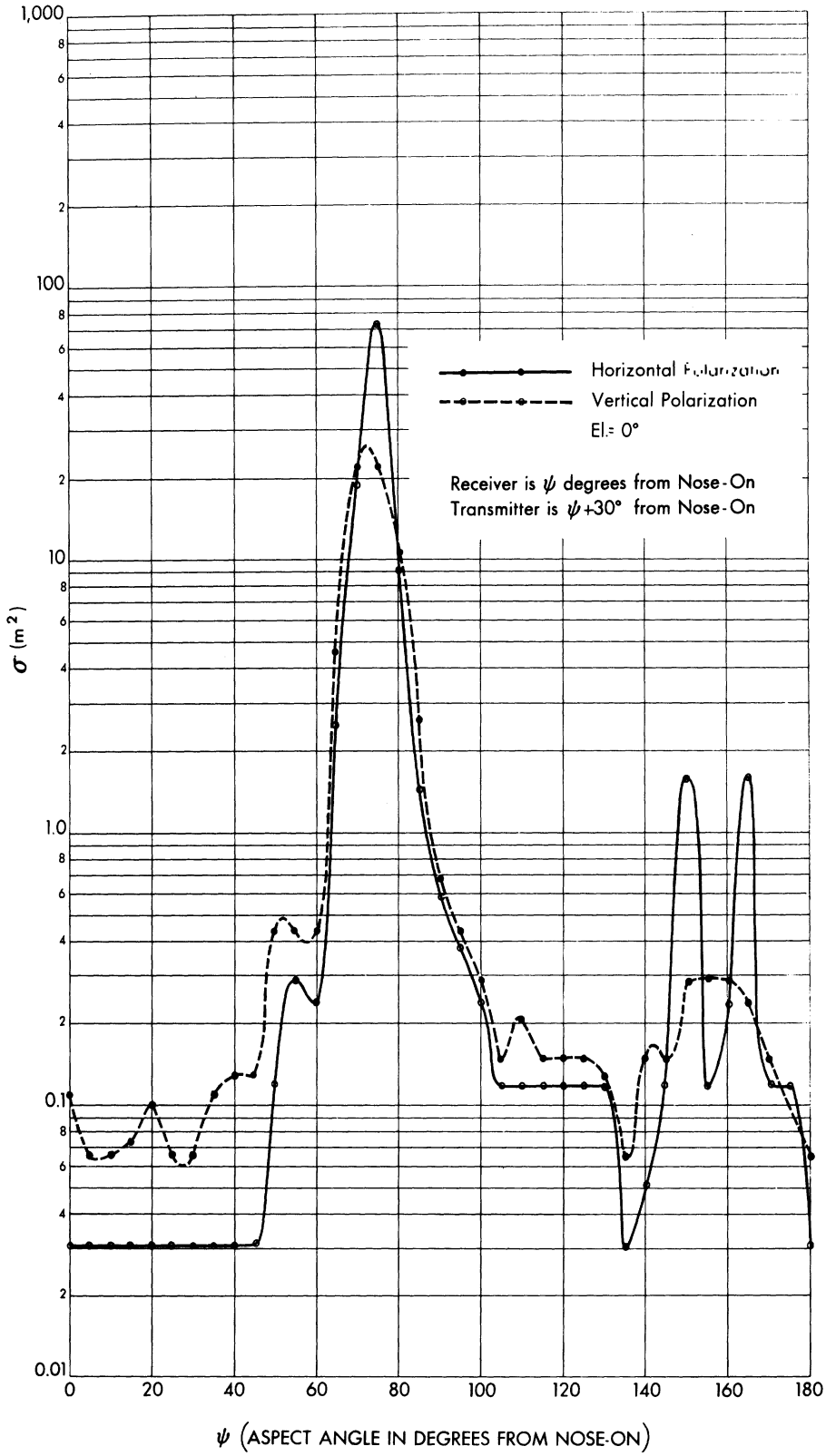

FIG. 5.4.9-6 BISTATIC CROSS-SECTION OF WAC AT 1,200 MC (O.S.U.)

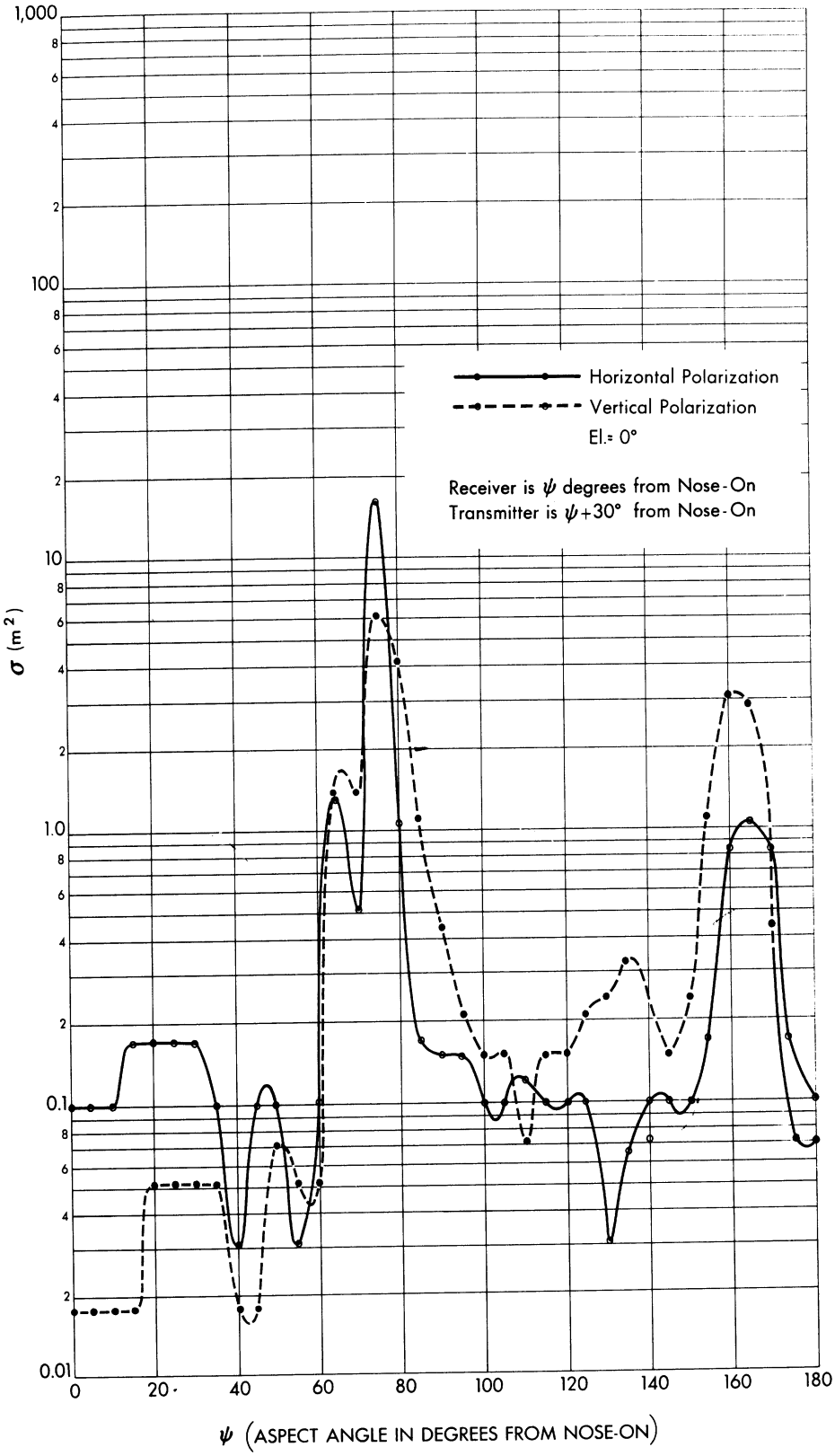

FIG. 5.4.9-7 BISTATIC CROSS-SECTION OF WAC AT 2,900 MC (O.S.U.)

5.5 V-2 Type Missiles - The Sperry Gyroscope Corporation

The Sperry Corporation conducted static tests on V-2 type missiles having a 6-to-1 length-to-diameter ratio (Ref. 50). The experiments were carried out at a wavelength of 3.2 cm on models which were 2.25, 3.6, 4.8, 6, and 12 inches long. Thus, the results scaled to full V-2 dimensions* give data on V-2 cross-sections at frequencies of approximately 40, 60, 80, 100, and 200 Mc (Figs. 5.5-1 through 5.5-6).

Sperry drew the following general conclusions from the results of their experiments (Ref. 50):

1. "For missiles up to approximately 3λ in length, the effect of fins on the back scattering of the rockets is negligible within experimental accuracy. This represents a V-2 seen at wavelengths down to 3 meters.

2. "The scattering from missiles of greater lengths than 4λ is affected markedly, particularly at aspects other than head-on, by addition of fins. In general, for aspects other than head-on, the echo from a target with fins mounted is 2 to 15 times greater than the corresponding echo from the missile without fins. Rotation of the missiles (with fins mounted) about the longitudinal axis, that is changing polarization with respect to fins, gives markedly different results at aspects other than head-on, the effect increasing with aspect. (These remarks apply to a V-2 type missile seen at wavelengths less than 2 meters.)"

A discussion of the experimental technique employed appears in Appendix 2.

*It is to be noted that these models have a length to diameter ratio different from that for a V-2.

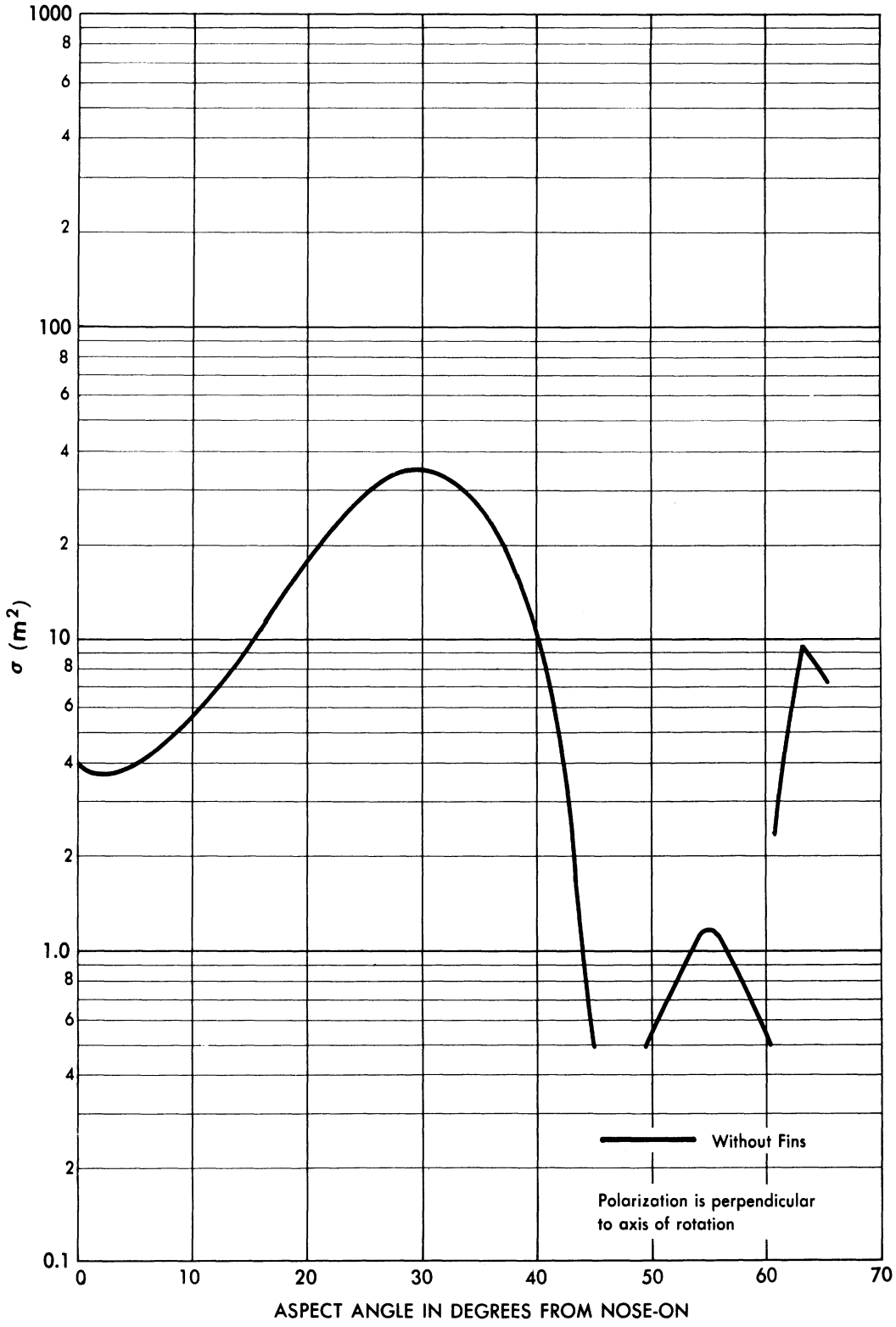

FIG. 5.5-1 CROSS-SECTION OF A V-2 TYPE MISSILE AT ~ 40 MC (SPERRY CORP.)

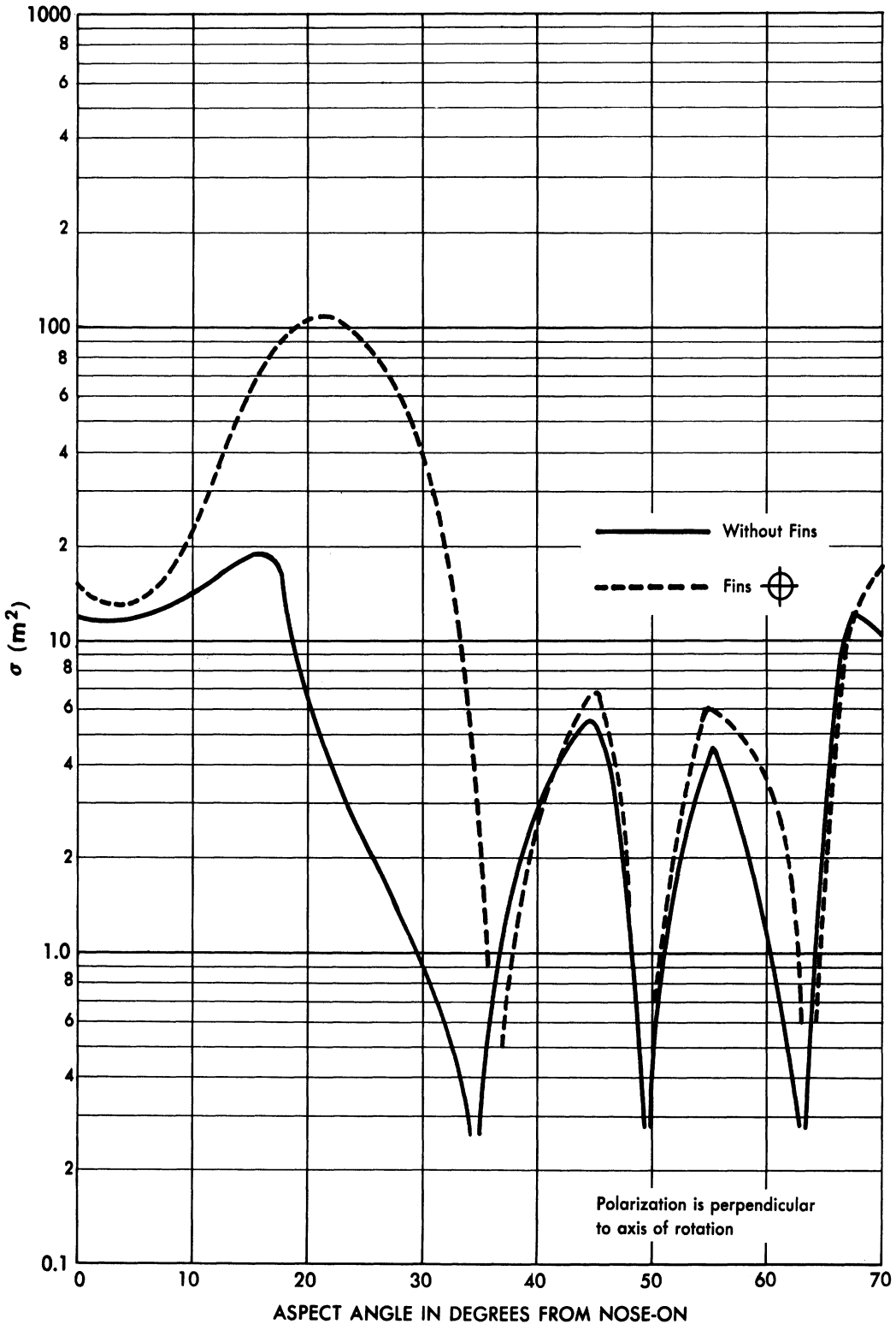

FIG. 5.5-2 CROSS-SECTION OF A V-2 TYPE MISSILE AT ~60 MC (SPERRY CORP.)

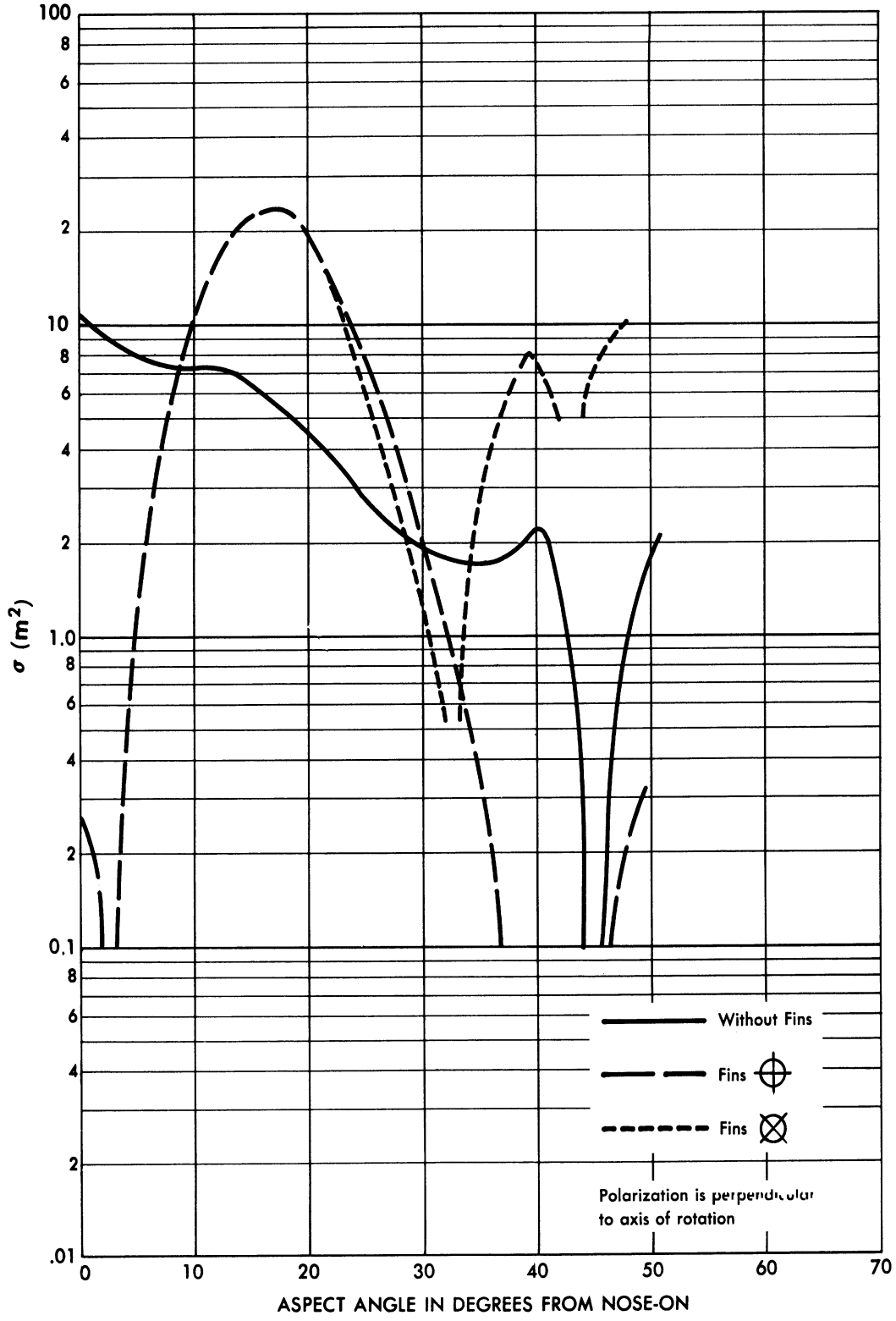

FIG. 5.5-3 CROSS-SECTION OF A V-2 TYPE MISSILE AT ~ 80 MC (SPERRY CORP.)

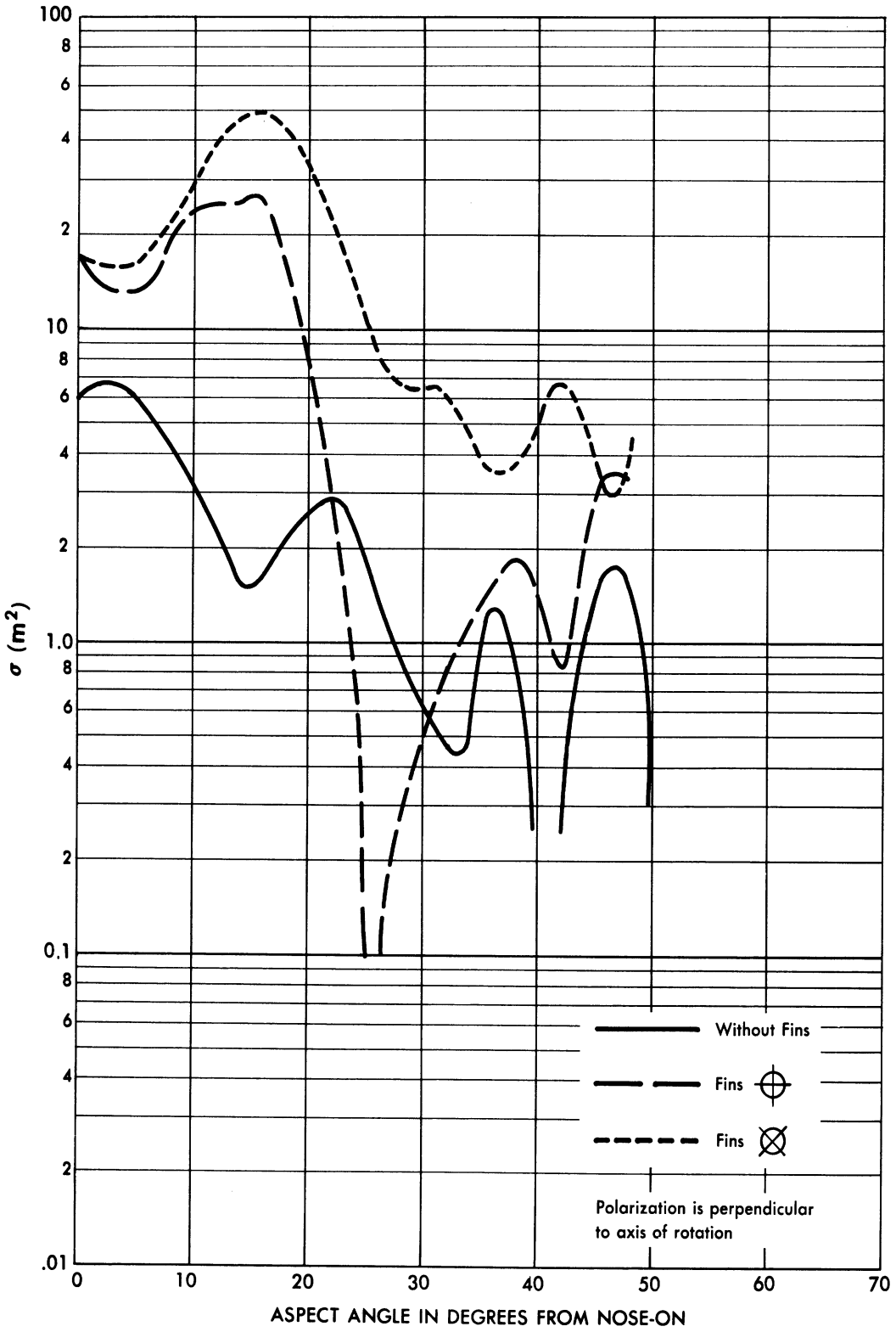

FIG. 5.5-4 CROSS-SECTION OF A V-2 TYPE MISSILE AT ~ 100 MC (SPERRY CORP.)

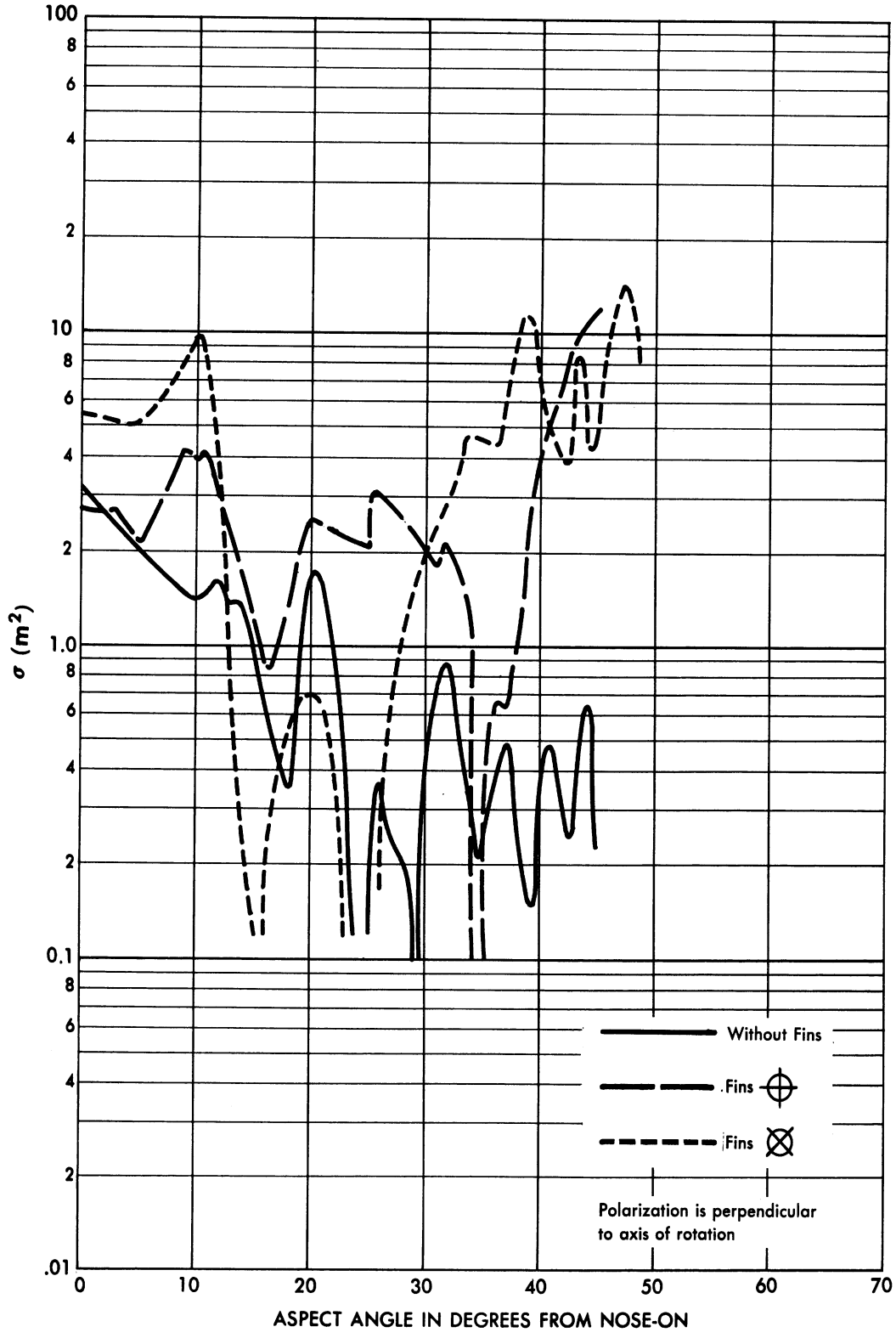

FIG. 5.5-5 CROSS-SECTION OF A V-2 TYPE MISSILE AT ~ 200 MC (SPERRY CORP.)

5.6 V-2 Type Missiles - Federal Telecommunication Laboratories, Inc.

The experiments conducted at the Federal Telecommunications Laboratories (Ref. 34) are summarized in this section in Figures 5.6-1 through 5.6-9.

The experiments resulted in data on the cross-section of a V-2 at the equivalent full-scale frequencies of 50, 100, 110, 200, 250, 300, 500, 750, and 1000 Mc for both vertical and horizontal polarizations (Figs. 5.6-1 through 5.6-9).

Figure 5.6-10 shows a plot of the cross-section of the V-2 nose-section at 2000 Mc. In the experiments the models were rotated about a vertical axis (keeping two of the fins perpendicular to the ground) for three different elevation angles, (0, 45, and 90 degrees). Only the 0 degree elevation cases are presented in the figures of this section.

These measurements were made using the radar set method (a lay-out plan of the measuring equipment is shown in Figure 5.6-11). Appendix 2 contains a description of the method employed.

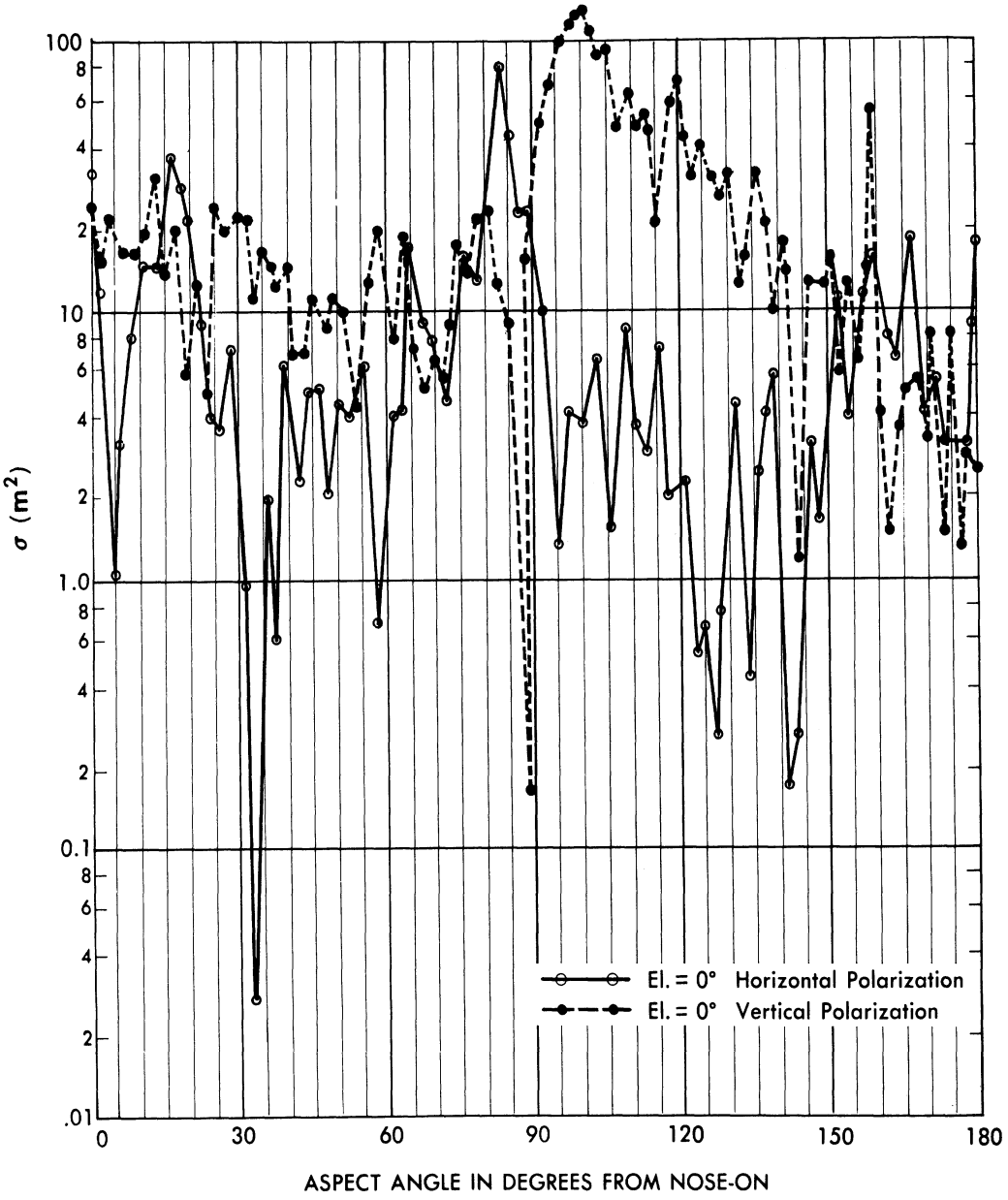

FIG. 5.6-1 CROSS-SECTION OF A V-2 AT 50 MC (FED. TEL.)

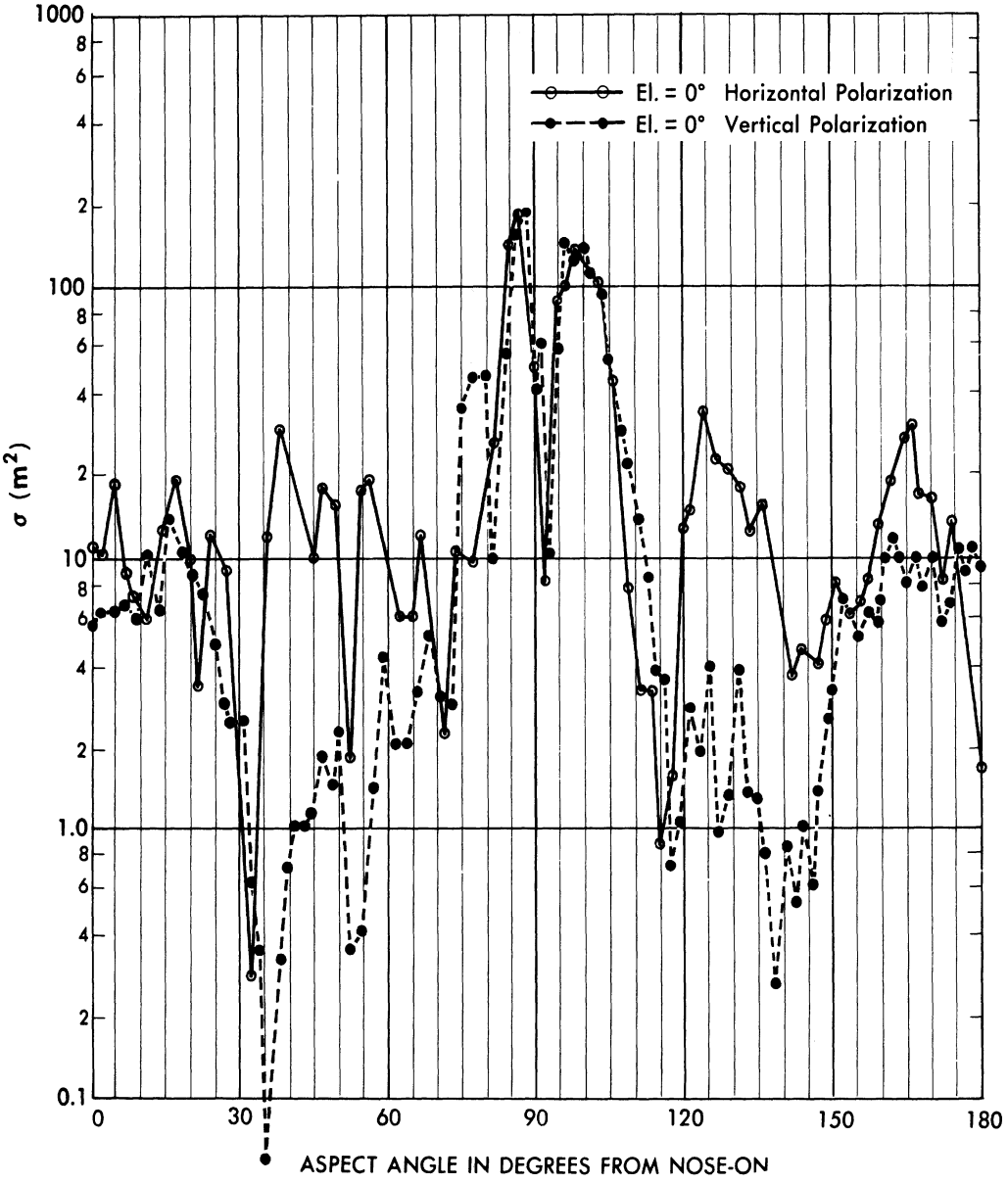

FIG. 5.6 - 2 CROSS-SECTION OF A V-2 AT 100 MC (FED. TEL.)

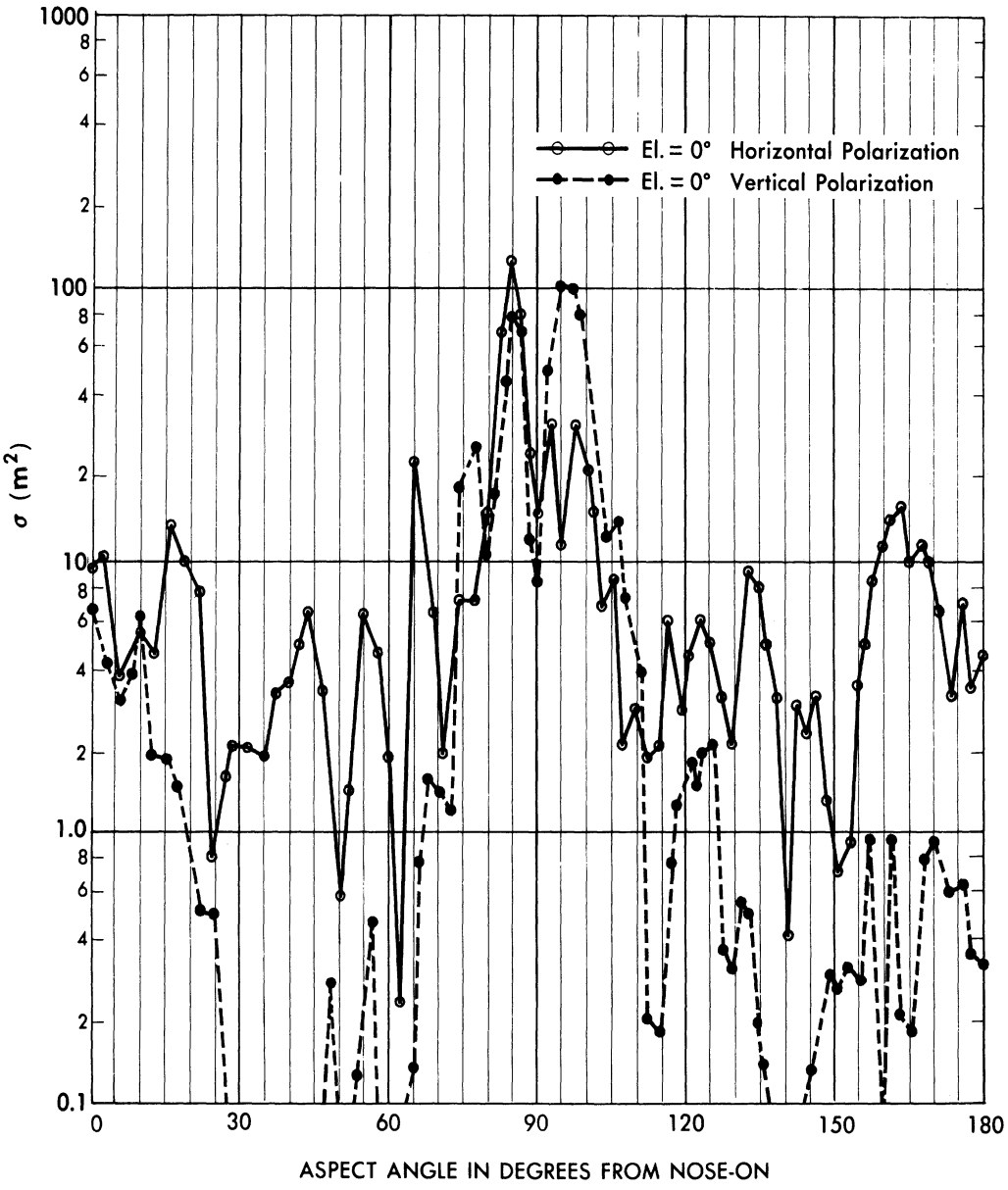

FIG. 5.6-3 CROSS-SECTION OF A V-2 AT 110 MC (FED. TEL.)

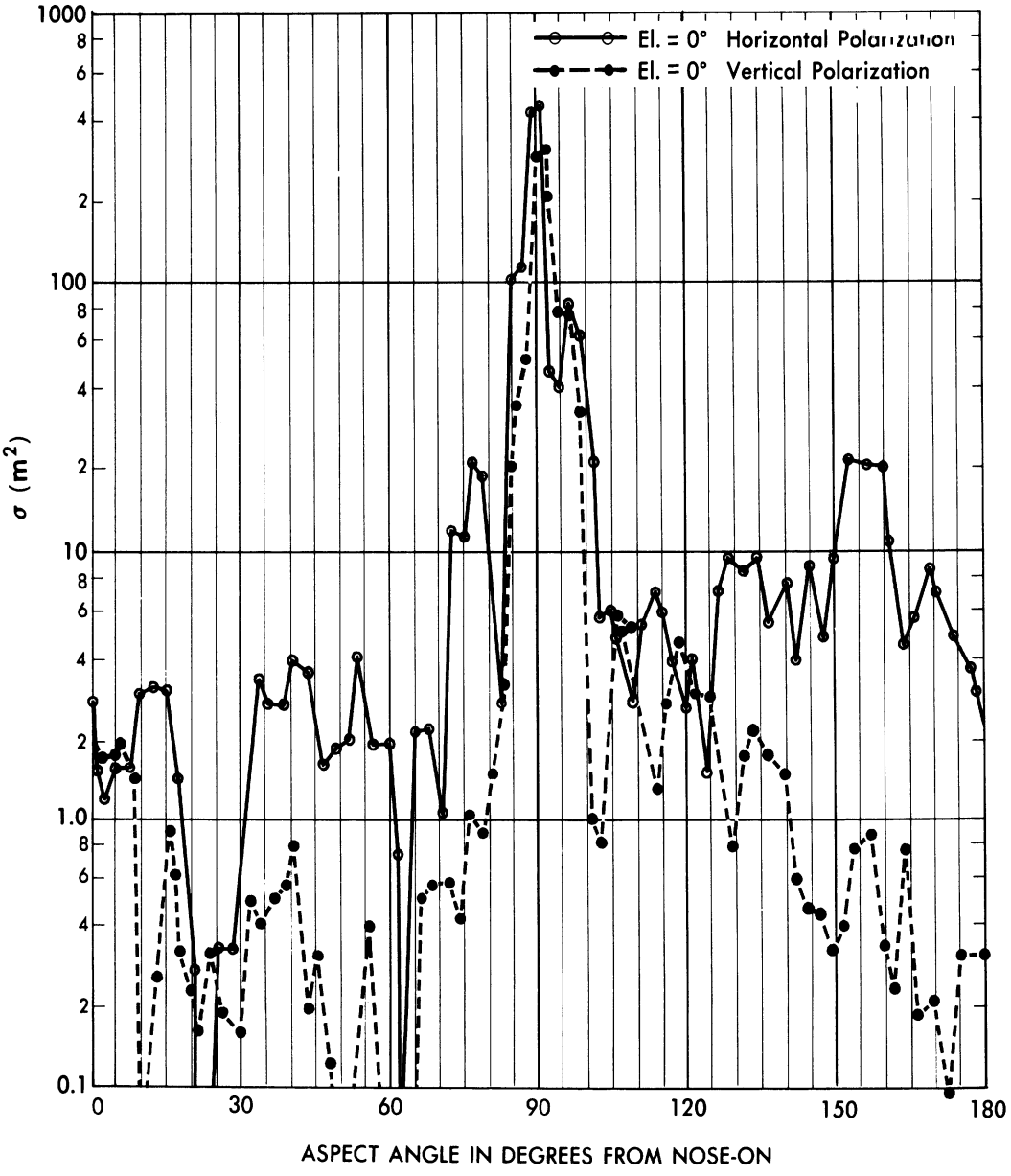

FIG. 5.6-4 CROSS-SECTION OF A V-2 AT 200 MC (FED. TEL.)

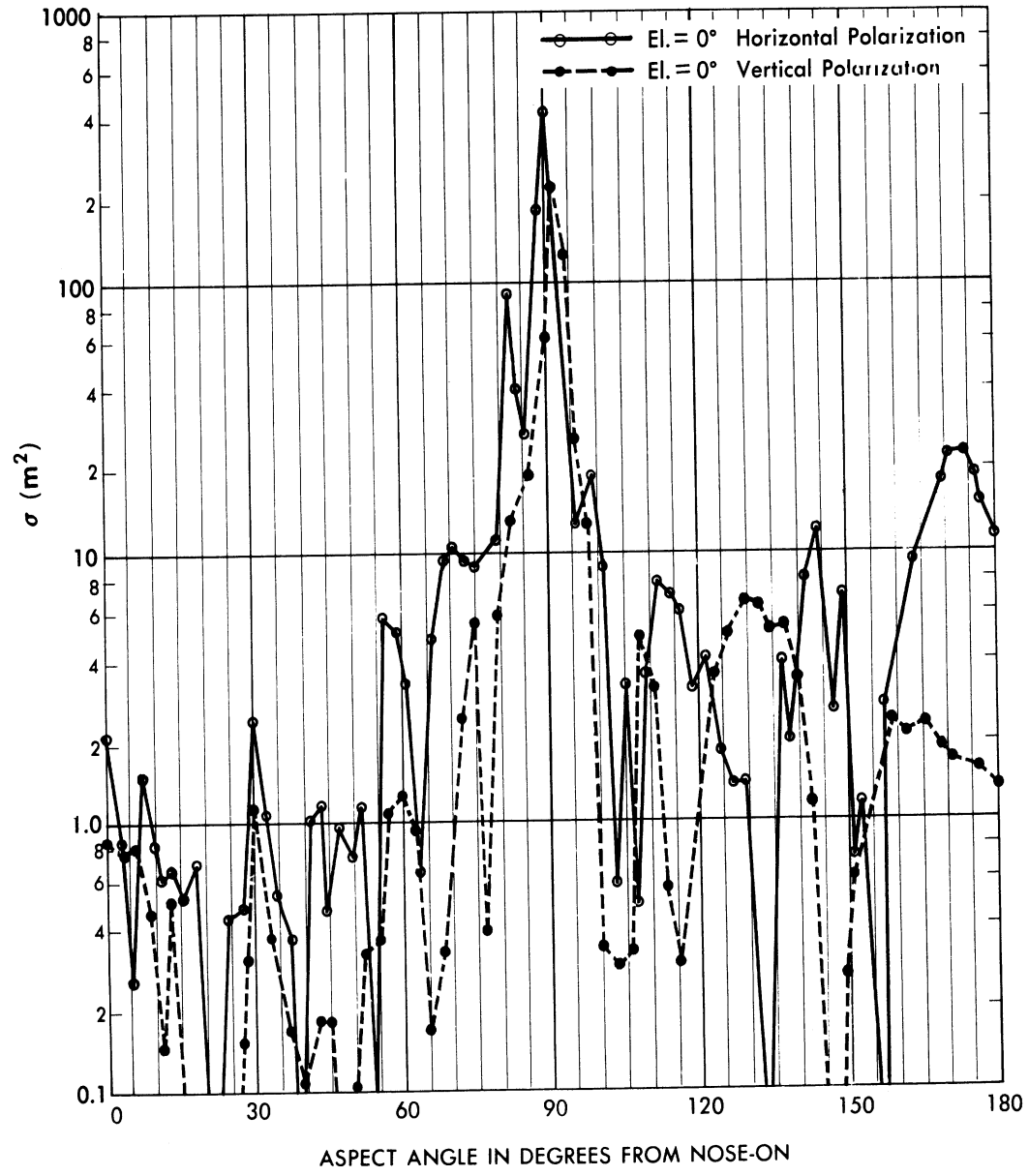

FIG. 5.6-5 CROSS-SECTION OF A V-2 AT 250 MC (FED. TEL.)

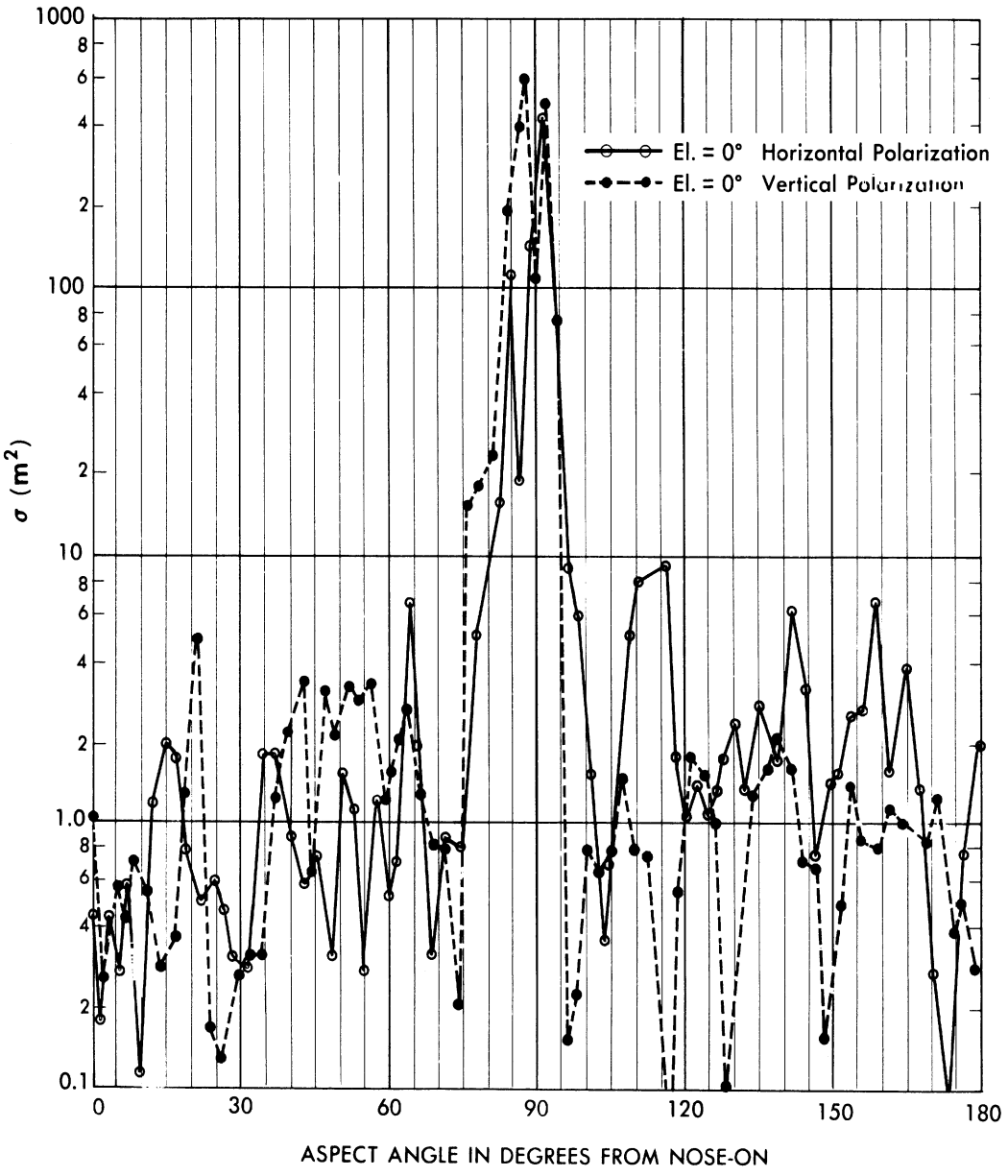

FIG. 5.6-6 CROSS-SECTION OF A V-2 AT 300 MC (FED. TEL.)

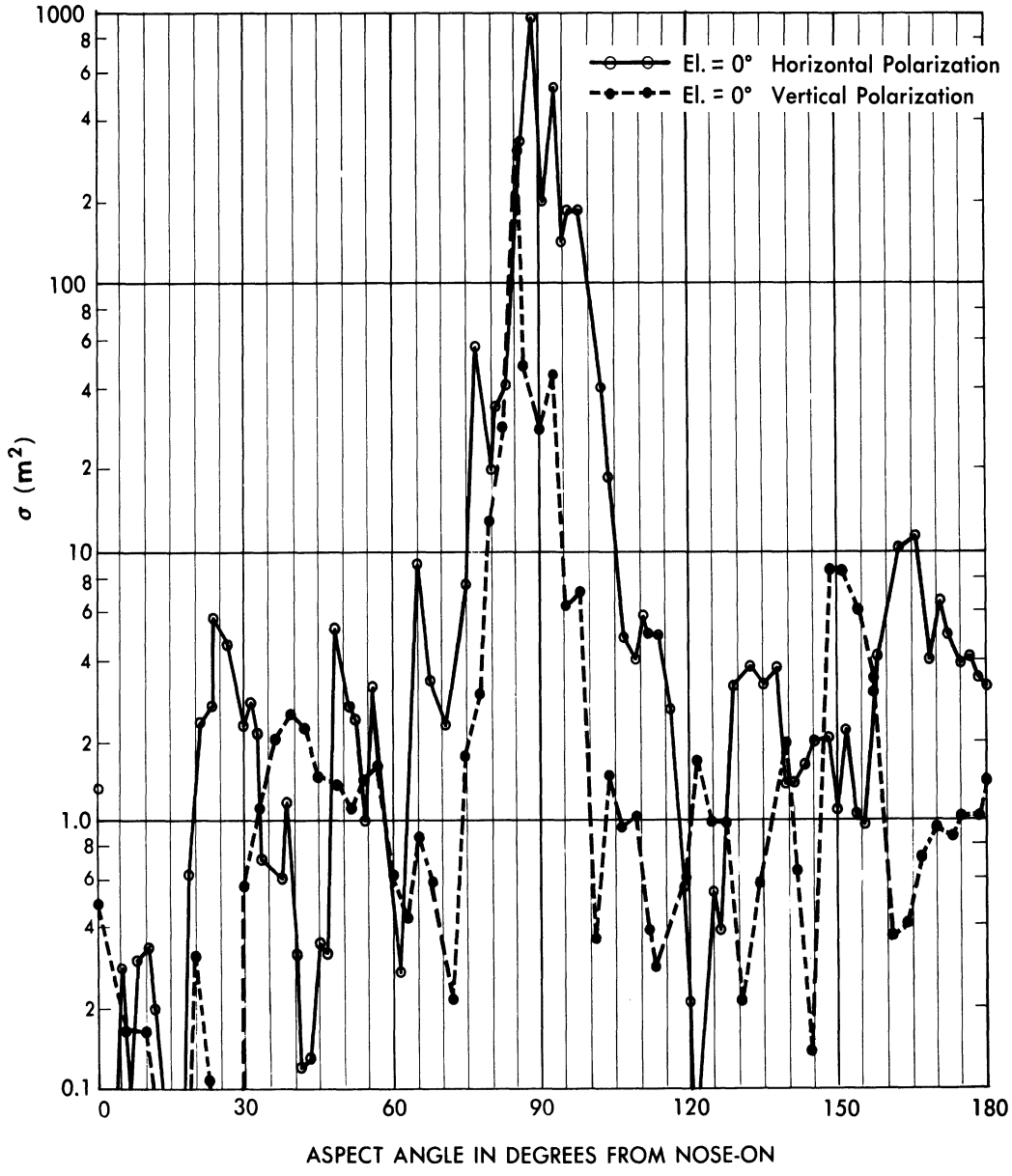

FIG. 5.6-7 CROSS-SECTION OF A V-2 AT 500 MC (FED. TEL.)

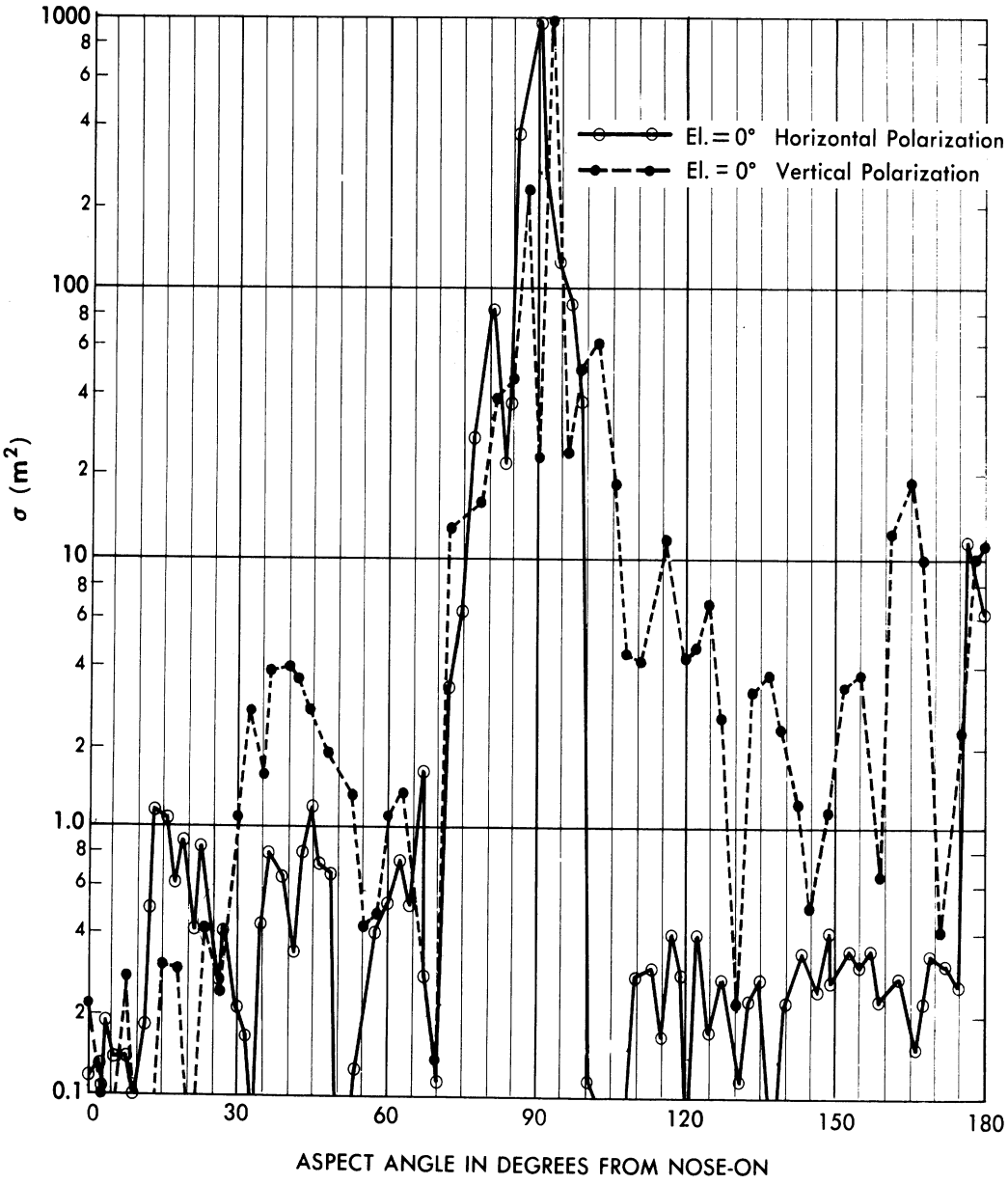

FIG. 5.6-8 CROSS-SECTION OF A V-2 AT 750 MC (FED. TEL.)

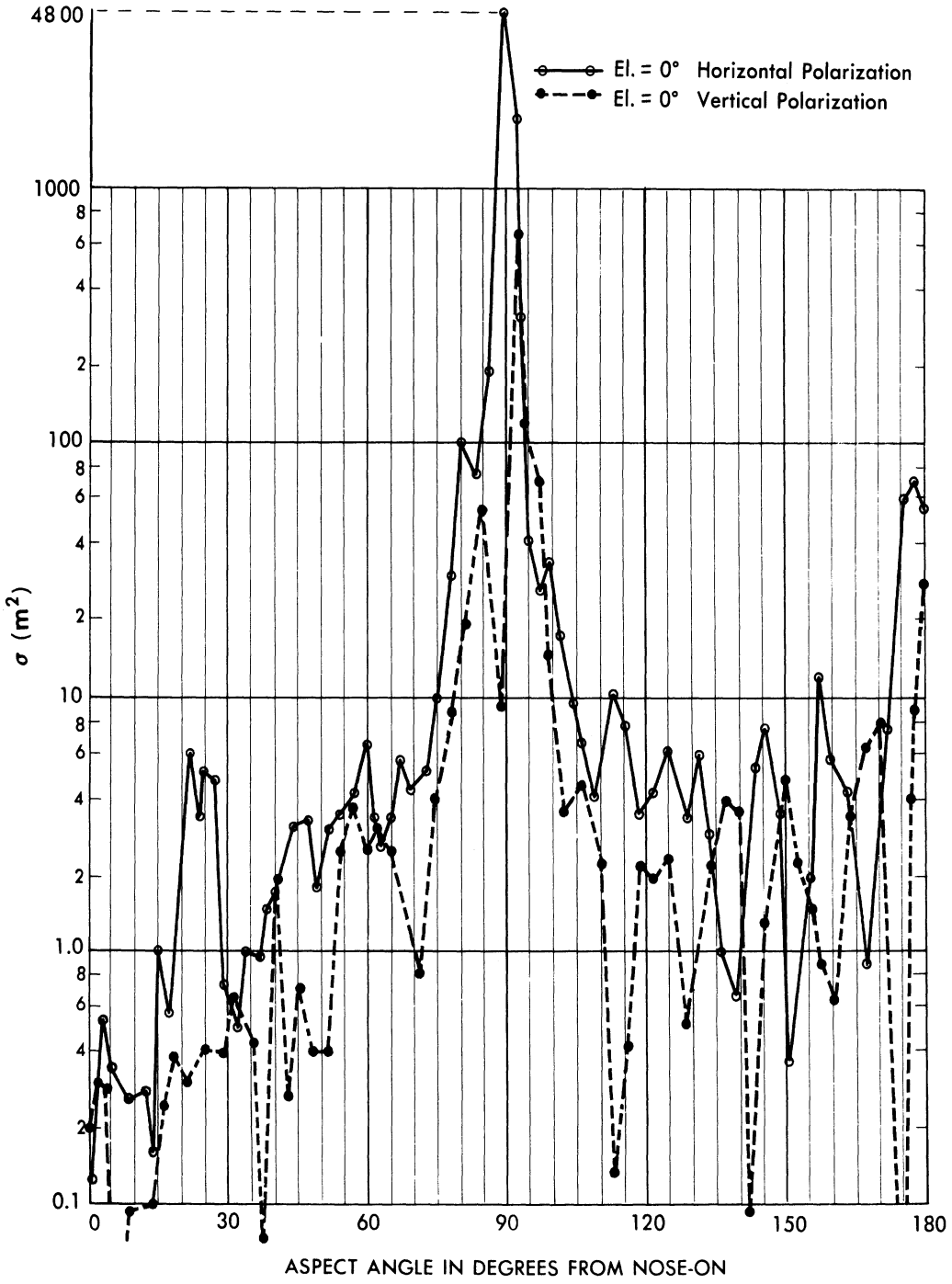

FIG. 5.6 - 9 CROSS-SECTION OF A V-2 AT 1,000 MC (FED. TEL.)

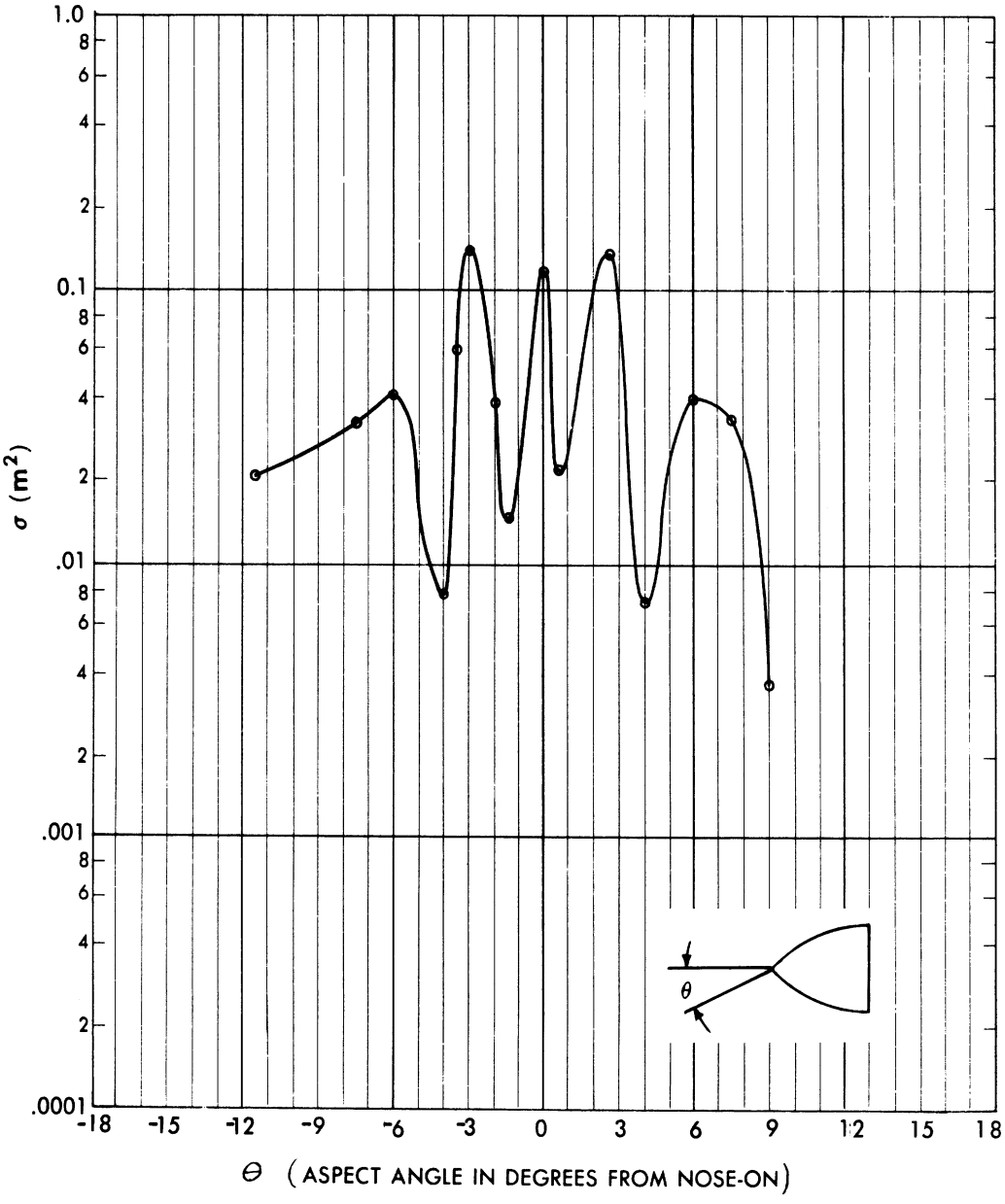

FIG. 5.6-10 CROSS-SECTION OF THE NOSE OF A V-2 AT 2000 MC (FED. TEL.)

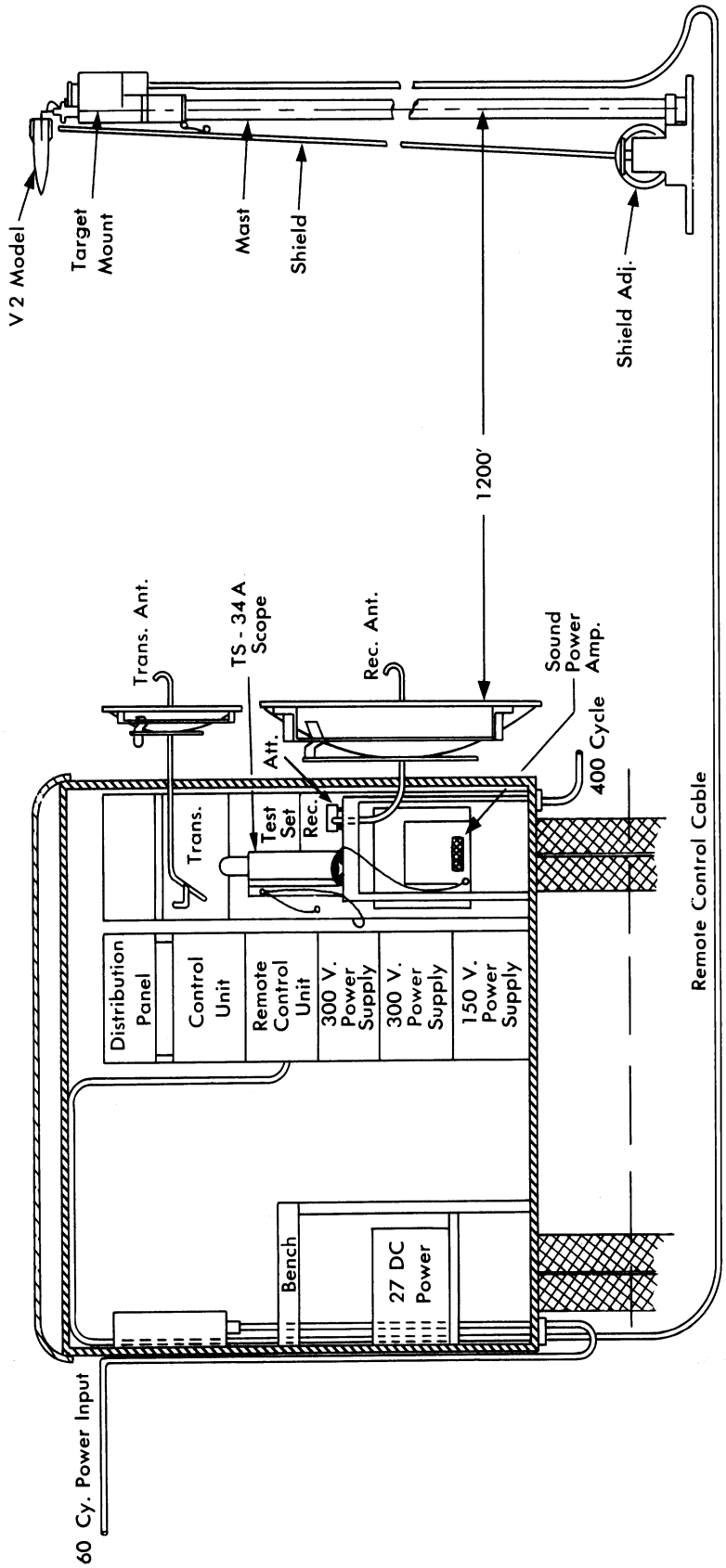

FIG. 5.6-11 A LAYOUT PLAN OF THE MEASURING EQUIPMENT AT FEDERAL TELECOMMUNICATIONS LABORATORY

5.7 V-2 Type Missiles - Radar Research and Development Establishment

The experiments conducted on missile models at the Radar Research and Development Establishment in England (Ref. 52) are summarized in Figures 5.7-1 through 5.7-9. These experiments were conducted at an actual wavelength of 3.22 cm on finned and unfinned models which varied in length from 3.88λ to 30.59λ; the diameters of the models varied from 0.5λ to 4λ.

Measurements were made with two different nose shapes (see Figure 5.7-1). Figures 5.7-2 and 5.7-3 show the effect of the different nose shapes.

The method of measurement is described in Appendix 2.

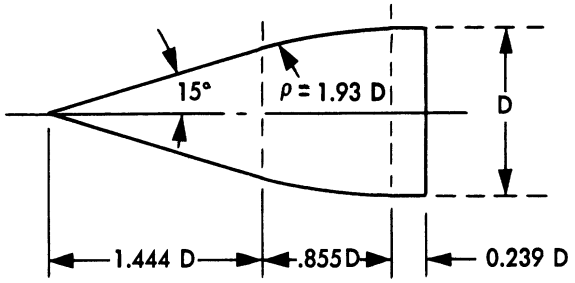

Nose Shape "A"

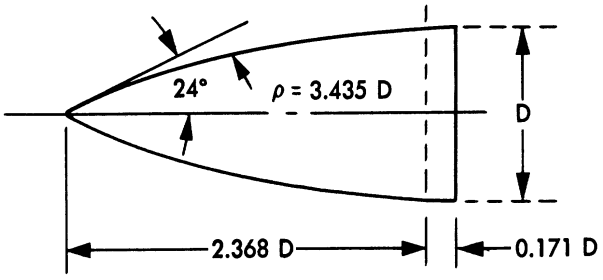

Nose Shape "B"

FIG. 5.7-1 NOSE SHAPES USED IN THE R.R.D.E EXPERIMENTS

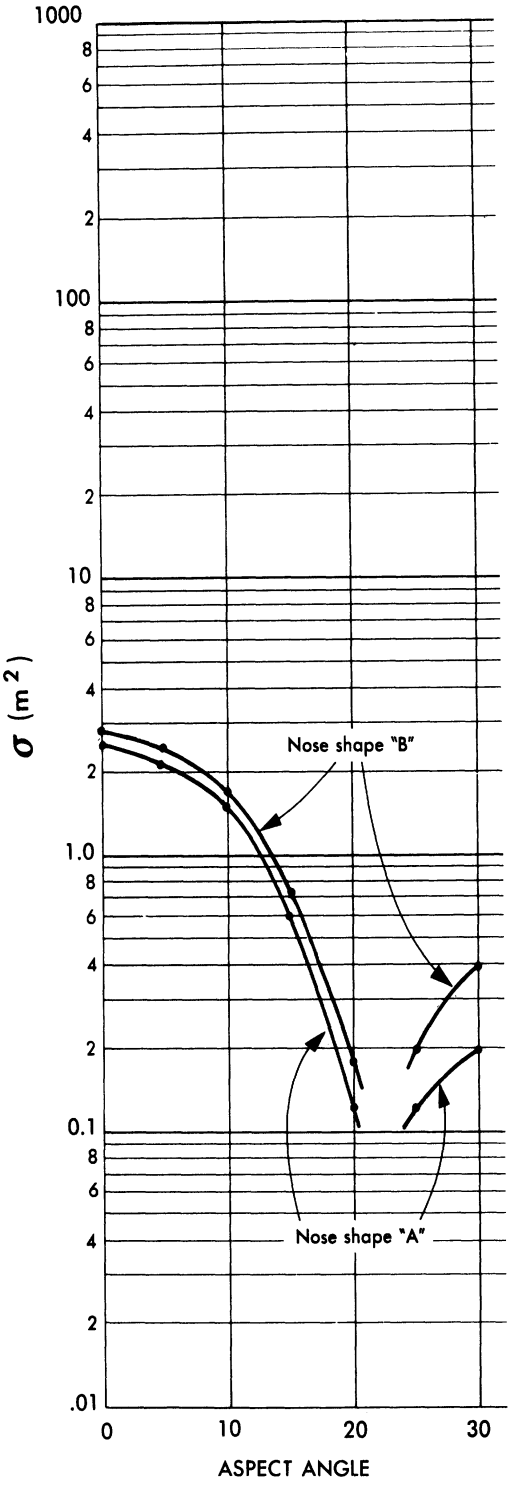

FIG. 5.7-2 CROSS-SECTION OF A FINLESS V-2 TYPE MISSILE AT ~80 MC (RRDE)
Horizontal Polarization

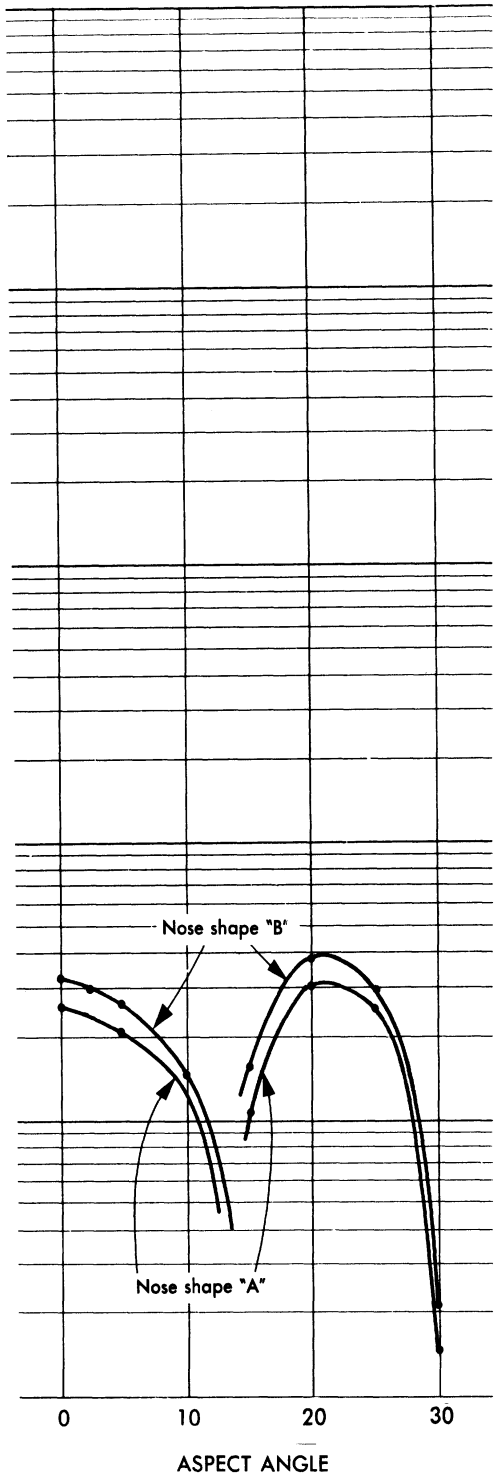

FIG. 5.7-3 CROSS-SECTION OF A FINLESS V-2 TYPE MISSILE AT ~165 MC (RRDE)
Horizontal Polarization

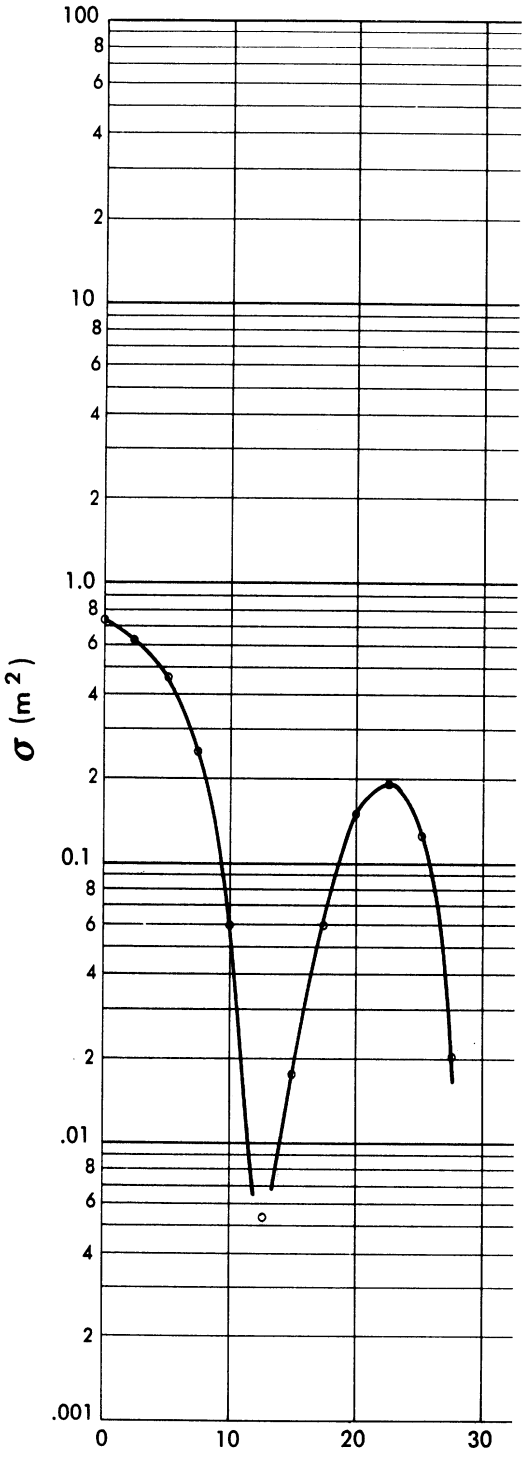

FIG. 5.7-4 CROSS-SECTION OF A FINLESS V-2 TYPE MISSILE AT ~ 210 MC (RRDE)
Horizontal Polarization Nose shape "A"

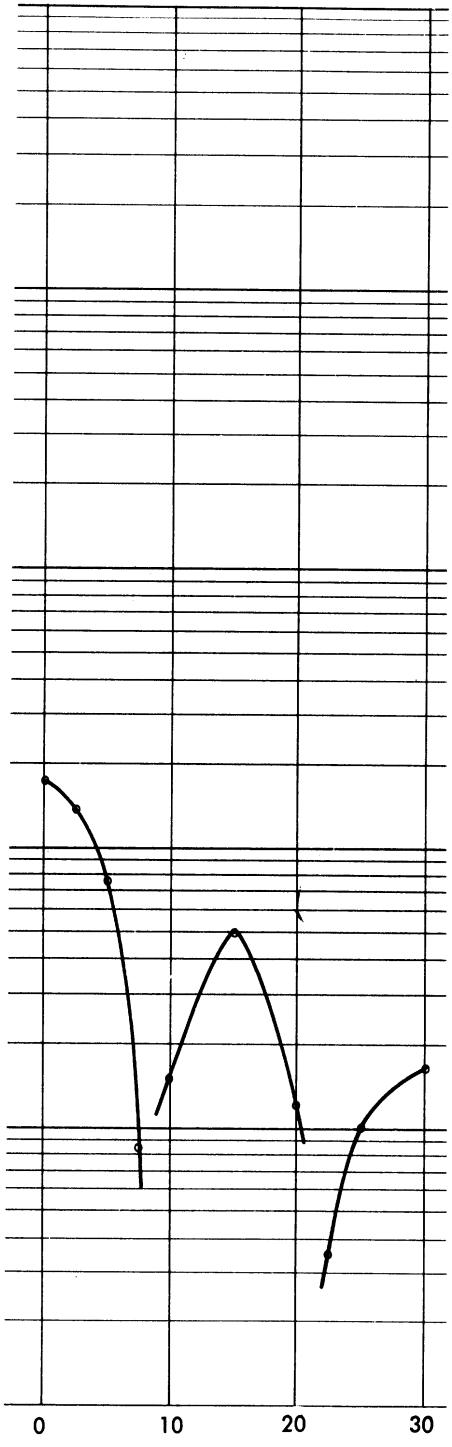

FIG. 5.7-5 CROSS-SECTION OF A FINLESS V-2 TYPE MISSILE AT ~ 325 MC (RRDE)
Horizontal Polarization Nose shape "B"

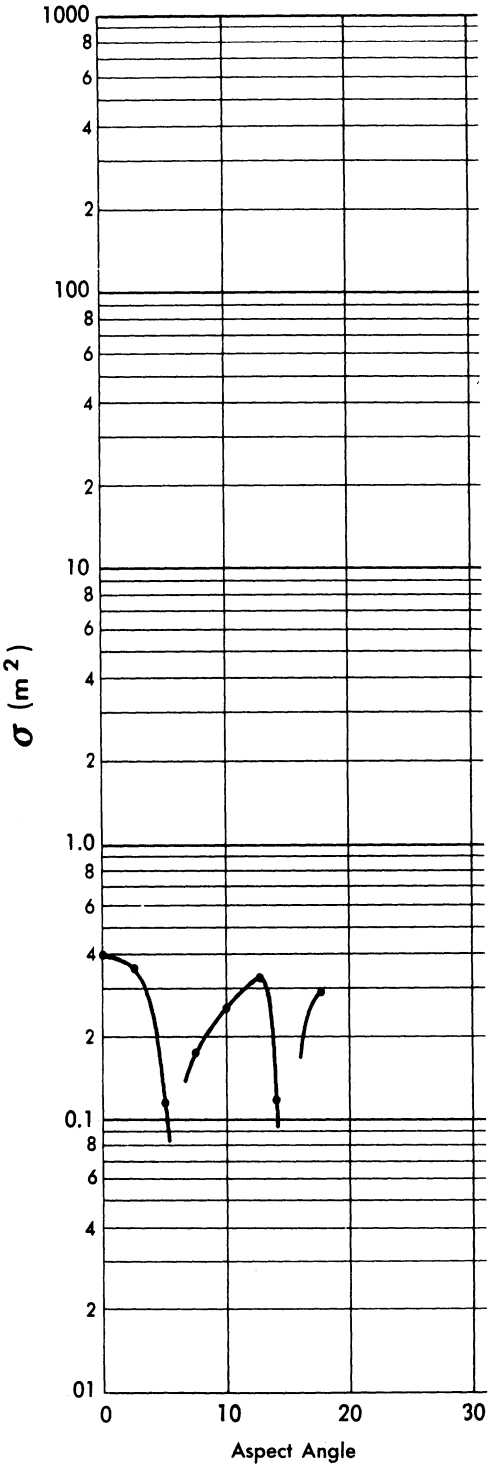

FIG. 5.7-6 CROSS-SECTION OF A FINLESS V-2 TYPE MISSILE AT ~650 MC (RRDE)
Horizontal Polarization Nose shape "B"

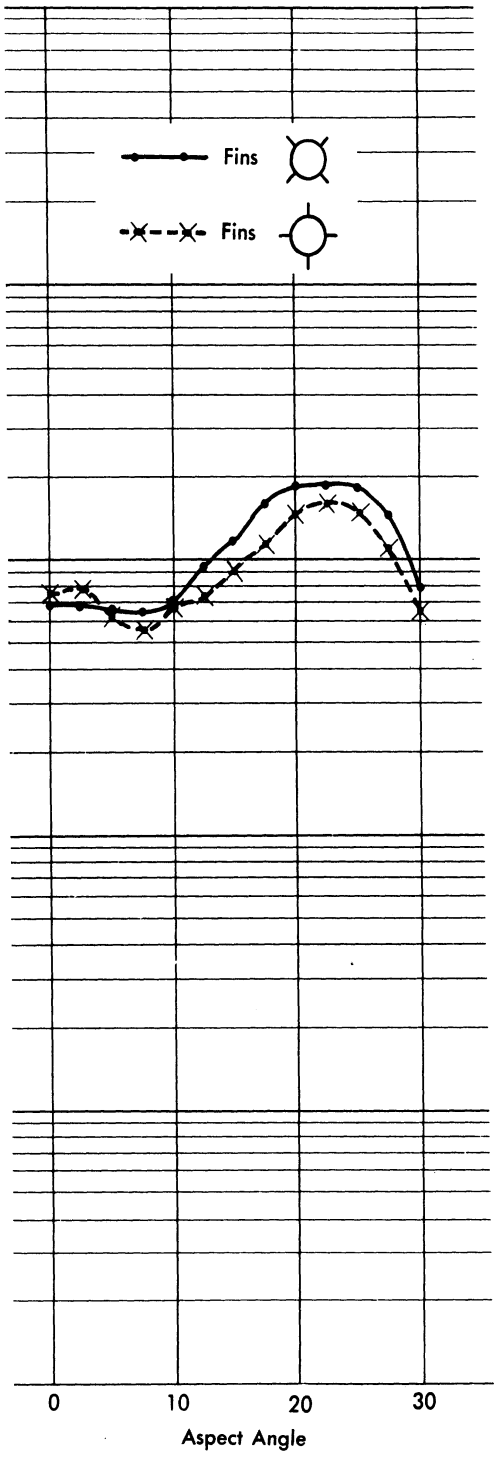

FIG. 5.7-7 CROSS-SECTION OF A V-2 TYPE MISSILE AT ~70 MC (RRDE)
Horizontal Polarization

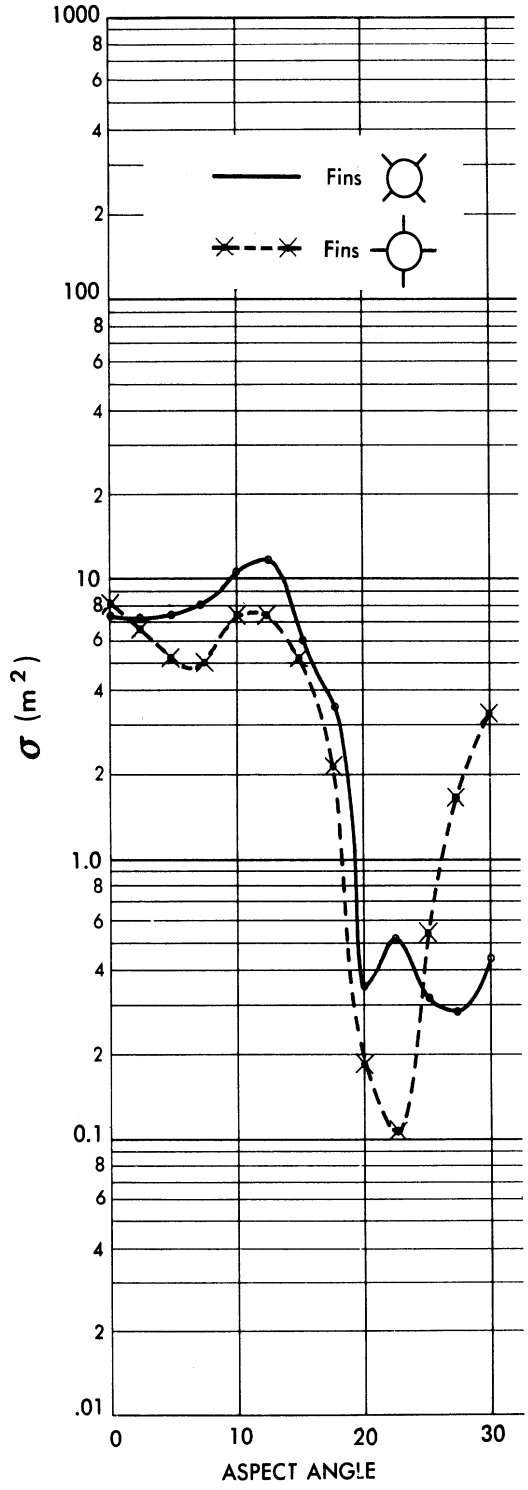

FIG. 5.7-8 CROSS-SECTION OF A V-2 TYPE MISSILE AT ~185 MC (RRDE)
Horizontal Polarization

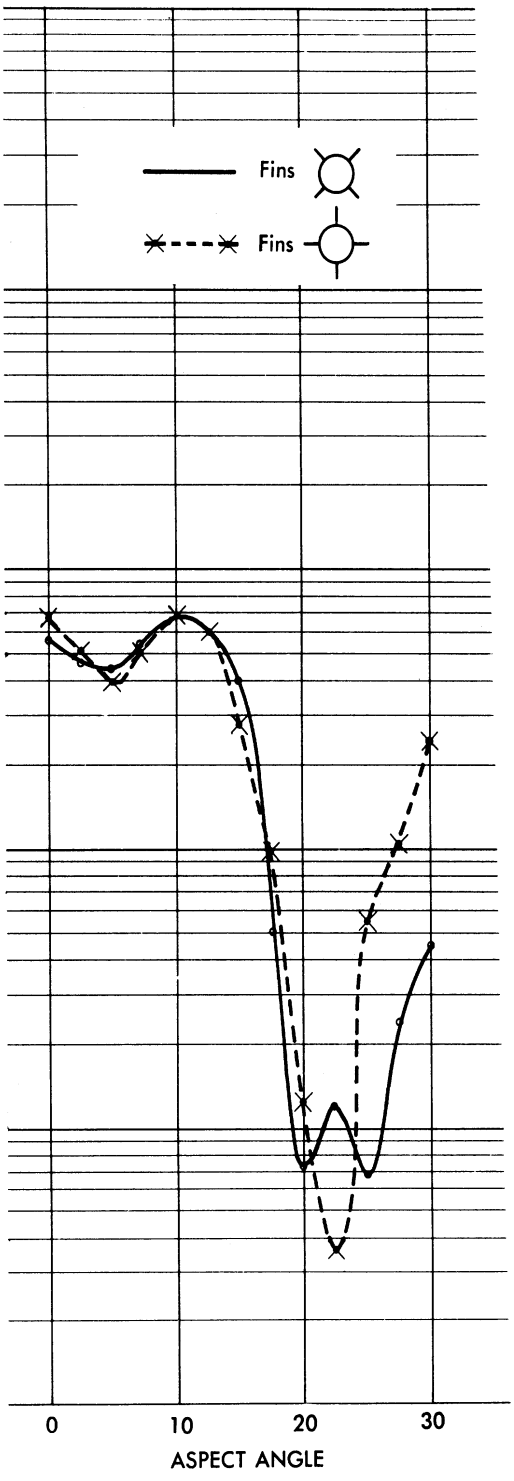

FIG. 5.7-9 CROSS-SECTION OF A V-2 TYPE MISSILE AT ~225 MC (RRDE)
Horizontal Polarization

5.8 V-2 Type Missiles - The General Electric Co.

The General Electric Co. conducted some experiments on Missile Echoing Area using an underwater sound analogy (Ref. 53 and Appendix 2). The Model used was one of the Hermes A missile (a V-2 type). The results (Fig. 5.8-1) are for an equivalent full-scale wavelength of 17.8 cm (i.e. approximately 1690 Mc).

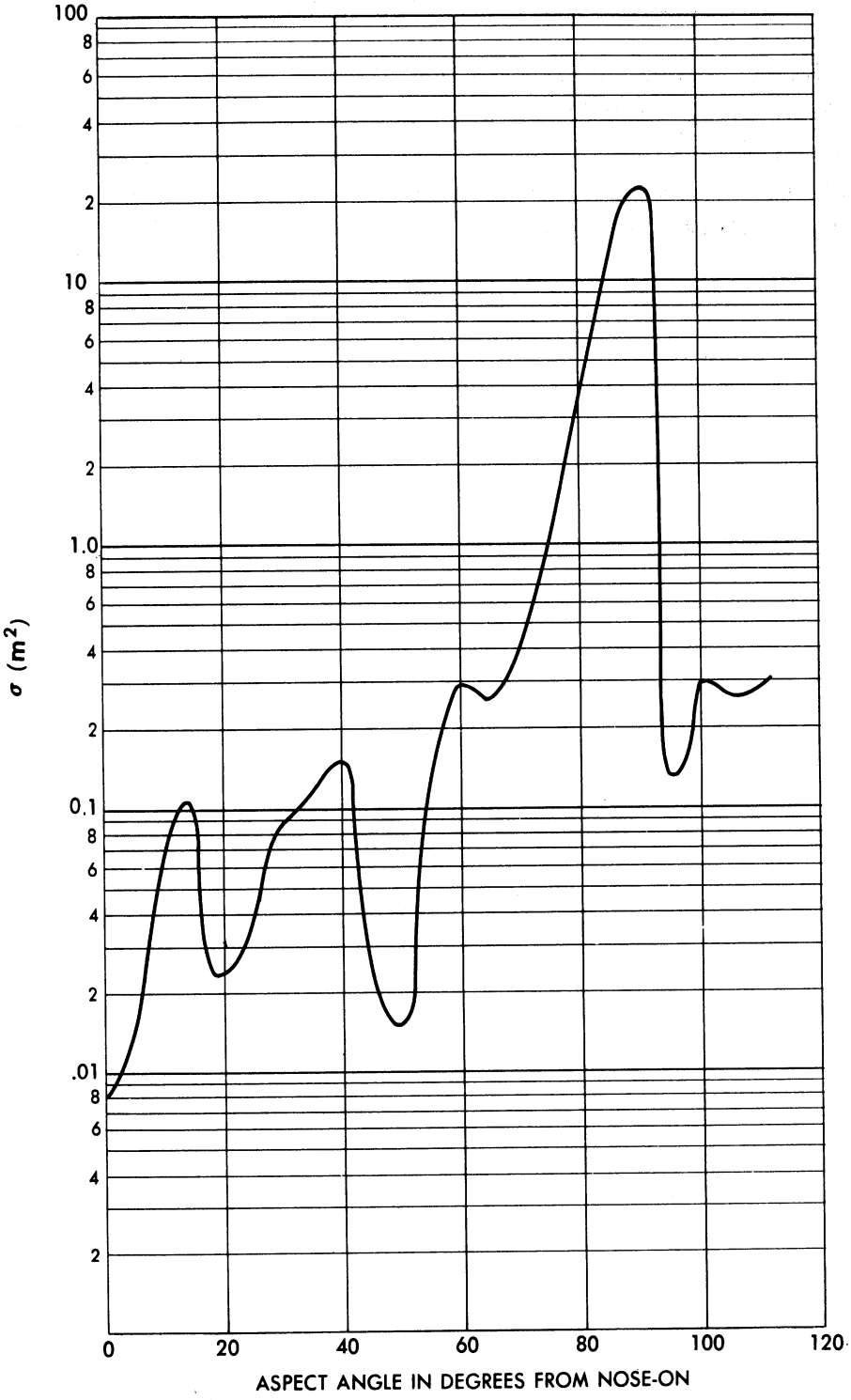

FIG. 5.8-1 CROSS-SECTION OF THE HERMES A AT A WAVELENGTH OF 17.8 cm (FREQ. ≈ 1,690 MC) - (G.E.)

5.9 Comparison of Static Experiments

The static experiments on Atlas type missiles were conducted at 75, 225, 333, and 1000 Mc and since all of these data appear in Section 5.2, it is not necessary to summarize them here.

The range in frequency involved in the V-2 type experiments is quite large, and since the number of experiments and experimenters is comparatively large some summarizing comments are called for. Table 5-3 presents a summary of the contents of Sections 5.3 through 5.8, indicating the range in frequency and the experimenter.

Examination of this table indicates that the frequencies of 50, 100, 300, and 1000 Mc were covered by more than one experiment. Figures 5.9-1 through 5.9-3 contain comparisons of horizontal polarization data at 50, 100, and 300 Mc and Figure 5.9-4 contains a comparison for vertical polarization at 1000 Mc. Figure 2.2 is repeated here for the purpose of comparing the experimental data obtained from these various sources in the vital nose-on region.

TABLE 5-3

Summary of Static Cross-Section Experiments (V-2)

Frequency (Mc)	Microwave Radiation Co.	Ohio State Univ.	Sperry Gyro. Co.	Fed. Tel. Lab.	Radar Res. & Dev. Est.	General Electric Co.
20		X				
40			X			
50		X		X		
60			X			
70					X	
80					X	
100		X	X	X		
110				X		
165					X	
185					X	
200			X			
210					X	
225					X	
250				X		
300		X		X		
325					X	
400		X				
500				X		
600		X				
621		X				
650					X	
710	X					
721	X					
750				X		
1000	X			X		
1200		X				
1690						X
2000				X*		
2900		X				

(* Nose-cone only)

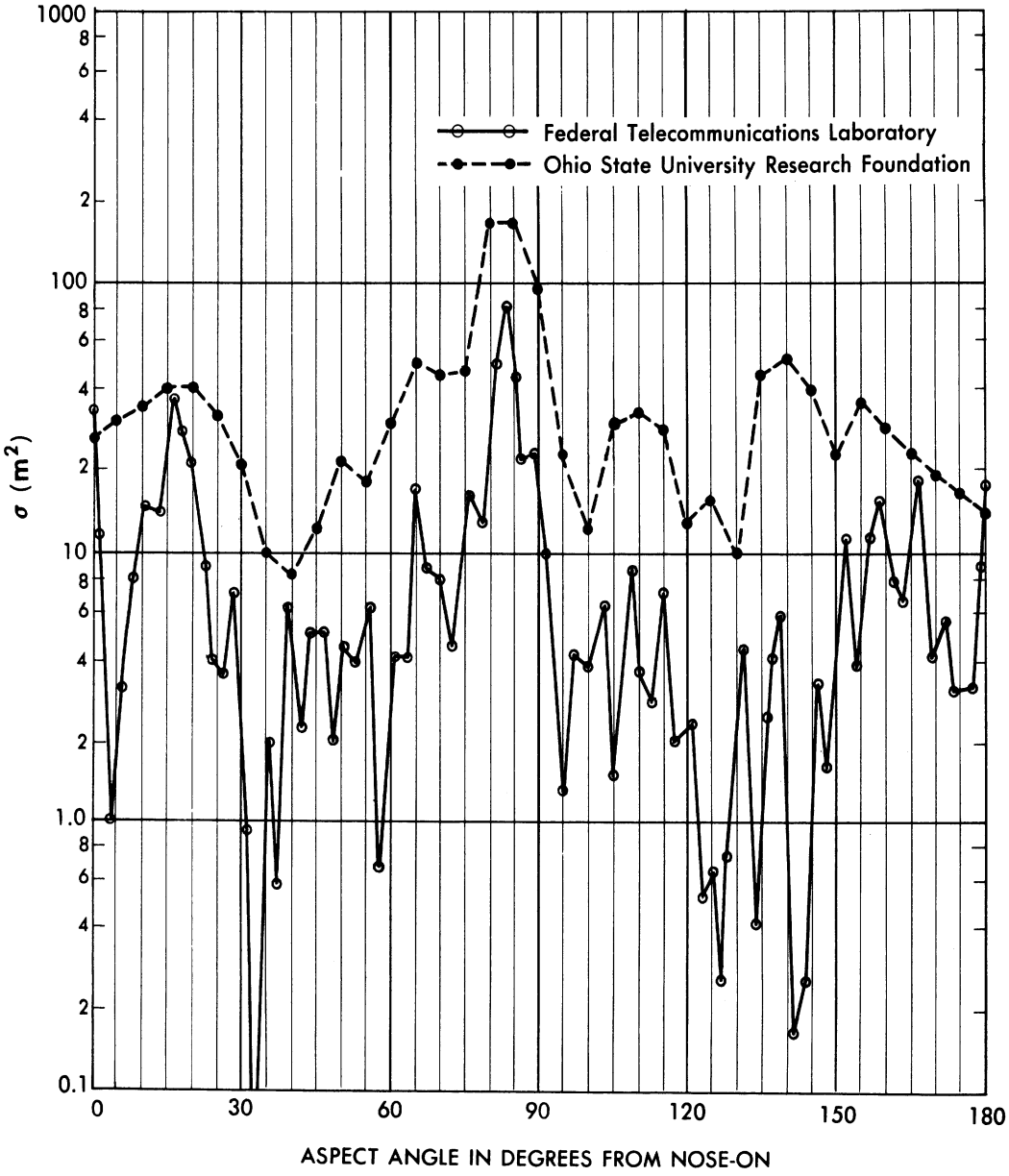

FIG. 5.9-1 CROSS-SECTION OF A V-2 TYPE MISSILE AT 50 MC FOR HORIZONTAL POLARIZATION - A SUMMARY OF DATA FROM STATIC EXPERIMENTS

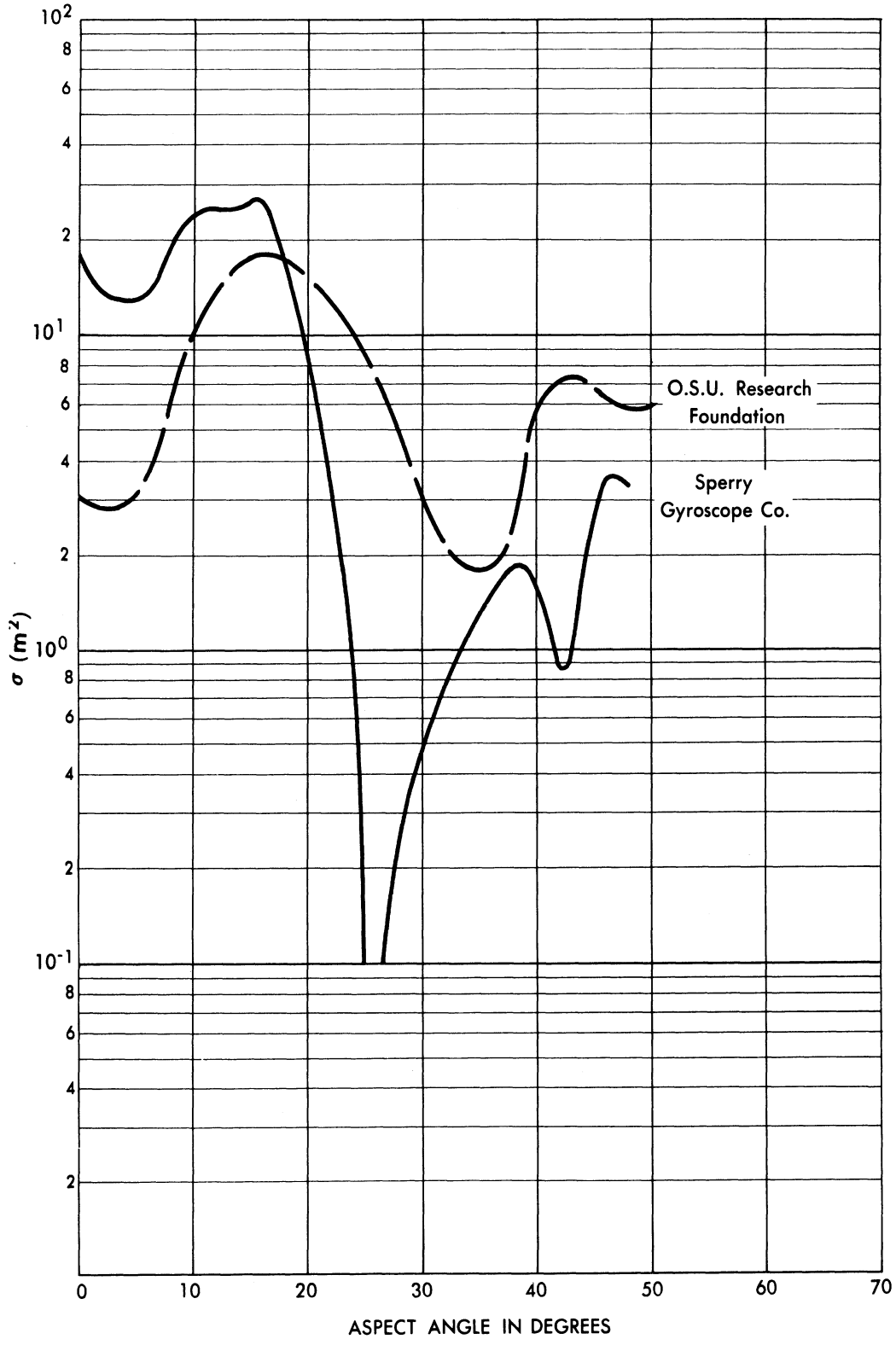

FIG. 5.9-2 CROSS-SECTION OF A V-2 TYPE MISSILE AT 100 MC - A SUMMARY (Horizontal Polarization)

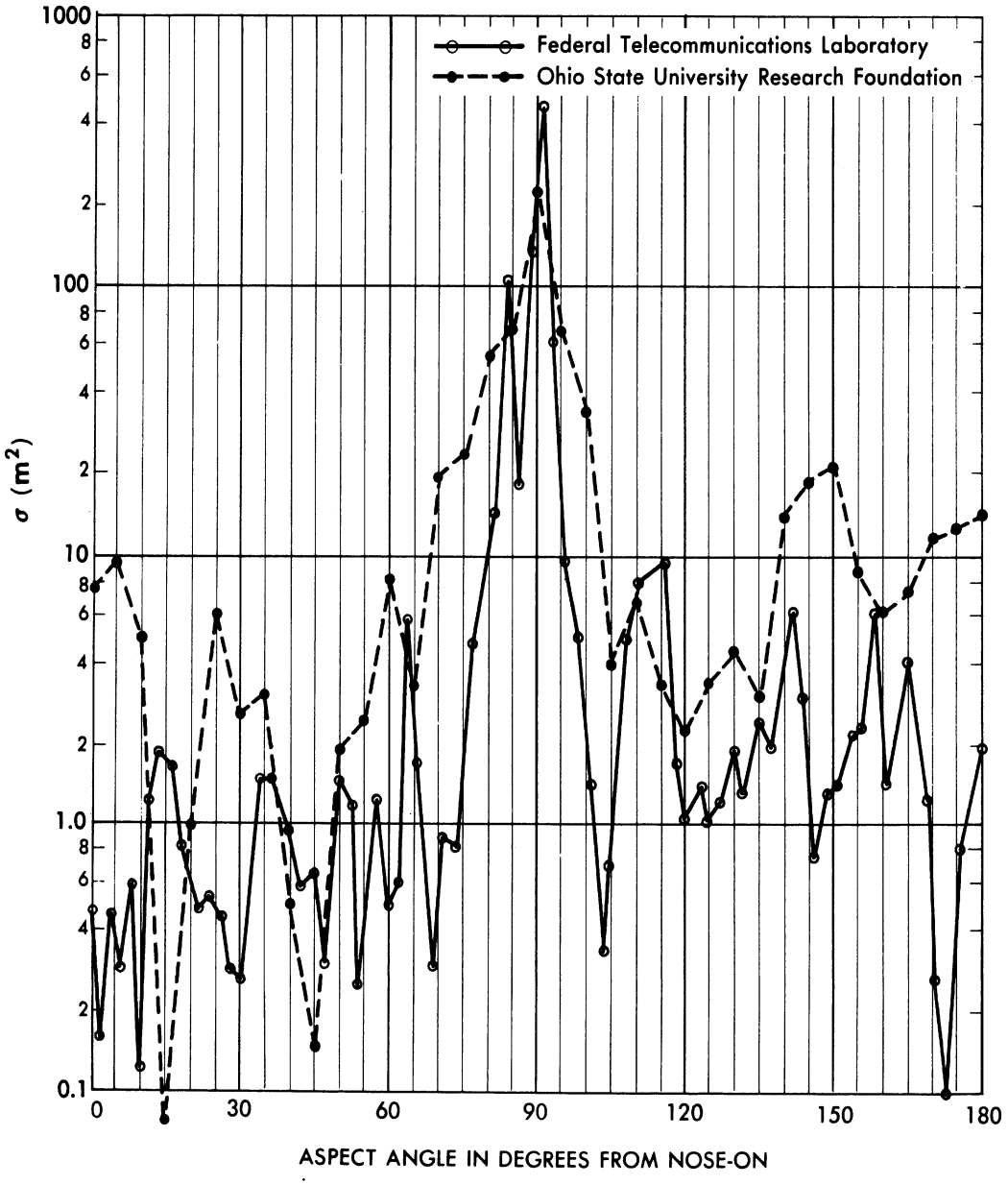

FIG. 5.9-3 CROSS-SECTION OF A V-2 TYPE MISSILE AT 300 MC FOR HORIZONTAL POLARIZATION - A SUMMARY OF DATA FROM STATIC EXPERIMENTS

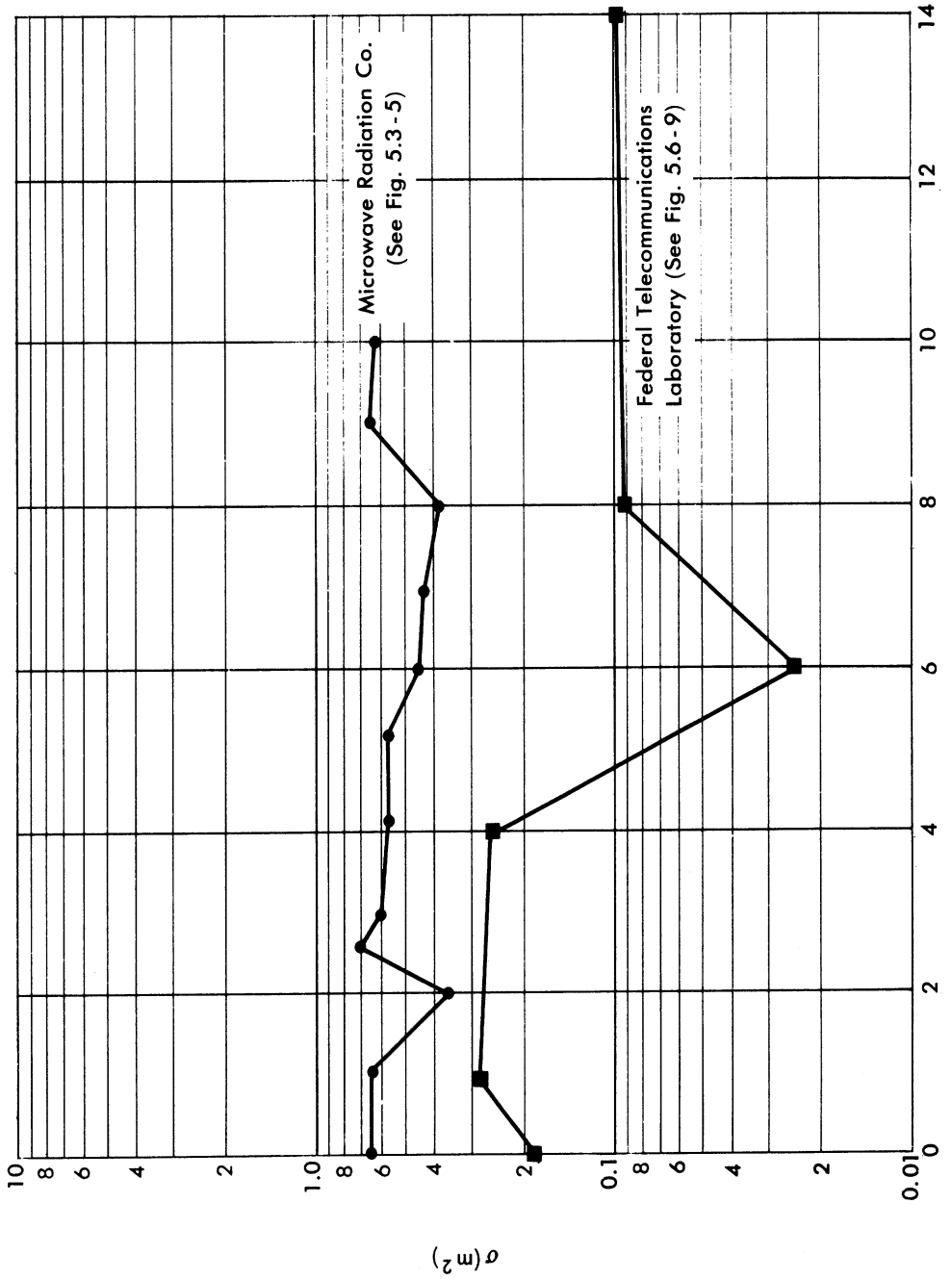

FIG. 5.9-4 CROSS-SECTION OF A V-2 TYPE MISSILE AT 1,000 MC
(Vertical Polarization) - A SUMMARY OF DATA FROM STATIC EXPERIMENTS

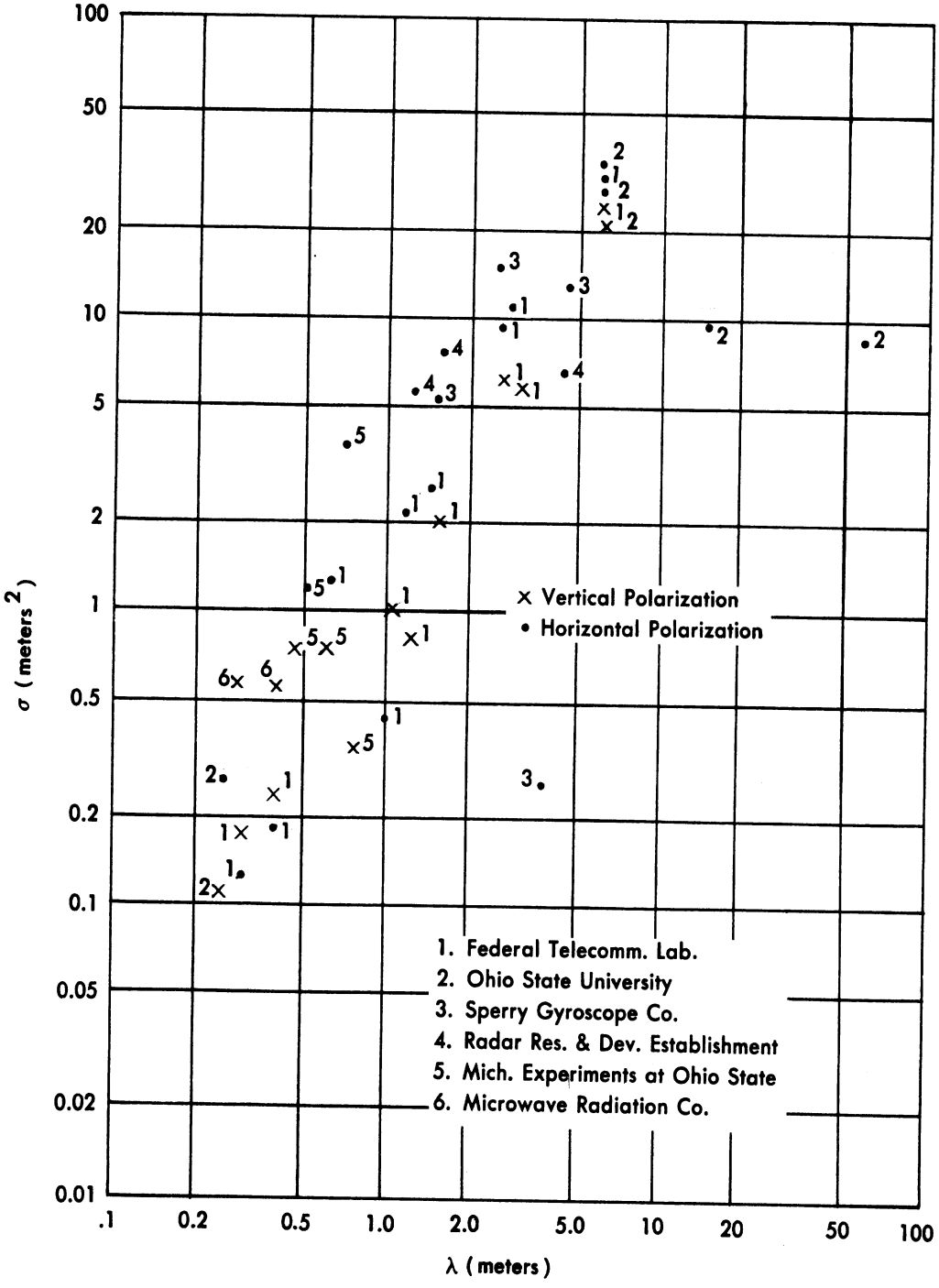

FIG. 2-2 EXPERIMENTAL NOSE-ON V-2 RADAR CROSS-SECTION (IN SQUARE METERS) AS A FUNCTION OF WAVELENGTH (IN METERS).

VI

REFLECTIONS FROM THE MISSILE SURFACES - DYNAMIC EXPERIMENTS

6.1 Willow Run Research Center Experiments

After a study * of the static experiments on V-2's was made, it was concluded that the results obtained in the past were not very accurate in the vital nose-on region.

In order to evaluate the different static experiments in the nose-on region and in order to have a more realistic check between theory and experiments, the Willow Run Research Center embarked on a dynamic measurement program in which V-2 type models were to be dropped from aircraft and their cross-sections near nose-on measured by ground-based radars. This experiment was undertaken after a search of the literature in the field indicated no dynamic nose-on V-2 type missile cross-section data were available.

One-third scale V-2 type models (Fig. 6-1) were used in the dynamic experiments. Static comparisons of the drop-test models were made by the Microwave Radiation Co., Inc. It was believed that their facility was capable of doing very accurate work. An attempt to have other facilities make similar static experiments was unsuccessful, since other facilities contacted felt that the accuracy of their experiments would be too open to question to warrant such experimentation.

The methods used in the dynamic tests are reported in Reference 40. Great care was taken to set up an experiment which would be as accurate as possible in the field. While these efforts were generally successful, the precision of the experiments was degraded by errors in the data reduction which, according to the operational set-up at HAFB,** was not

* Reference 69

** Holloman Air Force Base

under the control or even surveillance of the Willow Run Research Center. However after the data reduction (by Telecomputing Corporation at HAFB) was completed, the Willow Run Research Center obtained the raw data, and, to the extent that time and money allowed, re-reduced the data, thus eliminating the effects of some of the worst errors. However the errors could not be entirely removed in the allotted time, so that the data should be looked on as not necessarily accurate to better than 10 db.

Despite all this, several important conclusions may be drawn:

1. A feasible method of dynamic testing of missiles with small nose-on cross-sections has been developed.

2. The nose-on cross-section of ballistic missiles is sufficiently large that such missiles can be seen with properly adjusted and maintained present-day radars.

3. Theory, many static experiments, and dynamic experiment have produced radar cross-sections of the same order of magnitude.

4. As the aspect angle varies, there are more and deeper minima than those predicted by static experiments.

Unfortunately, certain questions which require high precision of test data cannot be answered; on the other hand, several theoretical conjectures have now been verified experimentally in the field.

Figures 6.—2 through 6.—20 present the data obtained in the dynamic drop tests for V-2 type missiles with square and swept-back fins. The models were 1/3 scale; thus X- and S-band radars yielded full-scale results at S- and L-band respectively.* Figures 6.—2 through 6.—11 are plots of the maximum and minimum cross-sections obtained for the models as a function of the angle off nose for the model frequencies (X- and S-band). The two curves result from the fact that at each angle

*The frequencies actually used in the experiment were 2839 Mc and 9376 Mc.

off nose, data were usually obtained for a set of aspect angles; thus there will, in general, be a set of cross-section values for each angle off-nose. Figure 6 - 12 shows the A-scope return vs time for a typical sphere drop, to indicate quality of the radar performance. The remaining eight figures are plots, corresponding to full-scale V-2, of the mean cross-sections vs aspect angle for horizontal and vertical polarizations. These polarizations are of interest for comparison with static experiments.

Horizontal and vertical polarizations are defined in those cases where there exists a plane containing the radar site and an arbitrarily chosen fin of the model. In these instances, the angle off nose is measured in this plane. The incident radiation is said to be vertically polarized when the electric vector is perpendicular to this plane and horizontally polarized when the electric vector is parallel to this plane.

It is apparent from Figures 6 - 13 through 6 - 20 that the circumstances corresponding exactly to horizontal and vertical polarizations occurred at relatively few angles off nose. The term latitude angle used in Figures 6 - 13 through 6 - 20 is the angle off-nose measured in the plane of the fins.

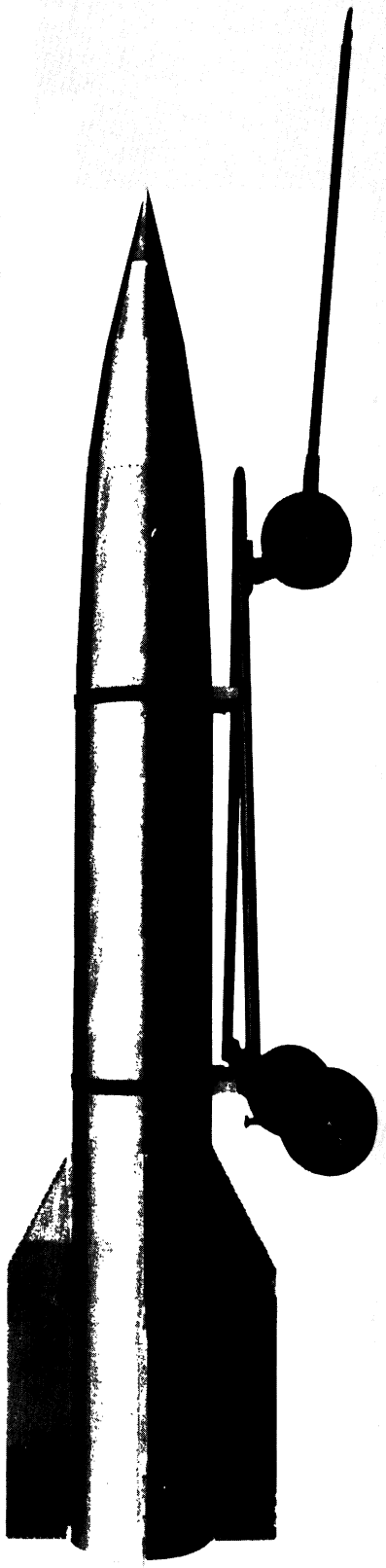

FIG. 6-1 PHOTOGRAPH OF THE MISSILE MODEL USED IN THE WILLOW RUN RESEARCH CENTER TESTS

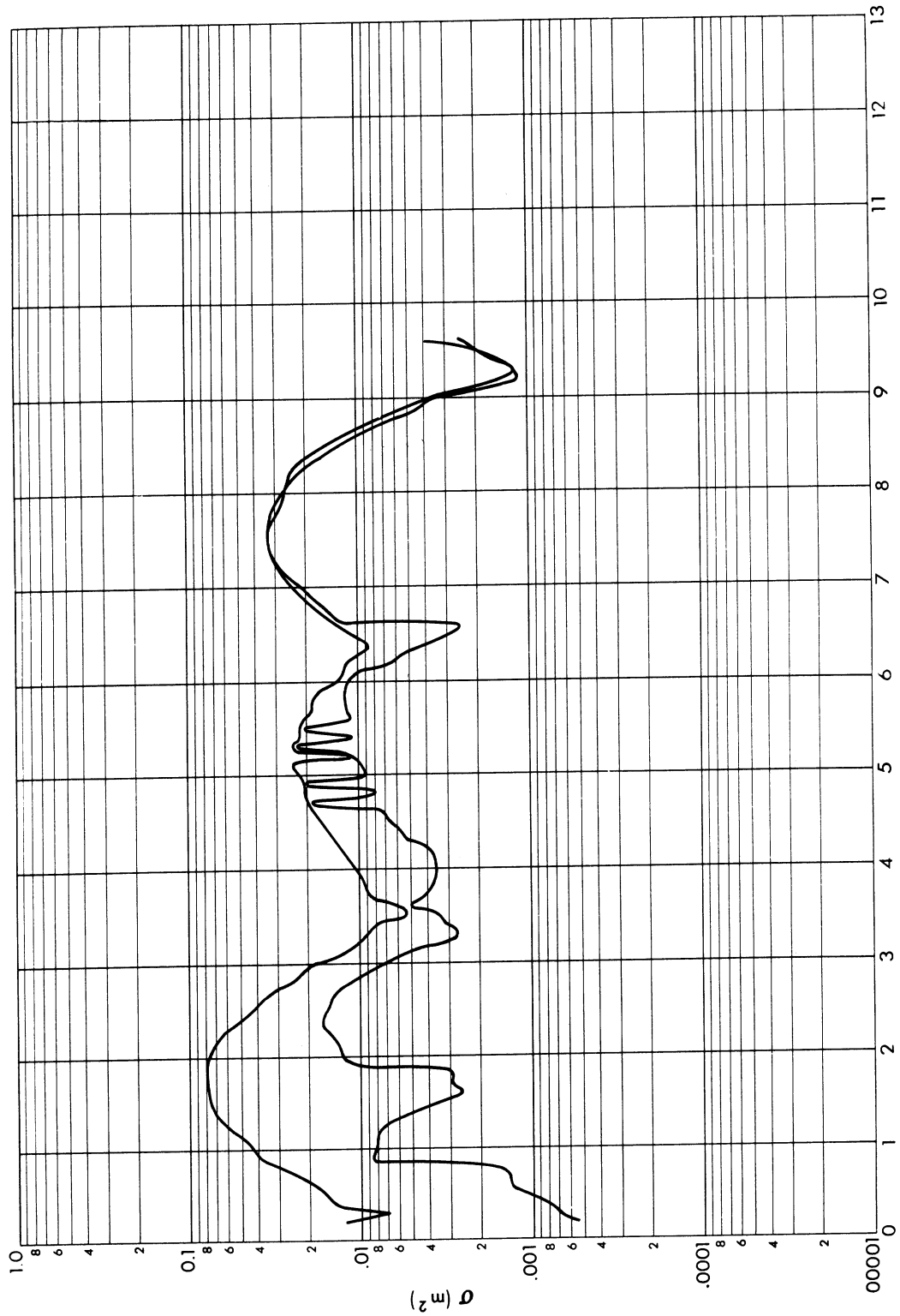

FIG. 6-2 RADAR CROSS-SECTION IN SQUARE METERS vs. ANGLE OFF NOSE
1/3 SCALE MODEL S-BAND MODEL "A" SWEPT FINS

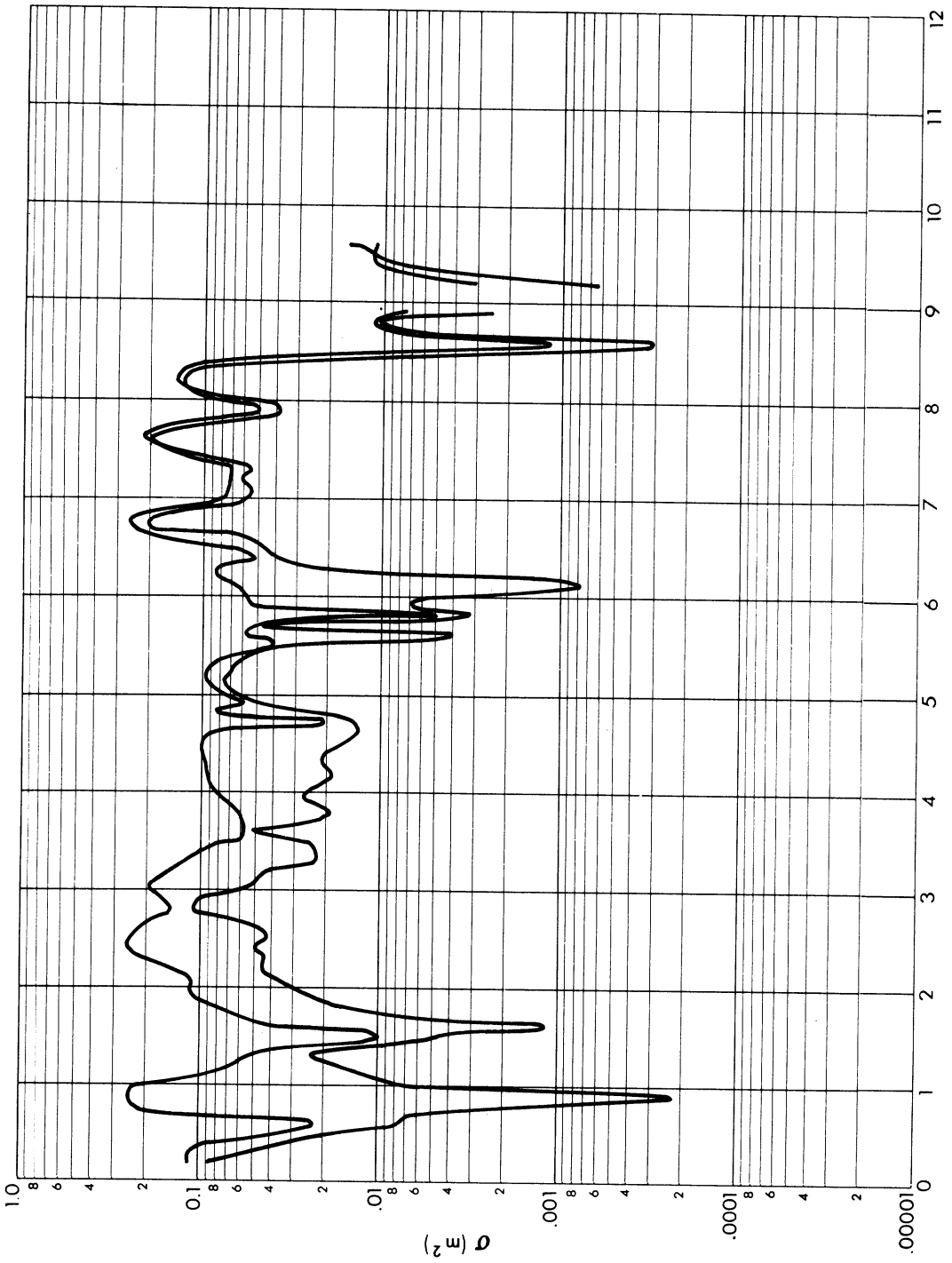

FIG. 6-3 RADAR CROSS-SECTION IN SQUARE METERS vs. ANGLE OFF NOSE
1/3 SCALE MODEL X-BAND MODEL "A" SWEPT FINS

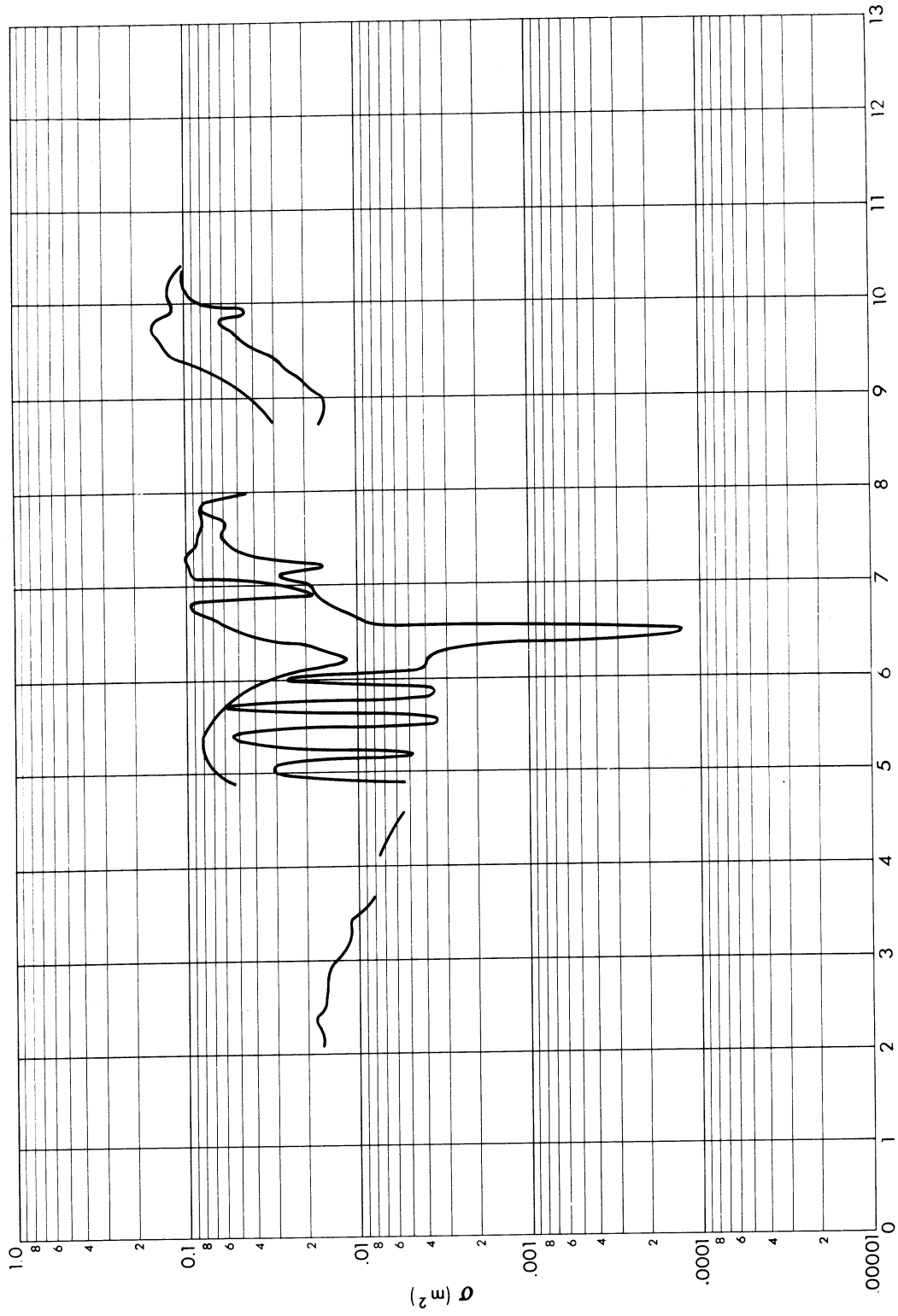

FIG. 6-4 RADAR CROSS-SECTION IN SQUARE METERS vs. ANGLE OFF NOSE
1/3 SCALE MODEL S-BAND MODEL "B" SWEPT FINS

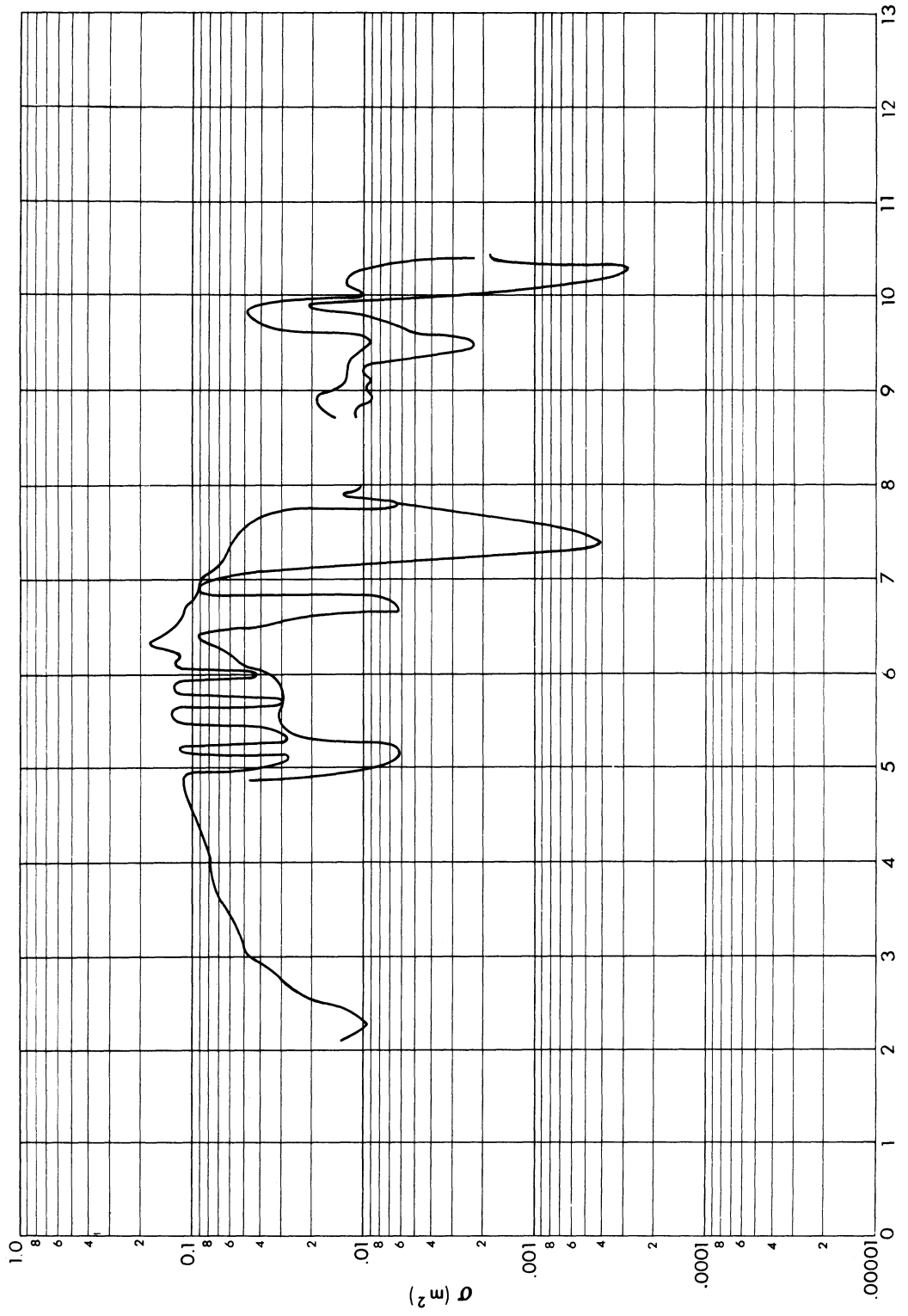

FIG. 6-5 RADAR CROSS-SECTION IN SQUARE METERS vs. ANGLE OFF NOSE
1/3 SCALE MODEL X-BAND MODEL "B" SWEPT FINS

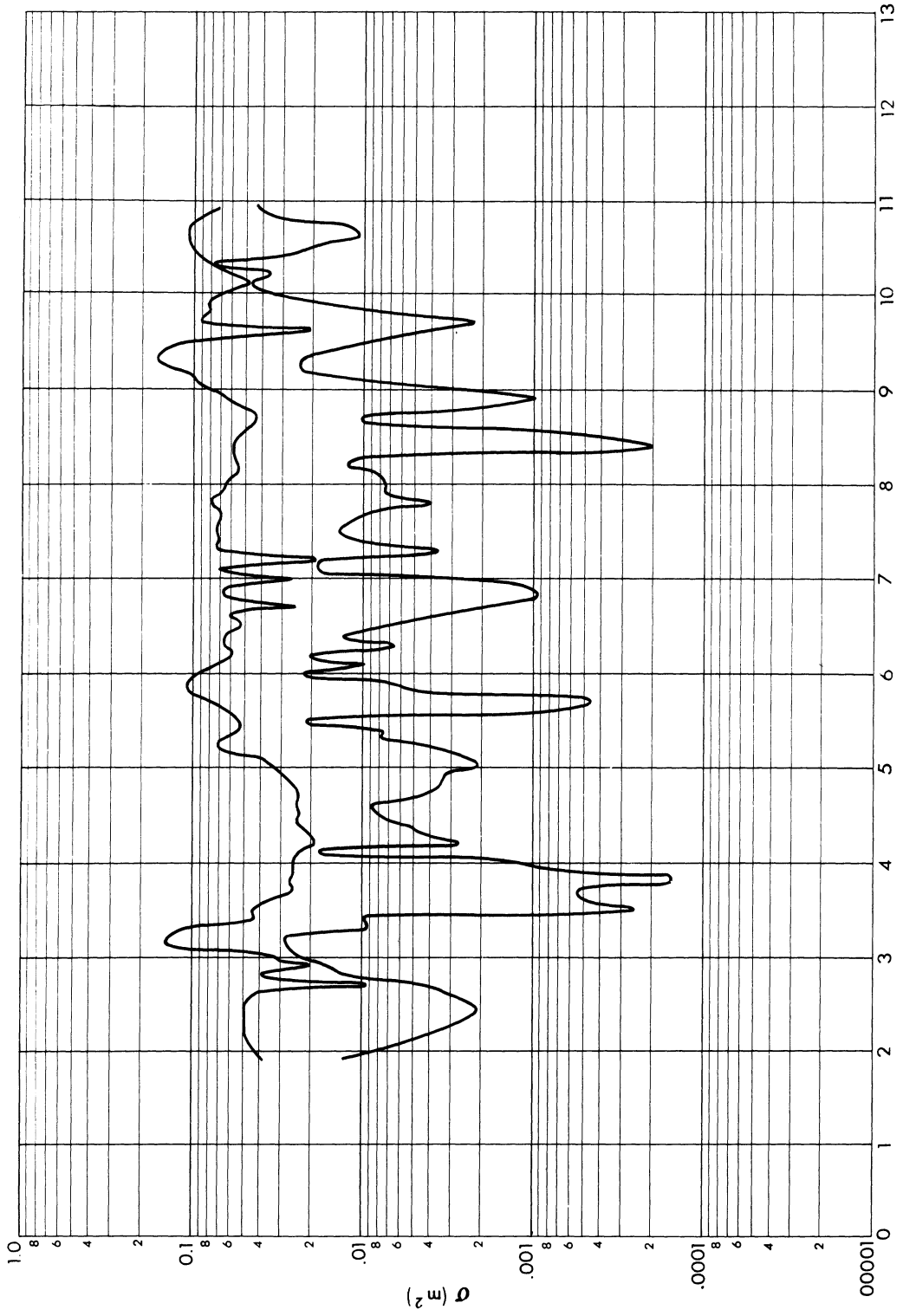

FIG. 6-6 RADAR CROSS-SECTION IN SQUARE METERS vs. ANGLE OFF NOSE
1/3 SCALE MODEL S-BAND MODEL "C" SWEPT FINS

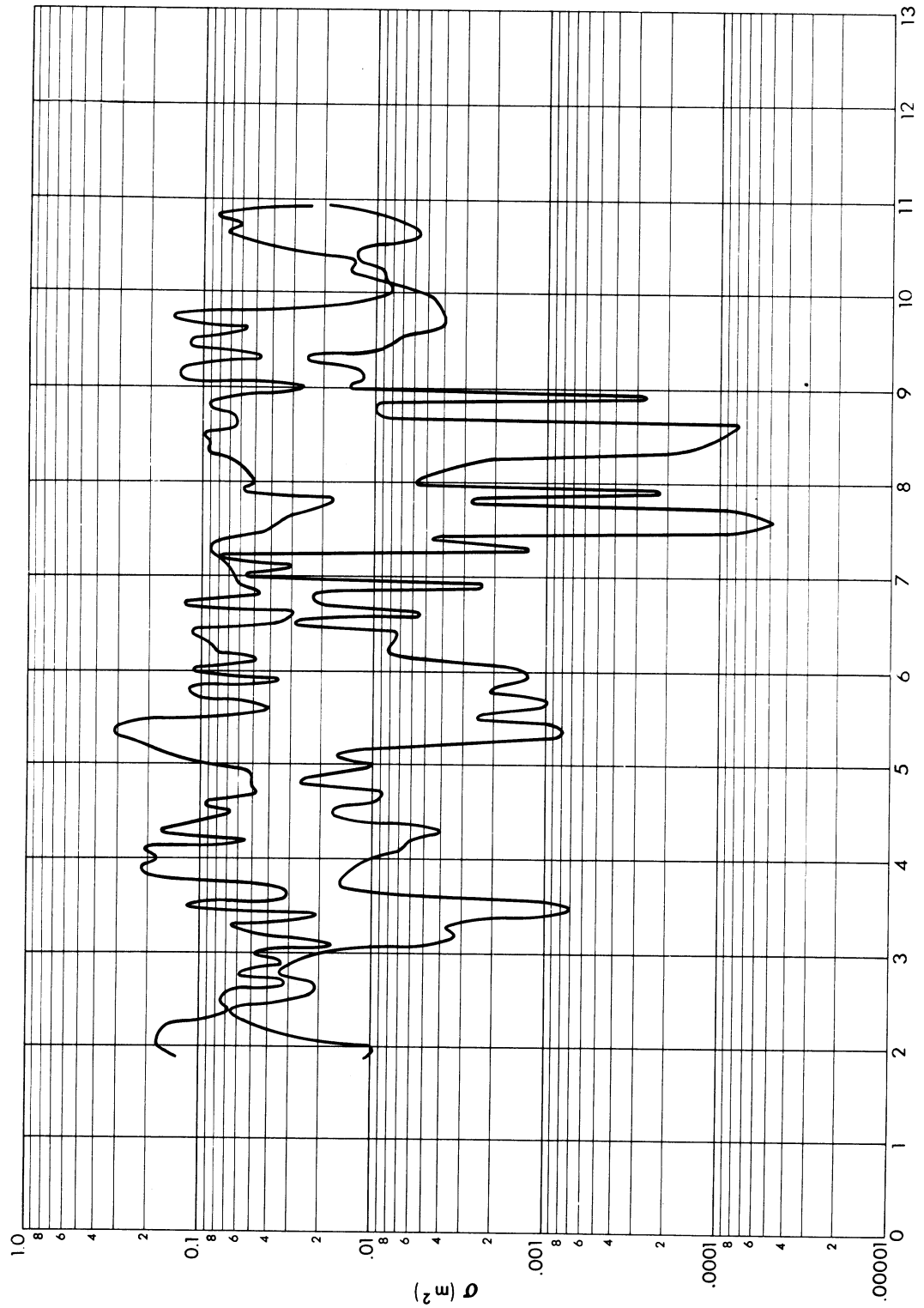

FIG. 6-7 RADAR CROSS-SECTION IN SQUARE METERS vs. ANGLE OFF NOSE
1/3 SCALE MODEL X-BAND MODEL "C" SWEPT FINS

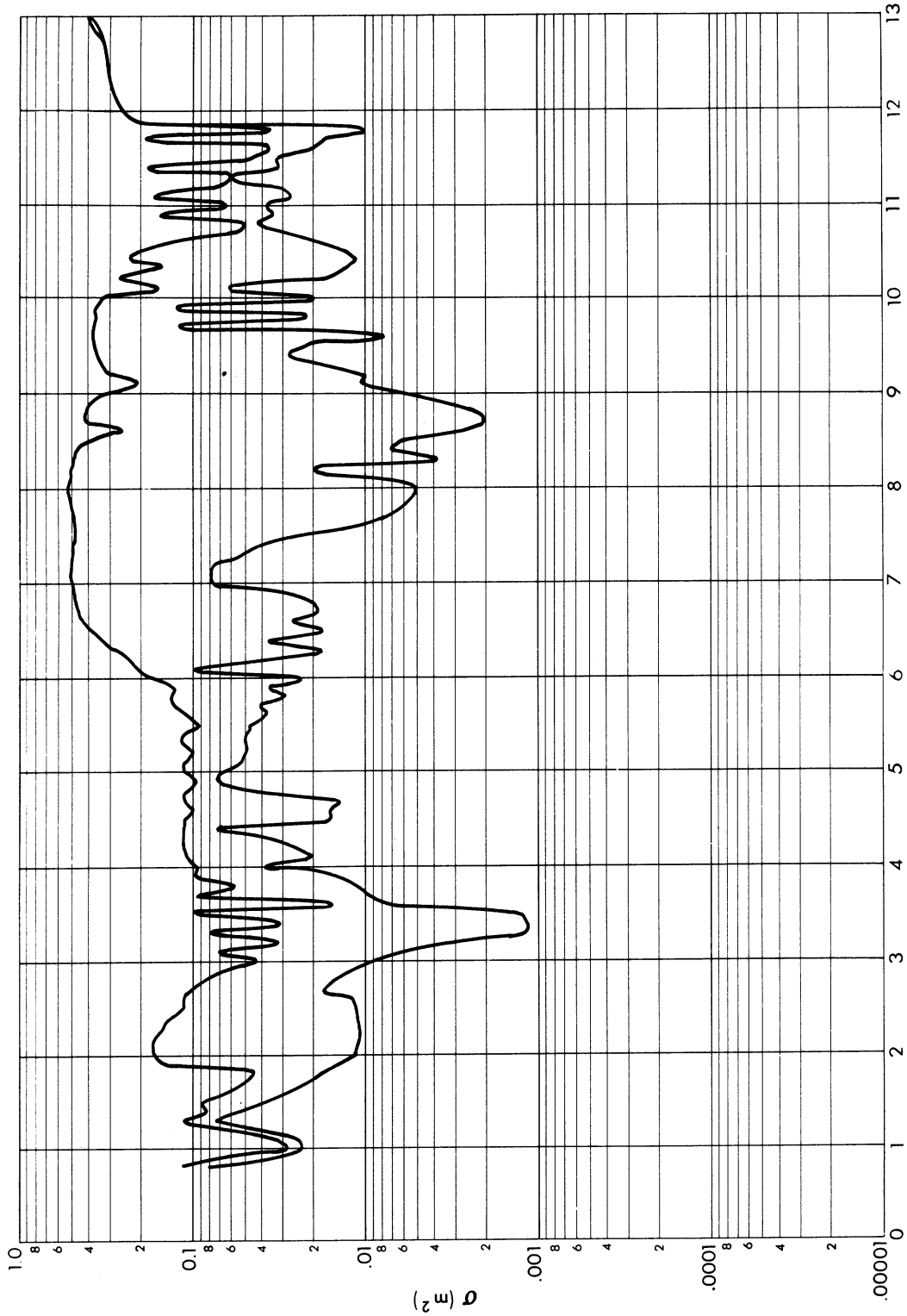

FIG. 6-8 RADAR CROSS-SECTION IN SQUARE METERS vs. ANGLE OFF NOSE
1/3 SCALE MODEL S-BAND MODEL "D" SQUARE FINS

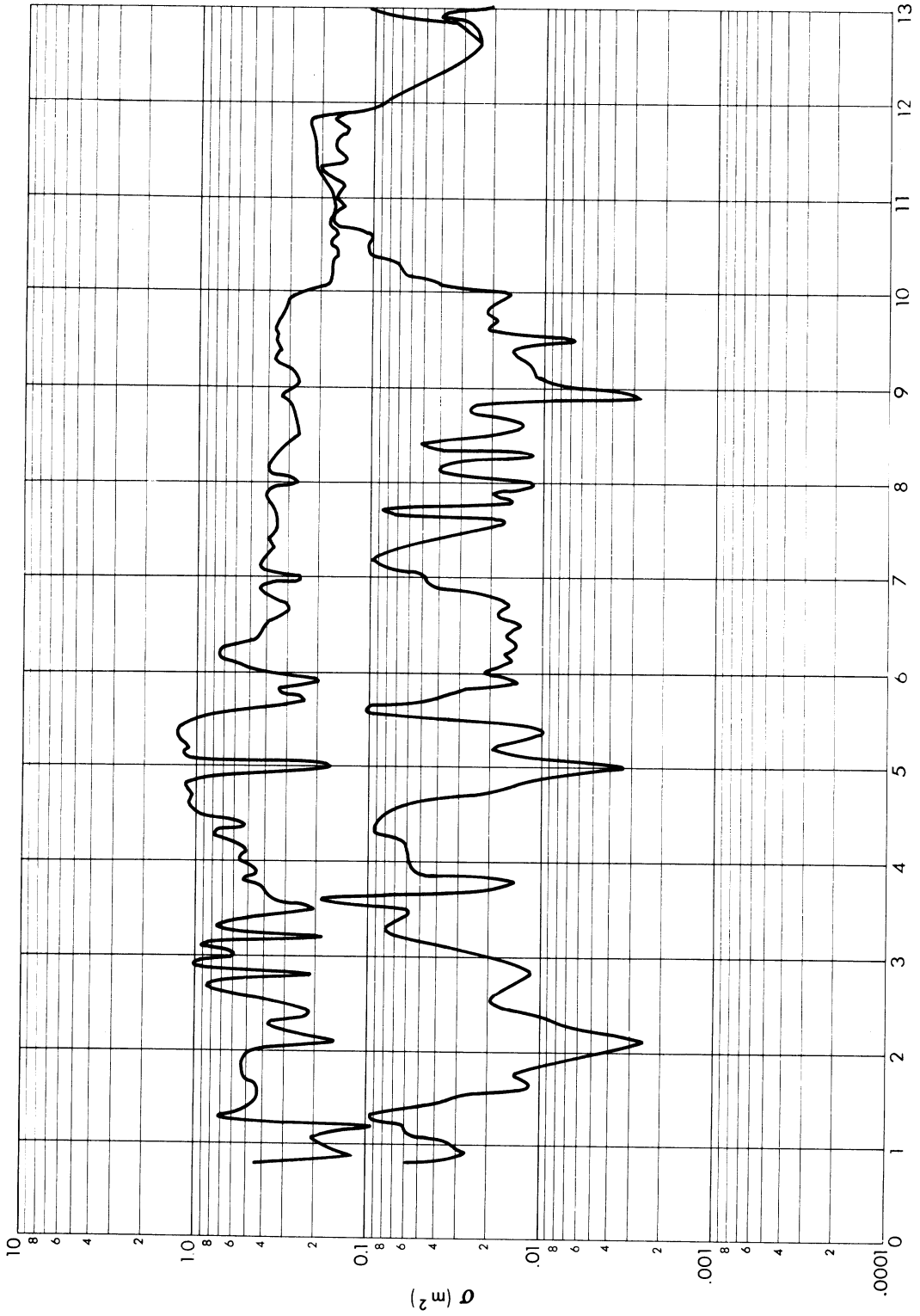

FIG. 6-9 RADAR CROSS-SECTION IN SQUARE METERS vs. ANGLE OFF NOSE
1/3 SCALE MODEL X-BAND MODEL "D" SQUARE FINS

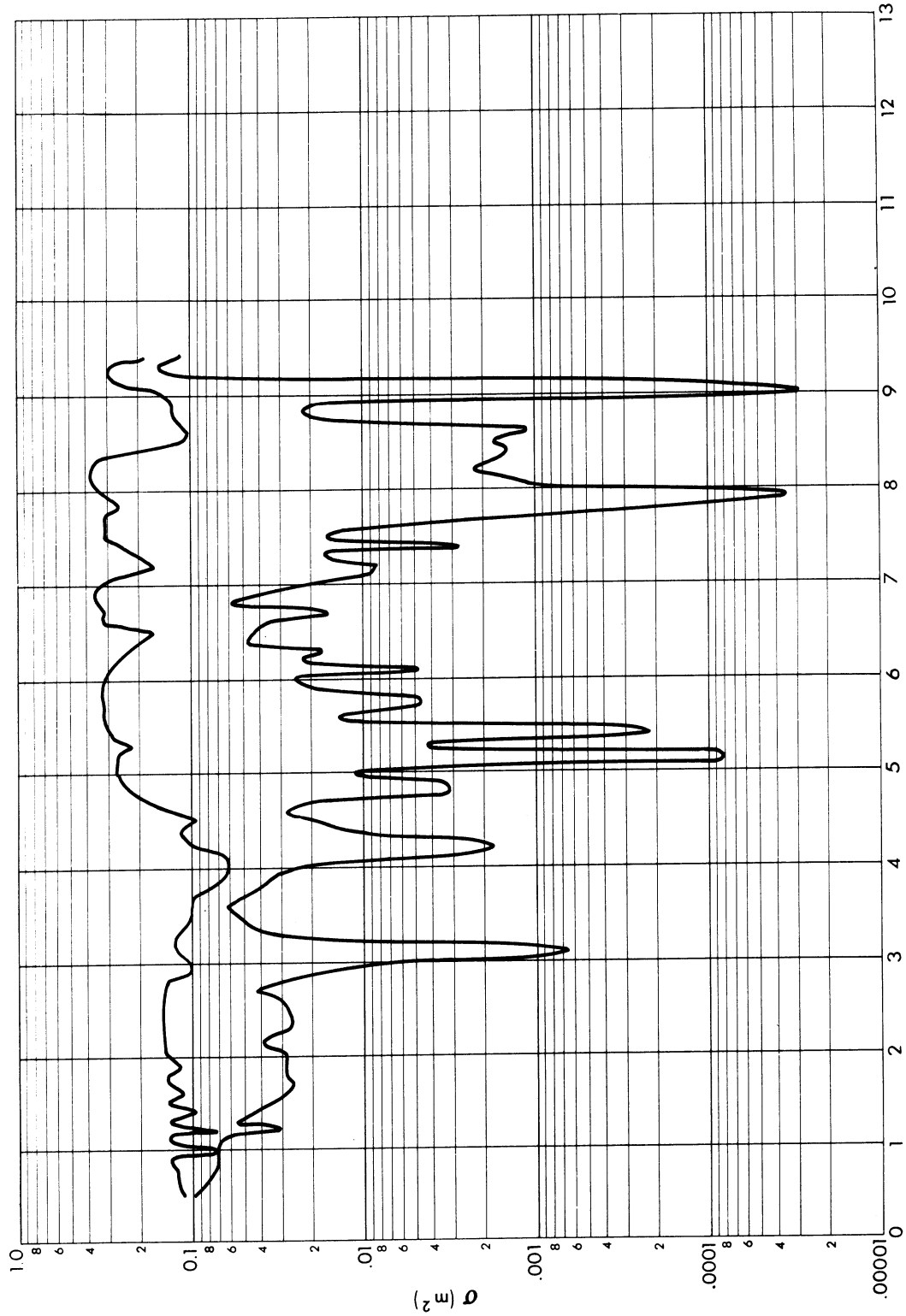

FIG. 6-10 RADAR CROSS-SECTION IN SQUARE METERS vs. ANGLE OFF NOSE
1/3 SCALE MODEL S-BAND MODEL "E" SQUARE FINS

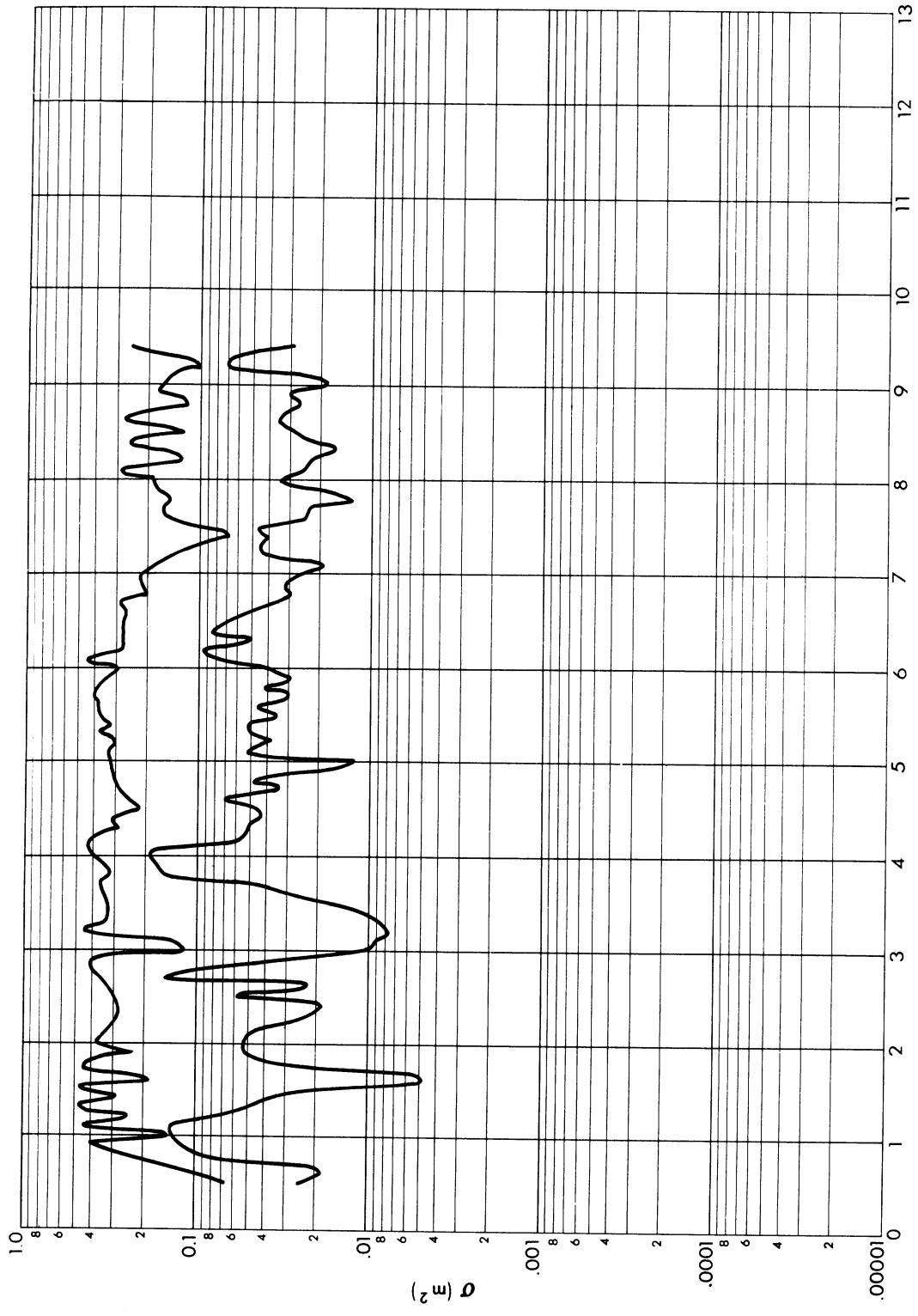

FIG. 6-11 RADAR CROSS-SECTION IN SQUARE METERS vs. ANGLE OFF NOSE
1/3 SCALE MODEL X-BAND MODEL "E" SQUARE FINS

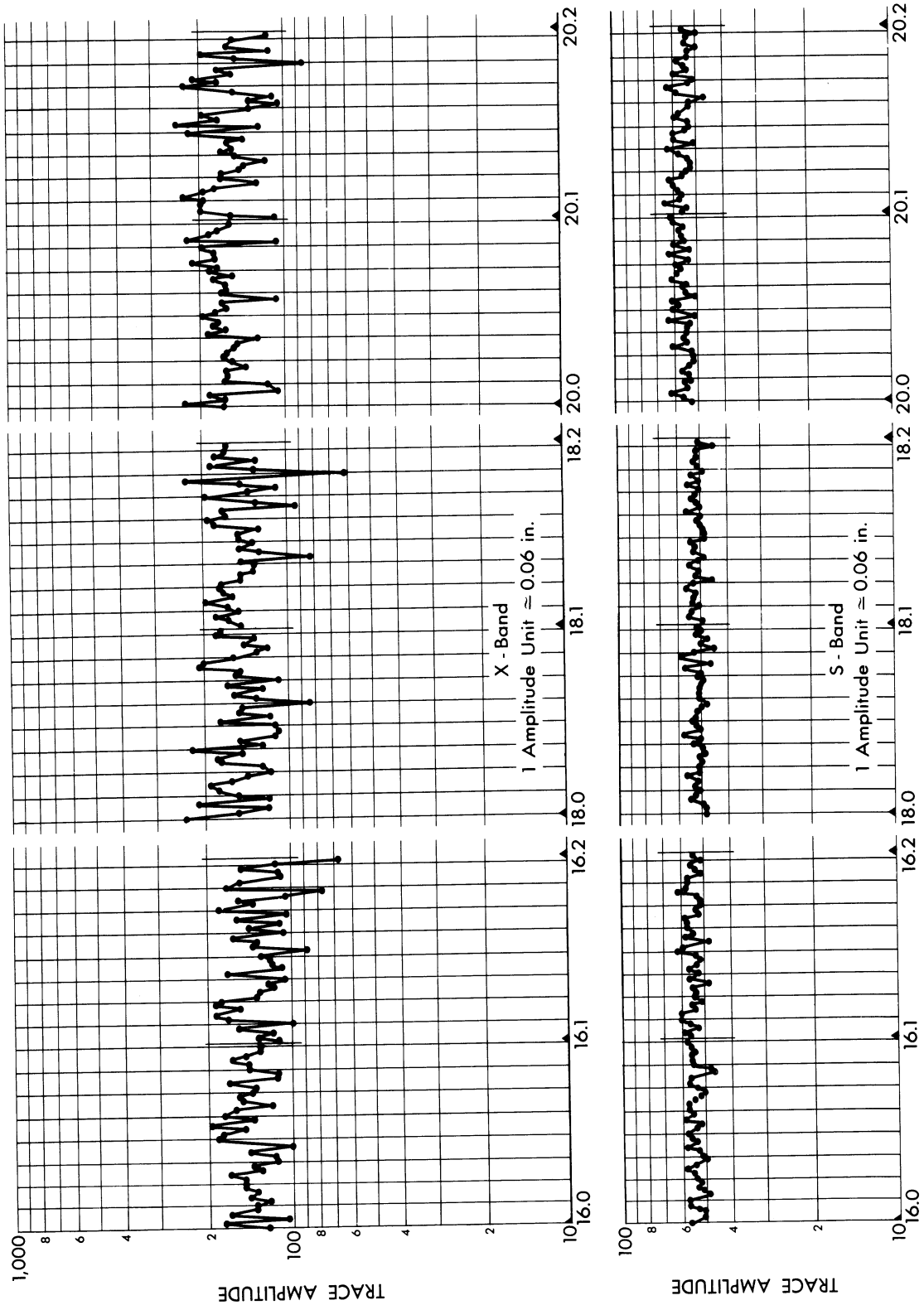

FIG. 6-12 A-SCOPE AMPLITUDE vs. TIME FOR SPHERE 18

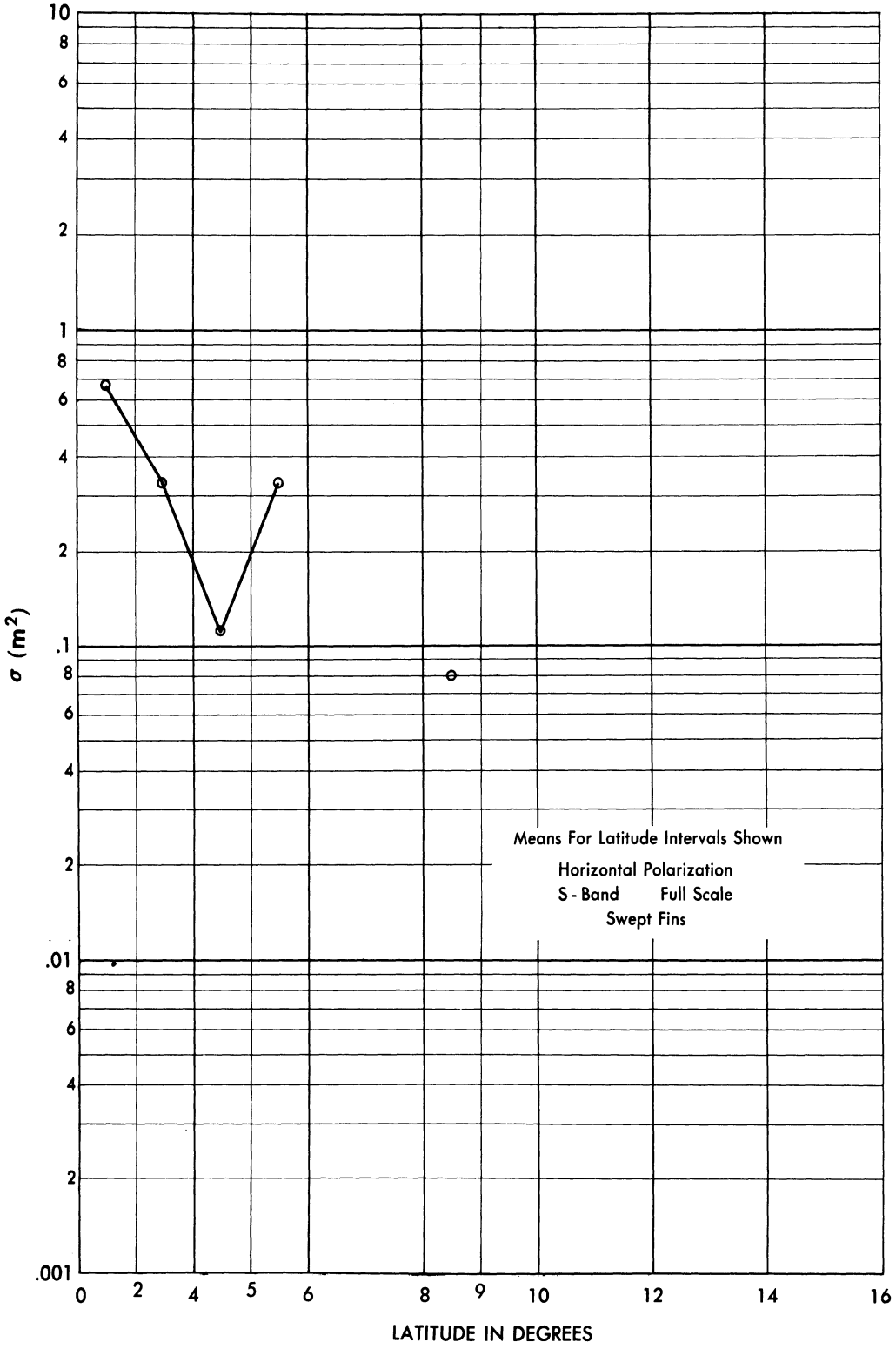

FIG. 6 - 13 MEAN CROSS-SECTION vs. LATITUDE ANGLE

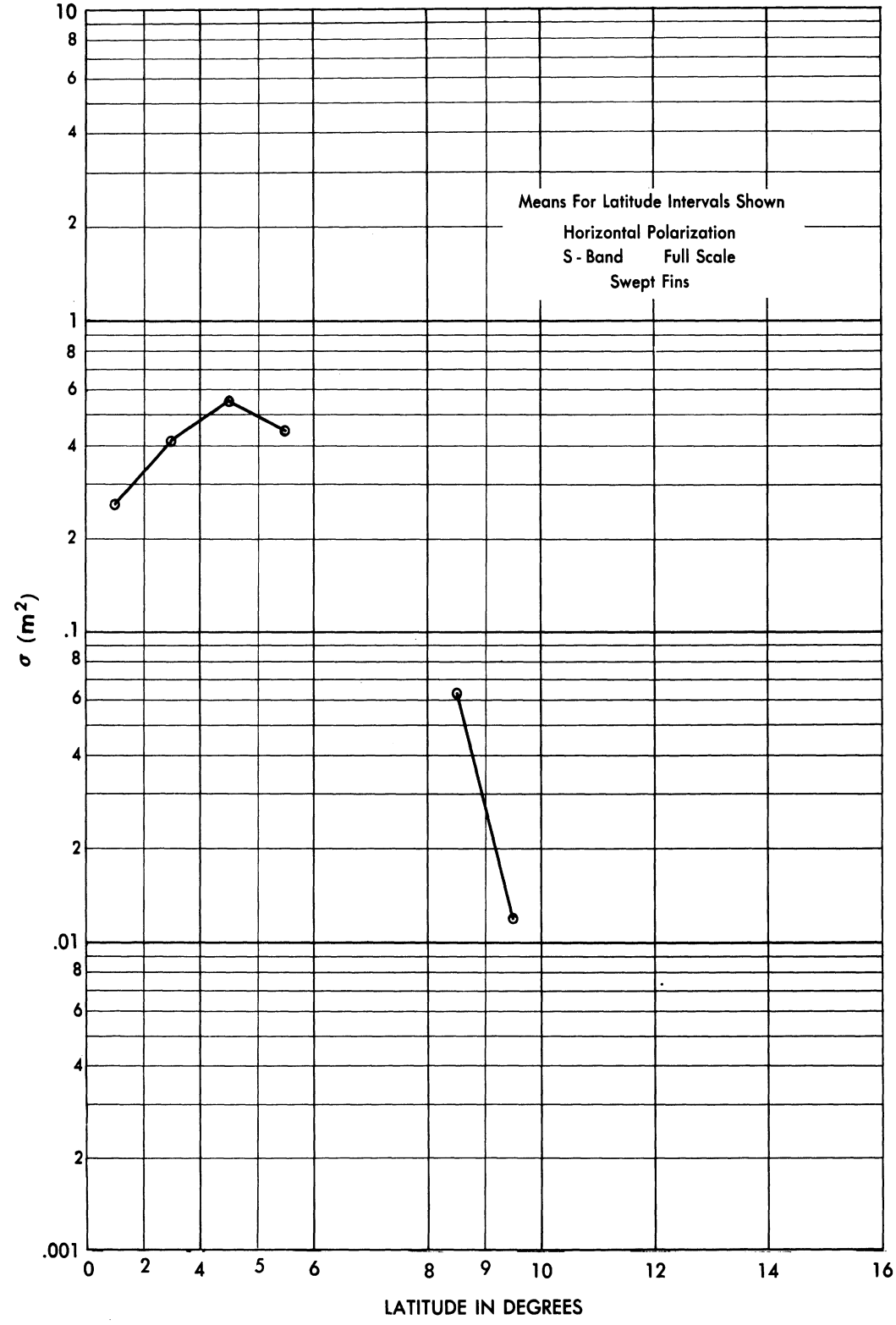

FIG. 6 - 14 MEAN CROSS-SECTION vs. LATITUDE ANGLE

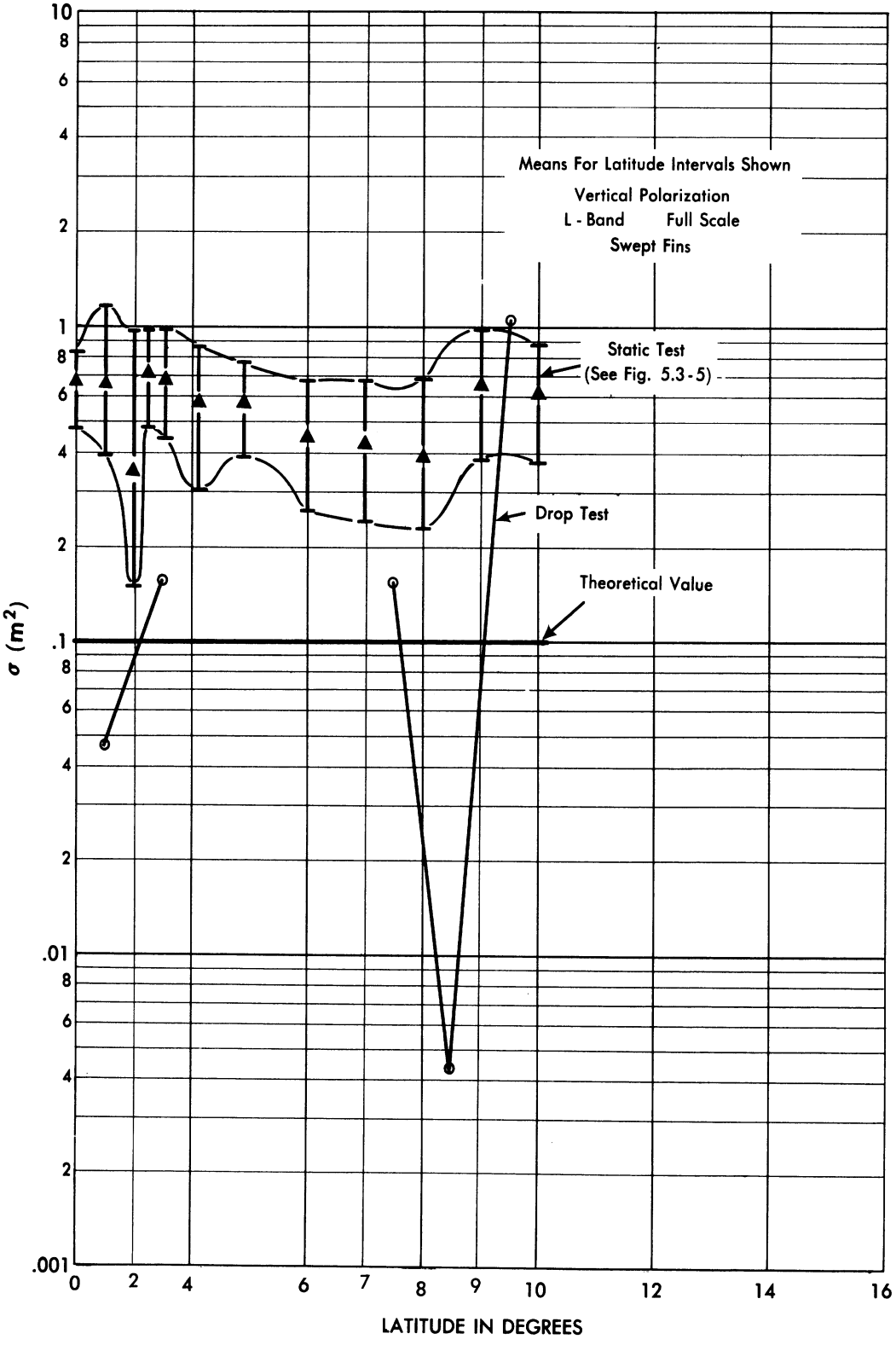

FIG. 6-15 MEAN CROSS-SECTION vs. LATITUDE ANGLE

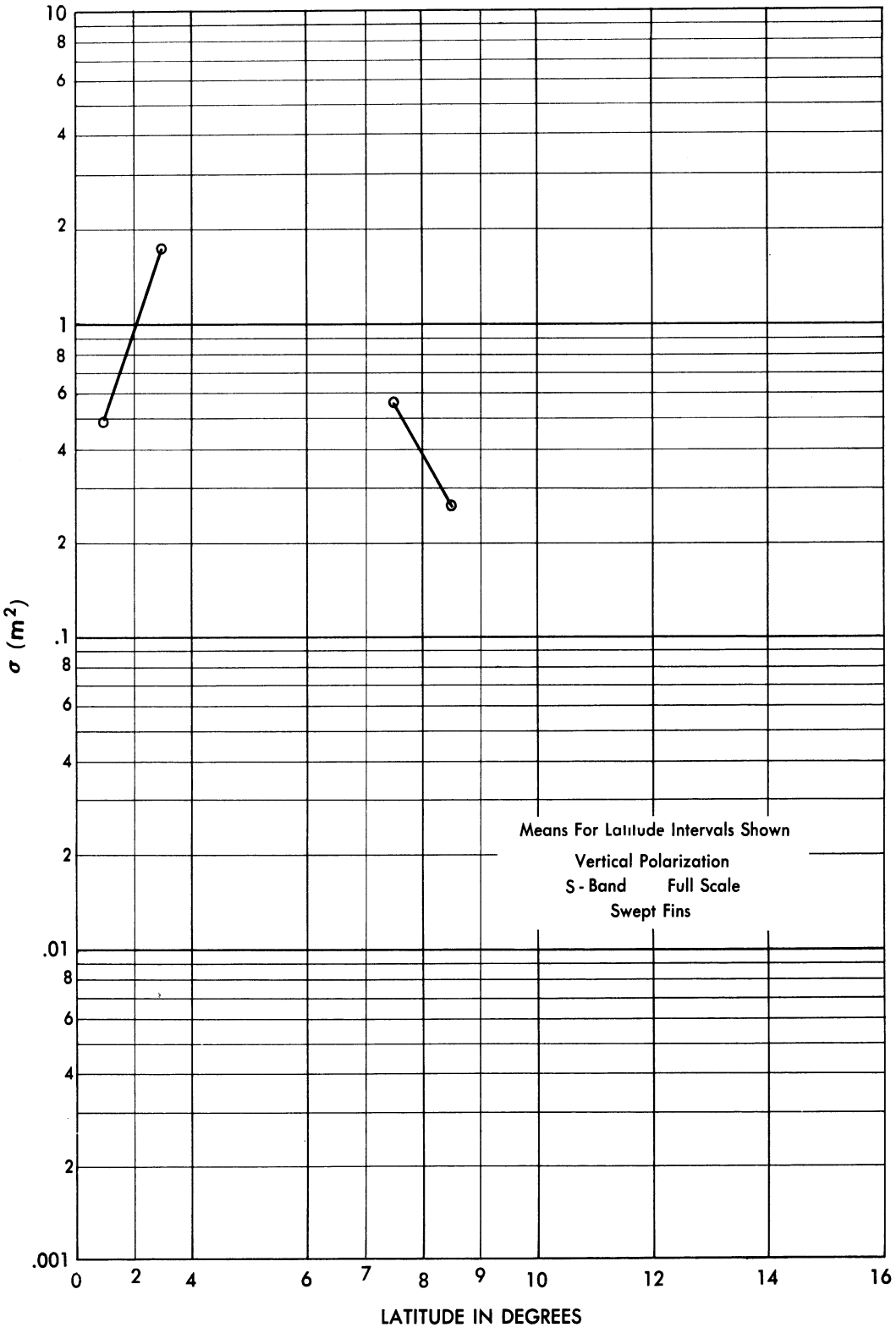

FIG. 6-16 MEAN CROSS-SECTION vs. LATITUDE ANGLE

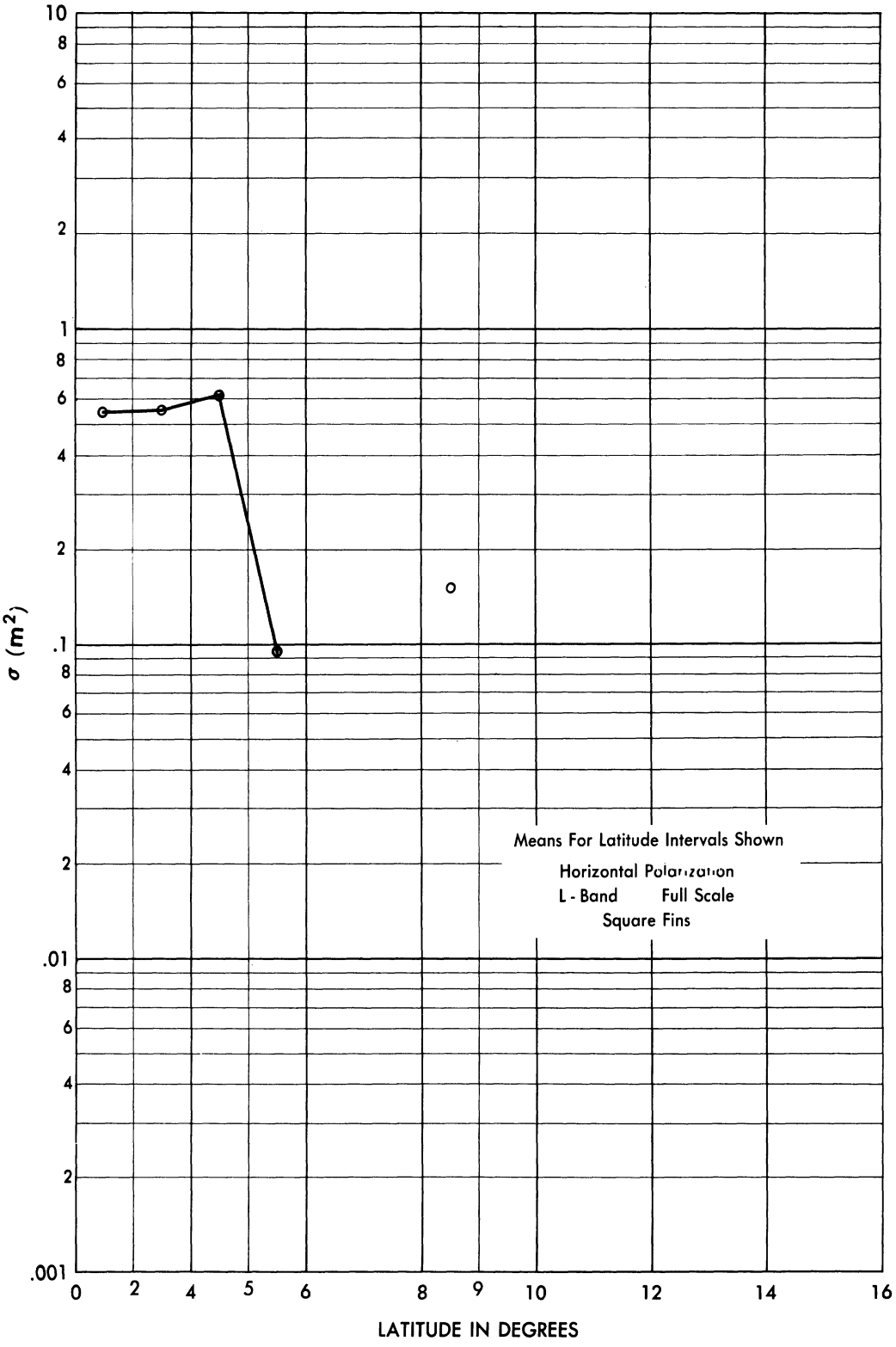

FIG. 6 - 17 MEAN CROSS-SECTION vs. LATITUDE ANGLE

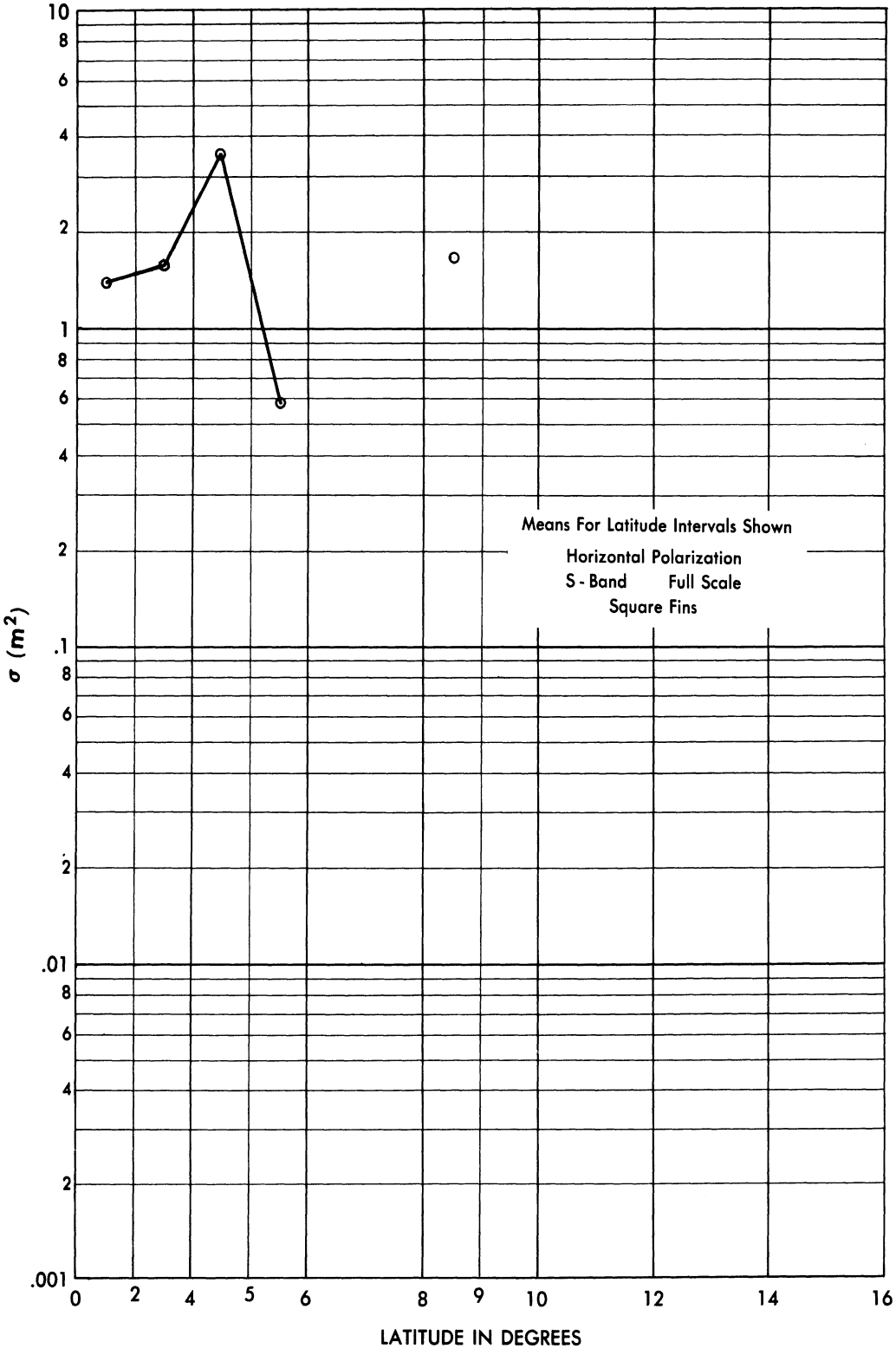

FIG. 6-18 MEAN CROSS-SECTION vs. LATITUDE ANGLE

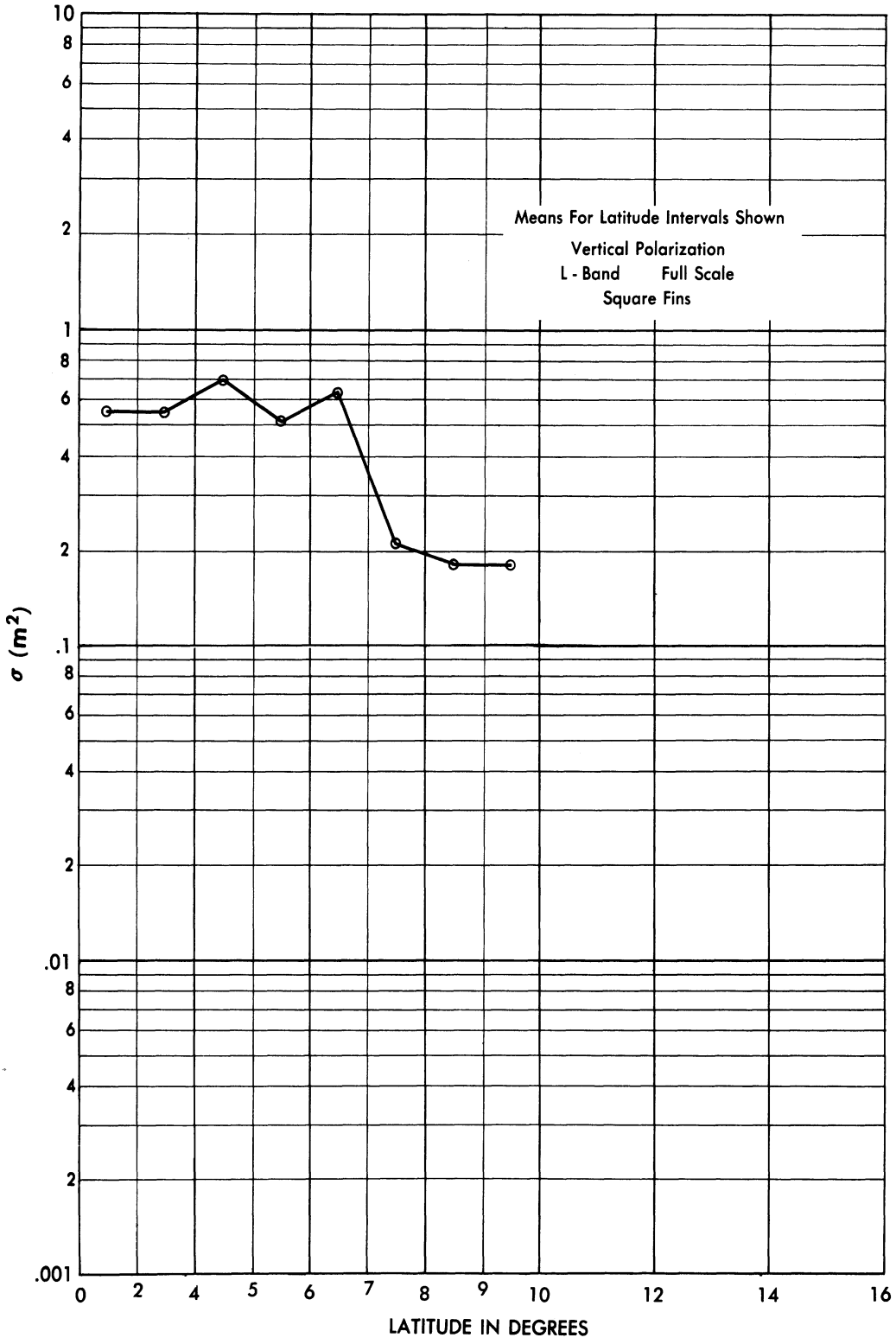

FIG. 6-19 MEAN CROSS-SECTION vs. LATITUDE ANGLE

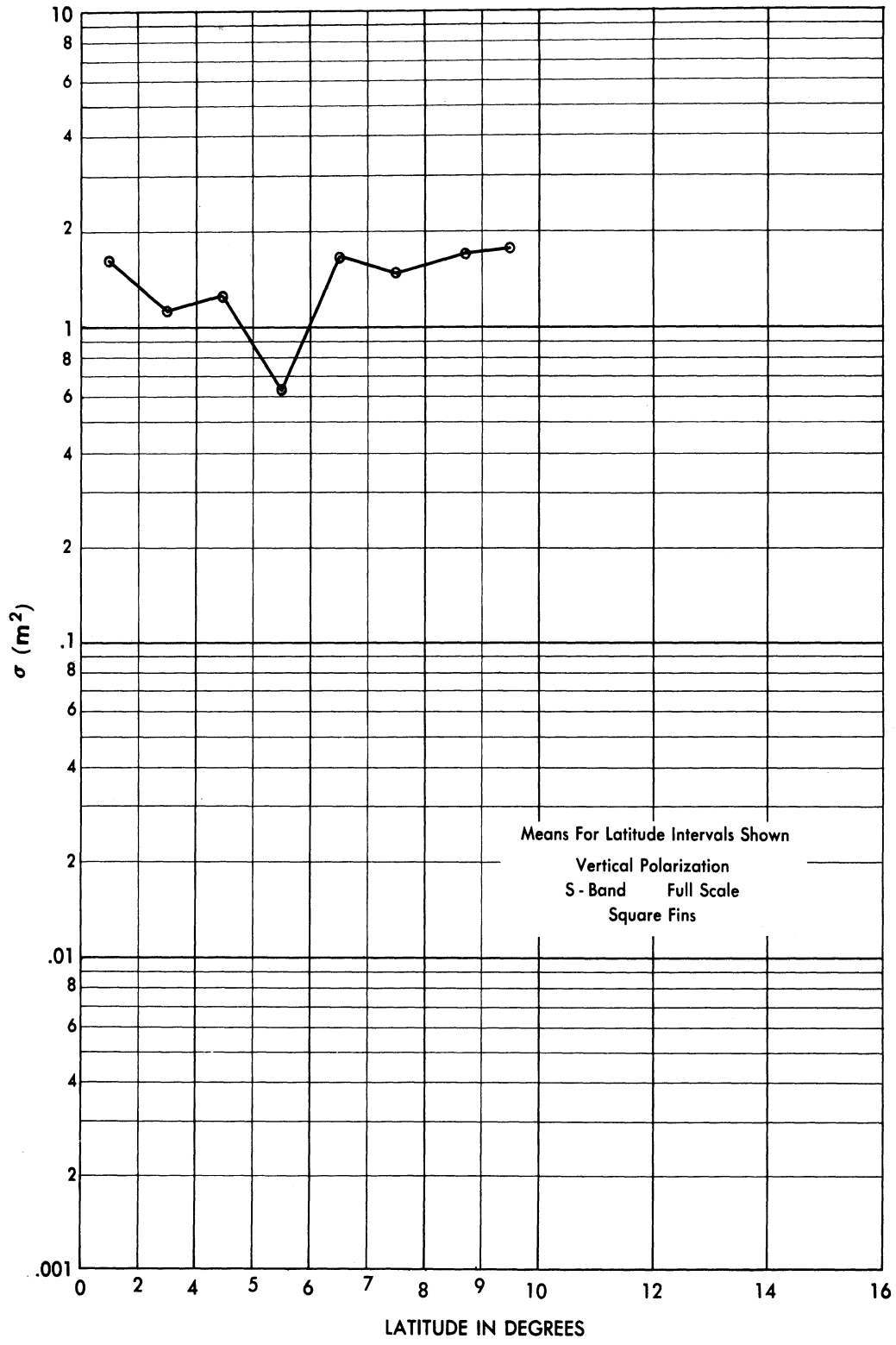

FIG. 6-20 MEAN CROSS-SECTION vs. LATITUDE ANGLE

6.2 Other Dynamic Experiments: Aspects Other than Nose-on

The Naval Research Laboratory, Washington D.C., has conducted dynamic measurements of V-2 cross-sections (Ref. 19 and 55). Measurements were made at White Sands, New Mexico between 20 February and 17 April 1947 employing an SCR-270 radar. Values of cross-section were obtained by comparison with the cross-section of a balloon covered with wire mesh. The conclusions reached from this test were (Ref. 19):

> "At 100 Mc the V-2 missile has a peak radar area of 150 square meters and shows a fluctuation of about 3 db before fuel cut-off. An accurate knowledge of the ground reflected energy might reduce this value to between 25 and 65 square meters. After fuel cut-off, the peak radar area varies from 0.3 square meters to 3 square meters and fluctuates more than 10 db."

Tests were also conducted at White Sands by NRL on 27 May 1948. The measurements were made at 1250 Mc and at 2825 Mc. In describing the method of measurement, NRL states that (Ref. 55):

> "The antennas were pointed optically throughout the flight. The S-band antenna is an 8 ft. diameter parabolic dish with a small section cut off the top and bottom. The L-band antenna is a 4 ft. x 15 ft. parabolic section. The peak powers of both radars are nominally 750 kw. Both radars were pulsed at 120 c.p.s.
>
> "The received signals were recorded on two cameras per radar. The first camera, a 35 mm movie camera, recorded the A-Scope presentation. The second camera, a continuous film camera, recorded the amplitude of each pulse by the following method. The radar video is applied to the horizontal deflection plates of a CRT. There is no signal applied to the vertical deflection plates. The positive range gate pulse applied to the control grid of the CRT makes the spot visible only for the duration of the pulse. Thus, horizontal deflection is only visible when a signal is in the range gate. The vertical travel of the film serves

to separate on the film the individual appearances of the range gate.

"Time was recorded on each film by means of seconds counters within view of the cameras. A fifth camera recorded a dial box showing time, range, bearing and elevation.

"The output of a calibrated signal generator was also recorded on the A-Scope and continuous films. In order to convert received signal into radar area, the various radar parameters were measured before the flight."

The results obtained from these tests were (Ref. 55):

"At 1250 Mc, the radar area was frequently of the order of one square meter. This value is verified by the upward portion of the trajectory and by the general level when the rocket was tumbling downward.

"The conclusions obtained at 2825 Mc were not nearly so definite. A tail view of the rocket after fuel cut-off gave values of radar area between 10 and 300 square meters. The tumbling period after blowoff indicated that the usual level considering all aspects is below 40 square meters."

VII

THEORETICAL CALCULATIONS AND COMPARISONS WITH EXPERIMENT

7.1 Approximate Methods

7.1.1 The Physical Optics Approximation

During World War II, Dr. R. Spencer, now of the Cambridge Research Center, generalized and simplified the methods for applying physical optics to electromagnetic scattering problems (Ref. 54). This procedure was originally proposed by Kirchhoff and later criticised by Poincaré (see Ref. 56). The major objections to applying physical-optics approximations to electromagnetic theory have been:

1. A shadow region is completely black according to Kirchhoff's theory whereas experiments show that such regions are not completely black.

2. The boundary between the "illuminated" and shadow regions is, according to Kirchhoff's theory, sharp and precisely defined. Again, experiment shows that there is no such definite boundary. Also, the concept of a sharp boundary around a black shadow region is untenable mathematically as it implies conditions on the total field which cannot be made consistent with the usual boundary conditions at the body and the radiation condition at infinity.

3. Since Kirchhoff's approximations were used and derived for optical problems where the wavelength (λ) of the radiation is small with respect to the characteristic dimension (ℓ) of the scatterer, it was felt such approximations would be poor in the resonance region, i.e., when $\lambda \approx \ell$.

The objections to using Kirchhoff's theory have not disappeared; however increased experience in the electromagnetic scattering field validates Spencer's methods. It is now known for example, that Kirchhoff's method predicts the exact solution for the scattering of electromagnetic waves by a paraboloid when the incident Poynting vector is on the axis of symmetry (Ref. 57). It is also known now that, for axially symmetric backscattering (Ref. 5) and for small angled cones in the bistatic case with the transmitter located on the axis of symmetry (Ref. 58), the Kirchhoff approximation is extremely close to the exact solution. (Note that this is in contradiction to 3.) Furthermore, a dihedral corner reflector with angle of separation between sides of π/n (n an integer), the Kirchhoff approximation is the exact result (Ref. 59). Agreement between Kirchhoff's theory and experiment even for such complex shapes as a B-47 at wavelengths from 3 cm to 5 meters is quite good (Ref. 60).

7.1.2 Conically Pointed Bodies

It was originally expected by Hansen and Schiff (Ref. 61) for physical reasons that, in the nose-on region, the cross-section of a semi-infinite cone and an ogive (the body described by the rotation of a circular arc about its chord) would be approximately equal if the nose angles were equal and the chord length exceeded λ. Similar reasoning would show that the radar cross-section of any rotationally symmetric pointed body which fitted within the cone tangent at the nose (a conically pointed body) whose contour curved smoothly into the shadow region before terminating could be approximated in the nose-on region by the cross-section of the semi-infinite cone whenever the length of the body was large with respect to the wavelength. The validity of this approach is exemplified by the experiments of Sletten (Ref. 62) for ogives. He obtained excellent agreement between both the theoretical and experimental cross-section of the ogive and the theoretical cross-section of the semi-infinite cone.

There has always been some uncertainty as to the validity of the physical optics approximation for a finite cone because of the circular discontinuity of "zero" dimensions at the base and because when the length of the finite cone is large with respect to the wavelength, its predicted physical optics cross-section in the nose-on region appeared to be so much larger than that for an infinite cone. Specifically

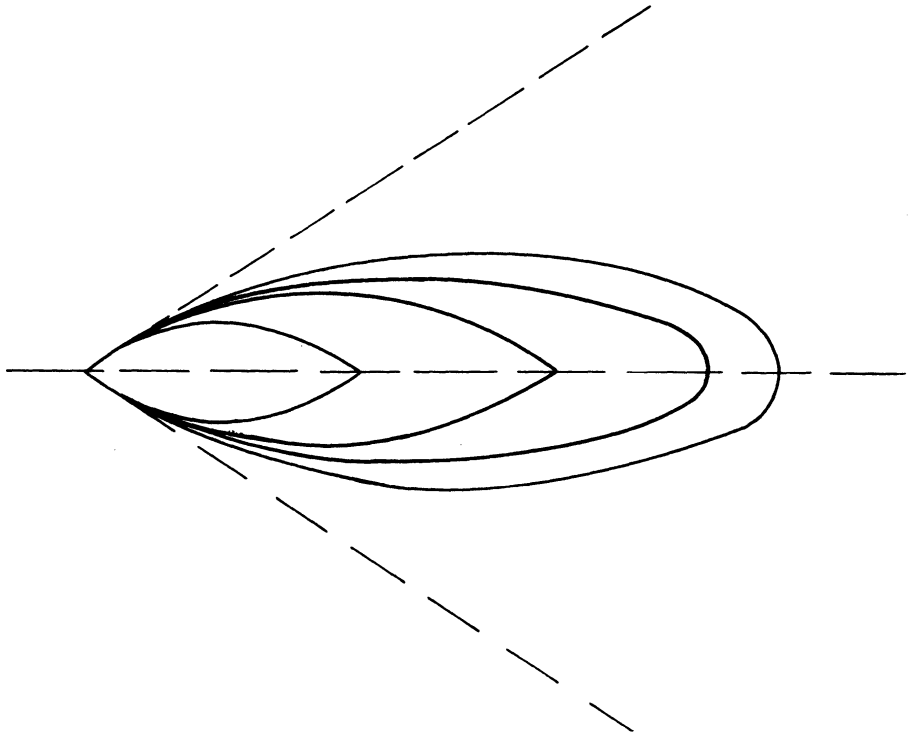

FIG. 7.1-1 CONICALLY POINTED BODIES

$$\sigma_{\infty \text{ cone}} \approx \frac{\lambda^2 \tan^4 \alpha}{16\pi} \qquad \sigma_{\substack{\text{finite} \\ \text{cone}}} \approx \pi H^2 \tan^4 \alpha \ ,$$

where H = length of finite cone, and $\alpha = \frac{1}{2}$ cone angle.

However, static experimental data obtained by the Federal Telecommunications Laboratories (Ref. 34) show that the physical-optics approximation is fairly close to being correct for the finite cone (Fig. 7.1-2). The theoretical curve shows marked oscillations whereas the experimental curve does not. The nulls of the static measurement are not as deep and the values of σ are generally slightly higher than those of physical-optics theory. Experience has shown that most recording devices tend to smooth over the nulls and hence that the physical-optics nulls could easily be more representative of the true situation. In any case, it seems clear that the physical-optics result is not inconsistent in predicting the amplitude of peaks. The experimental results indicate that the nose-on σ predicted for the finite cone by physical optics is either right or too small. It certainly is not too large as had originally been believed. This shows the great difference between having an abrupt termination of a body in the edge of the "lighted" region as compared with having it well into the "shadow" region.

7.1.3 Other Bodies

For several shapes, such as the circular flat plate (Ref. 63), the physical-optics approximations are quite good even in parts of the Rayleigh region ($\lambda >> \ell$) where σ is proportional to λ^{-4}. For those shapes for which physical optics gives poor results in relation to the exact theoretical solution in the resonance region, such as the sphere and the prolate spheroid (Ref. 64), other methods of approximation must be used. For example, it now appears as though wire theory (Ref. 65) making use of the new tables for thin wires (Ref. 66) makes it possible to predict the successive maxima in the σ versus $\frac{\ell}{\lambda}$ curve. A knowledge of the σ of the sphere, the σ of a 10/1 prolate spheroid, and wire theory will probably make it possible to predict the cross-sections of most other prolate spheroids.

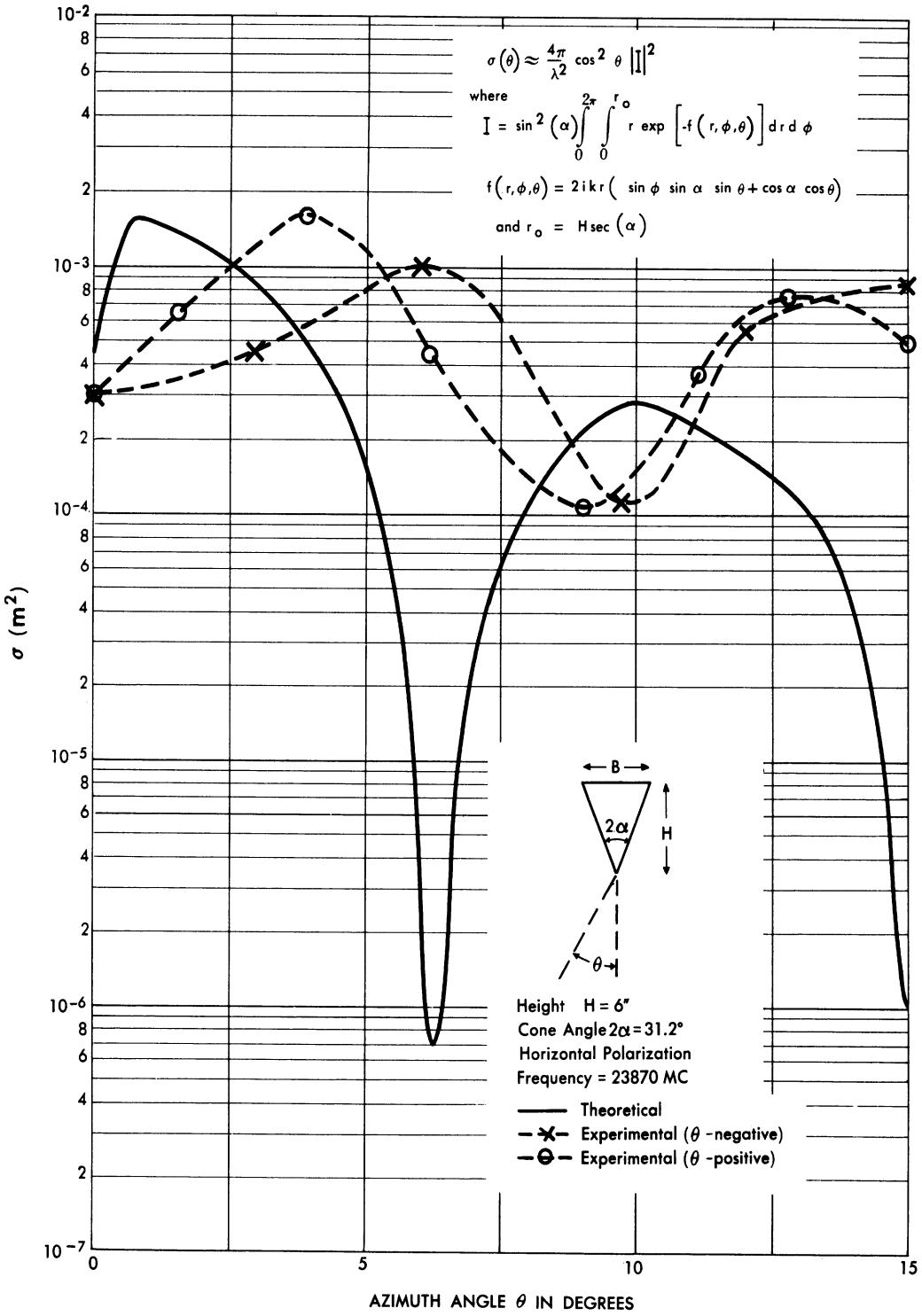

FIG. 7.1-2 ECHOING AREA OF A CONE

7.1.4 Approximation for the V-2

The physical reasoning which allows an ogive to be approximated by a semi-infinite cone in the nose-on region, similarly allows certain kinds of fins to be approximated with a section of an infinite wedge. Other types of fins can be replaced by finite cylinders with radii of curvature both large and small with respect to the wavelength. From theoretical considerations the fin contribution as a function of the wavelength will be considered to be in the form

$$\sigma_{fin} = k_1 \lambda^n, \text{ where } n \leq 2, \text{ and } k_1 \text{ is independent of } \lambda.$$

For off nose-on incidence, if the radius of curvature of the edge of the fin is small with respect to the wavelength, $n \approx 2$; if the radius of curvature is large with respect to the wavelength, $n \leq 1$. Since, in most cases, the V-2 body configuration is similar to that of an ogive, $\sigma_{\text{body (no fins)}} = k_2 \lambda^2$, where k_2 is independent of λ.

Since n can be less than 2 for the fins, it becomes clear that at large wavelengths the body contribution to σ may dominate while at small wavelengths the fin contributions might easily dominate.

In the resonance region other types of approximations must be used. One of these methods (successfully used by Franz and Depperman, Reference 67, for the cylinder), based on the interference of a specularly reflected wave with an exponentially damped wave which has crept around the object, has been used for missile cross-sections in the resonance region.

On the basis of the above arguments, the variation of the V-2 cross-section with frequency should appear as shown in Figure 7.1-3.

The question remaining is that of determining the constants k_i. (Region "A-B" would not exist if $k_2 \ll k_1$.) "Best fit" curves to the experimental data shown in Figure 2-2 imply that a region may exist. "Best fit" curves indicate that V-2 nose-on cross-sections depend on an exponent between one and two. Many laws, varying in accuracy and

convenience of application with different exponents and constants, can be arrived at on the basis of the available data. For example, in the wavelength region $0.3 < \lambda < 5$*meters, a convenient "rule of thumb" of $\sigma = 1.2\lambda^{-2}$ has been used at WRRC for the nose-on cross-section of missiles of the V-2 class, with swept-back fins. Such laws will, in general, be of sufficient accuracy for first-order system design purposes and experimental work, providing care is used in applying them only in the appropriate wavelength region and range of aspect angles and only to the particular class of missiles for which they are derived.

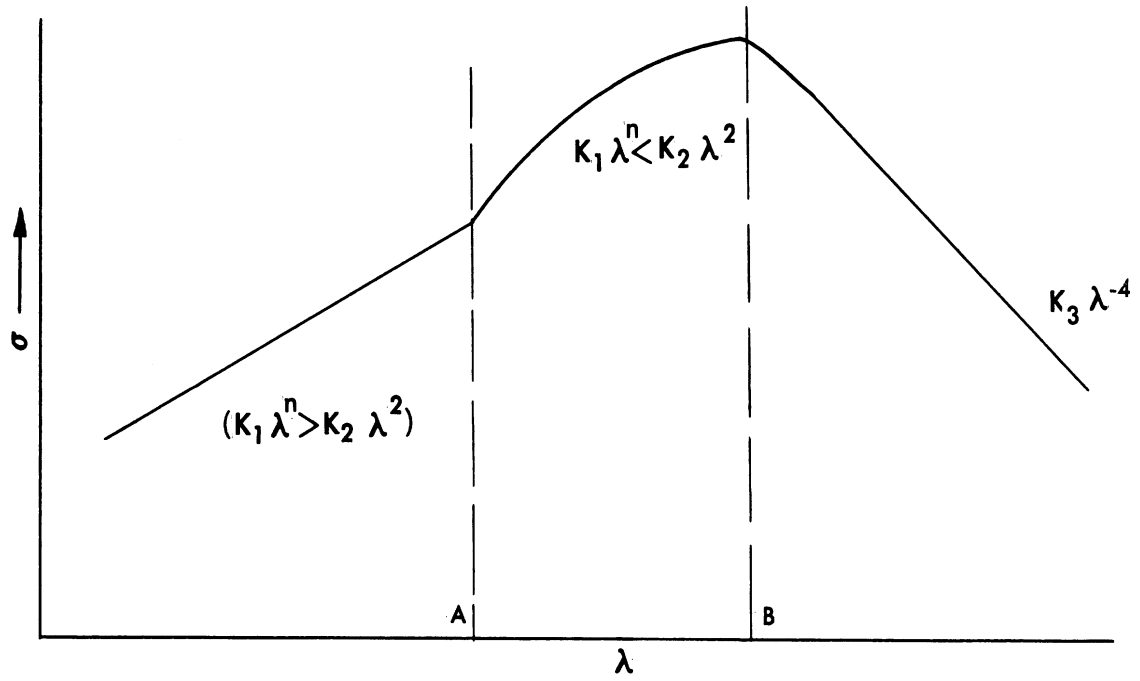

FIG. 7.1-3 GENERAL SHAPE OF V-2 CROSS-SECTION CURVE

*This explains why no comparison was made between theory and the dynamic experimental data for the smaller wavelength in Section VI. For small wavelengths, the cross-section must be approaching the optics answer. We can observe that the cross-sections at S- and L-bands are fairly close to each other and as a result it seems clear that the optics answer for a V-2 must be fairly close to the experimental S-band results obtained.

7.2 Atlas Type Missiles

Theoretical radar backscattering cross-sections have been computed for the 7-OC Atlas intercontinental ballistic missile (Fig. 5.1-1) at several frequencies between 25 and 1000 Mc. Cross-sections have been determined for the warhead alone; warhead with booster, and booster alone. In addition, the cross-sections of the "needle-nose" intercontinental ballistic missile (Fig. 5.2-2) have been computed.

7.2.1 Theoretical Calculations

7.2.1.1 Cross-Sections of the 7-OC Warhead Between 25 and 100 Mc

The final stage (warhead) of the Atlas ballistic missile has a length L, of about 20 feet and and average diameter of about 2 feet. Computations were made at wavelengths of approximately 40 feet (25 Mc), 13.3 feet (75 Mc), and 10 feet (100 Mc). The region of interest is one in which the quantity L/λ is approximately one and hence one in which the applicability of physical optics is doubtful.

A theory, which makes use of ideas similar to those presented by Franz and Depperman in their paper on the semi-infinite cylinder (Ref. 67) has been used to make an estimate of the Atlas warhead nose-on backscattering cross-section. Briefly, the theory involves considering the backscattering cross-section to be due to the sum of two contributions. One of the contributions is the radiation scattered from the first Fresnel zone on the body or, in the case of a pointed body, from the tip of the body. The other is due to radiation which creeps about the rear of the body and comes back to interfere with or add to (depending on the relative phase) the radiation scattered from the forward part of the body. In the limit of small wavelengths, this latter contribution is negligible. However, in the resonance region under consideration, it is an important contribution. Thus, the oscillations in σ as a function of wavelength which occur for the nose-on cross-sections of a sphere and a prolate spheroid in the resonance region may be thought of as being due to the interference of the two contributions. At the peaks they are in phase and in the valleys they are 180 degrees out of phase. For a pointed body

with a well rounded rear such as the Atlas 7-OC warhead, the main contribution to the nose-on cross-section is the contribution of the radiation which creeps about the rear of the body and comes back in the forward direction, since the contribution from the tip is very small. An estimate of the magnitude of this contribution can be obtained from a knowledge of sphere cross-sections. Thus, by the above argument:

$$\sigma_{peak} = \left[A_{G.O.} + A_{rear}\right]^2$$

where σ_{peak} is the sphere cross-section at a peak in the resonance region, $A_{G.O.}$ is proportional to the field amplitude due to the first Fresnel zone, and may be taken to be $\sqrt{\pi a^2}$, and A_{rear} is the contribution due to the radiation which creeps about the rear of the body. Values for σ_{peak} may be read off existing graphs such as the one in Kerr (Ref. 68) and the above equation may be solved for A_{rear}. This procedure indicates that $(A_{rear})^2$ is equal to $.033\lambda^2 \sqrt{\lambda/a}$. By setting a = 2 feet (the approximate radius of the rear bulb of the warhead), values of σ of 1.5 square meters and 0.8 square meter are obtained for the nose-on cross-section of the Atlas at 75 and 100 Mc respectively.

For off-nose aspects for 75 and 100 Mc, the results of thin wire theory were applied. At 75 Mc, $L/\lambda \cong 1.5$ and at 100 Mc, $L/\lambda \cong 2$. Curves for these cases drawn in Reference 65 were used to determine the cross-sections.

Although the experimental data for a V-2 for the $L/\lambda = 1$ and $L/\lambda = 2.5$ cases (Ref. 48) do not involve the specific ratios under consideration, the data for these V-2 cases can be used as a guide to the order of magnitude of the cross-section to be expected for off-nose aspects at 75 and 100 Mc for the Atlas 7-OC warhead. As the V-2 length is about twice that of the Atlas (the ratios of length to average diameter are about the same), the V-2 cross-sections were scaled down by a factor of four. In addition, the results for $L/\lambda = 1$ and $L/\lambda = 2.5$ were averaged for each aspect. This average curve was regarded mainly as a guide to the order of magnitude to be expected of the cross-section rather than the shape of the curves to be expected at 75 and 100 Mc.

Finally with the aid of the values computed, thin wire theory, and the experimental data for the V-2, judicious estimates were made as to the true cross-sectional curves at 75 and 100 Mc. These curves appear in Figure 7.2-1.

Nose-on values for 25 Mc ($a/\lambda = .05$) cannot be obtained by the method used for 75 and 100 Mc as these values were derived with the aid of Kerr's curve from points for which $a/\lambda \geq 0.15$. For the sphere, $a/\lambda = .05$ is within the Rayleigh region and there is little scattering from the rear bulb. The scattering from the tip is also very small. The application of physical optics to a cone of dimensions approximating those of the warhead for $\lambda = 40$ feet yields $\sigma < 0.001$ square meter for a rounded base and $\sigma < 0.005$ square meter for a flat stern base.

For the estimation of the cross-section of the Atlas at 25 Mc, the experimental results for a thick wire for $L/\lambda = 0.5$ were used. The results, scaled by the factor $\left[\frac{L(\text{Missile})}{L(\text{wire})}\right]^2$, also appear in Figure 7.2-1.

7.2.1.2 Cross-Section of the 7-OC Warhead Between 225 and 1000 Mc

Values of the cross-section for 225, 600, and 1000 Mc were computed by means of the methods of physical optics. The technique of polynomial approximation outlined in Reference 57 was used to obtain monostatic radar cross-sections at various aspect angles ranging from 0 to 50 degrees. The following table of values was obtained:

σ in square meters

	1000 Mc	600 Mc	225 Mc
0°	.28	.14	.26
5°	.089	.018	.18
15°	.014	.036	.079
30°	.018	.006	.19
50°	.071	.15	.11

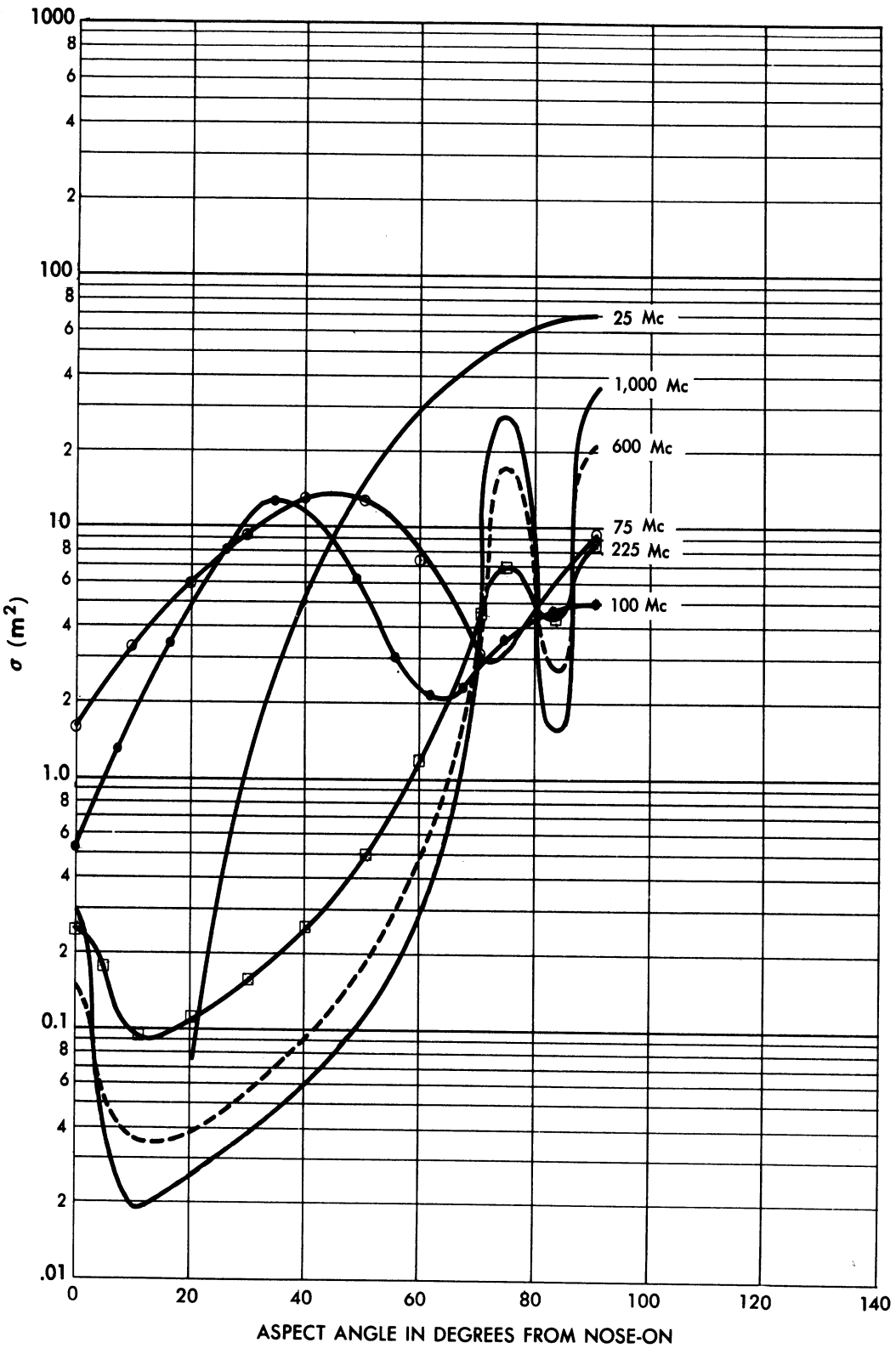

FIG. 7.2-1 THE THEORETICAL CROSS-SECTION OF THE 7-OC WARHEAD AS A FUNCTION OF FREQUENCY AND ASPECT ANGLE

For angles of incidence ranging from 75 to 90 degrees evaluation of the physical-optics cross-section by the technique of stationary phase (see Ref. 57) yielded the following values:

σ in square meters

	1000 Mc	600 Mc	225 Mc
75°	27.8	16.7	6.2
83°	1.5	2.5	3.3
90°	35.0	21.0	7.8

It is apparent from the first table shown that the cross-section is highly oscillatory in nature as is to be expected for a configuration such as the Atlas 7-OC warhead which consists of cones attached to cylinders. The contributions of the conical and cylindrical components to the cross-section alternately cancel and reinforce each other. In addition, study of the physical-optics cross-sections of cones and cylinders indicates that each of the individual contributions of the conical and cylindrical sections oscillates in magnitude. It would be highly desirable to use a technique whereby the averaged value (i.e., averaged over an oscillation period) of the cross-section may be obtained easily. Therefore, the methods of stationary phase outlined in Reference 57 were used to obtain formulas for the cross-section of the conical and cylindrical components. These values for the cross-section contributions were added assuming arbitrary phase (i.e., assuming all possible phases equally likely). These results also appear in Figure 7.2-1.

It is important to remember in using Figure 7.2-1 that the oscillations have been averaged out. Although the cross-section for the most part is expected to remain within a factor of 10 of these curves, there may be points at which nulls occur. The stationary phase formulas from which the curves are derived appear in Section 7.2.1.5.

7.2.1.3 Cross-Section of the Atlas Booster

The radar cross-section of the Atlas 7-OC Booster (see Fig. 5.1.1) has been computed by the method of physical-optics. Curves of the cross-section of the booster at 1000, 600, and 225 Mc are shown in Figure 7.2-2. To compute the near nose-on cross-sections, it was assumed that the total energy scattered from the interior was in equilibrium with the amount incident upon the nose aperture. In addition, a cos θ directional dependence was assumed. For the purposes of a rough estimate, this assumption was deemed adequate.

In addition, the composite cross-sections of the warhead attached to the booster for 1000, 600, and 225 Mc were computed as shown in Figure 7.2-3. As the interior of the booster is no longer visible, the first assumption concerning the nature of the interior of the booster is of no importance for these cases.

7.2.1.4 Cross-Section of the Needle-Nose Warhead

Values of the radar cross-section of the needle-nose warhead (Fig. 5.2-2) were also computed by the method of physical-optics. Curves of cross-sections at 1000, 600, and 225 Mc appear in Figure 7.2-4.

7.2.1.5 Stationary Phase Formulas Used in Atlas Computations

The formulas used in the stationary phase method of computing σ for the Atlas missile are listed in the section. In these formulas the symbols are defined as follows:

$$\beta = l_o + L_1 \frac{\tan\theta}{\tan\alpha - \tan\theta}$$

l_o = length of nose cone of missile warhead

L_1 = length of cylindrical section

$L - l_o$ = length of rear truncated cone

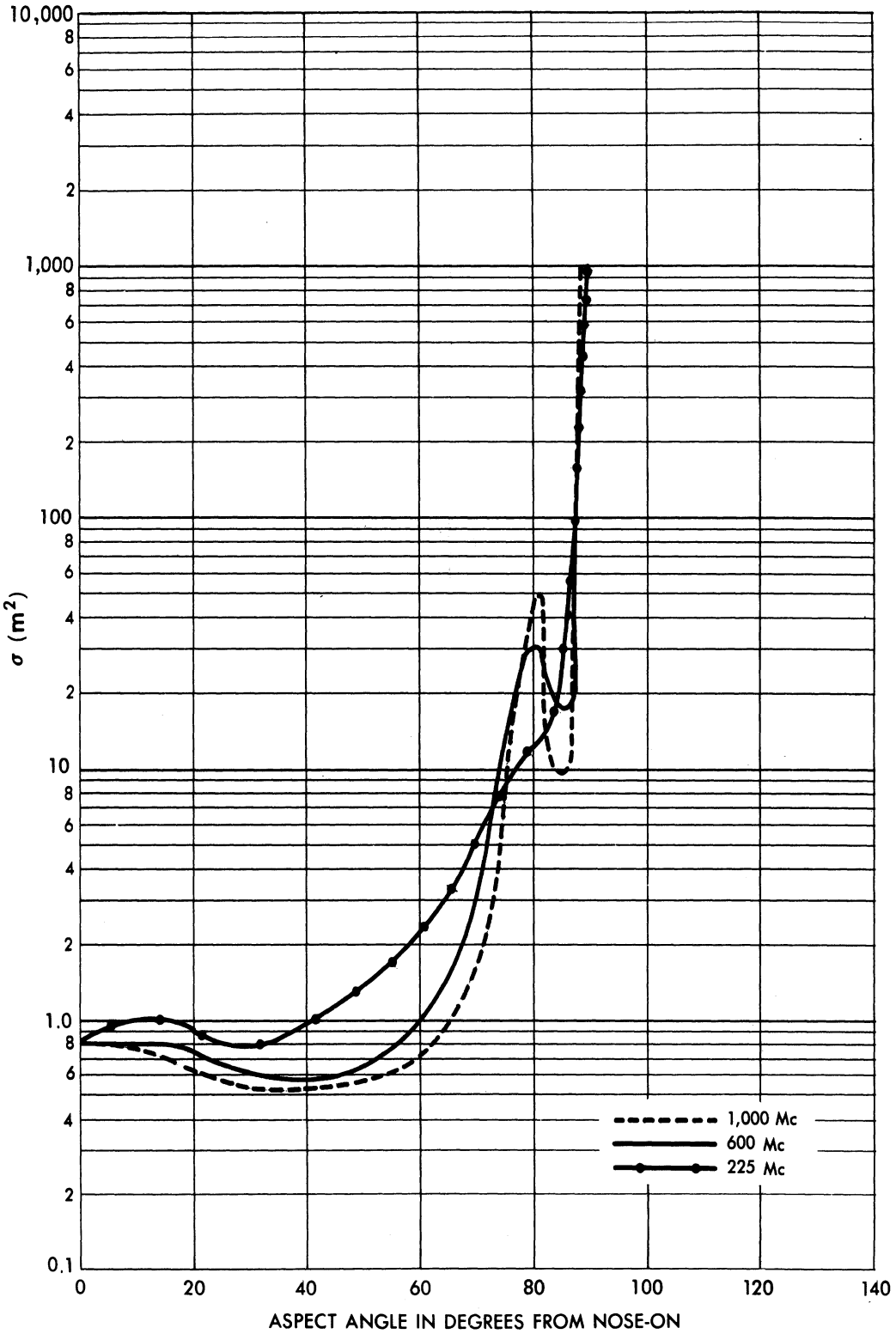

FIG. 7.2-2 THE THEORETICAL CROSS-SECTION OF THE 7-OC BOOSTER AS A FUNCTION OF FREQUENCY AND ASPECT ANGLE

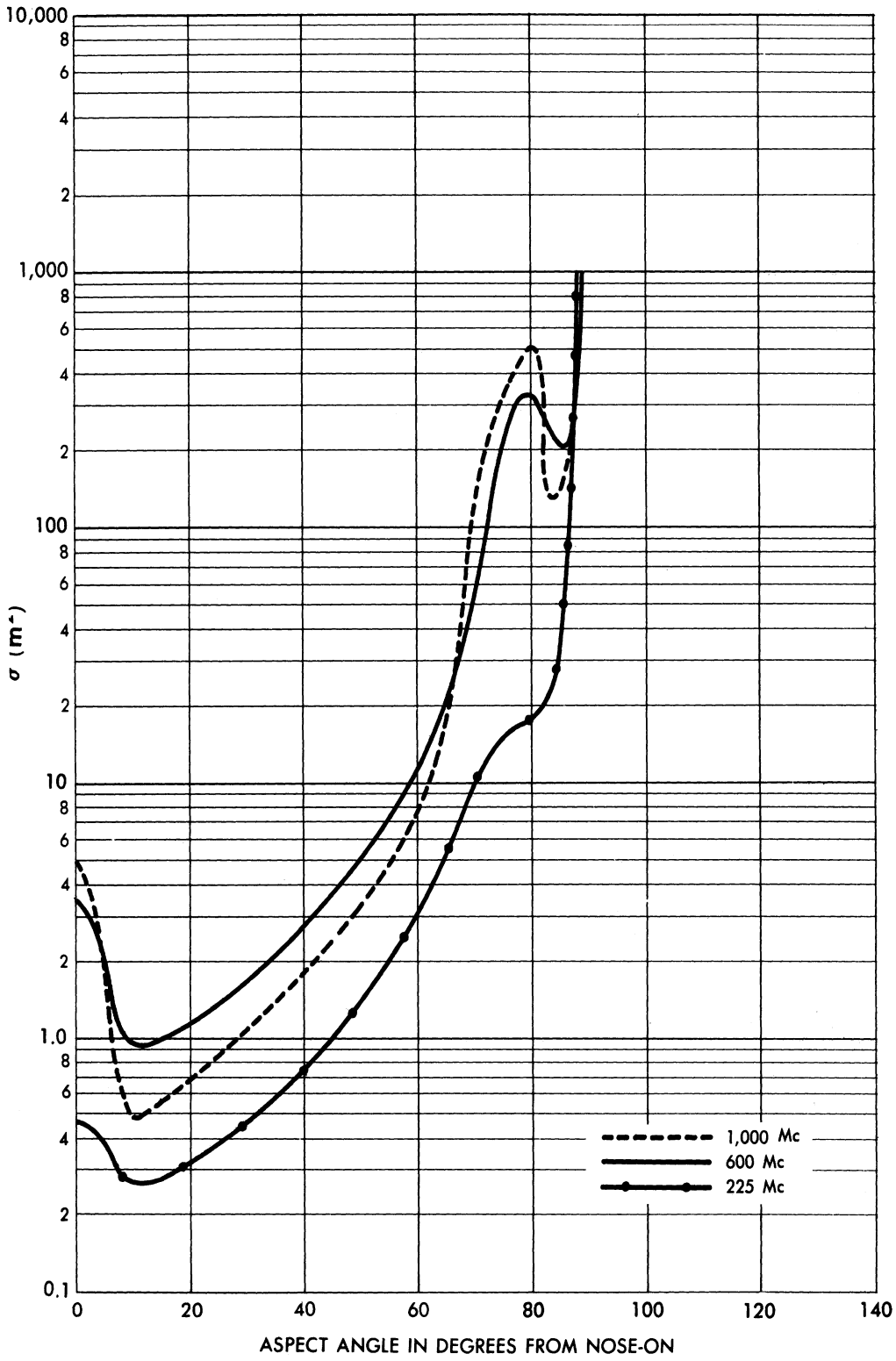

FIG. 7.2-3 THE THEORETICAL CROSS-SECTION OF THE 7-OC MISSILE (Warhead plus Booster) AS A FUNCTION OF FREQUENCY AND ASPECT ANGLE

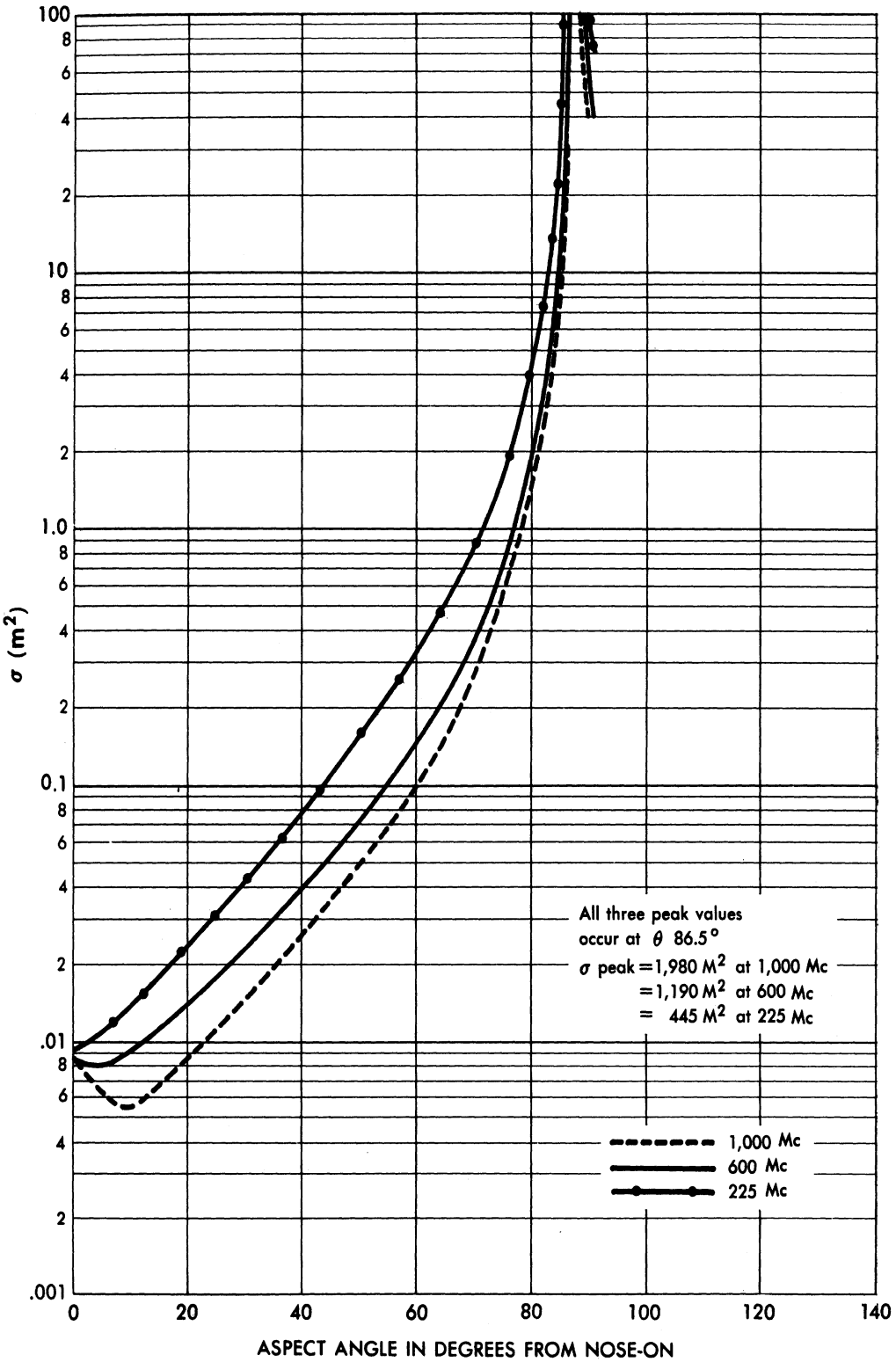

FIG. 7.2-4 THE THEORETICAL CROSS-SECTION OF THE "NEEDLE NOSE" INTERCONTINENTAL BALLISTIC MISSILE (Final Stage) AS A FUNCTION OF FREQUENCY AND ASPECT ANGLE

ρ = radius of cylindrical portion of missile

α = half cone angle which is 15° for the 7-OC warhead.

θ = angle of incidence

$U(x)$ = unit function $\quad U(x)=0 \quad x \leq 0$, $\quad U(x)=1 \quad x>0$

$k = 2\pi/\lambda$

Nose Cone Contribution

$$\sigma = \frac{4\pi}{\lambda^2} |g_1|^2$$

$$g_1 = \sqrt{\frac{\pi \tan \alpha}{4k^3 \sin\theta}} \left[i\, U(\alpha+\theta) \tan(\alpha+\theta)\, e \sqrt{l_o}\, \frac{2ikl_o\cos(\alpha+\theta)}{\cos\alpha} + U(\alpha-\theta) \tan(\alpha-\theta) \sqrt{l_o}\, e^{\frac{2ikl_o\cos(\alpha-\theta)}{\cos\alpha}} \right]$$

This formula is not valid for $\theta = 0^0$ and for $\alpha \pm \theta = 90^0$.

Cylinder Contribution

The physical optics contribution of the cylinder may be obtained exactly, but the stationary phase formula given here is a much simpler one to use computationally.

$$\sigma = \frac{4\pi}{\lambda^2} |g_2|^2$$

$$g_2 = \left(e^{2ikL_1 \cos\theta} - 1 \right) e^{-2ik\rho|\sin\theta|} \sqrt{\frac{\pi\rho|\tan\theta|}{4k^3\cos\theta}}$$

Shadowed Truncated Cone

$$\sigma = \frac{4\pi}{\lambda^2} \left| g_3 \right|^2$$

$$g_3 = \sqrt{\frac{\pi \tan \alpha}{4k^3 \sin\theta}} \left[i\, U(\alpha+\theta) \tan(\alpha+\theta) \left\{ \sqrt{L}\, e^{2ikL\cos(\alpha+\theta)} - \sqrt{\beta}\, e^{\frac{2ik\beta\cos(\alpha+\theta)}{\cos\alpha}} \right\} \right.$$
$$\left. + U(L-\beta)\, U(\alpha-\theta) \tan(\alpha-\theta) \left\{ \sqrt{L}\, e^{\frac{2ikL\cos(\alpha-\theta)}{\cos\alpha}} - \sqrt{\beta}\, e^{\frac{2ik\beta\cos(\alpha-\theta)}{\cos\alpha}} \right\} \right]$$

This formula is not valid for $\theta = 0^0$ and for $\alpha \pm \theta = 90^0$.

Averaged Cross-Section

$$\sigma_{\substack{\text{most} \\ \text{angles}}} = \frac{\lambda}{8\pi} \left\{ \frac{\tan\alpha}{\sin\theta} \left[(L+2l_o) \tan^2(\alpha+\theta) + l_o \tan^2(\alpha-\theta)\, U(\alpha-\theta) \right.\right.$$
$$\left. + (L+\beta) \tan^2(\alpha-\theta)\, U(L-\beta)\, U(\alpha-\theta) \right]$$
$$\left. + \frac{2l_o}{\cos\theta} \tan\theta \right\}$$

This formula is not valid at nose-on, broadside, or for angle of incidence perpendicular to a cone generatrix. The following formulas apply for the latter two cases.

$$\sigma_{\perp \text{ to cone}} = \frac{8\pi \sin\alpha}{9\lambda \cos^3\alpha \sin\theta} \left[L^3 + l_o^3 - 2 l_o^{3/2} L^{3/2} \right]$$

$$\sigma_{\text{Broadside}} = \frac{2\pi\rho L_f^2}{\lambda}$$

7.2.2 Comparison Between Theory and Experiment of the Cross-Section of Atlas Type Missiles

The results of static experiments on Atlas type missiles (Sec. 5.2) and the theoretical computations on Atlas type missiles (Sec. 7.2.1) were compared in Figures 5.2-5, 5.2-8, 5.2-13, 5.2-16, and 5.2-18. These figures are repeated here for reference.

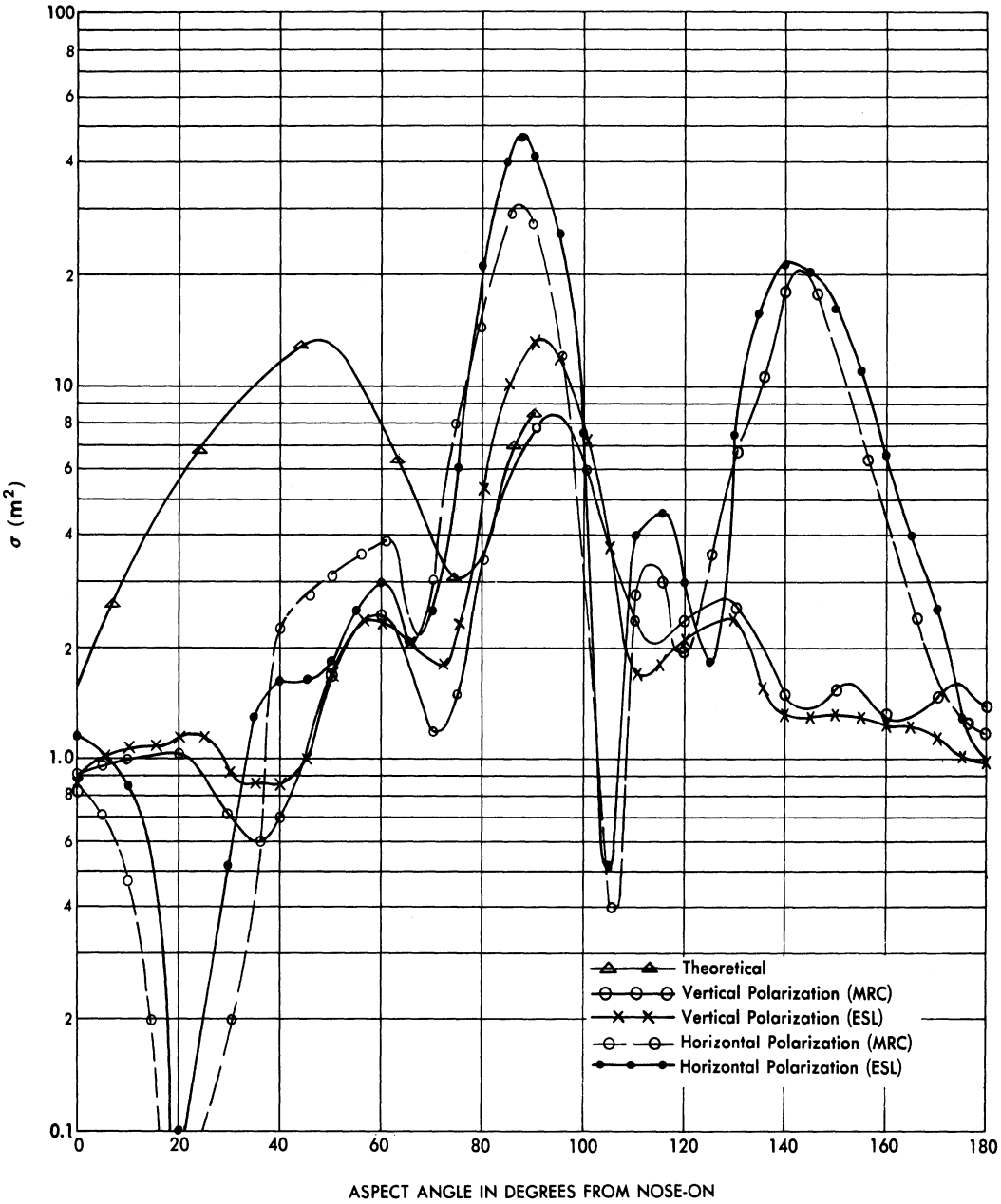

FIG. 5.2-5 CROSS-SECTION OF THE 7-OC WARHEAD AT 75 MC

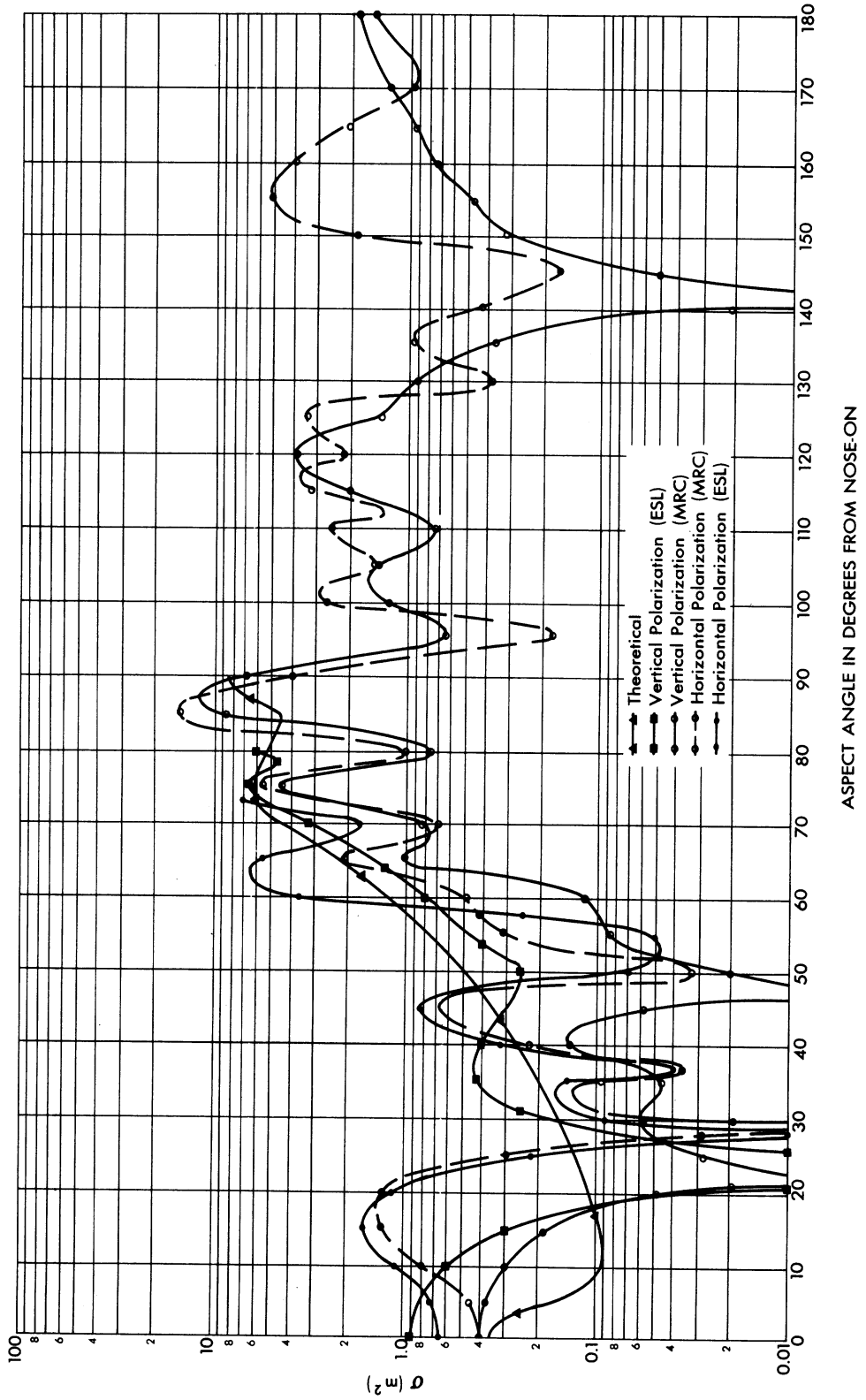

FIG. 5.2-8 CROSS-SECTION OF THE 7-OC WARHEAD AT 225 MC

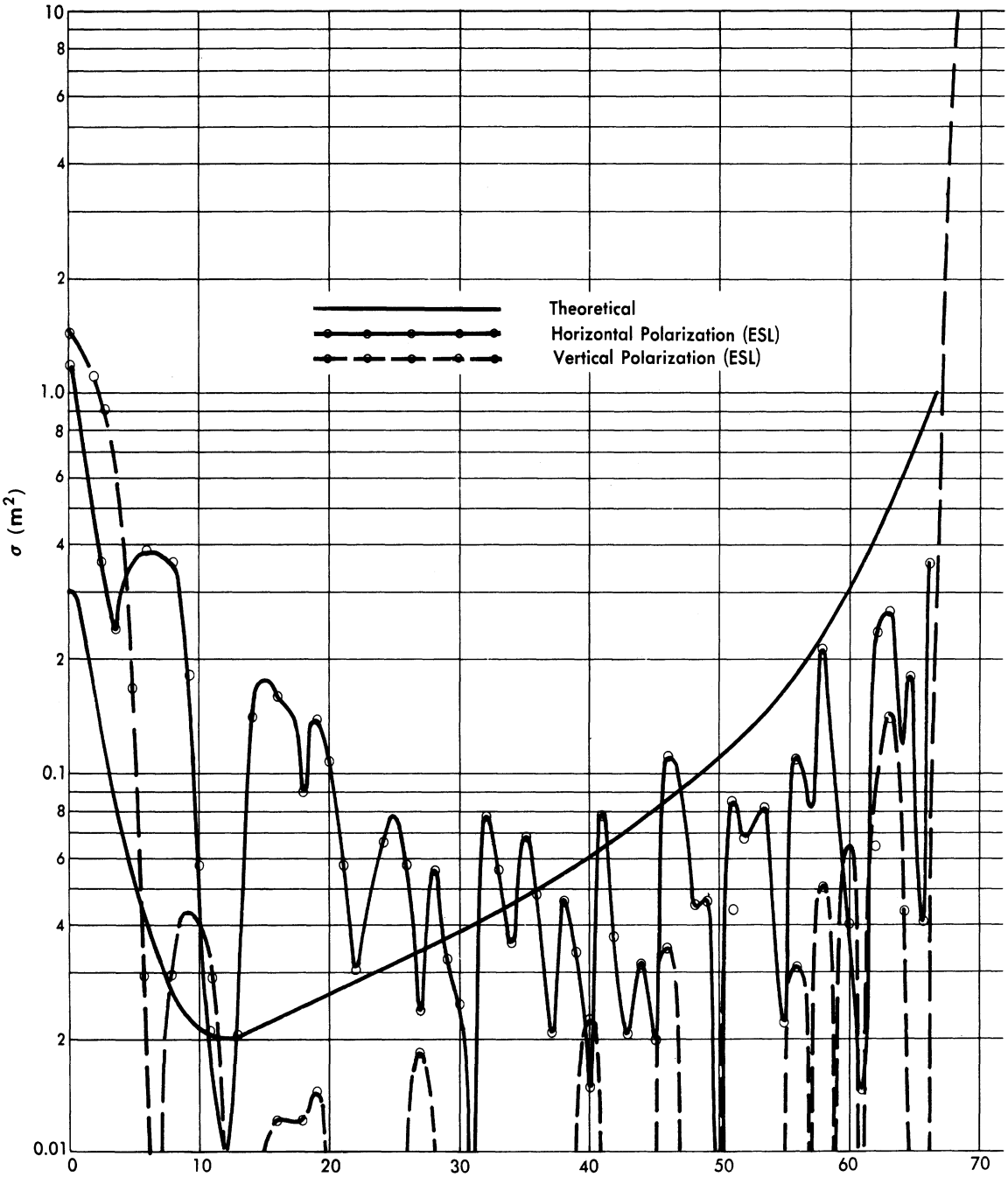

FIG. 5.2-13 CROSS-SECTION OF THE 7-OC WARHEAD AT 1,000 MC

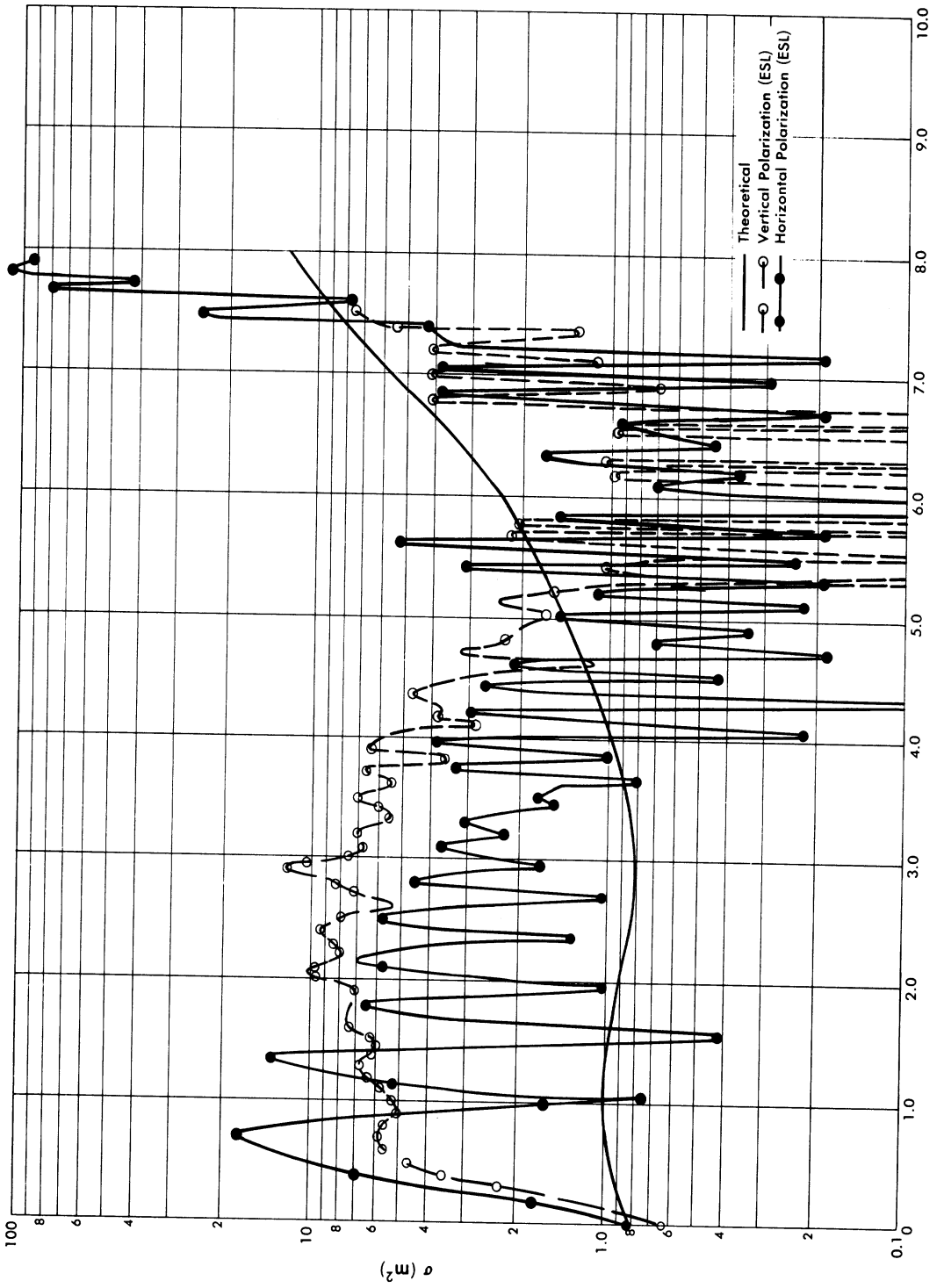

FIG. 5.2-16 CROSS-SECTION OF THE 7-OC BOOSTER AT 225 MC

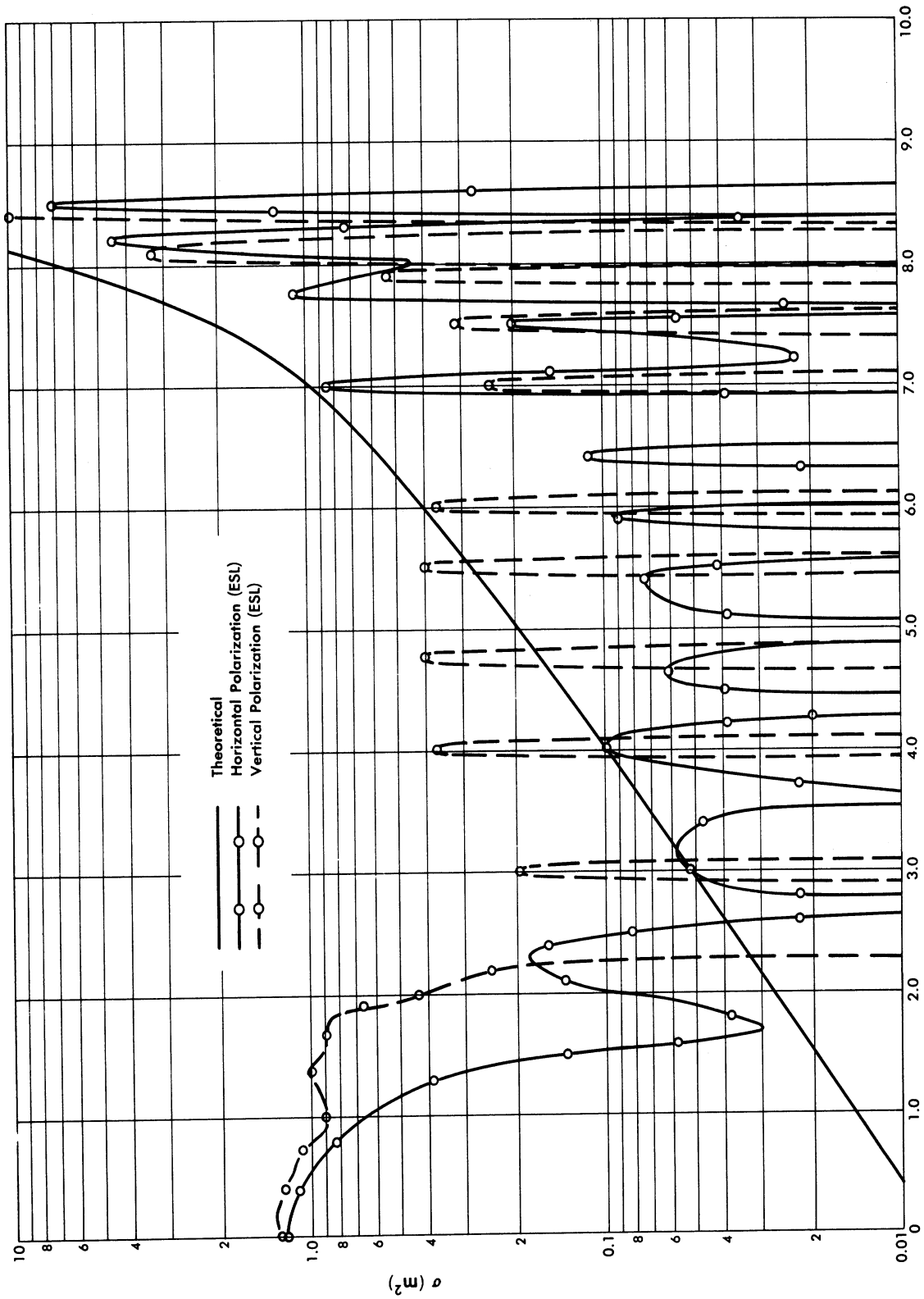

FIG. 5.2-18 CROSS-SECTION OF THE "NEEDLE-NOSE" WARHEAD AT 225 MC

7.3 Theoretical Determination of the Monostatic Cross-Section of V-2 Type Missile (144-1000 Mc).

For purposes of the theoretical computations, a V-2 type missile was assumed to be comprised of the following three components:

(1) the body, which was considered as a surface of revolution starting at a conical tip and tapering gently to a cylinder-like rear portion.

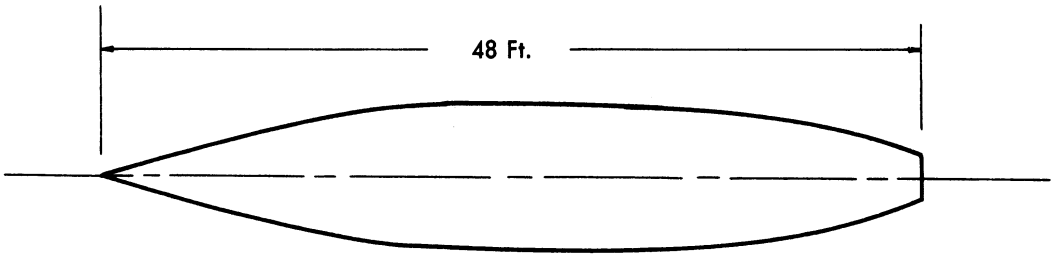

(2) the fins, which were considered to be thin flat plates of the shape depicted below,

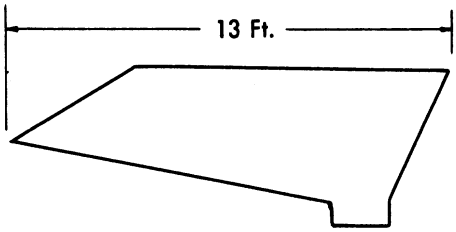

(3) the motor, which was considered to be comprised of an exterior flat plate ring and an open interior cone.

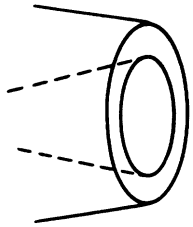

The cross-sections due to these components were computed separately by the methods of physical optics and then summed to give the cross-section of the entire missile.

7.3.1 Contribution of the Body

The physical optics backscattering cross-section of the body is given by:

$$I = \frac{4\pi}{\lambda^2}\left|\int_{z_0}^{z_{end}} e^{i2kz}\, d\,[A(z)]\right|^2, \quad k = \frac{2\pi}{\lambda},$$

where z is measured along the line of propagation of the incident ray, z_o is the point where the wavefronts first meet the body, and $A(z)$ is the projection onto the plane $z = z_0$ of the surface area lying between the plane $z = z_0$ and a plane coincident with the wavefront at z. The plane parallel to the wavefronts and farthest removed from z_0 but still in contact with the missile is denoted by $z = z_{end}$.

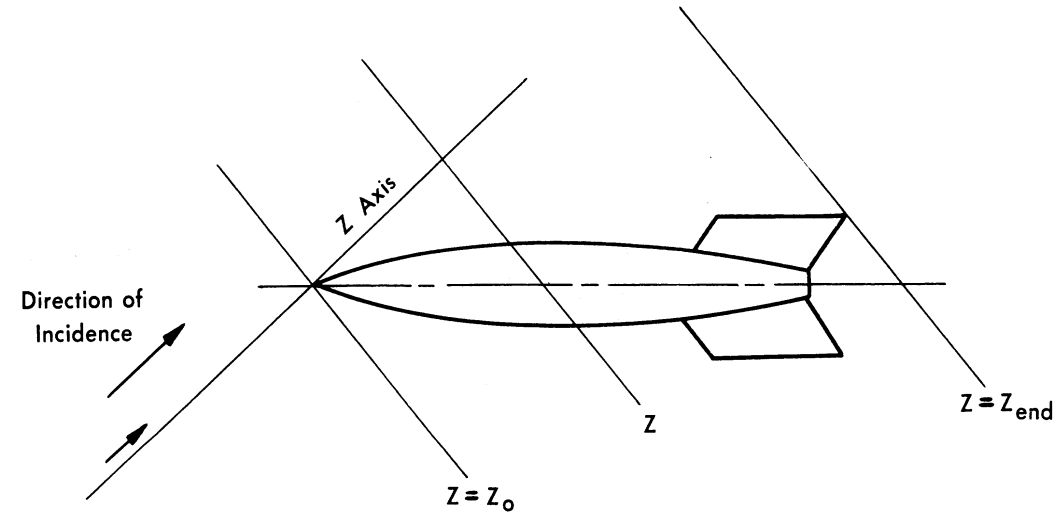

To evaluate the integral I in closed form is usually difficult. To obtain values for the V-2 body radar cross-section, the integral has been approximated by making use of the vibration curve analysis used in physical optics.

The idea of a vibration curve arises when considering an integral $\int_{x_1}^{x_2} e^{i\alpha x} f(x)dx$ as the limit of a sum of the form

$$\sum_{n=1}^{N} e^{i\alpha(x_1 + nh)} f(x_1 + nh)h \qquad \text{as } N \to \infty$$

where $h = \frac{x_2 - x_1}{N}$.

If a complex number is represented as a vector in the complex plane, then the magnitude of the above sum is the same as the magnitude of the resultant to the polygon formed by a series of these vectors, the n'th vector of which is oriented at an angle of $\alpha(x_1 + nh)$ to the real axis and has a magnitude of $hf(x_1 + nh)$.

In the limit, the vibration polygon becomes a smooth curve (if f(x) is continuous) and the magnitude of the resultant to this curve is equal to the magnitude of the integral,

$$\int_{x_1}^{x_2} e^{i\alpha x} f(x)\, dx.$$

The radius of curvature of the vibration curve at a point is given by:

$$R' = \frac{f(x)}{\alpha}$$

since $f(x)\,dx$ is the element of arc length along the curve and αdx is the element of angle through which the curve has turned about its instantaneous center of curvature.

The V-2 body has a conical tip portion tapering gently into a tail which is almost cylindrical. Hence $A(z)$ is continuous and $A'(z)$, the first derivative of $A(z)$, exists so that

$$\int_{z_0}^{z_{end}} e^{i2kz}\, dA(z) = \int_{z_0}^{z_{end}} e^{i2kz}\, A'(z)\, dz.$$

Furthermore, $A'(z)$ is continuous, although $A''(z)$ is not. The continuity of $A'(z)$ implies a continuously changing radius of curvature for the corresponding vibration curve since the magnitude of the radius of curvature for the curve is given by $\frac{\lambda}{4\pi} A'(z)$.

Another important characteristic of $A'(z)$ for the V-2 body is that at $z = z_{end}$, $A'(z) = 0$ for all aspects. This means that the vibration curve has a zero radius of curvature at $z = z_{end}$ so that the resultant of the vibration polygon also marks the final position of the center of curvature. If it were possible to trace the positions of the center of curvature, the desired value for

$$\left| \int_{z_0}^{z_{end}} e^{i2kz}\, A'(z)\, dz \right|$$

would be obtained. Fortunately, there are a great many qualitative statements that can be made about the motion of the center of curvature. Where the radius of curvature is rapidly varying, the center of curvature also moves about rapidly. Where the radius of curvature varies slowly, the center of curvature remains essentially constant. For a body for

which $A'(z)$ increases at first rapidly and then decreases very slowly to zero, the vibration curve would at first spiral out rapidly, and hence the center of curvature would move away from its original position. For a conical tip body $A'(z_o) = 0$ for angles of incidence with respect to the axis of the body which are less than the complement of the cone angle, so that the original position of the center of curvature would be the origin of coordinates. If the body tapers gradually from the initial conical tip, then in the region of gradual taper the radius of curvature decreases very gradually so that the vibration curve spirals in, gradually retaining a practically constant center of curvature and finally, as $A'(z)$ goes to 0, ending up at this constant center of curvature. Thus the variation of $A'(z)$ during its period of increase in the conical portion of the body accounts almost entirely for the final position of the center of curvature; or equivalently, the value of the integral $\int_{z_0}^{z_{end}} e^{i2kz}\, dA(z)$ may be accounted for largely by tip scattering. Such is the case for the V-2 body (without fins) when viewed nose-on. As the aspect is moved off-nose, $A'(z)$ still increases rapidly at the conical tip and then less rapidly in the tapered portion of the missile. During the rapid rise, the center of curvature assumes its tip scattering position and this position remains approximately constant during the subsequent gradual change of $A'(z)$. However, when passing into the transition region at the base of cylinder, $A'(z)$ rapidly decreases to zero with a consequent motion of the center of curvature. The vector denoting the resultant motion is called the base scattering contribution.

The tip scattering vector added to the base scattering vector gives the final position of the center of curvature, and the magnitude of this resultant gives the magnitude of the desired integral. The tip scattering and the base scattering contributions have been added assuming random phase, i.e., the cross-section for the body, σ_{body}, was taken as $\sigma_{tip} + \sigma_{base}$, where σ_{tip} and σ_{base} were computed as being $\frac{4\pi}{\lambda^2}$ times the square of magnitude of the tip scattering vector and the base scattering vector respectively. This procedure may be justified by noting that small changes in the length of the body will completely change the phasing

of the tip and base contributions for the wavelengths considered. When considering a V-2, it is well to assume all phasings are equally likely because the dimensions of one V-2 may differ by several wavelengths from another.

7.3.1.1 Computation of Tip Scattering

The tip scattering contribution may be found by computing the value of the integral:

$$\int_{z=0}^{z=\infty} e^{i2kz}\, dA(z)$$

for an area function whose first derivative has the same initial rise as the area function of the body which is of interest and then very gradually sinks to 0. Assuming that

$$dA = \left[\sum_{s=0}^{\infty} \alpha_s e^{-B_s z} \sum_{n=0}^{\infty} A_n z^n\right] dz \qquad \text{where} \quad \sum_{s=0}^{\infty} \alpha_s = 1$$

$$\int_0^{\infty} e^{i2kz}\, dA(z) = \sum_{s=0}^{\infty} \sum_{n=0}^{\infty} \frac{\alpha_s A_n\, n!}{(B_s - 2ik)^{n+1}} \quad \text{which in the limit as}$$

$B_0, B_1, \ldots, B_s, \ldots \longrightarrow 0$, is equal to $\sum_{n=0}^{\infty} \frac{A_n\, n!}{(-2ik)^{n+1}}$.

For large k, the 1/k term dominates the expansion so that the integral

$\int_0^{\infty} e^{i2kz}\, dA(z)$ is approximately given by $\frac{A_0 i}{2k} = i\frac{A_0 \lambda}{4\pi}$, providing $A_0 \neq 0$.

Since, for z small, $A_0 z$ is approximately the area function, A(z), the above expression is simply (i/π) (Area of the first Fresnel zone). For $A_0 = 0$, $A_1 \neq 0$ the $1/k^2$ term dominates the expansion so that

$$-\int_0^\infty e^{i2kz}\, dA(z) \cong \frac{2}{\pi^2}\frac{\lambda^2}{16} A_1 = \left(\frac{2}{\pi^2}\right)\left(\text{Area of first Fresnel Zone}\right).$$

The case for $A_0 = 0$, $A_1 \neq 0$ corresponds to a conical tip. For the V-2 body this is the case for angles of incidence which are less than the complement of the cone angle. For angles greater than the complement of the cone angle, the first formula above applies as $A_0 \neq 0$.

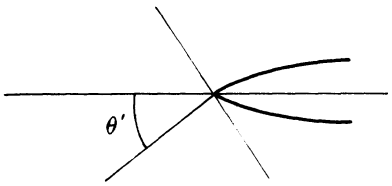

$A_0 = 0$

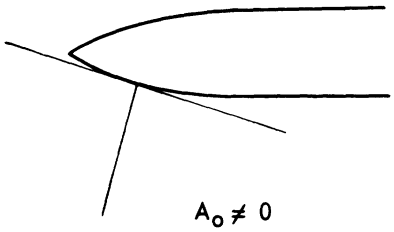

$A_0 \neq 0$

The expression for the area function, A(z), for a cone for various angles of incidence has been obtained analytically: For angles of incidence less than the cone angle,

$$A(z) = \frac{z^2 \pi \tan^2 \theta}{\cos^3 \theta' (1 - \tan^2 \theta' \tan^2 \theta)^{3/2}}$$

where θ' is the angle of incidence and θ is the half cone angle, $\theta' < \theta$. For A(z) given by this formula, the tip scattering contribution to cross-section is, using the results developed above,

$$\frac{4\pi}{\lambda^2}\left|\frac{2}{\pi^2}\frac{\lambda^2}{16}\frac{\pi \tan^2 \theta}{(1 - \tan^2 \theta \tan^2 \theta')^{3/2} \cos^3 \theta'}\right|^2 = \frac{\lambda^2}{16\pi}\frac{\tan^4 \theta}{(1 - \tan^2 \theta \tan^2 \theta')^3 \cos^6 \theta'}$$

For $90^0 - \theta > \theta' > \theta$ we have

$$A(z) = az^2 \left[b \cos^{-1} \left(-\frac{b}{c}\right) + \sqrt{c^2 - b^2}\right]$$

where

$$a = \frac{\tan \theta}{\cos \theta' \, (1 - \tan^2 \theta \tan^2 \theta')^{1/2}},$$

$$b = \frac{\tan \theta}{\cos^2 \theta' (1 - \tan^2 \theta \tan^2 \theta')}, \text{ and}$$

$$c = \frac{\tan \theta'}{\cos^2 \theta \, (1 - \tan^2 \theta \tan^2 \theta')}.$$

For angles of incidence such that $90^0 - \theta \leq \theta' \leq 90^0$, the tip scattering cross-section contribution is $\frac{4\pi}{\lambda^2}\left[\frac{A_0}{\pi}\frac{\lambda}{4}\right]^2 = \frac{A_0^2}{4\pi}$.*

A_0 was evaluated graphically for the third case.

For $\theta' > 90^0$ the wave fronts strike the cylindrical base of the model first; and, as the function $A'(z)$ decreases very gradually at the conical tip of the missile, tip scattering represents, for these cases, a contribution small compared to that of base scattering.

7.3.1.2 The Base Scattering Contribution to the Cross-Section

Case I: $\theta' < 90^0$

The wavefronts for these cases approach the cylindrical edge as shown below

*For $\theta' = 90^0$ (broadside) this tip scattering contribution is the sole contribution to the cross-section since $A'(z)$ approaches 0 gradually at $z = z_{end}$.

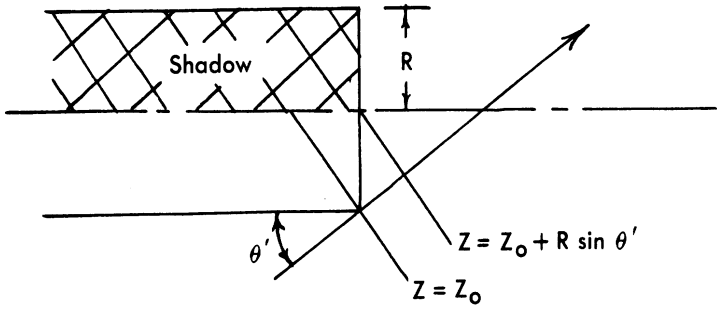

Let $z' = z - z_0$ where as before, z is the distance along the incident rays, and z_0 now represents the coordinate of the "transition edge" depicted in the diagram above.

The area function $A(z')$ is, to within an additive constant (which is not important in the process outlined below), given by the expression

$$A(z') = 2Rz' \tan\theta' + \frac{R \sin\theta' - z'}{\cos\theta'} \sqrt{2Rz' \sin\theta' - z'^2}$$

$$- R^2 \sin\theta' \tan\theta' \cos^{-1}\left(1 - \frac{z'}{R \sin\theta'}\right)$$

where θ' is angle of incidence and R is the radius of the cylindrical base.

The numerical magnitude of the radius of curvature, R', of the vibration curve at a point corresponding to the edge of the transition region is given by $\frac{\lambda}{4\pi} 2R \tan\theta'$. The center of curvature for the curve will lie along the normal to the curve at a distance numerically equal to R'. The final position of the center of curvature relative to this position may be obtained by integrating $e^{i2kz'} A'(z')$ with respect to z' over the transition region and adding to the resultant complex number, a complex number equal in magnitude to the radius of curvature at the edge of the region and having a phase $\left(\frac{4\pi}{\lambda} z_0 - \frac{\pi}{2}\right)$. The diagram below illustrates this process.

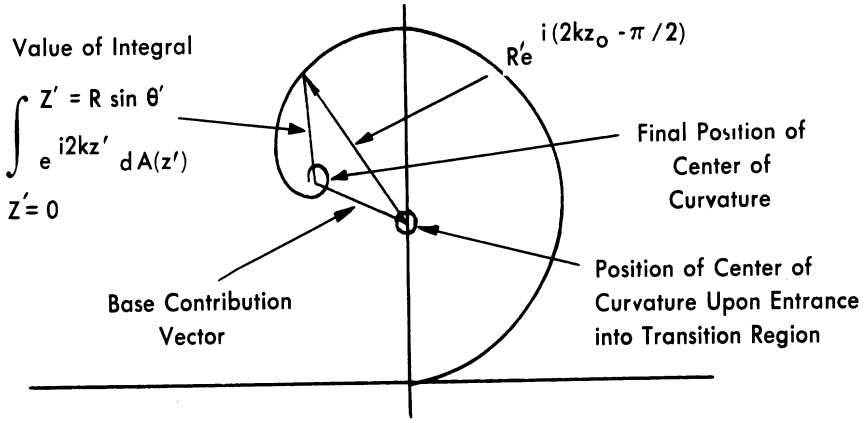

This procedure yields:

$$A'(z') = 2R\tan\theta' - \frac{2}{\cos\theta'}\sqrt{2R\,z'\sin\theta' - z'^2}.$$

The desired integral is evaluated readily.

$$I = \int_0^{R\sin\theta'} e^{i2kz}\left[2R\tan\theta' - \frac{2}{\cos\theta'}\sqrt{2R\,z'\sin\theta' - z'^2}\right] dz,$$

where $z' = z - z_0$.
Integrating the first term:

$$I = \frac{\lambda}{4\pi i}\,2R\tan\theta'\,\exp[(4\pi iR\sin\theta'/\pi) - 1]$$

$$- \frac{2}{\cos\theta'}\int_0^{R\sin\theta'} e^{i2kR\sin\theta'}\sqrt{R^2\sin^2\theta' - (R\sin\theta' - z')^2}\,dz.$$

Let $1 - \frac{z}{R\sin\theta'} = \phi$. Then

$$I = \frac{\lambda}{4\pi i} 2R \tan\theta' \left[\exp(4\pi iR\sin\theta'/\lambda) - 1\right] - \frac{2R^2 \sin\theta'}{\cos\theta'} \int_0^{\frac{\pi}{2}} e^{\frac{4\pi i}{\lambda} R \sin\theta' (1-\cos\phi)} \sin^2\phi \, d\phi.$$

The integral on the right is expressible in terms of the Bessel and Struve functions of 1st order.

$$I = \frac{\lambda}{2\pi i} R \tan\theta' \left[\exp(4\pi iR\sin\theta'/\lambda) - 1\right] - \frac{\lambda}{4} R \tan\theta' \, e^{i2kR \sin\theta'} \left[J_1(2kR \sin\theta') - iS_1(2kR \sin\theta')\right]$$

From this expression, the base contribution to the cross-section can be computed.

$$\sigma_{base} = \frac{4\pi}{\lambda^2} \left| I + \frac{\lambda}{4\pi i} R \tan\theta' \right|^2 .$$

In the above equation, care has been taken to add the radius vector in its proper phase.

Case II, $\theta' > 90^0$

For $\theta' > 90^0$, the base contribution is the main contribution since the conical tip contribution is negligible (Sec. 7.3.1.1). The value of σ_{base} was computed in a manner which was completely analogous to the technique used for $\theta' < 90^0$ except that allowance was made for the fact that the wavefronts approach the body so as to strike the base portion of the body first. $A'(z)$ increases from the value 0 at $z = z_0 = 0$ to the value $2R \tan(180^0 - \theta')$ at the end of the transition region.

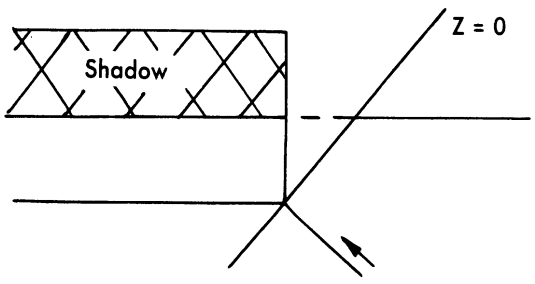

The value of the integral, $I = \int_0^{R \sin(\pi - \theta')} e^{i2kz} A'(z)\, dz$ added to

$$\frac{\pi}{4} \, 2R \tan(\pi - \theta') \, e^{i(2kR \sin(\pi - \theta') + \pi/2)}$$

gives the desired resultant position of the center of curvature. This is illustrated in the diagram below

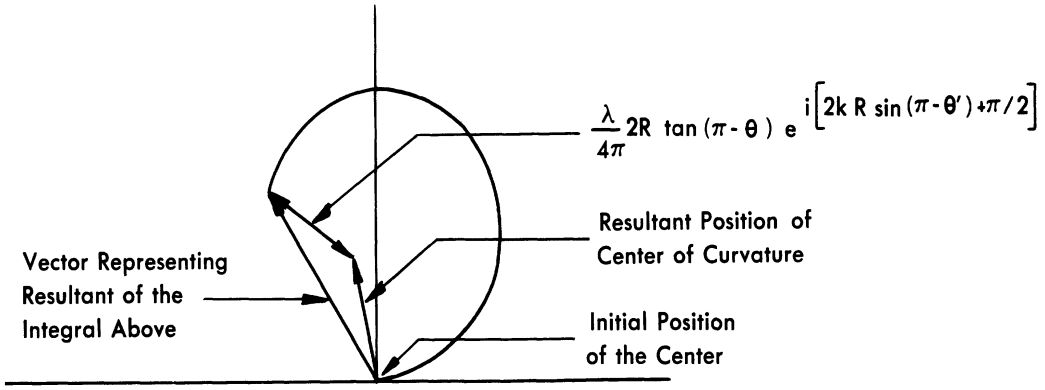

The area expressions and the resulting integrals are entirely similar to those encountered for $\theta' < 90^0$ and, as might be expected

$$\sigma_{base}(\pi/2 + \psi) = \sigma_{base}(\pi/2 - \psi).$$

Therefore, it is unnecessary to use any additional formulas for Case II.

7.3.2 Motor Contribution

It was assumed that the return ($\theta' > 90^0$) from the motor portion of the missile would emanate primarily from the nozzle (1) and the annular plate (2) shown in the figure below. The basis for this assumption is that the geometry of the combustion chamber combined with the roughness of the head (3) suggests that the entire combustion chamber may be considered a black body to within the accuracy of this method.

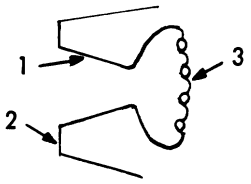

The physical optics backscattering cross-section for the plate portion may be expressed as

$$\sigma = \frac{4\pi}{\lambda} \left| \cos\theta' \int_{\substack{\text{Plate} \\ \text{Surface}}} e^{i2kx \sin\theta'} \, dA(x) \right|^2$$

where $\theta'' = 180^0 - \theta'$ (θ' is the angle of incidence of rays to missile axis) and where x and dA(x) are defined as in the diagram below.

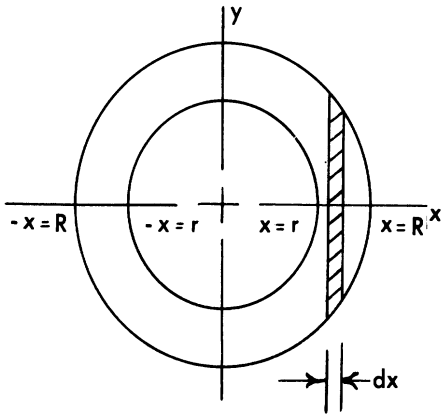

R = Radius of Outer Ring
r = Radius of Inner Ring

The integral $\int_{\substack{\text{plate} \\ \text{surface}}} e^{i2kx \sin\theta'} \, dA(x)$ is expressible as

$$2\left[\int_{x=-R}^{x=R} e^{i2kx}\sin\theta''\sqrt{R^2-x^2}\,dx - \int_{x=-r}^{x=r} e^{i2kx}\sin\theta''\sqrt{r^2-x^2}\,dx\right]$$

Making the substitutions $x/R = \cos\alpha$ and $x/r = \cos\alpha'$ respectively for these integrals

$$2\left[R^2\int_0^{\pi} e^{i2k\,R\cos\alpha\sin\theta''}\sin^2\alpha\,d\alpha - r^2\int_0^{\pi} e^{i2kr\cos\alpha'\sin\theta''}\sin^2\alpha'\,d\alpha'\right]$$

$$= 4\left[R^2\int_0^{\pi/2}\cos(2kR\cos\alpha\sin\theta'')\sin^2\alpha\,d\alpha - r^2\int_0^{\pi/2}\cos(2kr\cos\alpha'\sin\alpha')\sin^2\alpha'\,d\alpha'\right].$$

These integrals may be easily evaluated to give

$$4\left[R^2\frac{\sqrt{\pi}\,\Gamma\left(\frac{3}{2}\right)}{2kR\sin\theta'}J_1(2kR\sin\theta') - r^2\frac{\sqrt{\pi}\,\Gamma\left(\frac{3}{2}\right)}{2kr\sin\theta'}J_1(2kr\sin\theta')\right].$$

From this expression the cross-section, σ, may be computed.

The contribution of the interior cone was obtained by projecting graphically the "visible" portion of the interior cone lying between the two planes depicted in the diagram below and separated in distance by $\lambda/4$ onto a phase plane; the area thus obtained was measured. This area of course corresponds to the area of the first Fresnel zone (see diagram below).

The cross-sectional contributions of this interior cone were computed by squaring the above area and multiplying by $\frac{4\pi}{\lambda^2}$.

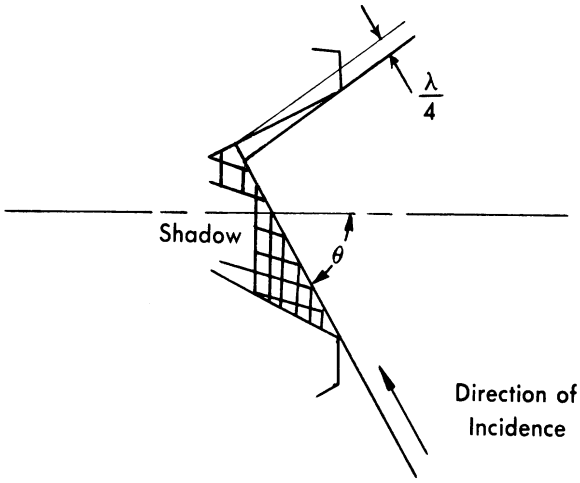

7.3.3 The Fin Contribution

The major differences in cross-section at high frequencies (S, X, and K bands) among different members of the V-2 class are due principally to different type fins (Sec. 7.1). Theoretical V-2 cross-section results at these frequencies are very sensitive to the type of simple shape used to approximate the fin. For some V-2 type missiles, thin wire theory appears most appropriate, for others small flat plates appear appropriate while for still others, when the leading edge has been made almost knife sharp, wedge theory appears appropriate.*

In the graphs shown in Section 7.3.4, the choice of which method to use was weighted by available experimental cross-section data. For these computations, the fins were considered to be thin plates. Their edges were swept back. This plate method minimizes the contribution of the fins in the nose-on direction so that it became necessary to assume that the nose-on fin-body interaction dependence is proportional to λ^2. The fins were assumed to be mounted so that two of them were

*It had been hoped that precise information would be obtained from the dynamic V-2 experiments (Sec. 6.1) to help decide which of the many possible approximation methods is best suited. Unfortunately the dynamic test data were too inaccurate to answer this question.

perpendicular to the plane defined by the axis of the missile and the incoming rays, so that for broadside incidence the fin contribution was $\frac{4\pi}{2}(2A)^2$, where A was the surface area of a fin. For angles of incidence other than broadside or nose-on, the fin contribution was obtained by evaluating the physical optics integral for the fin shape.

7.3.4 The Over-All V-2 Cross-Section

The back scattering cross-sections for the V-2 body computed are shown in Figure 7.3-1 where σ is plotted against angle of incidence. Since the cross-sectional contributions of the various portions of the missile were added assuming arbitrary phase, no scintillations or rapid oscillations due to phasing of the components is exhibited in these curves. Also the oscillations which would normally occur due to the flat plate areas (the fin and motor) have been averaged out so that the resultant curves are smooth. The theoretical computations were carried out for the representative frequencies of 144, 225, 400, 600, and 1000 Mc.

7.4 Theoretical Determination of Bistatic Cross-Sections of V-2 Type Missiles

The study of the radar cross-section of the V-2 included consideration of the case of bistatic radars, that is, radars in which the transmitter and receiver are geographically separated. The purpose of this bistatic study was to determine whether increased effective cross-section of a V-2 could be obtained by use of this mode of operation. These studies were carried out for frequencies of 225 and 1000 Mc for vertical and horizontal polarization, and for the V-2 fins in the plane defined by the missile heading and the transmitter location, or at 45° to this plane.

The monostatic and bistatic radar cross-sections of the V-2 as functions of θ (Fig. 7.4-1) are plotted in Figure 7.4-2 for frequencies of 225 Mc and 1000 Mc and for three different values of α(Fig. 7.4-1). In this graph the target line of flight, transmitter, and receiver are assumed coplanar ($\beta = 0$). The horizontal fins of the V-2 and the direction of the electric vector are in this plane. That is, the polarization of the electric vector is horizontal at both the transmitter

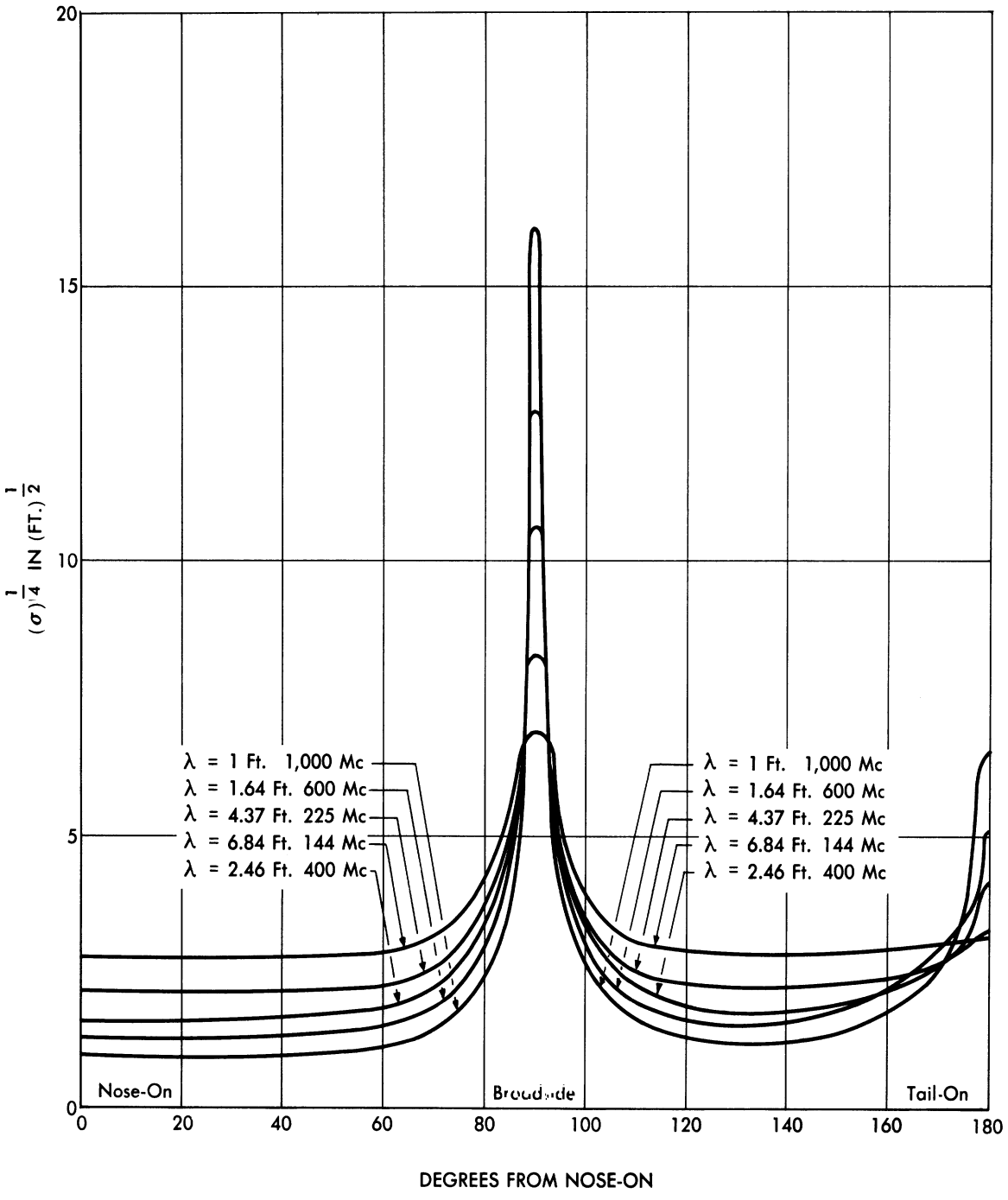

FIG. 7.3-1 COMPOSITE PLOT OF THE MONOSTATIC RADAR CROSS-SECTION OF A V-2 AT FIVE REPRESENTATIVE FREQUENCIES

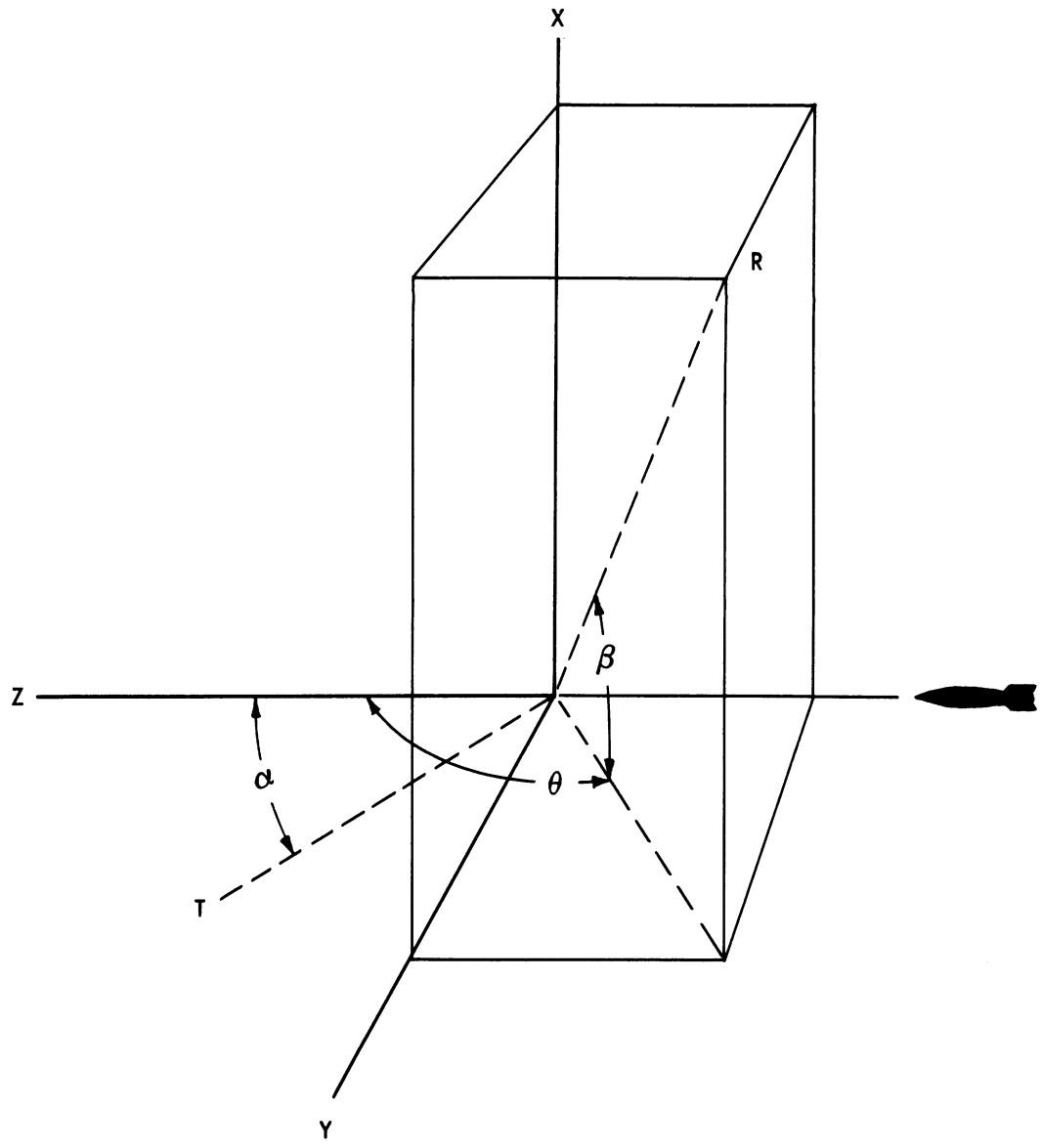

R = Receiver
T = Transmitter

FIG. 7.4-1 THREE NON-PLANAR ANGLES USED TO STUDY BISTATIC CROSS-SECTION OF THE V-2

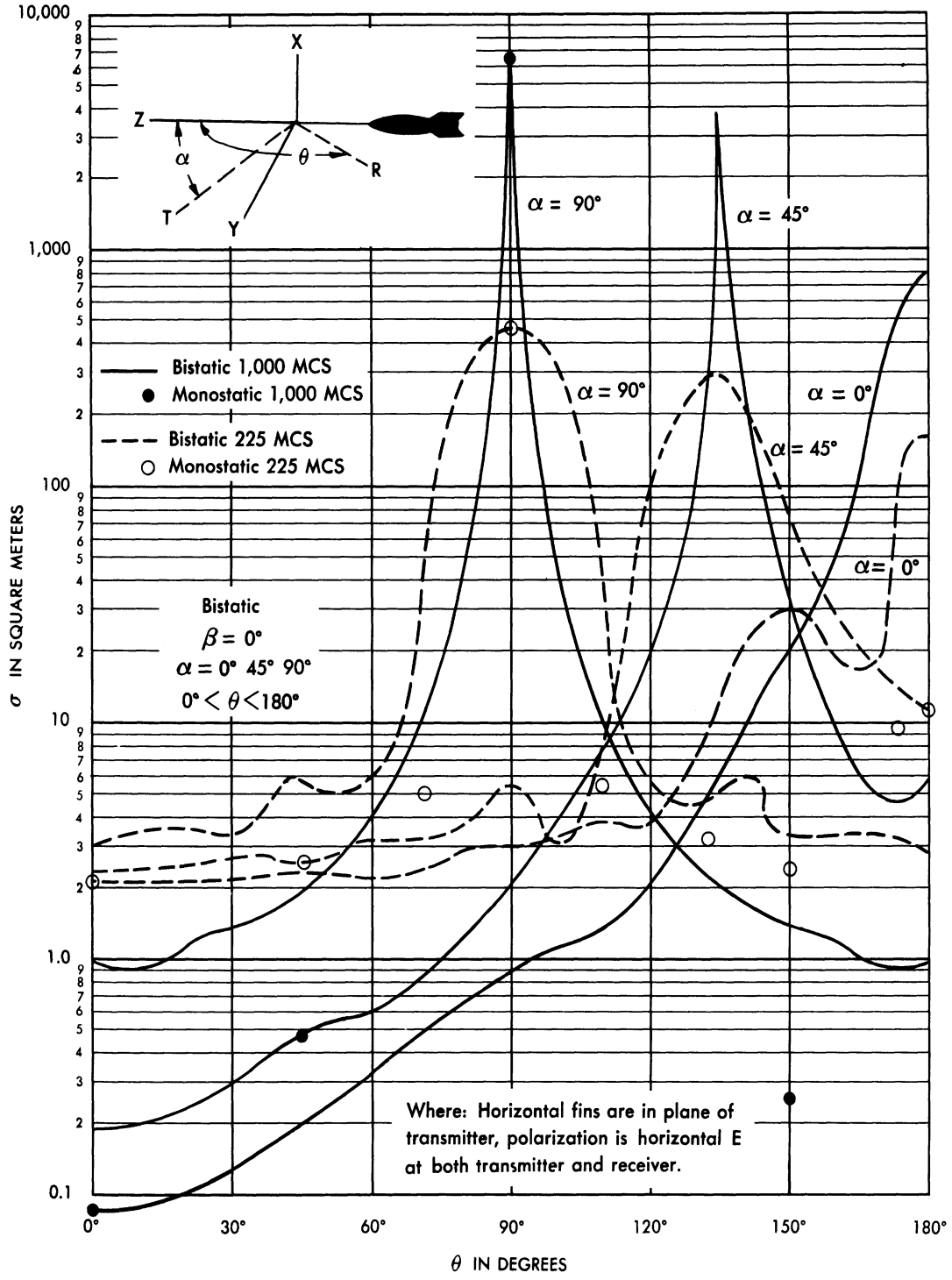

FIG. 7.4-2 RADAR CROSS-SECTION OF V-2 vs. ASPECT ANGLE θ AT 1,000 MCS AND 225 MCS

and the receiver. It can be seen from this graph that the largest bistatic cross-section is obtained when $\alpha + \theta = 180^0$, providing both α and θ are restricted to be less than or equal to 180^0. If α and θ are both restricted to small angles, such as angles less than 45^0, then there is little advantage to be gained from bistatic operation. It can also be seen that although the peak cross-section obtained at 1000 Mc is greater than that at 225 Mc, the latter frequency is more advantageous if comparatively large cross-sections are desired for a wide range of receiver angles.

The effect of transmitter, receiver, and V-2 heading being non-coplanar ($\beta \neq 0$) is shown in Figure 7.4-3. This figure, drawn for the case of forward scattering ($\alpha = \theta - 180^0$), shows that the cross-section decreases as the angle β increases. It can be seen that the 225 Mc frequency yields higher cross-sections than the 1000 Mc frequency for most orientations if β varies appreciably from zero degrees.

The variation of cross-section with polarization, fin angle, and frequency is illustrated in Figure 7.4-4. The differences between horizontal and vertical polarization, and between 0^0 and 45^0 orientations of the missile fins with respect to the plane of the transmitter, are both less than a factor of five. The frequency variation for vertical polarization is the same as that for horizontal polarization.

The methods used in arriving at Figures 7.4-2, 7.4-3, and 7.4-4 are described in detail in Appendix 3.

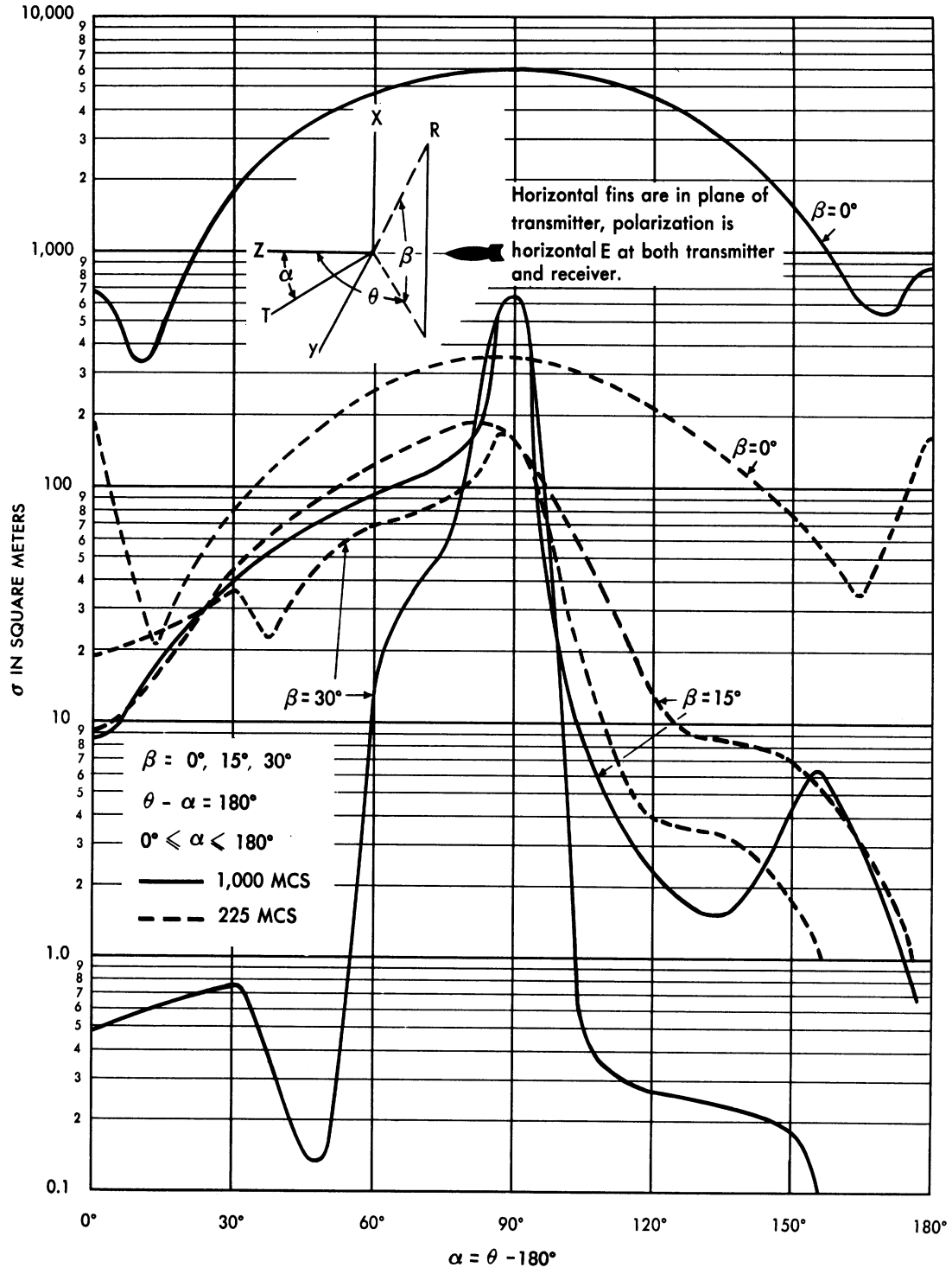

FIG. 7.4-3 RADAR CROSS-SECTION OF V-2 vs. ASPECT ANGLE α, θ AT 1,000 MCS AND 225 MCS

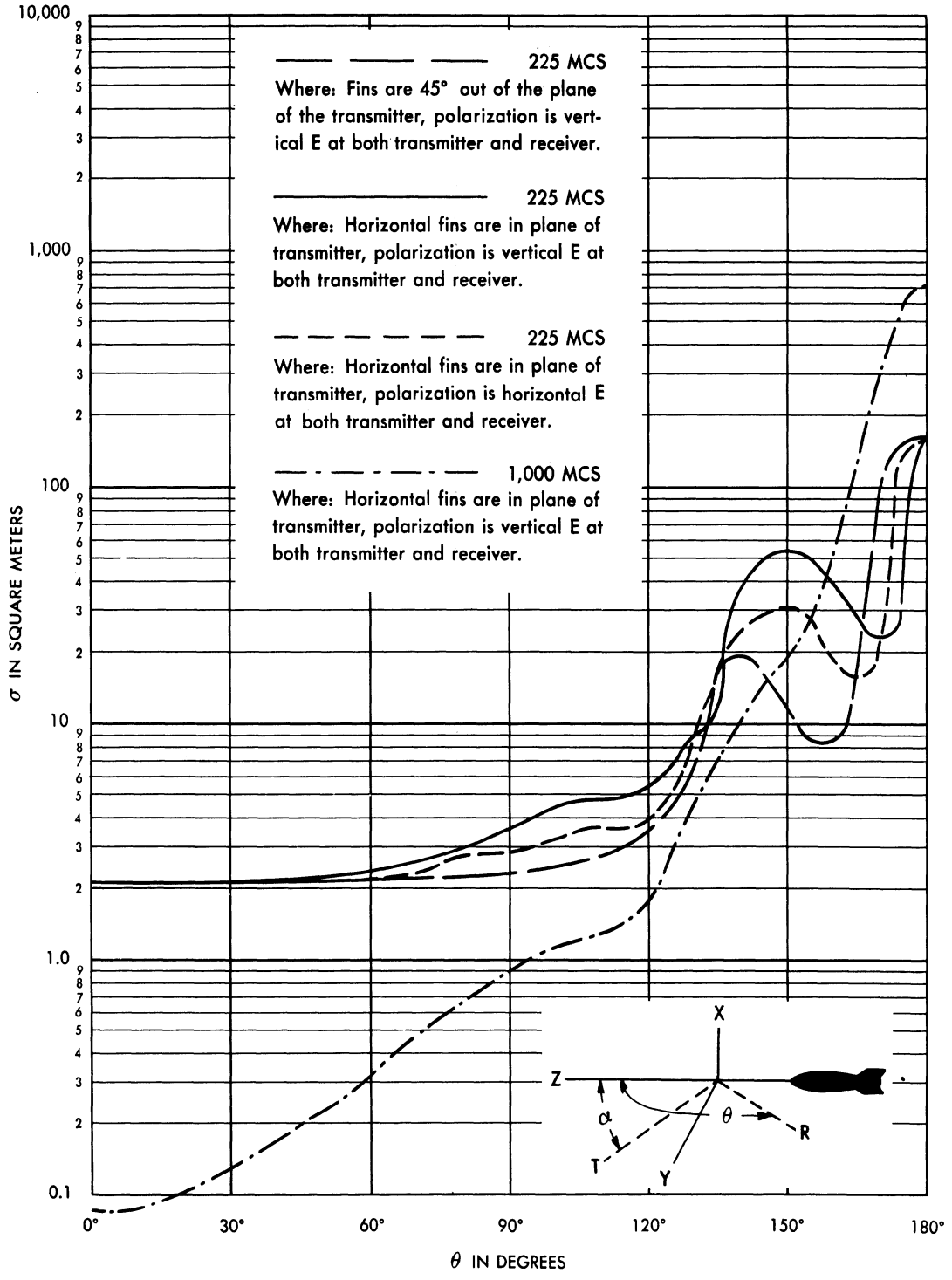

FIG. 7.4-4 BISTATIC CROSS-SECTION OF V-2 vs. ASPECT ANGLE θ FOR DIFFERENT FIN ANGLES, FREQUENCIES AND POLARIZATIONS ($\beta = 0°$; $\alpha = 0°$)

7.5 Comparison Between Theory and Experiment of the Cross-Section of V-2

A great deal of work has been done both experimentally and analytically in an attempt to determine the monostatic radar cross-section of V-2 type missiles. In this section, the monostatic cross-sections of a V-2 as a function of aspect angle obtained experimentally and theoretically are compared. Very little experimental work has been done on the bistatic case (Sec. 5.4.9); hence no attempt is made here to compare theory and experiment for the bistatic case.

In May 1950, Ohio State University made static cross-section measurements on WRRC models with removable fins (Sec. 5.4.8). O.S.U.'s c-w Magic T equipment was at X-band, and the models were three feet and two feet in length. Thus, in real V-2 dimensions, the corresponding radar frequencies were about 400 and 600 Mc. The results of the Ohio State experiments, (presented in Section 5.4.8) and the theoretical results (discussed in Section 7.3) are compared in Figures 5.4.8-2 through 5.4.8-5 which are repeated here. The theoretical curves appearing in these figures have had the nulls which were obtained theoretically "smoothed over".

The agreement is excellent considering that the V-2 and the UMA-1 (an early "Wizard" model) do not have identical dimensions and that the computations were done at a slightly different frequency than the experiments.

As discussed in Sections 5.3 and 6.1, both static and dynamic experiments have been conducted on WRRC V-2 models which yielded 1000 Mc cross-section data. These experimental data and the theoretical results were compared in Figure 6-15.

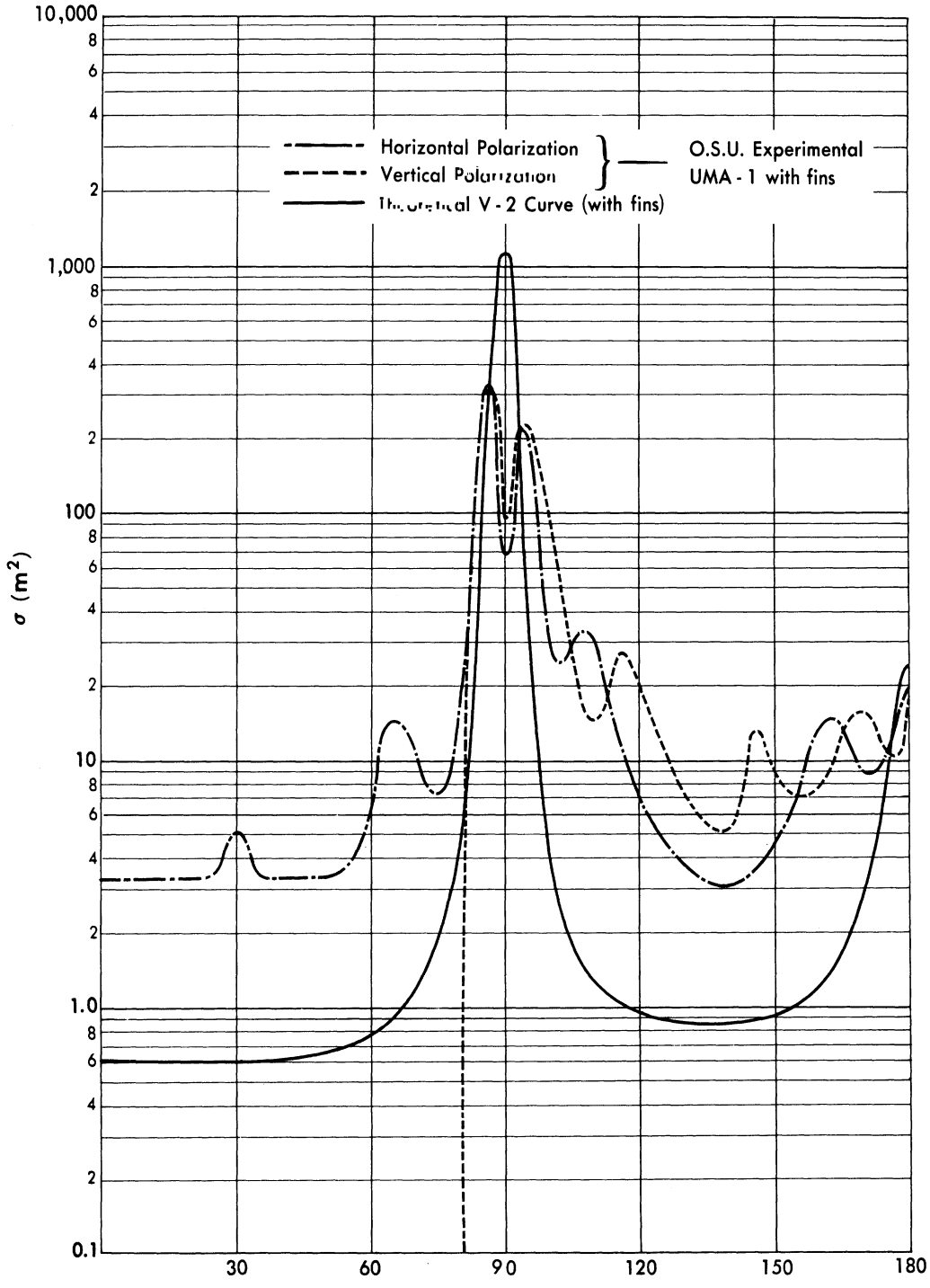

FIG. 5.4.8-2 COMPARISON BETWEEN THE THEORETICAL V-2 CROSS-SECTION AND THE EXPERIMENTAL UMA-1 CROSS-SECTION AS A FUNCTION OF ASPECT ANGLE AT ~400 MC/S - I

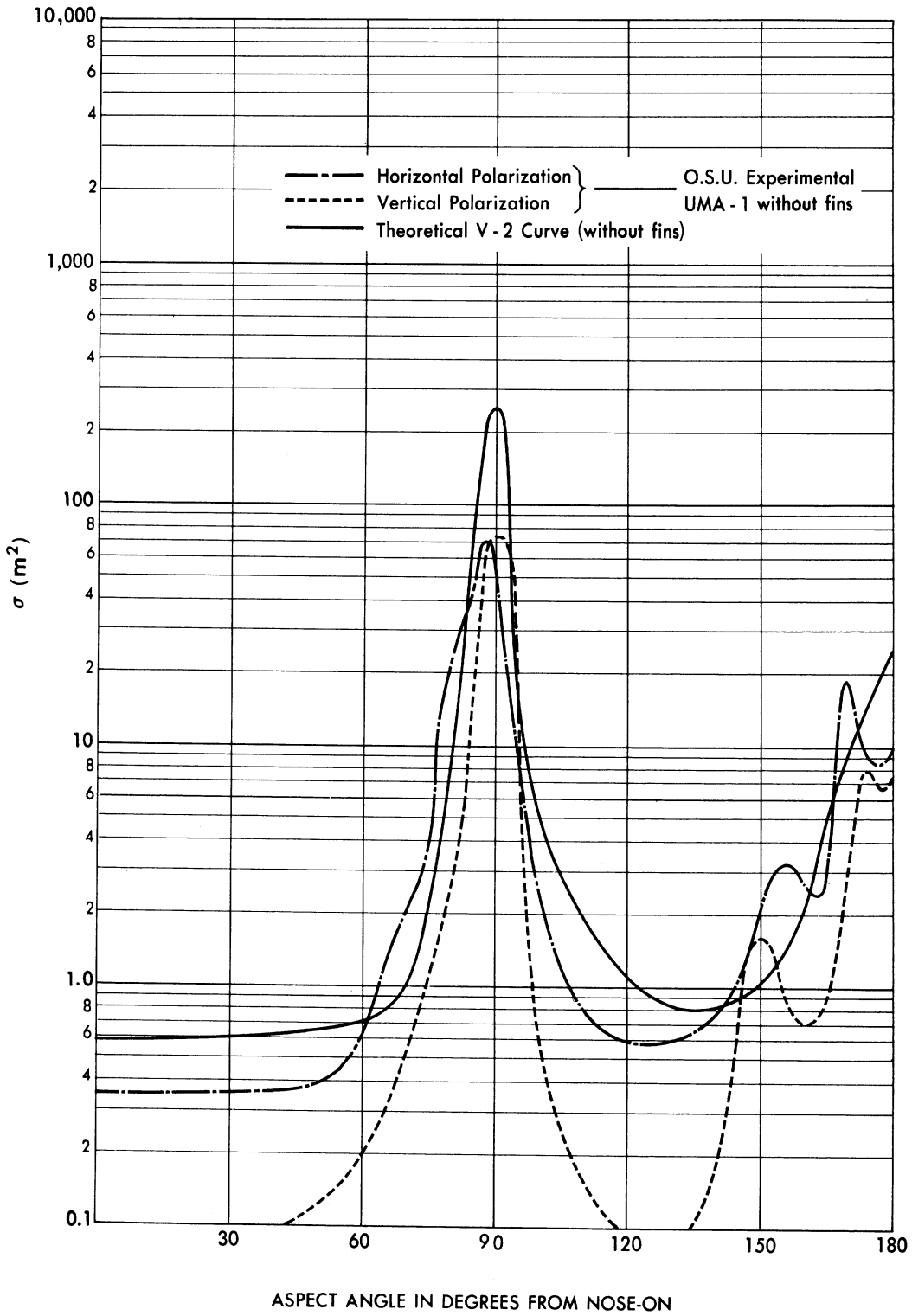

FIG. 5.4.8-3 COMPARISON BETWEEN THE THEORETICAL V-2 CROSS-SECTION AND THE EXPERIMENTAL UMA-1 CROSS-SECTION AS A FUNCTION OF ASPECT ANGLE AT ~400 MC/S - II

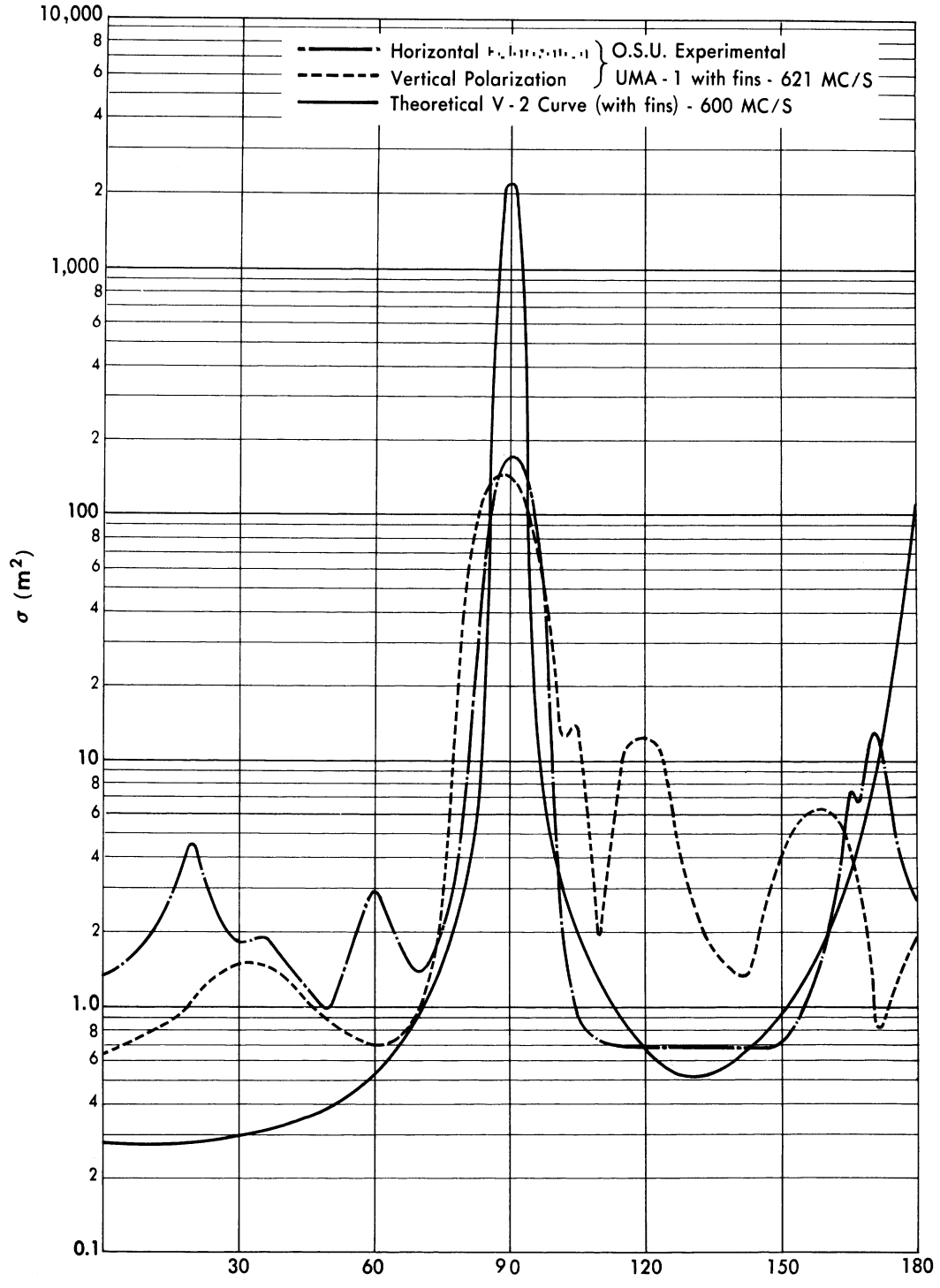

FIG. 5.4.8 - 4 COMPARISON BETWEEN THE THEORETICAL V-2 CROSS-SECTION AND THE EXPERIMENTAL UMA - 1 CROSS-SECTION AS A FUNCTION OF ASPECT ANGLE AT ~ 600 MC/S - 1

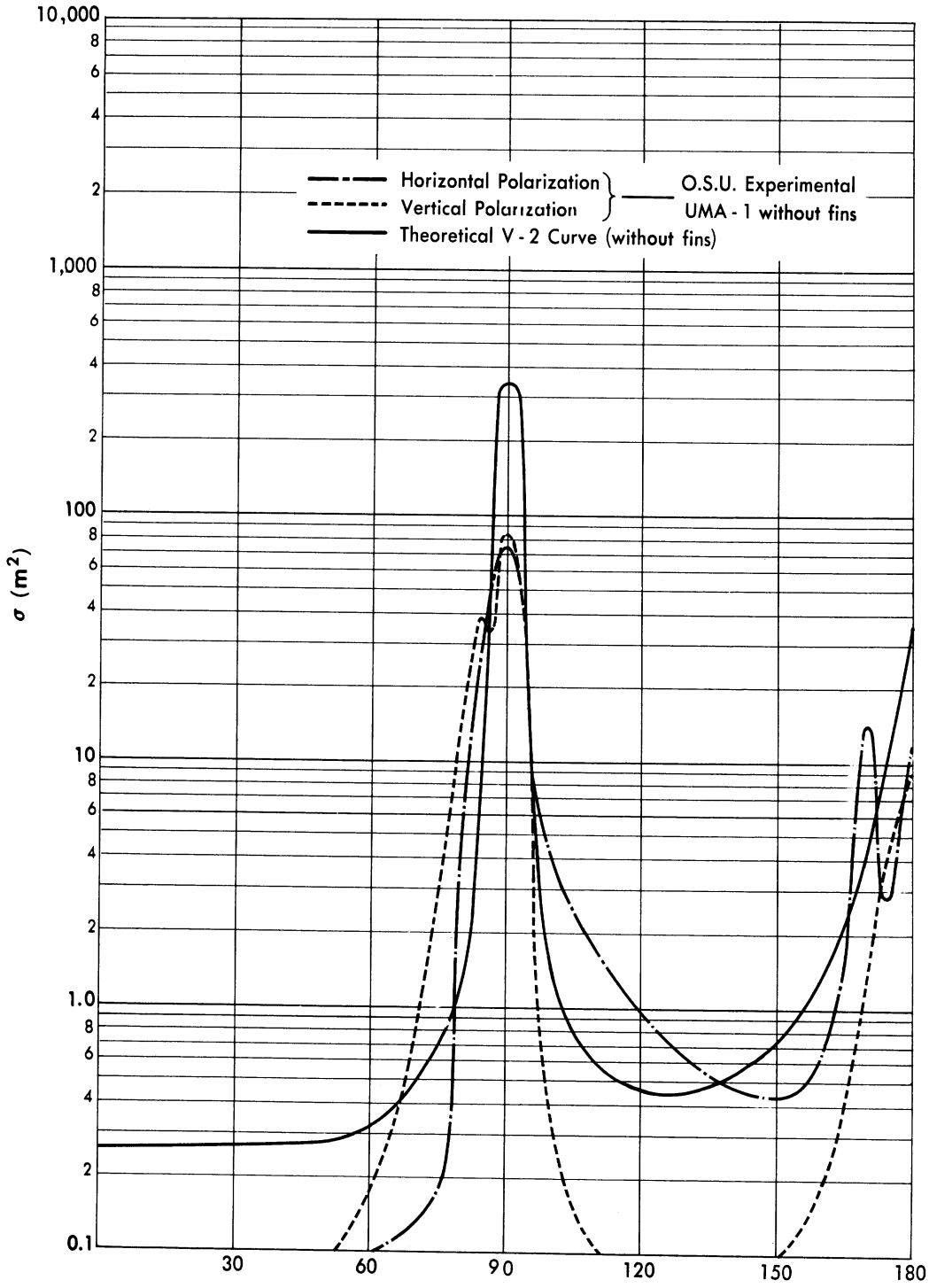

FIG. 5.4.8-5 COMPARISON BETWEEN THE THEORETICAL V-2 CROSS-SECTION AND THE EXPERIMENTAL UMA-1 CROSS-SECTION AS A FUNCTION OF ASPECT ANGLE AT ~ 600 MC/S - II

VIII

CONCLUSION

Inroads have been made on the major physical problems in the ballistic missile radar cross-section field. It is felt that sufficient knowledge now exists so that one can state what theoretical and experimental radar cross-section work should be done on Intercontinental Ballistic Missiles. It is further felt that enough is now known so that numbers may be specified which have physical meaning. The attainment of this knowledge and the ability to specify numbers has been the purpose of WRRC's work in the ballistic missile radar cross-section field.

APPENDIX I

THEORETICAL CONSIDERATIONS ON IONIZATION

The radar return to be expected from the ionic clouds produced by a high-speed missile depends upon the number of ions and free electrons produced, their distribution about the missile, and the aspect from which the cloud trail is viewed. Unfortunately, the experimental data available are insufficient for accurate computations of either the number of charged particles produced by such a missile or their spatial distribution. However, enough can be said to conclude that at altitudes above 200 km there will be insufficient ionization to appreciably affect the radar cross-section of a missile traveling at speeds below 10 km/sec.

In this appendix it is first established that a minimum missile speed of about 12 km/sec is required to form an appreciable number of potential ion producers above 200 km on the basis of various models for the ionization process, although a small number may be formed even at 10 km/sec. Even the latter speed is above that presently contemplated for intercontinental ballistic missiles. However, the analysis is continued on the assumption of sufficient ion production to estimate the expected spatial distribution of the ions (and associated free electrons) and the effects of such clouds on radar cross-section. These computations are then used to show that, for the radar cross-section to be appreciably enhanced, the required ion densities can be achieved only if several free electrons are produced by each energized atom or molecule. Although no data are available on the ionization probabilities for the primary type of collision of interest ($0 + 0 \longrightarrow 0 + 0^+ + e$), any type of collision where more than one electron is freed is so improbable, at the energies available, that the situation required for radar cross-section enhancement can be considered impossible.

In carrying out the various computations, wherever data or theory is lacking, the computations have been made so as to overestimate the

radar cross-section contribution of the ion cloud. The above conclusions were obtained in spite of these overestimations.

In making radar cross-section computations, a distinction is made between ionic clouds in which the density, N, of charged particles is above a certain critical density, N_c, and clouds in which the density is below that value. Where $N \geq N_c$, the index of refraction for the cloud is imaginary or zero. If the density of a cloud of charged particles is high near the cloud's center and decreases to zero at the edges, the inner part of the cloud will be bounded by a surface on which $N = N_c$. Then the outer part acts as a diffuse scatterer of incident electromagnetic energy, while the surface on which $N = N_c$ acts as a perfect reflector.

For a gas with primarily one type of scatterer, the index of refraction is given by (Ref. 7, p. 327, for example):

$$n = \sqrt{1 - \frac{N q^2}{4\pi^2 f^2 m \epsilon}} \qquad \text{(A.1-1)}$$

Setting $n = 0$ gives

$$N_c = \frac{4\pi^2 m \epsilon f^2}{q^2} \qquad \text{(A.1-2)}$$

Where m = mass of charged particle,
ϵ = dielectric constant of free space,
f = frequency of the radiation,
and q = magnitude of the charge on the particles.

In an ionic cloud, it is the free electrons which do most of the scattering, rather than the positive ions or the heavy negative ions formed by attachment, since the electrons have less mass and are thus more readily set into oscillation by the incident electromagnetic field. Thus, for scattering purposes, an ionic cloud should be thought of primarily as a free-electron cloud. For a free-electron cloud, Equation (A.1-2) becomes:

$$N_c = \frac{f^2}{81} \times 10^6 \text{ electrons/cm}^3. \qquad \text{(A.1-3)}$$

where f is measured in Mc.

An alternate view of this phenomenon is that there is a critical frequency f_c which must be exceeded for the electromagnetic waves to penetrate an ionic cloud of given density. Thus, to observe by radar a missile, which will be in or above the ionosphere layers, it is necessary to use frequencies above the critical frequencies for these layers. The largest* of these ionospheric critical frequencies is about 8.5 Mc.

A.1.1 Estimates of Minimum Speed Necessary for Ionization

Any estimate of the minimum missile speed required to produce appreciable ionization depends on the mechanism assumed for ionization.

We shall consider the following mechanisms:

1. Elastic collisions of stationary air molecules and atoms with a rigid missile skin of infinite mass give these particles sufficient energy to ionize other air molecules and atoms by subsequent inelastic collisions.

2. Elastic collisions of air molecules and atoms with individual atoms of the missile skin give the rebounding air constituents sufficient energy to ionize other air molecules and atoms, as above. (This case is distinguished from (1) because we treat the atoms of the metal not as rigidly bound in a lattice, but as free bodies having finite mass.)

3. Emission of metal atoms by evaporation from local "hot spots" on the missile skin.

4. Primary collisions of types described in 1 and 2 directly ionizing the air molecules and atoms which collide with the missile.

Two altitudes will be considered: 400 km and 200 km.

*In practice one should not consider operating lower than 20 Mc.

At the higher altitude, the only important constituent of the atmosphere is atomic oxygen (Ref. 8). It is therefore not necessary to consider molecular processes such as excitation of vibrational and rotational levels which might compete for energy with ionization. Also, since a dense gas cap will not form at the altitudes considered, we have not dealt with collision of oxygen atoms with those in a gas cap. Neither will ionization caused by high temperatures associated with the passing of air through a shock wave be treated, since no shock wave is present at these altitudes.

Although the density of nitrogen molecules is roughly 10 percent of the atomic oxygen concentration at the lower altitude considered, we shall neglect competing molecular processes at this altitude too. We thus overestimate the ion production.

The first two processes considered involve the ionization of air atoms or molecules by collision with other air atoms or molecules which have acquired high velocities by striking the missile skin. In order to determine the missile velocities at which the phenomenon is initiated, we must first compute the velocity that an air molecule or atom must attain before it can ionize another. In our calculations we shall first neglect the thermal velocities of the atmospheric constituents and then show them unimportant in cases where they might conceivably effect our conclusions.

A.1.1.1 Molecular Velocities for Ionization

To obtain a rough idea of the minimum missile speeds required for ionization we shall for the moment neglect the thermal velocities of the air molecules. In Section A.1.1.3 the thermal velocities and their distribution are taken into account.

If a particle of mass m_1 and velocity v_1 collides with an initially stationary particle of mass m_2, the maximum amount of energy, u, which can be transferred to the second particle is

$$u = \frac{1}{2} \frac{m_1 \cdot m_2}{m_1 + m_2} v_1^2 \qquad \text{(A.1-4)}$$

Setting u equal to the first ionization potential of atomic oxygen, we find that an oxygen atom must exceed 18.1 km/sec in velocity to ionize another stationary oxygen atom. For a collision between two nitrogen molecules, the minimum v_1 is 14.6 km/sec. We shall not consider N_2-0 collisions since the probability of ionization in such collisions is much smaller than in those considered (Ref. 8). These figures assume that ionization occurs for u = ionization potential, whereas heavy particles usually require several times this ionizing energy before they become most effective in ion production. This is reflected in their ionizing probabilities.

Having estimated the minimum velocity that a gas particle must have acquired to ionize another one, we now turn to considerations of the mechanisms by which this velocity is imparted to the particles. The introduction of these models permits the computation of threshold missile velocities (those which impart the above minimum values of v_1 to the rebounding particles).

A.1.1.2 Specular Reflection

The first model considered, in which the gas atoms and molecules collide elastically with a rigid missile skin, is based on one due to Cobine (Ref. 6). In such a model, the missile is considered to have infinite mass. The speed of a gas particle rebounding specularly from a conical nose surface is $v_1 = 2V\sin\alpha$, where V is the missile speed and α is the half-angle of the cone. For α = 15 degrees (Atlas 7-OC), the minimum missile speed required to ionize atomic oxygen is then 36.1 km/sec, while a 28.8 km/sec missile speed is needed to ionize nitrogen molecules. This is considerably above the presently contemplated speeds of less than 10 km/sec.

A.1.1.3 Direct Momentum Transfer

The model which we treat next is a better approximation to the physical situation. The experiments of Compton and Van Voorhis (Ref. 10)

on accommodation coefficients for ions incident on platinum and molybdenum cathodes indicate considerable energy transfer to the metal surface. Therefore the direct momentum transfer model, which allows such energy transfer, appears to be more realistic.

This model assumes that the gas-metal collision is so rapid that the metal atom may be treated as if free, the lattice forces not having time to transfer appreciable momentum. According to this picture, the speed attainable by a stationary air particle of mass m, colliding with a missile atom of mass M and speed V, is given as a function of the angle θ_2 between the missile axis and the direction of rebound by

$$v = \frac{2VM \cos \theta_2}{m + M} \qquad \text{(A.1-5)}$$

Introducing the maximum v obtained from this formula into the expression for u, we find that the maximum energy available to ionize an atom or molecule of mass m' is

$$u = \frac{1}{2}\left(\frac{mm'}{m+m'}\right)\left(\frac{2MV}{M+m}\right)^2 \qquad \text{(A.1-6)}$$

Equating this energy to the ionization potentials of N_2 and 0 we obtain estimates for various types of missile skins of the minimum missile speeds needed for ionization. These speeds are displayed in Table A-1.

Table A-1

THRESHOLD SPEEDS FOR IONIZATION
BY SCATTERED AIR MOLECULES

Material	$0 + 0 \longrightarrow 0 + 0^+ + e$	$N_2 + N_2 \longrightarrow N_2 + N_2^+ + e$
Fe	11.5 km/sec	10.9 km/sec
Ni	11.4 km/sec	10.7 km/sec
M_gO	12.5 km/sec	12.3 km/sec
Al	14.3 km/sec	14.9 km/sec

It appears from Table A-1 that a 10 km/sec missile will produce no ionization if the skin is made of the above materials. Since thermal velocities of the 0 atoms and N_2 molecules struck by the rebounding particles have been neglected, it might seem that this conclusion is too severe. However, even on the assumption of an ambient temperature of 1000^0 K (Ref. 8), we shall show that only a small fraction of even those air constituents which have most favorably oriented velocities will have great enough speeds to undergo ionizing collisions.

The relative kinetic energy of two colliding particles of masses m_1 and m_2, with velocities v_1 and v_2, is

$$T_R = \frac{1}{2} \frac{m_1 m_2}{m_1 + m_2} (\vec{v_1} - \vec{v_2})^2 \qquad \text{(A.1-7)}$$

If we use for $|\vec{v_1}|$ the maximum rebound velocity of an oxygen atom from a 10 km/sec iron missile, 15.6 km/sec, assume both particles oxygen atoms, and equate T_R to the first ionization potential of atomic oxygen, 13.5 e.v., we obtain

$$\vec{v_2} \cdot \vec{v_2} - 2 \vec{v_1} \cdot \vec{v_2} = .82 \times 10^{12} \text{ cm}^2/\text{sec}^2 \qquad \text{(A.1-8)}$$

Then taking

$$\frac{\vec{v_2}}{|\vec{v_2}|} = - \frac{\vec{v_1}}{|\vec{v_1}|}$$

to obtain the smallest $|\vec{v_2}|$, we find $|\vec{v_2}| = 2.4$ km/sec.

But at 1000^0 K, the average speed, $\bar{v}$, of an oxygen atom is $.921\sqrt{\frac{3kT}{m}}$ or 1.15 km/sec (Ref. 51). Thus we require $\frac{|\vec{v_2}|}{|\vec{v_2}|} = 2.10$, and less than .01 of even those atoms whose velocities are favorably oriented have such speeds (Ref. 51).

For N_2 molecules, $|\vec{v}_1|$ = 13.2 km/sec, and the ionization potential is 15.5 e.v. Then

$$\vec{v}_2 \cdot \vec{v}_2 - 2\,\vec{v}_1 \cdot \vec{v}_2 = .38 \times 10^{12}\ \text{cm}^2/\text{sec}^2 \qquad \text{(A.1-9)}$$

and $|\vec{v}_2|_{\min}$ = 1.4 km/sec. Here $\bar{v}_2$ = .873 km/sec and the ratio $\frac{|\vec{v}_2|_{\min}}{\bar{v}_2}$ = 1.6 is attained by about 10 percent of the molecules.

Since we have neglected the directional distribution in velocities of the struck particles which requires less favorable directions and therefore improbably high speeds for an enormously high fraction of them, it is clear that thermal velocity of the ambient atmospheric constituents will not make it possible for our 10 km/sec missile to produce many ions by this model.

Furthermore, even if missile speeds greater than those of Table A-1 are attained, there will be a distribution in direction, and therefore, by Equation (A.1-5), in magnitude of rebound velocities. This distribution will reduce the number of rebounding particles which are potential ion producers. For a given V the minimum value of $\cos\theta_2$ which pemits ionization may be computed from Equations (A.1-4) and (A.1-5). We shall assume a probability density $\frac{1}{2}\cos\theta$ for a rebound at an angle θ from the normal to the cone side (Ref. 70). On this basis the probability that $\theta_2 | < y$ is found to be

$$\begin{aligned} P &= \sin\alpha \sin y, \quad y \le \alpha \\ &= \tfrac{1}{2}\left[1 - \cos(\alpha + y)\right], y > \alpha. \end{aligned} \qquad \text{(A.1-10)}$$

Then for an Fe skin typical results for the probability of rebounds sufficiently rapid to cause ionization in 0 - 0 collisions, neglecting thermal velocities are:

Table A-2

V km/sec	P
12	.066
15	.210

The direct momentum transfer model affords only a small number of sufficiently energetic collisions for a 10 km/sec missile. This fact will be shown to require an unreasonably high probability for ionization in such a collision in order that ionization sufficient to give rise to an observable radar cross-section be produced. We shall therefore be able, by our computation, to rule out this model as a significant source of ionization.

A.1.1.4 Local Heating

The "local heating" model, developed by Hippel and Blechschmidt and more recently by Townes, explains the sputtering of cathode material by high-speed ions (Ref. 11). According to this theory, the energy transfer when an ion strikes a metal surface takes place so quickly that there is no time for heat to be dissipated. High local temperatures are obtained, and atoms evaporate from the cathode. This model gives minimum missile speeds not significantly different from those in Table A-1. However, since the mechanisms stopping positive ions and neutral atoms in a metal differ, we think it unsound to base an expectation of ion-producer emission on this model. We are therefore forced to neglect it, with the reservation that more detailed analysis might show it to be significant.

A1.1.5 Ionization by the Primary Collision

Equation A.1-4 applied to collisions of O or N_2 with either the missile as a whole or a free Fe atom, shows ionization by direct elastic collision energetically impossible. We also neglect inelastic collisions, since energy transfer to the lattice rather than to the O or N_2 is to be expected physically.

A.1.2 Near Nose-On Aspects

The radar cross-section of the ion cloud for the nose-on aspect of a missile is of special interest since it is for this aspect that a missile body (having a pointed nose) yields its smallest radar return. For the ion cloud to have a large cross-section from aspects near nose-on, it must contain a dense supra-critical region, whose surface is rounded and sufficiently large with respect to the wavelength of the incident radiation when viewed from the radar. Section A.1.1 demonstrates, on the

basis of very simplified physical pictures, the possibility of an ion cloud of this shape (but not necessarily supra-critical density) forming about the missile in the upper atmosphere, provided sufficient ions and free electrons are produced.

A.1.2.1 The Shape of the Ionic Cloud

As the potential ion producers discussed in Section A.1 rebound from the missile skin the density of collisions and drops off as $Ae^{-x/\ell}$ where x is distance normal to the skin measured from the point of rebound, ℓ is mean free path, and A is a constant. Hence a contour of constant density will form at a distance

$$\delta = \frac{f(\ell,\rho)\ |\overline{V}'_n|}{|V' + \overline{V}_n|} \qquad (A.1-7)$$

from the missile, where $\overline{V}_n$ is the component of the missile velocity in the direction normal to the missile surface at the point in question, $\overline{V}'$ is the relative velocity of the rebounding ion producers and $\overline{V}'_n$ is the component of $\overline{V}'$ in the direction of $\overline{V}_n$. In using this formula at 200 km altitude and above it is probably safe to use the mean free path of the ambient atmosphere since it is not likely that an appreciable gas cap will have formed about the missile at these altitudes.

According to this model, the contour within which most of the ions would be initially formed about the conical nose of a missile would be a cone with a spherical tip. Certainly diffusion would smooth out the transition from cone to rounded tip, so the contour would roughly resemble a hyperboloid and will be taken of that shape in the cross-section computation.

A.1.2.2 Cross-Section of a Supra-Critical Density Cloud

We shall assume $N \gg N_c$ within a hyperboloid. Physical optics reasoning (Ref. 57) yields, for the radar cross-section of a hyperboloid whose radius of curvature at the nose is r_c and whose asymptotic cone has an half-angle θ_c:

$$\sigma = \pi r_c^2 + \frac{\lambda^2}{16\pi} \tan^4 \theta_c. \qquad \text{(A.1-8)}$$

In other words, the cross-section of this hyperboloid may be represented by the sum of the cross-sections of a sphere and a cone. These are discussed in Section A.1.4.1 below.

A.1.3 Effect of the Diffuse Part of the Cloud

The above considerations give no idea of the form taken by the more diffuse part of the ion cloud. This is now investigated on the basis of a simple diffusion theory. From the results, it is then shown that the diffuse region cannot increase the radar cross-section of the whole ion cloud above that of the critical-density region. We shall therefore consider only the critical-density region in computing the cross-section of the ion cloud.

A.1.3.1 The Electron Density Distribution

To consider the diffuse cloud, we begin by describing the distribution of electrons at a distance from the missile for altitudes above 200 km, where free molecule flow prevails and the effect of recombination may be neglected. For study of the distribution of electrons far from the missile (i.e. at distances large compared to both the mean free path and the missile dimensions), the missile may be considered to be a moving point source of electrons. The electrons spread by diffusion away from the missile. The equation which must be solved is the diffusion equation:

$$\nabla^2 N(\vec{r}) = \frac{1}{D} \frac{\partial N(\vec{r})}{\partial t} \qquad \text{(A.1-9)}$$

in which ∇^2 is the Laplacian operator, $\vec{r}$ is the position vector from the source to the point of observation, $N(\vec{r})$ denotes the electron density N, D is the diffusion coefficient, and t is the time. Consider a point source to be moving in the negative z-direction at a speed V, and producing η electrons per unit length of its path. The resultant density is equivalent to that due to integrating the contributions of a distribution of stationary

sources along the z-axis which initiated their effects at successive moments in the past. This integration yields the following solution of the diffusion equation for a time of observation t = 0:

$$N(\vec{r}) = \frac{\eta}{4\pi D r} V e^{-\frac{V}{2D}(r - z)} \qquad \text{(A.1-10)}$$

The integration was carried out over all past time and a constant D was assumed. This implies constant altitude flight. For vertical flight D is variable and in fact the missile was not in the atmosphere and acting like an ion source for more than a limited time. Numerical examination of the integrand for suitable parameter values and an average D showed that the error in using an infinite integration time would be negligible; on the other hand it greatly simplifies the integration. (The anisotropy introduced by the earth's magnetic field could have been taken approximately into account by using a tensor diffusion coefficient.)

The contours in space of constant density given by Equation (A.1-10) above may be put in the dimensionless form

$$\frac{\exp[\alpha(s - \rho)]}{\rho} = 1 \qquad \text{(A.1-11)}$$

where

$$\rho = \frac{r}{a}, \; s = \frac{z}{a}, \; a = \frac{\eta V}{4\pi N D}, \quad \alpha = \frac{Va}{2D} \qquad \text{(A.1-12)}$$

For each value of α a contour profile may be plotted. The factor, a, represents the scale of the contour, whereas α determines the contour shape. The contours represent surfaces of revolution about the s-axis. Figure A.1-1 depicts several profiles for values of α ranging from 0 to ∞. The condition $\alpha = 0$ corresponds to a spherical contour, $\alpha = 100$ corresponds roughly to an elongated cylinder with a spherical nose. $\alpha = \infty$ corresponds to a straight line.

Note that the succession of contours in Figure A.1-1 does not directly give the spatial distribution of electron density. Since both a and α are

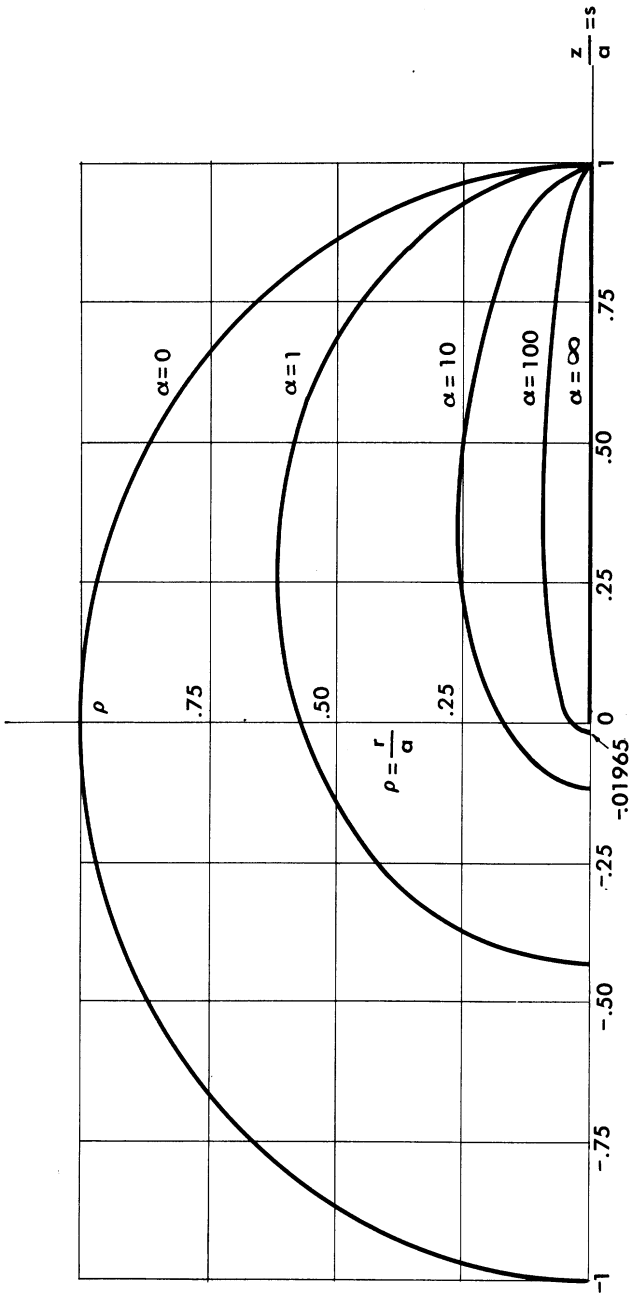

FIG. A.1 - 1 CONTOURS OF CONSTANT α

inversely proportional to N, the surfaces of constant density in rz space are small spheres of high density surrounded by larger elongated surfaces with rounded noses representing lower density. Even this picture, of course, does not describe the situation near the missile surface. We shall, however, use it to show that if the missile is surrounded by a critical-density cloud of electrons, the larger and more diffuse clouds of the type described above do not increase the cross-section of the innermost critical-density cloud. Thus, when in subsequent computations, we assume that the return from the ionic cloud accompanying the missile is essentially that of a metallic conductor having the shape of the critical-density cloud, we obtain an upper bound on the cross-section.

A.1.3.2 Refraction by the Low-Density Part of the Cloud

The index of refraction is given by

$$n^2 = 1 - \frac{Nq^2}{m_e \epsilon \omega^2} \qquad \text{(A.1-13)}$$

where $4\pi^2 f^2$ in (A.1-1) is replaced by ω^2, and m_e equals the mass of an electron.

Using Equation (A.1-10) for N, Equation (A.1-13) becomes

$$n = \sqrt{1 - \frac{V\beta}{Dr} e^{-V(r-z)/2D}}, \quad \text{where} \quad \beta = \frac{\eta q^2}{4\pi m_e \epsilon \omega^2} \qquad \text{(A.1-14)}$$

For rays incident nose-on close to the z-axis, the variation of the index of refraction is nearly radial. For points close to the negative z-axis, $z \cong -r$, and the expression for n becomes

$$n = \sqrt{1 - \frac{V\beta}{Dr} e^{-Vr/D}} \qquad \text{(A.1-15)}$$

We shall assume that this expression holds for $r > r_c$, the radius at the nose of the critical density hyperboloid. Since for wavelengths of interest, the critical density hyperboloid reflects like a sphere of radius r_c, the second term in Equation (A.1-8) being negligible, it is justified to replace it here by a sphere (Fig. A.1-2).

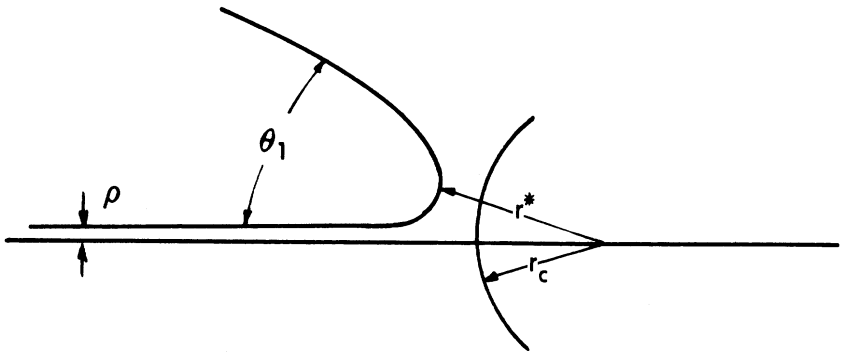

Fig. A.1-2

If a small bundle of rays is incident along the z-axis the incident rays furthest from the axis are refracted through some angle θ_1. For an index of refraction dependent only on r, such as we have here, an application of Luneberg's work (Ref. 9, Sec. 27) shows that θ_1 may be expressed as

$$\theta_1 = 2 \int_{r^*}^{\infty} \frac{\rho' \, dr}{r \sqrt{n^2 r^2 - \rho'^2}} \qquad \text{(A.1-16)}$$

where r^* is the minimum of r along the outermost rays of the bundle and ρ' is the radius of the incident bundle of rays. Here, r^* is given by the equation

$$(r^*)^2 \left[n(r^*)\right]^2 - (\rho')^2 = 0 \qquad \text{(A.1-17)}$$

For a ray coming in along the axis, that is in the limiting case as $\rho' \to 0$, $r^* \to r_c$, provided a density $N = N_c$ is achieved in the cloud.

The geometric optics approximation for the radar cross-section of this rounded ion cloud is

$$\sigma = \lim_{\rho' \to 0} 4\pi R^2 \frac{\pi \rho'^2}{\pi R^2 \tan^2 \theta_1} = \lim_{\rho' \to 0} 4\pi \frac{\rho'^2}{\theta_1^2}. \qquad \text{(A.1-18)}$$

We may write therefore

$$\sigma = \lim_{\rho' \to 0} \frac{4\pi\rho'^2}{4\left[\int_{r^*}^{\infty} \frac{\rho' dr}{r\sqrt{n^2r^2 - \rho'^2}}\right]^2} = \frac{\pi}{\left[\int_{r_c}^{\infty} \frac{dr}{nr^2}\right]^2}. \qquad \text{(A.1-19)}$$

For

$$n = \sqrt{1 - \frac{V\beta e^{-\frac{Vr}{D}}}{Dr}}, \qquad \text{(A.1-20)}$$

we have

$$\sigma = \frac{\pi}{\left[\int_{r_c}^{\infty} \frac{dr}{r^{3/2}\sqrt{r - \frac{V\beta}{D} e^{-Vr/D}}}\right]^2}. \qquad \text{(A.1-21)}$$

An upper bound on this expression for σ is $\sigma = \pi r_c^2$. We see, then, that a diffuse cloud of ions or electrons cannot increase the cross-section of a critical-density cloud which it surrounds.

A.1.4.1 Ionizing Efficiencies Required for Critical-Density Clouds, Nose-On

We shall assume that the minimum radar cross-section in the frequency range of interest will be π square meters (which is of the same order of magnitude as the broadside radar cross-section of the missile body), and inquire as to what efficiency of ion production is required to maintain a critical-density region of the missile nose which will have such a cross-section.

It will be recalled (Eq. A.1-8) that the radar cross-section of a hyperboloidal ion cloud of critical-density is given by

$$\sigma = \pi r_c^2 + \frac{\lambda^2}{16\pi} \tan^4 \theta_c.$$

Even at the lowest radar frequency which might be used in observing the missile (we shall consider 25 Mc, since higher frequencies require even higher critical densities and efficiencies), the second term is negligible compared to the first. We must then investigate the possibility of filling with ions a hyperboloid of 1 meter equivalent nose-radius. (If the ions are actually formed in a smaller region, the radar cross-section will be less than π square meters. To fill a larger region would require a still higher efficiency than that which we shall compute.)

We shall underestimate the required efficiency in two more ways. First, we shall neglect the variation in collision density with distance from the missile, which would require a supra-critical density interior to a critical-density surface. Second, we shall replace the hyperboloid which must be maintained at critical density with the included sphere of radius r_c.

The ionizing efficiency required may now be computed. In order to maintain critical-density in a sphere of 1 meter radius, the missile would have to produce $N_c V$ electrons or ions over a path length ℓ, where V is the volume between 2 spheres of 1 meter radius whose centers are displaced by a distance ℓ. (This is the new region to be filled as the missile proceeds forward.) This volume is $\pi \ell \ M^2$. Now if the efficiency E is the number of ions produced per air particle struck by the missile, r_o is the maximum missile radius, and N_0 is the ambient density of atoms and molecules, the missile will produce $N_0 \pi r_0^2 \ E \ell$ ions in a path of length ℓ.

Maintainence of critical density then requires

$$N_0 \pi r_0^2 \ E \ell = N_c \pi \ell \qquad \text{(A.1-22)}$$

or

$$N_0 \ E = \frac{N_c}{r_0^2}$$

Now E is the product of the probability (p_1) of the air particle struck by the missile acquiring sufficient energy to ionize another, the probability

(p_2) of colliding with another air particle, and the probability (p_3) of ionization if a sufficiently energetic collision occurs. p_2 will be taken as 1. (At the energies available, only one ionizing collision is possible.) The mechanism of direct momentum transfer yields a p_1 smaller than 10^{-2} for oxygen atoms at 10 km/sec. At 400 km then, where only oxygen atoms are of importance, only a value $p_3 > 1$ would permit $p_1\, p_2\, p_3$ to equal the required E. Such a value is, of course, impossible. At 200 km, where both nitrogen and oxygen are present, Equation (A.1-22) may be written more explicitly as

$$\frac{N_c}{r_0^2} = N_0^{N_2}\, E^{N_2} + N_0^0\, E^{0*} \qquad \text{(A.1-23)}$$

in which collisions between N_2 and 0 have been neglected, since ionization probabilities for mixed collisions are negligible compared to those for homonuclear collisions (Ref. 8).

The ambient densities at 200 km altitude are 4.3×10^9 nitrogen molecules/cm^3 and 1.75×10^{10} oxygen atoms/cm^3. Repeating the computation of Section A.1.1.3 for an ambient temperature of 640^0 K will lower p_1 for 0. The new value is less than 10^{-3}. For N_2, the probability of sufficient thermal speed is now < 0.02. If we overestimate the probability of favorable direction of the thermal velocity by counting all velocities within unit solid angle of $\vec{v}_1$, $p_1^{N_2}$ becomes $< 0.02/4\,\pi$ or 1.6×10^{-3} and p_1^0 becomes $< 0.8 \times 10^{-4}$. We may then write

$$8.68 \times 10^6/\text{cm}^3 \times \frac{1\ \text{m}^2}{.9\ \text{m}^2} = (4.31 \times 10^9/\text{cm}^3 \times 1 \times 1.6 \times 10^{-3}\ p_3^{N_2} + 1.75 \times 10^{10}/\text{cm}^3 \times 8 \times 10^{-5}\ p_3^0$$

or

$$2.24 \times 10^{-3} = 1.6 \times 10^{-3}\ p_3^{N_2} + 0.325 \times 10^{-3}\ p_3^0,$$

*The superscript identifies the molecule or atom to which the associated symbol refers.

which cannot be satisfied by values of p_3 less than 1. Since many factors which would increase the required efficiencies have been overestimated or neglected, we may conclude that for a 10 km/sec missile none of the mechanisms considered will produce sufficient ionization to yield a nose-on cross-section of π square meters even as low as 200 km altitude.

It should be noted that even at missile speeds slightly above threshold the previously mentioned distribution of rebound velocities will partially counteract the smaller contribution of thermal energy required, so that even then ionization may not be significant.

A.1.4.2 Off Nose and Broadside Aspects

From the previous sections it is evident that a critical density region can fill at best only a thin shell about the nose of a 10 km/sec missile. Furthermore there will be practically no ionization formed along the cylindrical sides of the missile by the mechanisms discussed. In the rare atmospheres under discussion, diffusion is quite rapid, and there is no reason to expect a large percentage of the electrons displaced radially by the missile in its passage through the electron cloud at its nose to remain near the cylindrical sides of the missile. Hence there is little reason to expect ionization of density exceeding N_c toward the rear of the cylindrical portion of the missile or in a trail behind it. The comparatively large radar cross-section of the off-nose and broadside aspects from the missile surfaces will therefore not be enhanced by ionization.

APPENDIX 2

MEASURING TECHNIQUES

A.2.1 Measurement Techniques and the Techniques Used at Microwave Radiation Company for Static Measurements*

A.2.1.1 Introduction

"The measurement of radar scattering cross-section is essentially the measurement and comparison of quantities which are related to the magnitude of the wave scattered by the target and the magnitude of the wave incident upon the target. The phase information is not necessarily used in the comparison procedure. The basic problem is to obtain a signal proportional to the scattered wave with as high a signal-to-noise ratio as possible. The noise is produced not only by the customary noise sources, but includes energy leaking directly from the generator to the receiver, scattering return from the ground and the support structure for the target, internal reflections in the microwave components and antenna, and additional noise sources peculiar to the basic circuitry being employed in the measurement device.

"Each of the three general techniques employed, pulse, f-m, and c-w, has its region of best use, as determined by model size and data required, and its fundamental limitations and inherent errors (Ref. 35). The regions of best use are specified by the target size in wavelengths at the full or scale frequency. Small targets are arbitrarily specified as from 0 to 50 wavelengths in extent, intermediate size targets are from 50 to 250 wavelengths in extent, and large targets are greater than 250 wavelengths in extent.

*This appendix, except for the notation used for references, sections, and figures, is quoted verbatim from a letter report by M. J. Ehrlich of the Microwave Radiation Company.

A.2.1.2 Measurement Techniques

"The pulse system is one in which the transmitted pulse is made extremely brief in time duration, and the transmitted signal and its induced effects in the receiver have ceased when the scattered signal reaches the receiver. One of the principal shortcomings of the pulsed system at present is the limitation of the minimum measurement range to values between 500 and 1,000 feet. This limitation arises from the high "Q" of the duplexer circuitry and/or the "recovery time" of the receiver. The resultant "ringing" is still of sufficient magnitude upon return of the scattered signal to cause excessive error. The minimum range allowed introduces considerable illumination of the ground between the target and transmitter. In order to reduce ground reflections, a large support structure is necessary. The support structure must be quite large in order to be out of the main beam and thus have little return. The relatively small back scattered signal of a thin needle-shaped target in the nose-on and quartering aspects may easily be lost in the return signal from the support structure and intervening ground. In addition, fluctuation in pulse height and variations in TR and ATR tube characteristics serve to introduce considerable error.

"Pulsed systems cannot accurately measure back scattering cross-section for the great majority of models at ranges of 1,000 to 2,000 feet at the present time. However, for very large models in terms of wavelengths, or full scale models, it is the only available technique and thus may find ample use despite its many shortcomings.

"The f-m or doppler system is one in which filters are employed to utilize the difference between the transmitter frequency at the time of return of the scattered signal and the frequency of the scattered signal. Variations of this technique employ moving or oscillating models to generate frequencies different than the transmitted signal, and thus furnish a basis for differentiating between the model return and the ground and support structure return.

"The f-m system is limited in use to the measurement of scattering cross-section of models large in terms of wavelength. The reason for

the limitation is the requirement of an appreciable frequency difference between transmitted and received signals. Implicit in the requirement is the assumption of a considerable range to the target which ensures ample time for the transmitter to change frequency by an adequate amount. The problems of return from structure and ground are thus also present in the f-m system. Reference 35 was somewhat optimistic in that larger bandwidths were assumed for the magic-T than may be feasibly obtained. The resulting amplitude modulation introduces large error signals in the i-f section and places further restrictions on required minimum range.

"There are other factors which at present preclude the use of an f-m system for the measurement of the scattering return of small and intermediate size targets. Among these is the fact that current f-m systems do not measure signal amplitude but measure instead relative velocity and range. The system circuitry has not been developed to measure signal amplitudes, and any such future development will be necessarily a long and costly procedure.

"A system is in use abroad which utilizes a rectilinear motion of the target toward the transmitter to produce a doppler shift for measurement of backscattering cross section. The system is, unfortunately, adversely affected by return from the moving model support, as it is unable to differentiate between model return and support return. The required complexity of model support and towing carriage, the length of tow required, and the relatively short time of measurement combine to make this system too inaccurate for precision measurement of any models but those very large in terms of wavelengths.

"The c-w technique is one in which the isolation qualities of a properly terminated magic-T are utilized to separate the transmitted and received signals, and thus allow the magnitude of the scattered signal to be determined. The experience gained by the Microwave Radiation Company, Signal Corps Evans Laboratory, McGill University, and Ohio State University have demonstrated the feasibility of use of the c-w system for the measurement of monostatic radar backscattering cross section of small and intermediate size targets. The technique is presented in some detail below.

A.2.1.3 Discussion of the C-W Measurement Technique

A.2.1.3.1 Theory of Operation

"The c-w technique employs the isolation obtained between the arms of a magic-T to separate the received from the transmitted signal as shown in Figure A.2-1. The transmit-and-receive antenna is connected to one symmetrical arm of the magic-T and a tuning network to the other arm. The receiver is connected to one of the asymmetrical arms of the magic-T and the transmitter is connected to the other. The tuning network is adjusted so that the field reflected from it into the receiver arm very nearly cancels the signal in the receiver arm arising from reflections from the symmetries in the antenna arm, discontinuities in the antenna, and back scattered signals from the ground, nearby objects, and the model support structure. The model is then placed in the support, and the output of the receiver is a measure of the back scattered signal from the model. A calibration of the absolute level is obtained by measuring the back scattered signal from spheres of different radii.

A.2.1.3.2 Error of Measurement

"The principal portion of the error of measurement in the c-w system is measured by the vector sum of the reflections coupled into the receiver arm from sources other than the model and the opposing reflection supplied by the tuning network. This vector sum, or residual signal, hereafter called the "cross-coupling error signal", is usually the preponderant part of the probable error of the measurement.

"The ratio of the amplitude of this residual signal to that of the generator output specifies the isolation of the magic-T.

"The cross-coupling error signal is extremely frequency sensitive because it is the vector sum of reflections arising at discontinuities many wavelengths apart. Hence, frequency stability of the klystron source, reduction of ground and support reflections, and reduction of mechanical vibration and thermal variation are essential. In addition, the tuning network, used to balance out the reflections causing the

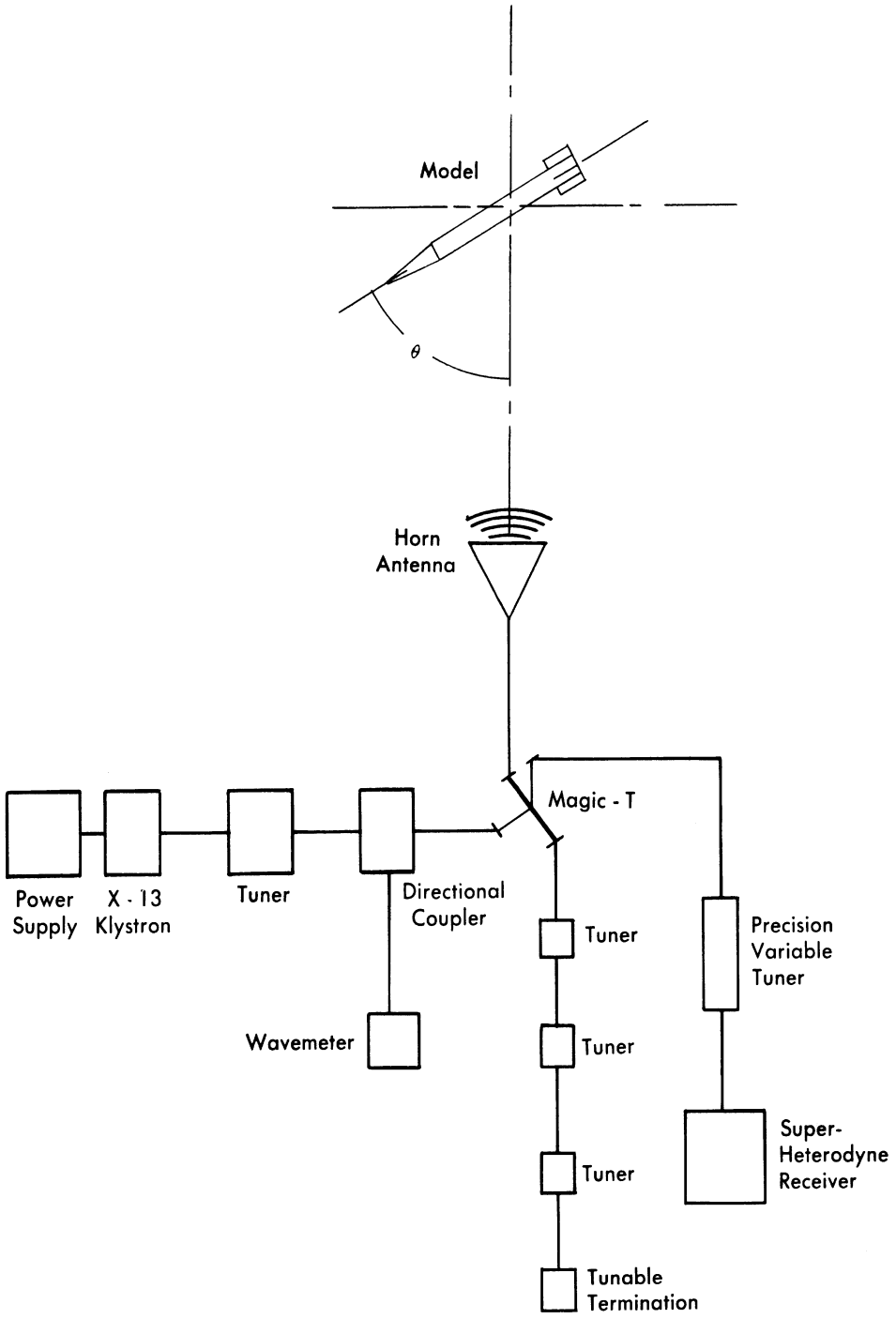
Model
θ
Horn
Antenna
Magic - T
Power
Supply
X - 13
Klystron
Tuner
Directional
Coupler
Tuner
Precision
Variable
Tuner
Wavemeter
Tuner
Super-
Heterodyne
Receiver
Tuner
Tunable
Termination

FIG. A.2-1

cross-coupling signal, must be of sophisticated design in order to have the required bandwidth and sensitive adjustment characteristics, so that the probable error of measurement may not become excessive.

A.2.1.3.3 Problems of Measurement of Monostatic Radar Back Scattering Cross-section Using a C-W System

"It is now evident that the fundamental limitation of the c-w system is the magnitude of the required isolation of the T. Very great isolation levels, in excess of 90 db, are required to measure accurately the return from missile and supersonic vehicle configurations. Since measurements must be made in the far zone of the target, it is qualitatively clear that, owing to the upper bound on feasibly obtainable isolation levels in the magic-T, an upper bound must exist on target size. Above this size limitation the errors increase rapidly. Contrary to intuition, the larger the model, the larger the required isolation. This seeming paradox arises from the fact that a larger model requires a greater distance between the model and antenna in order to ensure operation in their respective far zones, and hence the returned signal rapidly decreases with increasing distance. A quantitative relation has been obtained (Ref. 13) between the target size in wavelengths and the target reflection characteristics, in order to obtain a specified signal-to-noise ratio. The nose-on and quartering aspect returns of missile-like targets investigated have been found to have backscattering cross-sections 15 to 20 db less than the return from a sphere whose diameter is equal to the maximum dimension of the target. A graph of the isolation required to obtain a unity signal-to-noise ratio for a spherical target, as a function of sphere radius, is shown in Figure A.2-2. It is clear from the graph that in any feasible, physically realizable c-w system incorporating a magic-T, an upper bound must be placed on model size, in wavelengths, in order that the probable error of measurement not become excessive. It is seen from Figure A.2-2 that the isolation level required for a specified return signal-to-noise ratio is proportional to the square of the size of the target in wavelengths.

"Hence, a change in the scale frequency used to simulate the full scale problem does not serve to alter the isolation level requirement.

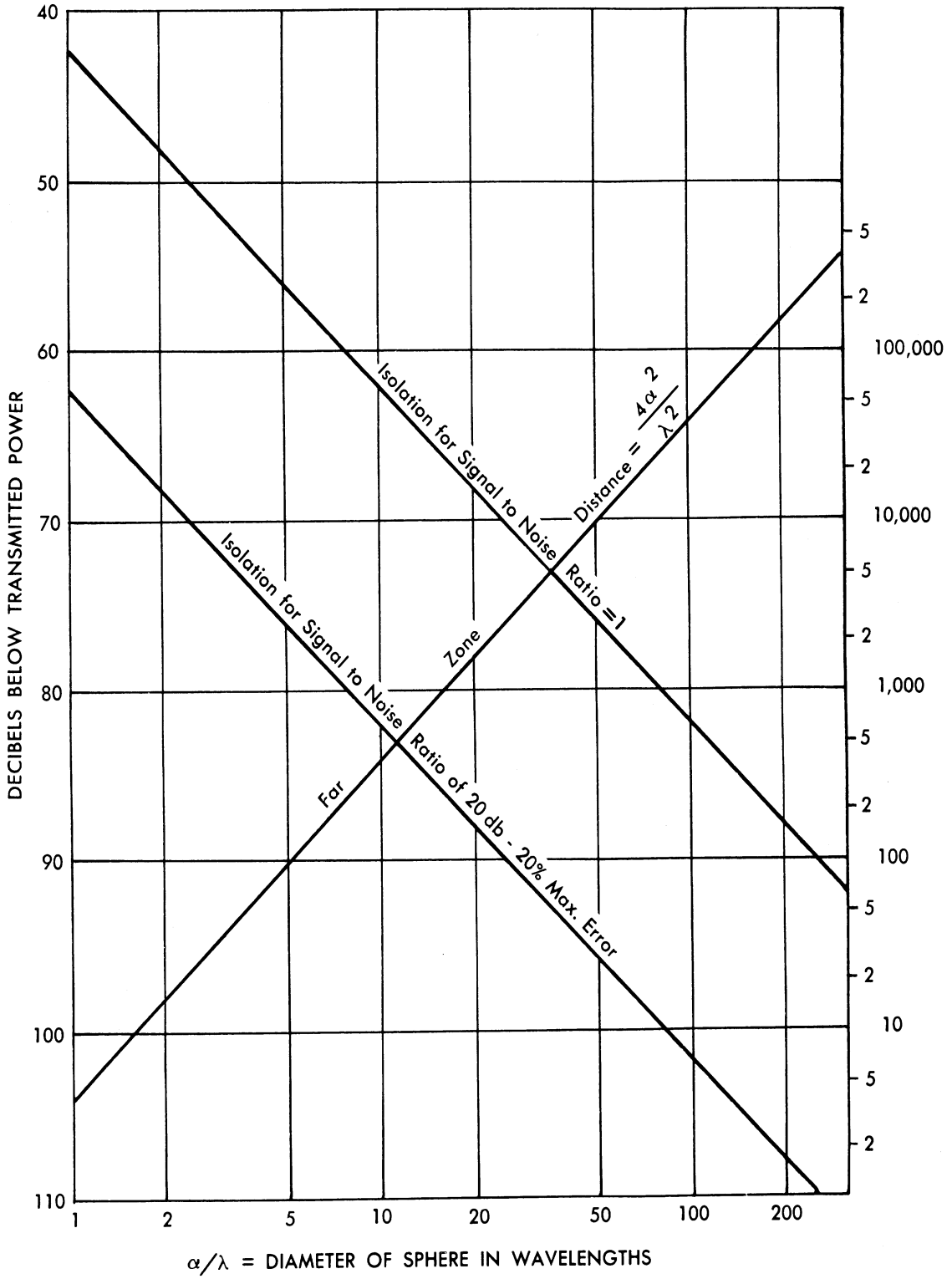

FIG. A.2-2 ISOLATION REQUIRED FOR SPHERE

It merely serves to change the dimension of the pattern range and c-w system microwave components. The general experience has been to limit the highest scaling frequency to X-band.

"It is to be noted that an increase in the power output of the transmitter does not improve the system performance, as it is the isolation level of the magic-T that specifies the performance. Adequate transmitter power is provided by a medium-power klystron. A check on transmitter power level is furnished by noting the presence of the cross-coupling error signal in the receiver output.

A.2.1.3.4 Optimum Size of the Transmitting Antenna

"Ideally the size of the antenna should be equal to the maximum dimension of the target (Ref. 35), assuming, of course, far zone operation, in order to realize maximum return signal. Inasmuch as a wide variety of targets of different dimension may be measured in the course of operation of the instrument, a compromise must be made regarding the number of different sizes of the antenna used. Usually the antenna will differ from the optimum, and the signal will be less than the theoretical maximum.

"The target is a passive scatterer, and the return signal is inversely proportional to the fourth power of the range. Hence, a severe penalty is paid in reduction of the signal-to-noise ratio for performing measurements at distances in excess of the allowable minimum. A pattern range of variable size is therefore implied in the foregoing discussion.

"Similar arguments as to size may be made regarding the target support structure. The support structure should be reduced in size for the smaller targets because the structure return signal contributes in a coherent manner to the target return signal. Thus a relatively large error may be introduced. Concomitant with the increased range introduced by large targets is an increased ground return signal. The frequency stability of the r-f source of the c-w system is such that the ground return is also a coherent signal and introduces substantial errors in the target return signal.

A.2.1.4 Revision of the Classical Far Zone Concept

"The majority of targets to be studied are long, needle-shaped objects with sharply swept back wings and/or fins. They have high aspect ratios and long tapering front ends. It is almost needless to state that the radar backscattering return signal from such targets is exceedingly small for all aspect angles except the near broadside and broadside aspects. The cross section information of principal concern, however, is in the region of small return, i.e., nose-on and quartering aspects off nose and tail.

"The range required between the target and antenna is the far zone of the target or antenna, whichever is larger. The far zone as specified by the maximum target or antenna dimension is much too great to obtain a usable signal-to-noise ratio for any but the broadside aspects of large models. Consequently, measurements of scattering return for the nose-on and quartering aspects may be in error by several orders of magnitude when measured at this maximum far zone distance.

"A revision of the classical far-zone concept (Ref. 14) has been made (Ref. 13) which shows that the far zone of the target, which is a passive scatterer, is a function of the target dimension and of the angle of incidence between the propagation vector of the incident plane wave and the longitudinal axis of the target.

"The required far zone is proportional to the angle of incidence. The smaller the angle of incidence, i.e., more nearly nose-on, the smaller the required far zone distance. At broadside the far zone distance of the target is given by

$$r = \frac{D^2}{\lambda},$$ where D = largest dimension of model, λ = free space wavelength;

and for the nose-on aspect

$$r = \frac{b^2}{\lambda}$$ where b = largest transverse dimension.

Thus the target may be placed closest to the transmitting antenna (the transmitting and receiving antenna being coincident in backscattering measurement) for the nose-on aspect and moved farther away as the incidence angle is increased.

"The magnitude of the back scattered signal is markedly increased in this manner, and more accurate data is obtained, provided the cross-coupling error signal is not allowed to increase above a specified maximum value. It is assumed, of course, that for all angles of incidence the target is in the far zone of the transmitting antenna, which is defined by the relation

$$r = \frac{A^2}{\lambda} \qquad \text{where } A = \text{maximum aperture dimension of transmitting antenna.}$$

"The size of the transmitting antenna should be increased as the angle of incidence is increased and the target is moved further away from the antenna, in order to take advantage of the allowed decrease in beamwidth as the range is increased.

"When the distance between antenna and target is adjusted to be near the optimum, i.e., computed from the greatest dimension of the model transverse to the line of sight between antenna and target, the spherical wave behavior of the transmitted wave ($\frac{1}{r}$ variation over the length of the target) introduces an error. Consideration of some simple targets shows that an upper bound may be placed on this error. The error introduced by the $\frac{1}{r}$ variation of the incident field is much less than that caused by the exceedingly small signal-to-noise ratio of the return signal for the low return aspects when the target is placed at the classical far zone distance. Thus a reasonable error whose upper bound is readily estimated is obtained in place of an intolerably large error of unknown magnitude. Experimental substantiation of this hypothesis has been obtained (Ref. 13) for a wide range of target sizes and aspects. Nose-on and quartering aspect returns may be measured in this manner with error less than 30 per cent.

A.2.1.5 Errors of the C-W System Arising from Thermal Variation, Mechanical Vibration, and Frequency Variation

"Great effort has been expended by many workers to reduce mechanical, thermal, and frequency fluctuations to tolerable levels in order to utilize automatic recording systems incorporating continuous rotation of the target and fixed pattern range size. It has already been pointed out that for the preponderant number of targets the range is too great to obtain adequate return signal for all but the broadside and near broadside aspects. It will be shown in the following sections that the use of afc circuitry alone is insufficient to reduce the cross-coupling error signal caused by mechanical and thermal fluctuation, and that the tuning network must be readjusted to effect the desired reduction.

A.2.1.5.1 Cross-coupling as a Function of Frequency

"The principal phenomenon causing difficulty in any c-w system is in the fact that the greater the isolation between the arms of the T, to which the receiver and generator are coupled, the narrower is the bandwidth over which the isolation is achieved. The bandwidth is measured at X-band (8200 - 12,400 mc) not in megacycles but in kilocycles. A numerical example serves to illustrate the case. A practical system, with 85 db isolation, has a maximum bandwidth of approximately 220 kilocycles, i.e., 9300 mc $\pm$ 110 kc, or $\pm$0.0011 per cent. The required frequency stability of the klystron is 1 part per 100,000. The same system with a 100 db isolation has a bandwidth of 50 kc, i.e., 9300 mc $\pm$ 25 kc, and the required stability is 5 parts per 1,000,000.

"Greater isolation and increased bandwidths have been obtained in c-w systems terminated in closed matched loads located at the immediate ends of the T. However, when the conjugate arms of the T are terminated in (1) an antenna many wavelengths in extent radiating into free space, and (2) a tuning network of geometry as nearly identical to that of the antenna as possible, the sources of reflection are large and separated by paths many wavelengths in extent. These inherent operating conditions of the c-w backscattering system result in reduced isolation and decreased bandwidth as compared to the closed magic-T network.

"It is clear from the consideration of the narrow bandwidth involved that frequency stabilization is essential to the system operation. A manually-monitored, free-running klystron immersed in oil or some form of afc system is usually used. The former has a purer output spectrum but requires a skilled operator; the latter has poorer spectrum purity but does not require as close attention. The spectrum purity is important when very great isolation levels are required, and the free-running klystron is customarily used to obtain these levels.

A.2.1.5.2 Contribution to the Cross-coupling Error Signal from Thermal and Mechanical Variation

"The effect of mechanical shocks and vibrations, and changes in dimension produced by thermal fluctuations cause large variations in cross-coupling error signal. The effects of thermal and mechanical variations on the system are (1) alteration of the impedance seen looking into the arms of the T, and (2) alteration of the impedances seen looking into the antenna, tuning network, receiver, and signal source. The changes in impedance produce very great increases in cross-coupling error signal, and the return signal-to-noise ratio suffers a correspondingly great decrease. Unless the tuning network is readjusted, the error of measurement rapidly becomes excessive.

"The backscattering ranges now in operation using a packaged automatic c-w system do not monitor cross-coupling level, the great source of error in the measurements. Instead, the frequency only is monitored and stabilized, a necessary but by no means sufficient condition to obtain accurate data.

"There is no currently available automatic system in which the cross-coupling error signal is monitored and the necessary compensatory changes made in the tuning adjustments as mechanical and thermal stresses deform the system. Adjustment of the frequency alone will not prevent the increase in the cross-coupling error signal produced by these deformations. The tuning network must be readjusted to affect the necessary reduction.

A.2.1.6 Technique Used at Microwave Radiation Company for Static Measurements

"The technique developed at the Microwave Radiation Company to overcome the errors arising from mechanical and thermal fluctuations and to utilize the shorter ranges obtained from the revised far-zone theory is one in which the measurements are made point by point. Cross-coupling level and frequency are checked before and after each measurement. Calibration data are taken before and after each point measurement and consist of the measurement of the backscattering of spheres of known radii. Several measurements are made at each point. Changes of range are made as a function of angle of incidence in order to increase signal-to-noise ratio for the nose-on aspect.

"The detailed study of the fin and body contributions to the total backscattering cross section of a V-2 as presented earlier in this appendix clearly demonstrates the fruits of this point-by-point variable range technique. The separate contributions and interactions were determined in detail. The resolution possible by use of the technique is to be contrasted to the experiences obtained using an automatic recording, fixed distance range, where it was found that the target could be resolved only for the broadside and near broadside aspects.

A.2.1.7 Conclusions

"The point-by point procedure as described takes longer and requires highly skilled personnel to perform the study and make the measurements. These requirements are stated by Fubini and Fails (Ref. 35):

> Conclusions and Recommendations
>
> A careful examination of the methods in use today for the measurement of radar cross-section (especially the Ohio State University system) leads to the conclusion that present methods though satisfactory for laboratory measurements are not yet ready to be packaged into a completely engineered unit. The most important reasons for this statement are the following:

1. The equipment is critical in adjustment and very sensitive to temperature variations and mechanical vibration.

2. The methods employed require skilled personnel to operate the apparatus and interpret the results...'

"These statements were made in 1949, and there have been no subsequent developments which in any way invalidate them. If anything, the problem is more severe because the scattering cross-sections of present sonic and supersonic targets are markedly less than those of the models measured in 1948-49. The measurement of radar scattering cross-section is a laboratory procedure utilizing laboratory instruments pushed to the ultimate limits of their sensitivity, and requires highly skilled personnel to perform the measurements and evaluate the data."

A.2.2 Measurement Techniques Used at Evans Signal Laboratory and Ohio State University Research Foundation

Radiating systems used by Evans Signal Laboratory were the same as those used by Ohio State University Research Foundation. Inasmuch as the same plumbing, horn beamwidths, and the like were used in both systems, the following direct quotation (except for designation of figures and references) from Appendix I of Reference 15 applies to both experiments.

"The microwave sources for production of the incident field and the receiving systems used in the measurements here were developed at the Antenna Laboratory of The Ohio State University during the past several years. Two operating frequencies are available for free-space wavelengths of 3.33 and 10 cm. The facilities for alternate operation at these different frequencies greatly increase the system flexibility since two choices of model size are possible for each frequency to be simulated.

"The microwave energy for measurements at either frequency is radiated by means of electromagnetic horns. The horns are required to radiate a sufficiently wide angle beam to provide substan-

tially uniform amplitude of the incident field over the model apertures. On the other hand, it has been found necessary to maintain the narrowest possible beam width in order to minimize the excitation of background objects with subsequent interfering reradiation. These conflicting requirements were met adequately with the use of horns having half-power beam widths of about seven degrees, both with an operating range of about 11 meters.

"Since the equipment is designed for the measurement of echo areas, it is necessary to use the same antenna for both transmission and reception. As a means of separating the received signal, of relatively low power, from the transmitted signal, a hybrid "T" waveguide section is used. The hybrid "T" is the wave guide counterpart of the hybrid transformers used in telephone systems. A discussion of the theory of the hybrid "T" can be found in any good book on microwave techniques (Ref. 16). Figure A.2-3 shows schematically the arrangement of the hybrid "T" section and the horn antenna used at either frequency.

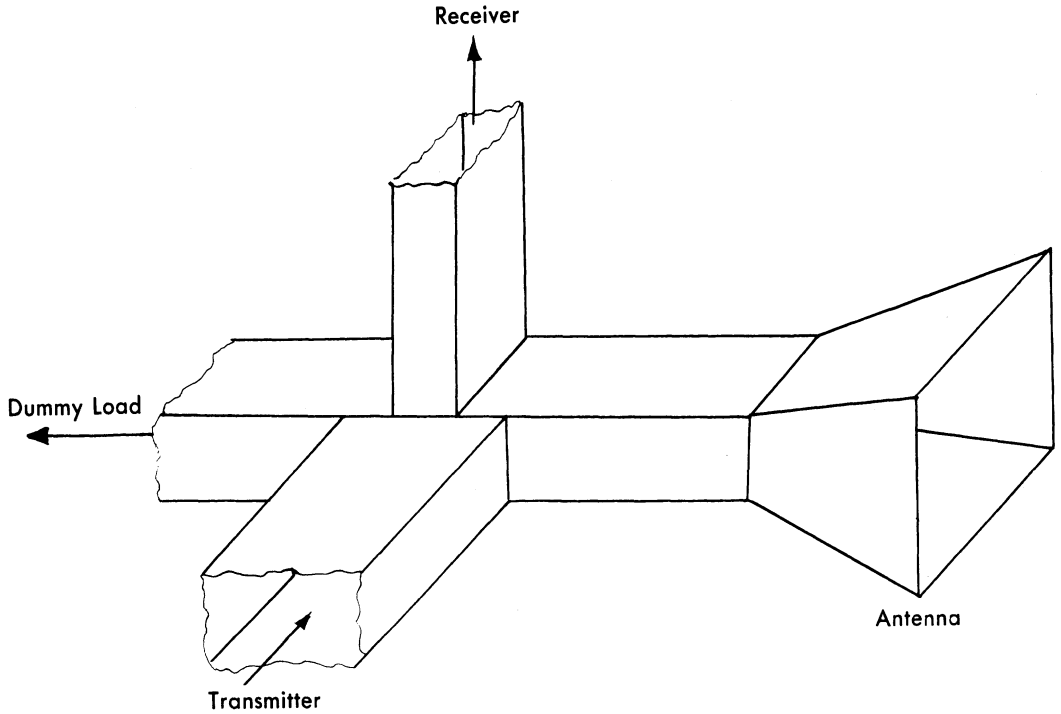

Fig. A.2-3. Hybrid "T" section with horn antenna.

"It has been found that in order to employ the above method of isolation of the transmitted and received signals, an exceedingly stable operating frequency must be used. For this reason the microwave signals are obtained by starting with the output of a crystal-controlled exciter, oscillating at a frequency of approximately 5 Mc. This output is unmodulated. By successive frequency multiplication and amplification, a frequency of 3000 Mc is obtained. This provides a free-space wavelength of 10 cm. For the 3.33-cm wavelength operation, the 10-cm output is used to excite a frequency tripler.

"The microwave signals for both 3.33- and 10-cm wavelengths are unmodulated as they are obtained from the output of the respective frequency multiplying klystrons. However, it is desirable to modulate the signals before radiation in order that the received echo signals can be demodulated to give an audio frequency voltage for recording of data. Consequently, each microwave signal is modulated by a square wave of fundamental frequency of 1000 cps before being delivered to the hybrid "T" junction which feeds the radiating horn. This modulation is accomplished by applying square pulses to the grids of amplifying klystrons used as final amplifiers in the transmitters.*

"The available transmitted power for 10-cm operation is sufficiently great to permit using direct crystal detection of the echo signal received from typical targets. The crystal is mounted in the receiving arm of the hybrid "T" section and delivers a square wave of 1000 cps fundamental frequency to an audio amplifier which drives a data recorder. The crystal has a good square-law characteristic, i.e., the peak audio-frequency output voltage is very nearly proportional to the square of the peak radio frequency voltage detected.

---

*Square wave modulation is used because this wave shape produced minimum detuning over a modulation cycle and yields maximum average radio frequency power for a given maximum instantaneous power.

As a consequence, the audio frequency voltage to the recorder varies directly with the received power.

"For 3.33-cm operation, the power output available from the klystron amplifier in the transmitter is very much lower than that in the 10-cm system. This necessitates the use of a superheterodyne receiver to offset the decreased inherent sensitivity of the system. The superheterodyne operation is accomplished by mixing the received microwave signal with a fixed microwave signal in a crystal located in the receiving arm of the hybrid "T". The fixed signal is obtained from a stabilized oscillator identical in design to the 3.33 transmitter, but it delivers a frequency 30 Mc higher than the transmitter frequency. The square-law crystal yields, among other things, a signal of 30 Mc frequency which varies directly with the received microwave voltage. The 30 Mc signal is then amplified and detected yielding an audio frequency output signal with a square-wave shape of fundamental frequency of 1000 cps. In this case, however, the audio voltage varies directly with the received microwave voltage and not with the received power.

"In both the 3.33- and 10-cm systems the audio output from the receiving system is used to drive a Speedomax recorder which records data by means of an inking pen moving radially on a sheet of polar-coordinate paper. These recorders have good linear characteristics, so that as the polar paper is rotated on a servo-controlled table, the recording pen traces out the polar plot of the received power with the equipment at 10-cm wavelength (or received voltage at 3.33-cm operation).

"As was mentioned before, a servo system positions the recording table to conform with the target rotation about a vertical axis. As a result, the polar plots are interpreted in terms of model echo area when the systems are calibrated.

"The calibration of the measuring equipment at both frequencies is done by using standard metal spheres as targets. The echo area of each of a series of calibrating spheres has been calculated so

that the recorder reading with a given sphere as a target can be interpreted as a known echo area. This provides a scale factor for the interpretation of recorded plots in terms of echo area when the law of response of the over-all system is known. The response curve for the over-all system has been obtained by checks of recorded data against a series of calculated echo areas of the targets producing the data."

In addition to the general technique described above, Evans Signal Laboratory (ESL) took special precautions in the very low-level reflection measurements.* A block diagram of the complete ESL system is shown in Figure A.2-4. The limiting factors in measuring reflection are insufficient sensitivity and secondary reflections from the model support members. The latter effect was determined by trying various methods of support. Limited sensitivity was partially combated by operating in the evening when low wind velocities resulted in the best possible mechanical stability of the plumbing. Another technique used was the repetition of patterns at two or more ranges. This did three things. First, the possibility of doubly reflected energy errors was diminished; second, the reliability of the measurements was improved; and third, a comparison was provided for evaluating the pattern deterioration resulting from the use of very short ranges.

A.2.3 Measurement Technique Used by the Sperry Gyroscope Corporation

The measurement system used at the Sperry Gyroscope Corporation consisted essentially of a 3-centimeter c-w klystron generator which fed power to an 18-inch diameter paraboloidal reflector through a magic-"T" bridge circuit. This doppler c-w radar was chosen because of the relatively high measurement accuracy attainable. In Reference 50 it is

*The following information was obtained in a letter from James T. Evers, Chief, Radar Development Branch, Radar Division, Evans Signal Laboratory.

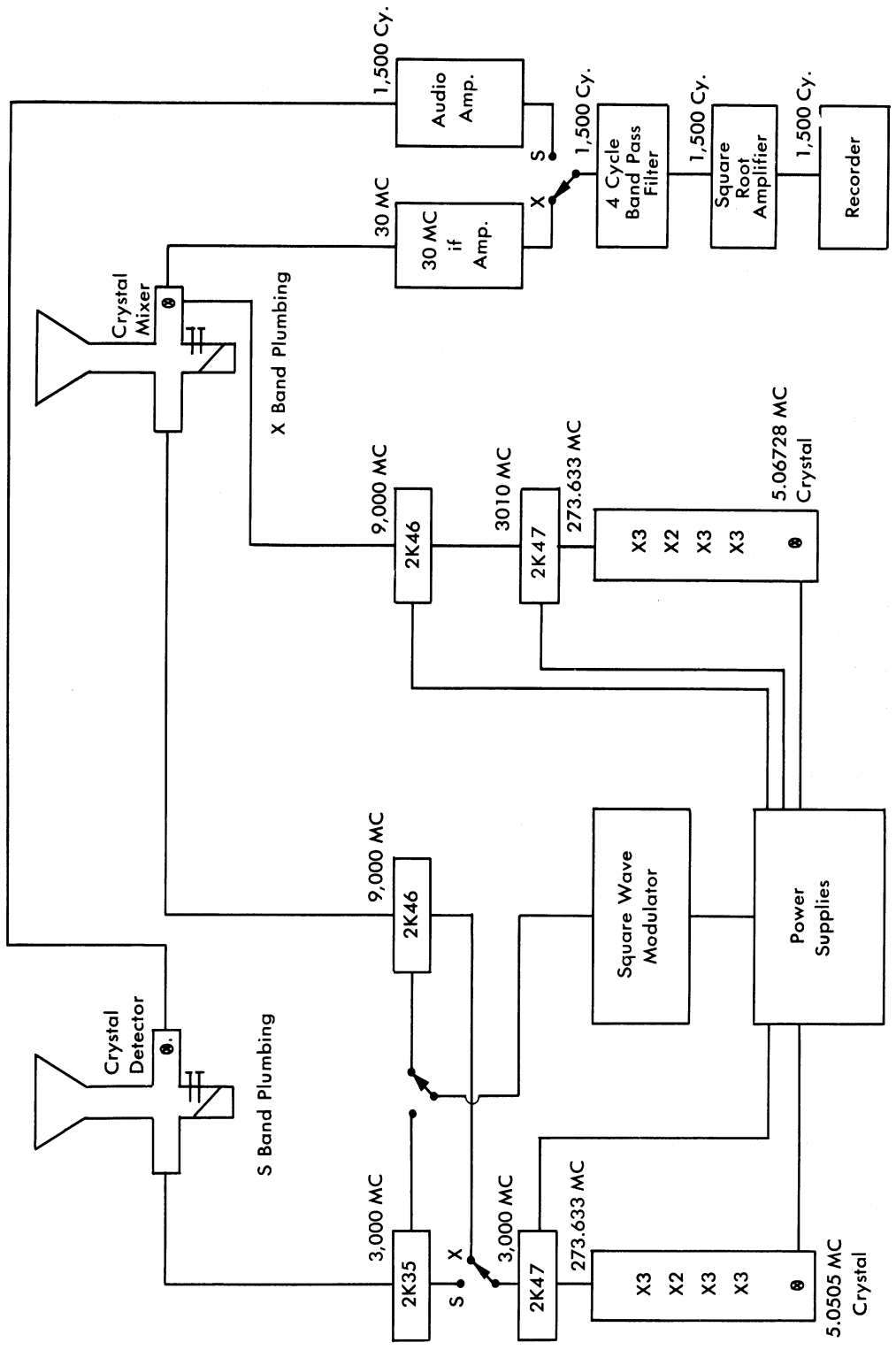

FIG. A.2-4 S & X-BAND REFLECTION MEASURING SYSTEMS

stated that an accuracy of 20 per cent was attainable over a wide range of σ (0.001 to 1000 square wavelengths) with a minimum of effort.

A description of the procedure used and the validity of the results obtained is quoted below from Reference 50.

> "The missile model whose echoing area was to be measured was supported by means of a nylon leader in the center of a six-foot square wooden frame (Fig. A.2-5). This frame could be rotated 360 degrees around either a horizontal or a vertical axis (the figure shows the set up for rotation about the vertical axis only). The nylon leader was used because it was found to give the smallest reflection (just barely detectable at the lowest end of the range of σ measurable) of all supports tested.
>
> "Measurements were made with the frame at distances of 7 to 25 feet from the transmitter.
>
> "The magic-tee bridge was unbalanced slightly so that, with the model held stationary in the field, the reflected energy mixed with a portion of the transmitted energy. The result was detected by means of a crystal detector, amplified by a d-c amplifier, and then recorded by an Esterline-Angus recorder.
>
> "For obtaining a measurement, the missile model was moved slowly along the axis of the antenna beam through about two wavelengths (at 3 cm). Moving the missile through a half wavelength in space resulted in the crystal output voltage going through a complete maximum-minimum cycle, the peak-to-peak value of which was a measure of σ.
>
> "The system as described was calibrated by measuring the reflections from a series of metal spheres of known diameter. The backscattering of a sphere is known accurately theoretically, and the metal spheres were so chosen as to cover the whole range of σ measurable. The calibration curves were obtained at every distance used in the actual measurements.

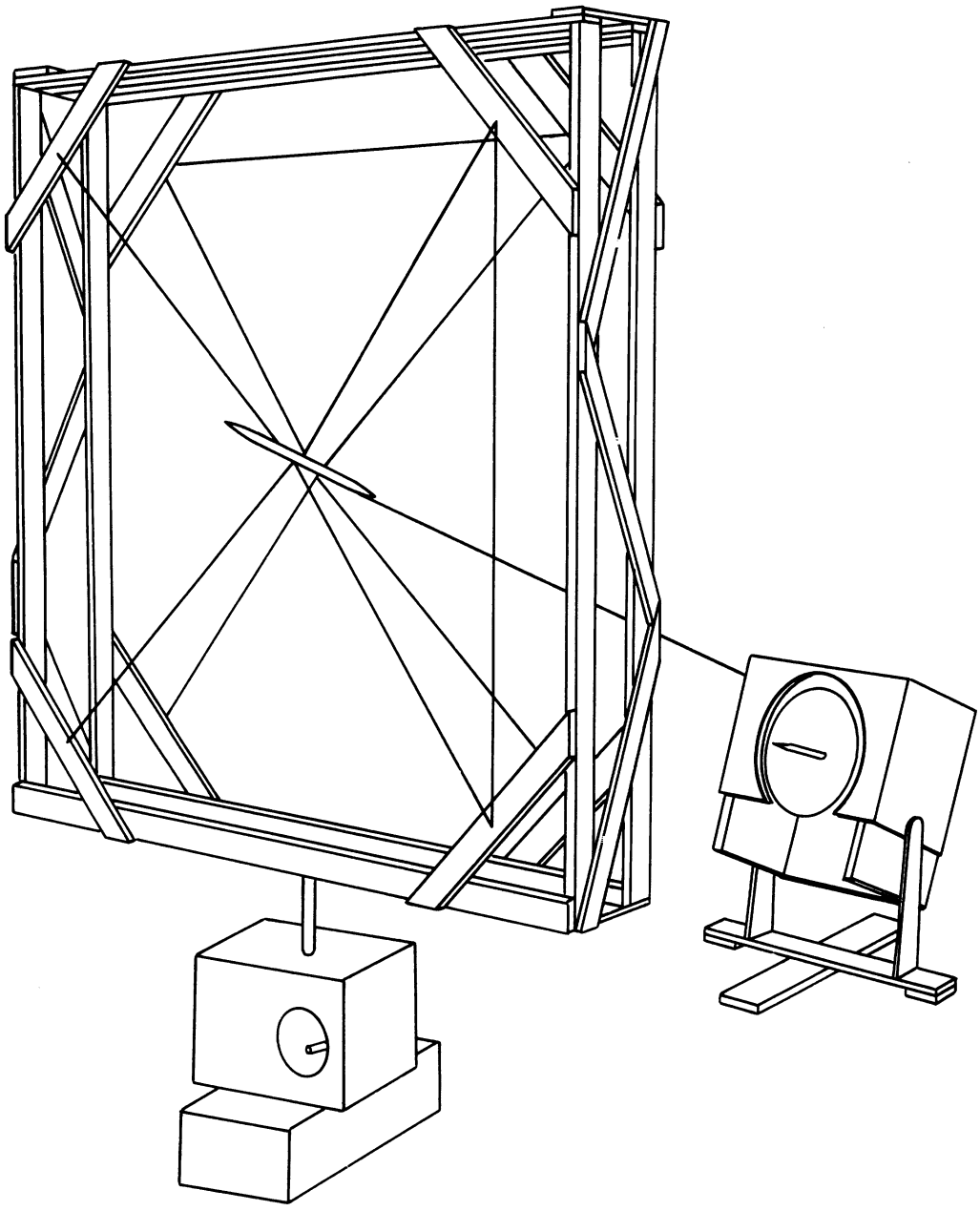

FIG. A.2-5 EQUIPMENT USED IN MEASURING THE EFFECTIVE ECHOING AREA

"Although the procedure just described did not permit the measurement of σ automatically on a continuous polar plot (it was felt the additional time and expenditure involved were not warranted), the results desired could be obtained quite rapidly and simply."

Sperry believes that some of the difficulties encountered in using null c-w methods and pulse methods were by-passed. Reference 50 goes on to state.

"For the doppler c-w method, reflections from steadily moving targets are measured. Hence, constant readjustment of a null balance is not necessary, and reflections from stationary or very slowly moving targets do not have to be accounted for. The nylon leader, although also in motion, has a barely detectable reflected signal. Thus, the signal from the model is the only echo actually measured. (If proper precautions are not taken, however, results may be in error due to multiple path reflections from the target.)

"To ensure the validity of the results obtained, particular precautions were taken to eliminate the possibility of multiple reflections occurring. The antenna was tilted at as large an angle from the ground as was possible with the equipment used, and metal plates were used to test for ground reflections over the entire ground surface between the antenna and the frame.

"Since power limitations and equipment sensitivity restricted measurements to a range of 7 to 25 feet from the antenna, within the Fresnel zone for the operating wavelength (3 cm), some time was spent investigating the effects of the Fresnel patterns on the results. This was done primarily by checking and cross-checking the results obtained at various distances, with proper regard for beamwidths at these distances. These results were found to check well within the accuracy of the experiment and so they can be considered satisfactory. These results, incidentally, corroborate similar results obtained by investigators at Ohio State University who found measurements obtained by their "close-in method" to be correct for distances as close as seven feet.

"The calibration method, which used spheres as standards, served as a further check on the accuracy of results obtained. By plotting σ in square meters (or square wavelengths) versus the reading on the Esterline-Angus recorder for the spheres at a given distance, a straight line is obtained on log-log paper. In a typical case most of the actual points lay on this line, with some scattering well within the 20 per cent accuracy figure quoted previously. This calibration with spheres was checked constantly, and for a given distance it was found that approximately the same straight-line calibration was obtained at all times. For various distances the different calibration curves were found to be parallel to one another, as was to be expected. These results, obtained on spheres at various distances, are an indication of the consistency of the measurements."

A.2.4 Measurement Technique Used at the Federal Telecommunications Laboratory

The measurements at Federal Telecommunications Laboratories were made with an AN/TPQ-2 radar set at equivalent full-scale frequencies of 50, 100, 110, 200, 250, 300, 500, 750 and 1000 Mc. Both horizontal and vertical polarizations were employed, and three elevation settings were used for each polarization (model axis horizontal, vertical, and 45 degrees above horizontal). In all measurements one set of fins was placed in a vertical plane.

Federal Telecommunications Laboratories give the following reasons for choosing the radar set method of measuring echoing areas in preference to the free space standing wave and c-w hybrid-"T" methods:

Although the standing wave procedure is simple and requires little apparatus, it is much less sensitive than the radar-set technique. The magic "T", on the other hand, is, in general, the most sensitive of the three set-ups. However, if its i-f bandwidth were much greater than the video bandwidth, noise would reduce its sensitivity below that of the radar set. Further, providing that the target distance is great enough that the radar echo is received after the end of the recovery time, the

radar-set method affords discrimination against extraneous reflections because of the difference in arrival times. Finally the echoing areas for pulsed and c-w illumination were expected to be different, and it was decided that pulsed operation would be of greater interest.

The range of operating frequencies was determined by the site, target size, and electronic equipment available. The target distance in wavelengths, a pure numeric, is not scaled. Obstructions, in front of which the target must be placed, restrict this distance and therefore the frequencies used. Also, if obstructions exist toward the sides, a frequency which allows use of a narrow-beam antenna should be chosen. Model size in wavelengths is also unaffected by scaling. A frequency range which permits a reasonable model size must therefore be selected. Finally, the state of development of components usually favors lower-frequency work. However, because of site requirements and the model length of 50 to 100 wavelengths, an operating frequency of 24,000 mc was necessary.

The AN/TPQ-2 radar set which has an 1/6 micro-second pulse width, a repetition rate around 5000 cps, peak power up to 50 KW, and a 10 Mc receiver bandwidth, was used.

Although the early work employed a transmitter and receiver duplexed on one antenna, simplex operation was found necessary to eliminate ringing and changes in gain of the receiver. In simplex operation, the transmitting antenna was a 2-foot-diameter parabola fed, with a "question mark" feed horn. The E-plane half-power width was 1.4 degrees and the H-plane half-power width was 1.5 degrees. The first side lobe was down 30 db. The receiving antenna, mounted below the transmitter, was a 4-foot-diameter parabola with a question mark feed horn. The E- and H- plane half-power widths were 0.7 degrees.

The target was mounted on a 15-foot galvanized iron mast, 1200 feet away from the radar. A mechanism for rotating the model in azimuth and a selsyn to indicate the angle were mounted on top of the mast. To minimize background reflections and those from the mast, half a steel I-beam 5 1/4 inches wide was attached to the top of the mast through a

swivel clevis. At the bottom of this shield, a screw (to allow tilt in elevation) and a turntable (for rotation in azimuth) were provided.

To measure cross-section, a corner reflector was first mounted on the mast, and the transmitter and receiver oriented for maximum return as observed on an oscilloscope. The shield was rotated to reduce background to a minimum steady value. The method of separating signal from background involved moving the target through about half a wavelength so the signal went in and out of phase with the background. From the maximum and minimum signal received in this "peaking" motion, the return from the target alone may be computed, since the background is constant. It was convenient to fix the noise level by adjusting the i-f gain of the receiver, and reduce the signal to twice noise level by means of a calibrated r-f attenuator between the receiving antenna and receiver. The signal strength was related to cross-section by using a calibrating sphere. For the 6-inch-radius sphere used, the operating frequency of 24,000 Mc is in the geometric optics region and hence this sphere had an echoing area of πa^2 at all aspects.

A.2.5 Measurement Technique Used at the Radar Research and Development Establishment*

The measurements made at RRDE were performed using the apparatus shown in Figure A.2-6.

The model under observation is supported on a tall tapering vane of plywood so shaped as to give minimum reflection from the vane to either the antenna or the model. The vane is carried on a trolley which is well out of the path of the incident radiation. The trolley, vane, and model travel at a constant speed, the model being in a c-w field radiated from a dipole at the focus of a parabolic reflector. A screen of absorbent material is placed behind the model. The signal reflected back from the moving model is shifted in frequency owing to the Doppler effect. This reflected signal received at the antenna is mixed with the oscillator signal

*Large portions of this appendix are quoted directly from Reference 52.

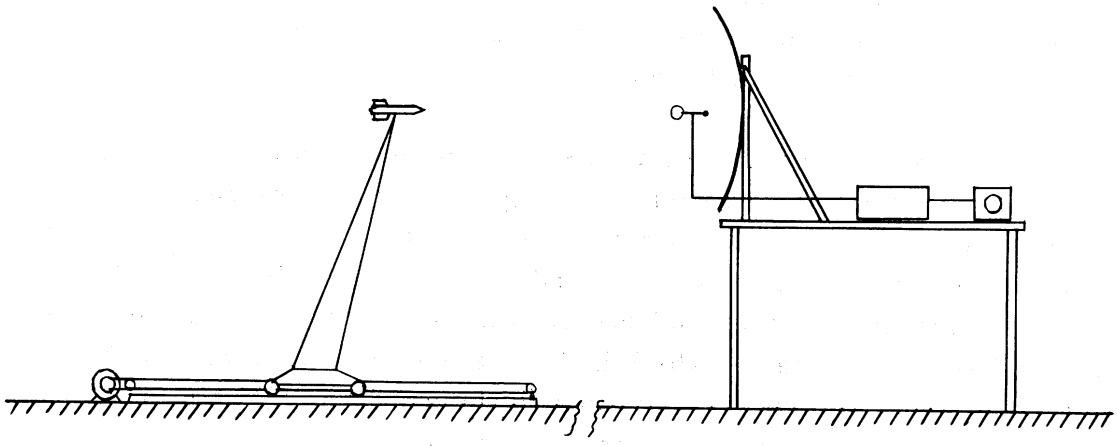

Fig. A 2-6

to give at the receiver amplifier a signal at the difference frequency of 10 cps. After passing through a tuned amplifier the output is measured on a valve voltmeter."

"The amplifier input/output characteristic was calibrated by means of a 10-cps signal generator. The region in which the model moves was then explored to ensure that the field presented a plane wave of constant amplitude in the vicinity. In making the measurements of echoing area a sphere of diameter 3.62 cm. was used as a standard. The receiver output was recorded with the sphere and then the missile model supported in turn on the moving vane. The supporting vane alone did not give a signal greater than $0.001\lambda^2$ which was the minimum detectable signal.

"The method was validated by measuring the echoing areas of spheres of different sizes compared with the standard, since for spheres rigorous theoretical computations are available."

A.2.6 Measurement Technique Used at the General Electric Company

The effective echoing area of a Hermes A missile was determined by use of underwater acoustic techniques. A 6-inch model and a frequency

range of 288 to 860 kc were employed to simulate a missile 30 feet long and 3.5 feet in midsection diameter, and to simulate wavelengths between 10 and 30 cm. The model was finless since preliminary tests had shown the fins important only at broadside.

The tests were conducted in a swimming pool, in order that the source-to-model distance would be large enough for the radiation incident on the model to approximate plane waves and in order to minimize echoes due to multiple reflections and side lobes. Unfortunately, because of attenuation in the water and the limited available signal power, the source-to-model distance which had to be used was so small that the incident waves could not be considered plane. (This effect was not considered in computing values of cross-section.)

Reflections from spheres and discs were used to calibrate the returned signal. At the lower frequencies, the sphere radius and the wavelength were almost equal, but it was still assumed that the effective area of the sphere is πa^2 (a = radius of sphere).

To obtain maximum model reflectivity, a hollow, air-filled model was used. These models were fabricated by first casting a solid model in a metal of low melting point (type unspecified), then plating this solid model with a few mils of nickel, and finally melting out the solid inner core.

The model was not rigidly supported, nor was the measurement of aspect angle precise, since most of the effort was directed toward obtaining additional power output rather than refinement of the measuring techniques.

A pulsed Hartley oscillator, which gave r-f pulses variable in length between 80 and 300 micro-seconds at a variable prf of 25 to 180 pps was used in the transmitter. A tube in the cathode circuit was used for keying, so that the oscillator could be cut off completely between pulses and the noise level thus could be kept low. With optimum coupling, 850-Volt r-f pulses (peak to peak) were obtained across the transducer crystal.

A double-conversion, superheterodyne receiver, which tuned over the frequency range, was found to have a sufficiently low signal-to-noise ratio. This receiver had a bandwidth of 15 kcs in order to be able to pass a 100 micro-second pulse and an input level below 2 micro-volts. The receiver's i-f frequencies were at 3 Mc and 455 kcs to minimize the beating of harmonics, which would have made several points in the frequency range unusable. An r-f stage output was used to improve the signal-to-noise ratio and a cathode follower to prevent loading of the i-f output.

Several crystal transducers were used in order to obtain the maximum frequency response everywhere in the frequency range. With 830 Volts output (peak to peak), a power of 0.35 watts was applied to the transducer. Assuming 30 per cent efficiency, a power of 0.105 watts was transmitted into the waver. The beamwidth was approximately 6 degrees. The t-r system used 1N34 crystals connected back to back. The transmitter coupling was a compromise between the requirements of matching the high impedance oscillator during transmission and having low impedance during receive time, the circuit being tuned for maximum echo strength.

The measurements of signal strength were made on an oscilloscope. The attenuation circuit and gain setting were calibrated for each setting on the scope. The receiver linearity was checked with a signal generator at the various gain settings. This method of taking measurements on the face of the scope, while not accurate, was within other experimental error values.

APPENDIX 3

THEORETICAL DETERMINATION OF THE BISTATIC CROSS-SECTION OF V-2 TYPE MISSILES

Applying the methods of physical optics to bistatic cross-sections as is shown in Reference 57, the theoretical values of the bistatic cross-section of a V-2 type missile at 225 Mc and 1000 Mc were computed. The computations were made for a V-2 type missile which had the following component parts:

1. A surface of revolution, forty-eight feet long in the form of a conical tip tapering gently back to a long, almost cylindrical, base of about five feet in diameter (Fig. A.3-1).

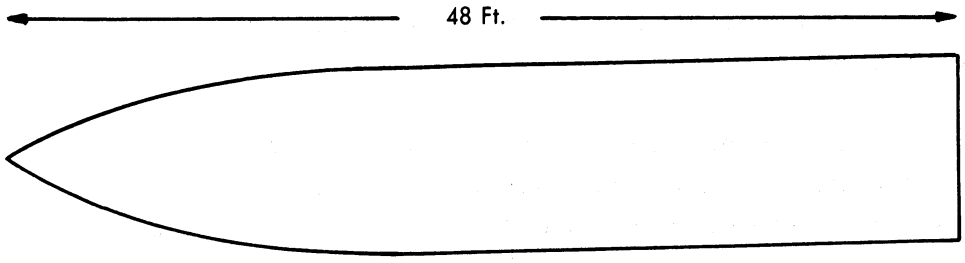

Fig. A.3-1

2. Four fins, which were flat plates of the shape depicted below mounted at right angles to one another (Fig. A.3-2).

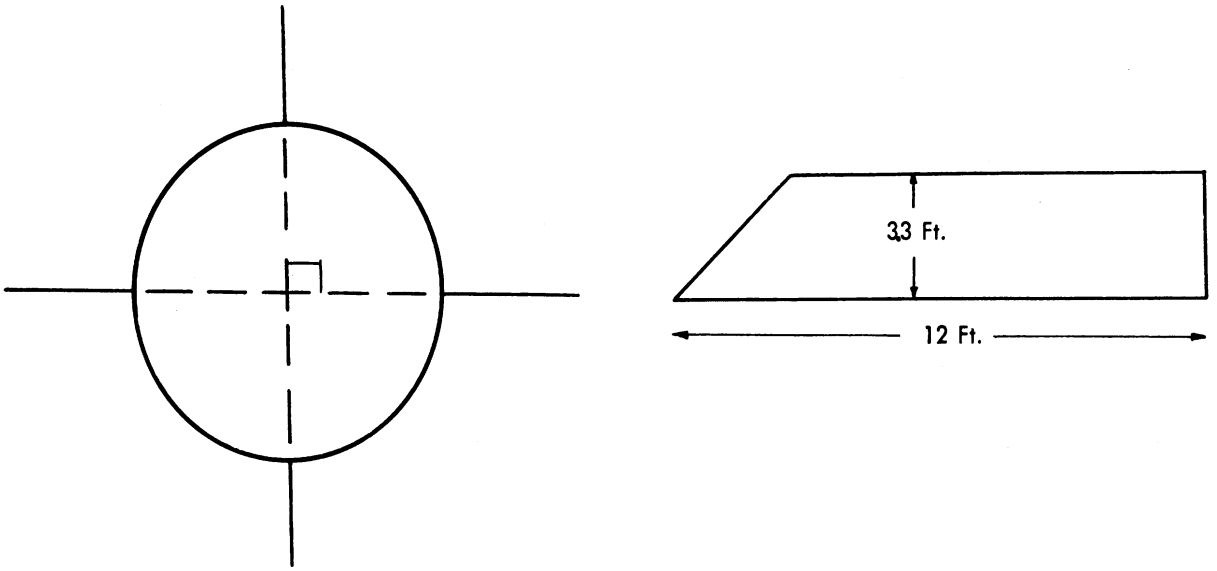

Fig. A.3-2

3. A flat rear portion in the form of a ring of outer radius of about 2.3 feet and an inner radius of about 1.2 feet (Fig. A.3-3).

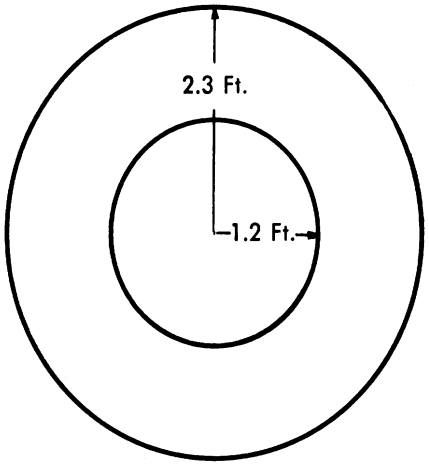

Fig. A.3-3

For any particular combination of polarizations of the transmitting and receiving antennas, it would be desirable to be able to compute the cross-section contribution of each of the three missile parts separately and then to add them together assuming random phasing as was done in computing the monostatic cross-sections. In most bistatic cases, however, some difficulty is encountered in attempting to do this as there is an interaction between the body and fin radiations. For example, radiation from the rear of the body may be specularly reflected to a fin and then deflected by the fin as shown in Figure A.3-4. Inasmuch as the fins extend along only one fourth of the body length, the amount of body radiation deflected by the fins from a given specular direction is small compared to the total amount of radiation which would reflect in that direction. Hence, the presence of the fins have a negligible effect in reducing

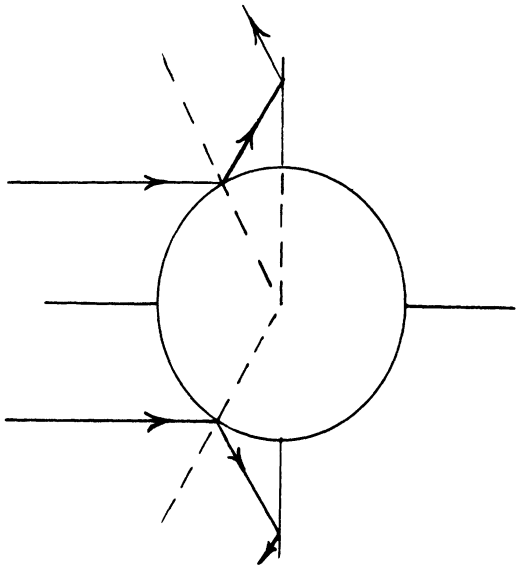

Fig. A.3-4

the cross-section in a direction of specular reflection. However, the radiation deflected by the fin into the mirror image (with respect to the fin) of the specular direction may constitute an important contribution in that direction especially if the cross-section in that direction in the absence of the fin would be small. Hence, the procedure was to compute

the body and fin contributions separately and, in certain directions, to add the contributions due to deflection of body radiation by the fins and fin radiation by the body. In general, the effect of such deflections is to spread the scattered radiation more uniformly throughout space and to create narrow peaks where they might not be expected. In treating the contribution of the fins it is not, in general, possible to treat each fin separately as reflections of radiation from one fin to its neighbor must be taken into account. In order to shorten the computations, use was made of reciprocity relationships which are believed to hold for the exact solutions to the scattering problem and extensive use was also made of the symmetries of the missile shape.

A.3.1 Body Contribution

Suppose that $\hat{a}$ is the direction of magnetic polarization of the transmitted waves and that $\hat{d}$ is the direction of the magnetic polarization of the receiving antenna. In addition, suppose that the axis of the missile lies along the $\hat{k}$ direction and that the direction from the transmitter to the body is $\hat{k}_0$ while the direction from the receiver to the body is $\hat{n}_0$. Then if the vector $\hat{g}$ is defined as being $\sqrt{4\pi R}\,\frac{\vec{H}_{sc}}{|\vec{H}_{inc}|}$, where $\vec{H}_{sc}$ is equal to the scattered magnetic field at a distance R in the far zone in the direction $-\hat{n}_0$ and $|\vec{H}_{inc}|$ is the magnitude of the incoming magnetic field, then $|\vec{g} \cdot \hat{d}|^2$ would represent the cross-sectional contribution of the body for the magnetic polarization direction $\hat{d}$ of the receiving antenna. The quantity $\vec{g} \cdot \hat{d}$ according to the methods of physical optics is given, to within a phase factor, by the expression

$$\sqrt{\frac{4\pi}{\lambda^2}} \left\{(\hat{d} \cdot \hat{a})(\hat{n}_0 \cdot \vec{v}) - (\hat{d} \cdot \vec{v})(\hat{a} \cdot \hat{n}_0)\right\}$$

where $$\vec{v} = \int_R \hat{n} \exp\left[ik\vec{r}' \cdot (\hat{n}_0 + \hat{k}_0)\right] ds,$$

$\hat{n}$ is the normal to the surface, $\vec{r}'$ is the radius vector from the origin to a point on the surface, and the region of integration R is that

portion of the surface which is "seen" by the transmitter. The main task, therefore, is to find a suitable method for approximating $\vec{v}$.

Direct evaluation of the integral defining $\vec{v}$ is difficult. However, the following line of reasoning leads to a choice of a suitable approximation. Consider a rounded body surface such as the one in Figure A.3-5. The planes of constant phase, which are given by the expression $\vec{r}\cdot(\hat{n}_0+\hat{k}_0)=c$, first strike the body at a point P_0. For a rounded body, such a point always exists and corresponds to what is known as the stationary phase point i.e., it is the point on the body for which

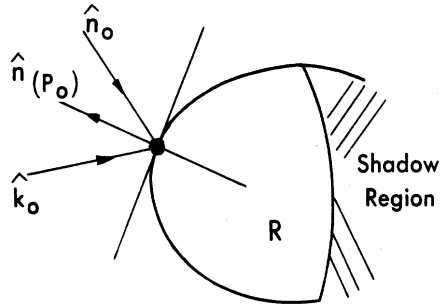

Fig. A.3-5

$\vec{r}\cdot(\hat{n}_0+\hat{k}_0)$ is a minimum. At the stationary phase point, the phase planes are tangent to the surface so that the normal to the surface at this point, $\hat{n}(P_0)$ would be given by $-\frac{\{\hat{n}_0+\hat{k}_0\}}{|\hat{n}_0+\hat{k}_0|}$ which is the negative of the direction of the phase planes $\vec{r}\cdot(\hat{n}_0+\hat{k}_0)=c$.

If, starting at the stationary phase point, the surface is sliced with phase planes spaced apart by some small fraction of λ (Fig. A.3-6), then on each slice of the surface the phase factor is approximately constant. Therefore, the integral $\int_R \hat{n}\exp[k\,i\,\vec{r}'\cdot(\hat{n}_0+\hat{k}_0)]$ may be approximated by the sum $\sum_j e^{ikc_j}\int_{s_j}\hat{n}ds_j$ where c_j is the phase factor

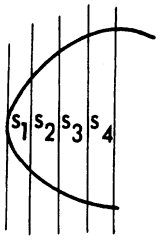

Fig. A.3-6

associated with the jth phase plane, i.e., for the jth plane $\vec{r} \cdot (\hat{n}_0 + \hat{k}_0) = c_j$, and where s_j is that portion of the body surface which is bounded by the jth and (j+1)th phase planes. Now, the integral $\int_{s_j} \hat{n}\, ds_j$ may be approximated fairly well by $\hat{n}(P_0)\, A_j$ where A_j is the surface area s_j projected into the direction of $\hat{n}(P_0)$. The reason for this is apparent from the geometry. For each tiny portion of s_j ds_j, with a normal direction, $\hat{n}_\theta$, making an angle of θ with the direction $\hat{n}(P_0)$, there is a portion of the surface ds_j', of approximately equal area lying on the opposite side of $\hat{n}(P_0)$. All components of the two vectors $\hat{n}_\theta\, ds_j$, and $\hat{n}'_\theta\, ds_j'$ except those lying along $\hat{n}(P_0)$ will nearly cancel.* The integral $\int_{s_j} \hat{n}\, ds_j$ may be approximated, therefore, by the expression $\hat{n}(P_0) \int_{s_j} \hat{n} \cdot \hat{n}(P_0)\, d s_j = \hat{n}(P_0)\, A_j$. Therefore, the integral $\int_R \hat{n} \exp (i k \vec{r}' \cdot (\hat{n}_0 + \hat{k}_0)\, ds$ may be approximated by $\sum_j \exp [ikc_j] \int_{s_j} \hat{n}\, ds_j$ which, in turn, may be approximated by $\hat{n}(P_0) \sum_j A_j e^{ikc_j}$. The smaller the surface division, s_j, the better is the first approximation so that $\hat{n}(P_0) \sum_j A_j \exp(ikc_j)$ may be

*This statement is "most true" in the region near the stationary phase point and "less true" away from it.

written as the integral $\hat{n}(P_0) \int_R e^{ik\vec{r}'} \cdot (\hat{n}_0 + \hat{k}_0) dA$ where dA is equal to $ds(\hat{n} \cdot \hat{n}(P_0))$.

The last integral may be written as

$$- \frac{\{\hat{n}_0 + \hat{k}_0\}}{|\hat{n}_0 + \hat{k}_0|} \left[\int \exp ikz \; |\hat{n}_0 + \hat{k}_0| \; dA(z) \right]$$

where z is the distance measured along the normal to the phase planes. Since, for a rounded body, dA(z) approaches zero as the shadow region is reached the absolute value of the bracketed integral above may be approximated by the expression A_0/π where A_0 is the area of the first Fresnel zone (Ref. 54). This zone is defined in this case as the surface area cut off by the phase plane

$$\vec{r} \cdot \left\{\hat{n}_0 + \hat{k}_0\right\} = \vec{r}(P_0) \cdot \left\{\hat{n}_0 + \hat{k}_0\right\} + \frac{\lambda}{2}$$

projected in the direction $\hat{n}(P_0)$. The final approximation to the integral

$$\int_R \hat{n} \exp \left[ik\vec{r}' \cdot (\hat{n}_0 + \hat{k}_0)\right] ds$$

is therefore

$$- \frac{\{\hat{n}_0 + \hat{k}_0\}}{|\hat{n}_0 + \hat{k}_0|} \; \frac{A_0}{\pi} \; .$$

Consider now the expression for $\vec{g} \cdot \hat{d}$ which is obtained by use of this approximation for the above integral:

$$\vec{g} \cdot \hat{d} = \frac{(\hat{a} \cdot \hat{d}) \; (1 + \hat{n}_0 \cdot \hat{k}_0) - (\hat{d} \cdot \hat{k}_0) \; (\hat{a} \cdot \hat{n}_0)}{|\hat{n}_0 + \hat{k}_0|} \sqrt{\frac{4\pi}{\lambda^2}} \; \frac{A_0}{\pi}$$

To obtain this expression, the fact that $\hat{a}$ and $\hat{d}$ are transverse to the transmitting and receiving directions respectively is used.

The above results can be extended to a body with a conical tip. Although a stationary phase point will not, in general, exist for each transmitter and receiver direction, the direction $-\frac{(\hat{n}_0 + \hat{k}_0)}{|\hat{n}_0 + \hat{k}_0|}$ is still defined as is the first Fresnel zone still defined if it is thought of as being the surface area cut off by the phase $\vec{r}\cdot(\hat{n}_0+\hat{k}_0) = \vec{r}_0 \cdot \{\hat{n}_0 + \hat{k}_0\} + \frac{\lambda}{2}$ ($\vec{r}_0$ is the radius vector to the conical tip) projected in the direction $-\frac{\{\hat{n}_0 + \hat{k}_0\}}{|\hat{n}_0 + \hat{k}_0|}$ (For cases when the phase planes do not strike the conical tip first, a stationary phase point exists.)

The evaluation of the area A_0 for a body like a V-2 type missile is not, however, easily done computationally. For this reason, it was felt that in order to facilitate computation, it would be well to use for the actual missile body, an "equivalent" well rounded body for which stationary phase points existed and for which the contribution of these stationary phase points might be easily expressed using the methods of geometrical optics. "Equivalent" refers, of course, to a body that would give approximately the same trends as the missile body. Comparison with theoretical monostatic cross-section data for the missile body (Sec. 7.3) would be a check on any "equivalent" body. A prolate spheroid seemed, therefore, a natural choice for an "equivalent" body, especially as its geometrical optics bistatic cross-section is readily expressible in a simple form. The semi-major and semi-minor axes of the "equivalent" prolate spheroid were determined by matching its nose-on and broadside cross-sections with the monostatic data computed for the missile body. Using these axes, the backscattering cross-sections were computed for angles of incidence varying from nose-on to 180 degrees. The values thus computed were in excellent agreement* with the data

*The agreement was so close in fact that the two curves were hardly distinguishable when plotted on 3 cycle semi-log paper.

obtained by more refined methods. Accordingly, an "equivalent" prolate spheroid was used to compute the magnitude of the bistatic cross-section contributions of the V-2 body.

The bistatic cross-section by geometrical optics for a prolate spheroid of major axis 2ℓ and the minor axis 2t is given by the expression

$$\sigma(\hat{k}_0, \hat{n}_0, \ell, t) = \frac{\pi \ell^2 t^4}{[\ell^2 \cos^2 \alpha + t^2 \sin^2 \alpha]^2}$$

where $\alpha = \cos^{-1}\left[\frac{\hat{k}\cdot(\hat{n}_0 + \hat{k}_0)}{|\hat{n}_0 + \hat{k}_0|}\right]$, and $\hat{k}$ is the direction of the major axis.

Using this "equivalent" prolate spheroid data and using $-\frac{\hat{n}_0 + \hat{k}_0}{|\hat{n}_0 + \hat{k}_0|}$ as the direction of $\vec{v}$, $\vec{g}\cdot\hat{d}$ becomes

$$\vec{g}\cdot\hat{d} = \left[\frac{(\hat{d}\cdot\hat{k}_0)(\hat{a}\cdot\hat{n}_0) - (\hat{a}\cdot\hat{d})\{1+\hat{k}_0\cdot\hat{n}_0\}}{\{1 + \hat{k}_0\cdot\hat{n}_0\}}\right] \sqrt{\sigma(\hat{k}_0, \hat{n}_0, \ell, t)}$$

This expression was the one which was used in the computations.

A.3.2 Computation of the Cross-Sectional Contribution of the Rear Flat Plate

The computation of the contribution of the rear flat plate was carried out by the methods of physical optics. The rear flat plate was oriented perpendicular to the axis of the missile, its center lying on the axis. If $\hat{k}$ is the direction of the missile axis, $-\hat{k}$ would be the outward normal to the rear flat plate. The physical optics expression for $\vec{g}\cdot\hat{d}$ is

$$\vec{g}\cdot\hat{d} = \sqrt{\frac{4\pi}{\lambda^2}}[-(\hat{d}\cdot\hat{a})(\hat{n}_0\cdot\hat{k}) + (\hat{d}\cdot\hat{k})(\hat{a}\cdot\hat{n}_0)] \int_T \exp[ik\vec{r}'\cdot(\hat{n}_0+\hat{k}_0)]\, ds$$

where T is the region of the plate "seen" by the transmitter.

It may be shown by a host of simple counter-examples that the above expression for $\vec{g}\cdot\hat{d}$ does not satisfy reciprocity relationships. In fact, in general, the physical optics expressions for flat plates are not reciprocal. In the computations, however, reciprocity relationships were assumed to hold for the flat plates since reciprocity is known to hold for the exact solution to the electromagnetic scattering problem (Ref. 57).

On carrying out the integration, the following expression was obtained for $\vec{g}\cdot\hat{d}$.

$$\vec{g}\cdot\hat{d} = \sqrt{\frac{4\pi}{\lambda^2}}\left[-(\hat{d}\cdot\hat{a})(\hat{n}_0\cdot\hat{k})+(\hat{d}\cdot\hat{k})(\hat{a}\cdot\hat{n}_0)\right]\frac{2\pi}{kf}\left[RJ_1(kRf)-rJ_0(krf)\right]$$

where $f = f(\alpha,\beta,\theta) = \sqrt{(\sin\alpha + \cos\beta\sin\theta)^2 + \sin^2\beta}$

R = outer radius of flat plate, J_0, J_1 = Bessel Functions of order zero and one,

r = inner radius of flat plate,

α = the $\cos^{-1}(\hat{k}\cdot\hat{k}_0)$

β = the angle the direction $\hat{n}_0$ makes with its projection on the plane spanned by $\hat{k}$ and $\hat{k}_0$,

θ = the angle between the projection of $\hat{n}_0$ in this plane and the $\hat{k}$ direction. (Fig. A,3-7)

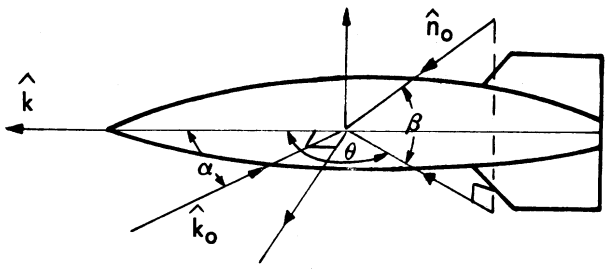

Fig. A,3-7

As the rear flat plate only enters into the view of the transmitter when $90^0 < \alpha < 270^0$ the rear flat plate contribution was computed only for these cases.

A.3.3 Computation of the Fin Contribution

For the cases in which the transmitter direction lay in the plane of a fin, the computation of the fin contribution was relatively simple. The fins were treated as flat plates of trapezoidal shape. At most three fins at a time were illuminated by the transmitter: the two fins vertical to the plane spanned by $\hat{k}$ and $\hat{k}_0$, and one of the fins lying in this plane. There was no overshadowing of one fin by another. The contribution of the illuminated horizontal fin was neglected. For $\hat{n}_0$ not in the plane spanned by $\hat{k}$ and $\hat{k}_0$, the contributions of the two vertical fins were added assuming random phase for, if λ is small with respect to the diameter of the body, the phase of the fins as $\hat{n}_0$ moves out of the plane of $\hat{k}$ and $\hat{k}_0$ depends critically on the diameter of the body. For $\hat{n}_0$ in the plane of $\hat{k}$ and $\hat{k}_0$, the fins were considered to be in phase. The expressions used to compute $\vec{g}\cdot\hat{d}$ were

$$\vec{g}\cdot\hat{d} = [(\hat{d}\cdot\hat{a})(\hat{n}\cdot\hat{n}_0)-(\hat{d}\cdot\hat{n})(\hat{a}\cdot\hat{n}_0)] \begin{Bmatrix} 2 \\ \text{or} \\ \sqrt{2} \end{Bmatrix} \int_{\text{fin}} \exp\left[ik\left\{\sin\beta y+(\cos\alpha + \cos\beta\cos\theta)z\right\}\right] dzdy$$

where $\hat{n}$ is the normal to fin surface and the angles α, β, and θ are as defined in the previous sub-section. The fin integral was evaluated with ease. The fact that the factor of 2 or $\sqrt{2}$ was used depending on whether or not $\hat{n}_0$ was in the plane of $\hat{k}$ and $\hat{k}_0$ occasions no great difficulty as far as continuity is concerned because of the size of the discrete steps in β used in the computations.

For the case in which the transmitter is in a plane making an angle of 45 degrees with the planes of the fins, the situation is more complex. Let us suppose that the transmitter lies on the same side of the missile axis as fins 1 and 2, and suppose that $\hat{k}_0$ lies in the plane of $\hat{i}$ and $\hat{k}_0$ (Fig. A,3-8).

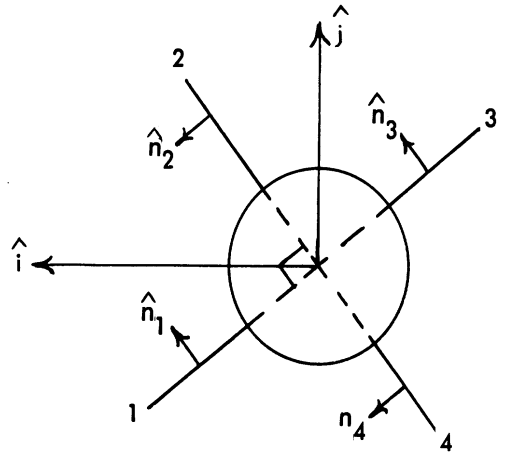

Fig. A$_1$3-8

In general, all four fins will be illuminated, although fins 1 and 2 in all cases (except in the transmitter nose-on cases) partially overshadow fins 4 and 3 respectively. When α = 90 degrees, the overshadowing is complete. In computing the contribution of fins 3 and 4, the integrations are carried out only over the regions of those fins which are not in the shadow of either fin 1 or fin 2 or the body. The contribution of fin 3 was computed by use of the formula

$$\frac{\lambda}{\sqrt{4\pi}}\vec{g}_3\cdot\hat{d} = [(\hat{d}\cdot\hat{a})(\hat{n}_0\cdot\hat{n}_3) - (\hat{d}\cdot\hat{n}_3)(\hat{a}\cdot\hat{n}_0)]$$

$$\int_{R_1} \exp\left[ik\left[\frac{(\sin\alpha+\cos\beta\sin\theta-\sin\beta)x}{\sqrt{2}}+(\cos\beta\cos\theta+\cos\alpha)\rho\right]\right]dx\,d\rho$$

The contribution of fin 4 was computed by use of the formula:

$$\frac{\lambda}{\sqrt{4\pi}}\vec{g}_4\cdot\hat{d} = [(\hat{d}\cdot\hat{a})(\hat{n}_0\cdot\hat{n}_4) - (\hat{d}\cdot\hat{n}_4)(\hat{a}\cdot\hat{n}_0)]$$

$$\int_{R_1} \exp\left[ik\left[\frac{(\sin\alpha+\cos\beta\sin\theta+\sin\beta)x}{\sqrt{2}}+(\cos\beta\cos\theta+\cos\alpha)\rho\right]\right]dx\,d\rho$$

The region of integration R_1 is the illuminated portion of the fins. For $0 \leq \alpha < 90^0$ (α is the angle between the $\hat{k}$ and $\hat{k}_0$ directions), the region R_1 appears as in Figure A.3-9. For $90^0 \leq \alpha \leq 180^0$ the region R_1 appears in Figure A.3-10.

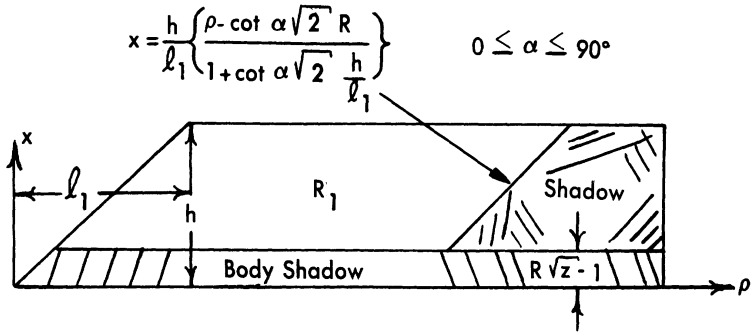

Fig. A.3-9

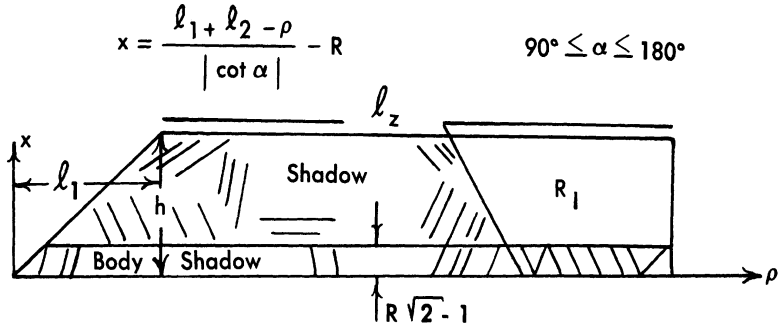

Fig. A.3-10

Although the expression for the general limits of integration are difficult, for each particular range of α the integrals may be carried out readily. For fins 1 and 2 some of the radiation incident on either fin is specularly reflected to the other and then deflected. For angles of incidence near broadside, these fins constitute a corner reflector system

and must be treated as such. Radiation reflected from one fin to its mate tends to decrease the cross-section in the direction of specular reflection off the first fin and enhance the cross-section in the direction of the mirror image in the second fin of the specular reflection direction. Accordingly, the contribution of a fin is evaluated by integrating the primary distribution of current due to the incident radiation over its entire surface and then adding, in the proper relative phase, an integral which takes account of the current induced on the neighboring fin by the radiation reflected specularly. The region of integration of the second integral will correspond to that region of the neighboring fin upon which specularly reflected radiation is incident. For α = 90 degrees this region corresponds to almost the entire area of the neighboring fin. In tracing the radiation from fin to fin, the magnetic polarization must be kept track of. Thus, for example, if radiation of magnetic polarization $\hat{a}$ is incident on fin 1, upon specular reflection the magnetic polarization of the scattered radiation incident on fin 2 will be $(\hat{a} - 2\hat{n}_1(\hat{n}_1\cdot\hat{a}))$. The contribution of fin 1 may be therefore expressed as

$$\vec{g}_1\cdot\hat{d} = \sqrt{\frac{4\pi}{\lambda^2}}\ [(\hat{d}\cdot\hat{a})(\hat{n}_1\cdot\hat{n}_0)-(\hat{d}\cdot\hat{n}_1)(\hat{a}\cdot\hat{n}_0)]$$

$$\int_{\substack{\text{entire}\\ \text{fin}}} \exp\left\{ik\left[\frac{(\sin\alpha+\sin\beta-\cos\beta\sin\theta)x'}{\sqrt{2}}+(\cos\beta\cos\theta+\cos\alpha)\rho\right]\right\}dx\,d\rho$$

$$+\ [(\hat{n}_2\cdot\hat{n}_0)\hat{d}\cdot(\hat{a}-2\,\hat{n}_1(\hat{a}\cdot\hat{n}_2))-(\hat{d}\cdot\hat{n}_2)((\hat{a}-2\hat{n}_1(\hat{a}\cdot\hat{n}_1))\cdot\hat{n}_0)]$$

$$\int_{R_2}\exp\left[\ ik\ \left[\left\{\frac{\sin\alpha-\sin\beta-\cos\beta\sin\theta}{\sqrt{2}}\right\}x'+(\cos\alpha+\cos\beta\cos\theta)\rho\right]\right]dx'd\rho$$

The region R_2 is that region of fin 2 which received reflected radiation from fin 1. For $0 \le \alpha \le 90^0$, R_2 is just the complement of the R_1 shown in Figure A.3-9. For $90^0 \le \alpha \le 180^0$, R_2 is the complement of R_1 shown in Figure A.3-10.

For fin 2 $\vec{g}\cdot\hat{d}$ is given by the expression

$$\vec{g}_2\cdot\hat{d} = \sqrt{\frac{4\pi}{\lambda^2}}\left\{[(\hat{d}\cdot\hat{a})(\hat{n}_2\cdot\hat{n}_0)-(\hat{d}\cdot\hat{n}_2)(\hat{a}\cdot\hat{n}_0)]\right.$$

$$\times\int_{R_2}\exp\left\{ik\left[\frac{x'(-\sin\alpha-\cos\beta\sin\theta-\sin\beta)}{\sqrt{2}}+\rho(\cos\theta\cos\beta+\cos\alpha)\right]dx'd\rho\right.$$

$$+\left.[(\hat{d}\cdot[\hat{a}-2\,\hat{n}_2(\hat{n}_2\cdot\hat{a})])\,(\hat{n}_1\cdot\hat{n}_0)-(\hat{d}\cdot\hat{n}_1)\,[\hat{n}_0\cdot(\hat{a}-2\,\hat{n}_2(\hat{n}_2\cdot\hat{a}))]]\right.$$

$$\times\int_{R_2}\exp\left\{ik\left[\frac{x'(\sin\alpha+\sin\beta-\cos\beta\sin\theta)}{\sqrt{2}}+(\cos\alpha+\cos\beta\cos\theta)\rho\right]dx'd\rho,\right.$$

where R_2 is defined as above.

The contributions for the 4 fins were added assuming random phase, since the relative phasing of the fin contributions for a small λ depends critically on the dimensions of the body. The total fin contribution to the cross-section is

$$\sigma_{fin} = \left|\vec{g}_f\cdot\hat{d}\right|^2_{fin} = \left|\vec{g}_1\cdot\hat{d}\right|^2_{fin\ 1} + \left|\vec{g}_2\cdot\hat{d}\right|^2_{fin\ 2} + \left|\vec{g}_3\cdot\hat{d}\right|^2_{fin\ 3} + \left|\vec{g}_4\cdot\hat{d}\right|^2_{fin\ 4}$$

A.3.4 Body-Fin and Fin-Body Reflection Contributions

Fin-body contributions to the cross-section refer to the contributions to the scattering cross-section of the radiation which is incident upon a fin and is specularly reflected from the fin to the body and then deflected.

Body-fin contributions to the cross-section refer to the contributions of the scattering cross-section of the radiation which is incident upon the body and specularly reflected to a fin from where it is deflected. The methods used to compute the body-fin contributions for the cases when the transmitter is normal to the axis of the missile are described first. With a few modifications the results may be extended to the other cases of interest.

Let the unit vectors $\hat{i}$, $\hat{j}$, and $\hat{k}$ form a right handed orthogonal coordinate system; let the $\hat{k}$ direction correspond to the axis of the missile, and let the transmitter direction, $\hat{k}_0$, correspond to the $-\hat{i}$ direction. Furthermore, let $\hat{n}_1$ be the normal to one deflecting fin and let $\hat{n}_2$ be the normal direction to the second deflecting fin. For the cases in which the fins are normal to the plan spanned by $\hat{k}_0$ and $\hat{k}$, $\hat{n}_1 = \hat{n}_2 = \hat{i}$. Let $\hat{n}\gamma$ be the unit outward normal to the body and let γ be the angle which this vector makes with the positive $\hat{i}$ direction. There exists a critical angle γ_0 such that the rays which strike the surface at points for which $\gamma_0 \leq |\gamma| \leq \pi/2$ are deflected by the fins (Fig. A,3-11). These rays induce currents on the surfaces of the fins which in turn are responsible for a diffraction pattern throughout space. In the computations the shape of this pattern was determined only in that region of space which is on the same side of the fins as the transmitter. Unfortunately, the integrations necessary to determine the shape of the pattern cannot be carried out by the methods of physical optics. For directions of the receiver, $\hat{n}_0$, such that $\hat{n}_0 \cdot \hat{k} = \hat{k}_0 \cdot \hat{k} = 0$ and such that $\hat{n}_0 \cdot \hat{i}$ satisfies the relationship $0 \leq \cos^{-1}(\hat{n}_0 \cdot \hat{i}) \leq \pi - 2\gamma_0$ there are stationary phase points on the surface for which $\gamma_0 \leq |\gamma| \leq \pi/2$. The magnitude of the cross-section as computed by the technique of stationary phase for these directions is $\frac{2\pi RD^2}{\lambda}$*, where R is the radius of the cylinder, and D is the length of the fin which is effective in deflecting radiation. The direction of the $\vec{H}$ field to be associated with these receiving directions is given by the expression:

$$\frac{[\hat{a} - 2\hat{n}\gamma(\hat{n} \cdot \hat{a})] - 2\begin{Bmatrix}\hat{n}_1\\ \hat{n}_2\end{Bmatrix}\left[\begin{Bmatrix}\hat{n}_1\\ \hat{n}_2\end{Bmatrix} \cdot \left\{\hat{a} - 2\hat{n}\gamma(\hat{n}\gamma \cdot \hat{a})\right\}\right]}{|\text{Magnitude of Numerator}|}$$

*At the edges of the range, stationary phase gives 1/2 this value. Actually the decrease to 1/2 takes place gradually over a range depending upon λ/R. In order to get the approximate shape of the pattern graphical addition of the elementary contributions may be carried out.

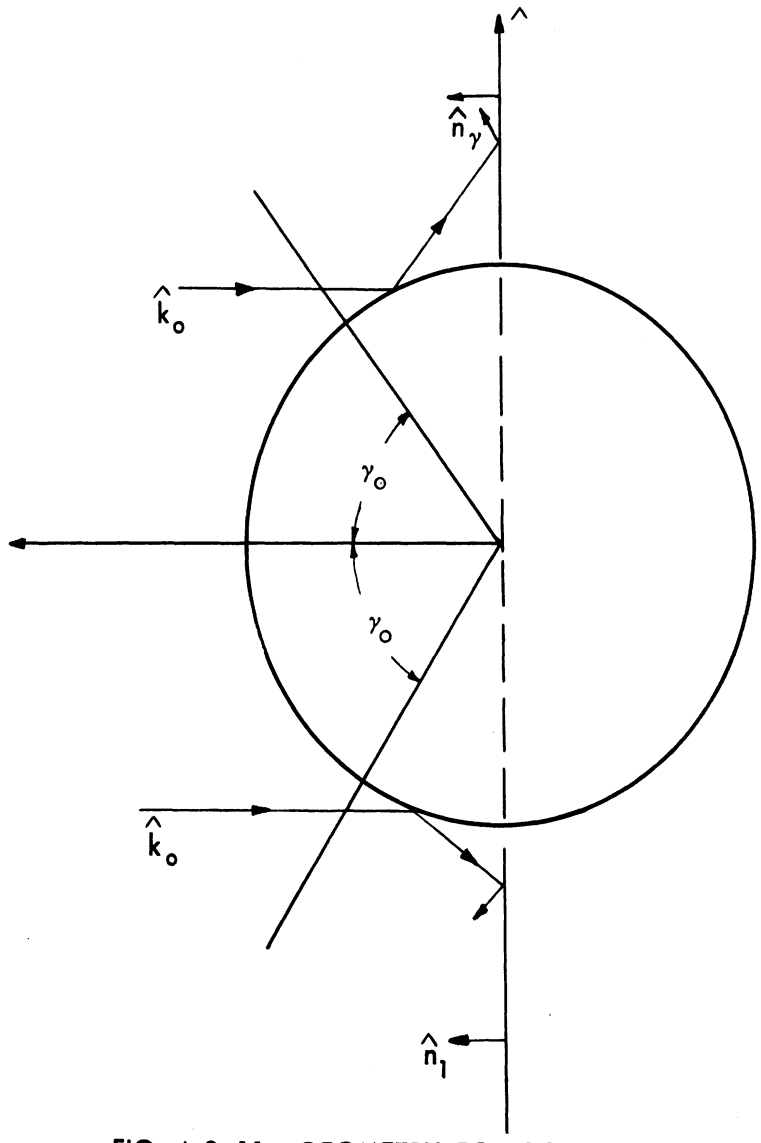

FIG. A.3-11 GEOMETRY FOR BODY-FIN DEFLECTION CONTRIBUTIONS

The half-width to be associated with the radiation pattern in the plane spanned by $\hat{j}$ and $\hat{k}$ will be taken as $\delta = \lambda/D$.

When $\hat{k}\cdot\hat{k}_0 \neq 0$, the body-fin deflection contributions will favor those receiving directions, $\hat{n}_0$, for which $\hat{n}_0\cdot\hat{k} = -\hat{k}_0\cdot\hat{k}$. All those directions, $\hat{n}_0$, which satisfy this condition and in addition satisfy the condition that $0 \leq \cos^{-1}(\hat{n}_0\cdot\hat{i}) \leq \pi - 2\gamma_0$ will have stationary phase points on the body for which $\gamma_0 \leq |\lambda| \leq \pi/2$. The magnitude of the cross-section in these directions is given by the expression $\frac{2\pi RD^2}{\lambda}$.* The direction of the scattered $\vec{H}$ field is as in the preceding paragraph. The half-width of the pattern in the plane spanned by $\hat{j}$ and $\hat{k}$ will be taken as λ/D.

The fin-body contributions may also be taken into account by such first-order approximations. These approximations are only good in the regions of the spectrum for which λ is much smaller than the radius of the body. The chief virtue of these approximations is that they are simple and that they do give a rough idea of the width and height of these deflection peaks.

A.3.5 Addition of the Component Contributions

For each polarization $\hat{d}$ of the receiving antenna, the $(\vec{g}\cdot\hat{d})$ of each component were added assuming arbitrary phase, i.e., the corresponding cross-section was obtained by adding the squares of the magnitudes of each $(\vec{g}\cdot\hat{d})$ for the various components;

$$\sigma_{\hat{a}\hat{d}} = \sum_{\text{components}} |\vec{g}\cdot\hat{d}|^2$$

where $\hat{a}$ denotes the incident magnetic polarization corresponding to the $\vec{g}$.

*D will be a function of $\hat{n}_0\cdot\hat{k}$.

Since $\hat{k}_0$ is transverse to $\hat{a}$ all possible polarizations of the incident field are expressible as linear combinations of the two polarizations

$$\hat{a}_1 = \frac{\hat{c} \times \hat{k}_0}{|\hat{c} \times \hat{k}_0|} \text{ and } \hat{a}_2 = \frac{\hat{k}_0 \times [\hat{c} \times \hat{k}_0]}{|\hat{k}_0 \times [\hat{c} \times \hat{k}_0]|}$$

where $\hat{c}$ is an arbitrary vector which is not parallel to $\hat{k}_0$. In computation, if the missile axis direction, $\hat{k}$, was not parallel to $\hat{k}_0$, $\hat{k}$ was chosen to be $\hat{c}$. Since, in the far zone, the radiated field is transverse to the direction of propagation, $-\hat{n}_0$, of the field, $\hat{g}$ is expressible as a linear sum of

$$\hat{d}_1 = \frac{\hat{b} \times \hat{n}_0}{|\hat{b} \times \hat{n}_0|} \text{ and } \hat{d}_2 = \frac{\hat{n}_0 \times [\hat{b} \times \hat{n}_0]}{|\hat{n}_0 \times [\hat{b} \times \hat{n}_0]|}$$

where $\hat{b}$ is arbitrary and not parallel to $\hat{n}_0$. Whenever $\hat{k}$ was not parallel to $\hat{n}_0$, $\hat{b}$ was chosen equal to $\hat{k}$. For each combination of $\hat{n}_0$ and $\hat{k}_0$, $\vec{g} \cdot \hat{d}$ was computed for the four combinations of $\hat{a}$ and $\hat{d}$: $\hat{a}_1\hat{d}_1$, $\hat{a}_2\hat{d}_2$, $\hat{a}_1\hat{d}_2$, and $\hat{a}_2\hat{d}_1$.

The following cases were considered:

(1) A fin was considered to lie in the plane of $\hat{k}_0$ and $\hat{k}$. For each position of $\hat{k}_0$ in this plane ($\hat{k}_0$ was rotated about $\hat{k}$ in steps of 15 or 30 degrees) cross-sections were computed for $\hat{n}_0$ varying throughout space in steps of 30 or 15 degrees in azimuth and zenith. Reciprocity relationships were then used to obtain the cross-sections for receiver and transmitter interchanged.

(2) The fins were rotated through 45 degrees but the plane spanned by $\hat{k}$ and $\hat{k}_0$ was unchanged. For each position of $\hat{k}_0$, cross-sections were obtained for $\hat{n}_0$ varying through space, in the same manner as in (1). The body and rear plate contributions remained the same as in (1) and only the fin contribution had to be recomputed.

In an effort to take account of the scattering from the sharp edges and fin-body junctions, an empirical constant, determined for the nose-on monostatic case, was added to all cross-sections computed thus shifting the curves upward by a constant amount as was done in the monostatic case. This extra contribution was assumed to have the same polarization as the body contribution. Except for nearly nose-on aspects this modification represents a very small percentage change in the cross-section.

Figures 7.4-2, 7.4-3, and 7.4-4 shown in Section 7.4, constitute only a small portion of the results which were obtained.

REFERENCES*

1. B. Bovarnick, "Microwave Detection of Shock Waves", Boston University Upper Atmosphere Research Laboratory, Technical Note No. 5, ATI 67554 (24 August 1949).

2. "Notes and Tables for Use in the Analysis of Supersonic Flow", National Advisory Committee for Aeronautics, Technical Note No. 1428, Ames Aeronautical Laboratory, Moffett Field, California (1947).

3. Z. Kopal, "Supersonic Flow of Air Around Cones", Technical Report No. 1, Dept. of Electrical Engineering, Center of Analysis, Massachusetts Institute of Technology (1947).

4. Z. Kopal, "Supersonic Flow Around Yawing Cones", Technical Report, Dept. of Electrical Engineering, Center of Analysis, Massachusetts Institute of Technology (1947).

5. K. M. Siegel, et al, "Studies in Radar Cross-Sections IV - Comparison Between Theory and Experiment of the Cross-Section of a Cone", Willow Run Research Center, University of Michigan, Report No. UMM-92, (June, 1953).

6. J. D. Cobine, et al, "Detection of High-Velocity, High Altitude Missiles", General Electric Company, Thumper Project Report No. 45846, ATI-1473 (11 March 1947), CONFIDENTIAL.

7. J. A. Stratton, Electromagnetic Theory, McGraw-Hill Book Co., Inc., New York (1947).

8. S. K. Mitra, The Upper Atmosphere, The Royal Society of Bengal Monograph Series, Vol. V (1948).

9. R. K. Luneberg, Mathematical Theory of Optics, Brown University, Providence, R. I., (1944).

*All references are unclassified unless otherwise marked.

10. K. T. Compton and C. C. Van Voorhies, "Accommodation Coefficients of Positive Ions of Argon, Neon, and Helium", Physical Review, Vol. 37 (June 1931).

11. H. S. W. Massey and E. H. S. Burhop, "Electronic and Ionic Collision Phenomena", Oxford University Press, London (1952).

12. "Thumper Project: The Meteor Problem (In Connection with High-Altitude, High-Velocity, Anti-Missile Research)", General Electric Company, Report No. TR-55308 (21 April 1947). CONFIDENTIAL.

13. M. J. Ehrlich and I. K. Wilhams, "Analysis of a C-W Radar Back Scattering Cross-Section Measurement System", Microwave Radiation Company, Report 102-6 (to be published).

14. S. Silver, Microwave Antenna Theory and Design, MIT Radiation Laboratory Series, Vol. 12, McGraw Hill Book Co., Inc., New York (1943).

15. "The Determination of the Radar Echoing Properties of Objects", The Antenna Laboratory, Ohio State University Research Foundation, Report 444-6 (29 February 1952).

16. C. G. Montgomery, R. H. Dicke, and E. M. Purcell, Principles of Microwave Circuits, Radiation Laboratory Series, Vol. 8, Chapter 9, McGraw Hill Book Company (1948).

17. T. R. Kaiser, "Radio Echo Studies of Meteor Ionization", Advances in Physics, Vol. 2, No. 8, p. 495 (October 1953).

18. W. W. Balwanz, "Reflections from the Exhaust Stream of the Jet Aircraft and Missiles", Memo - 5320-432A/54jw, Naval Research Laboratory (9 June 1954). SECRET.

19. F. C. MacDonald, "Radar Area Measurements of V-2 Rockets", NRL Report R-3220, Naval Research Laboratory (9 January 1948). RESTRICTED.

20. Daser, Gloeck, and Lutze, "The Effect of Ionized Gases on Electromagnetic Waves", Aviation Radio Research Institute Oberpfaffenhofen, F-TS-6446-RE (ATI-50151), AMC German Translation (April 1945). RESTRICTED.

21. Wessel, "On the Cause of the Reflection of Electric Waves by Thunderheads", Air Radio Research Institute Oberpfaffenhofen, Report F-TS-5494-RE (ATI-43271), AMC German Translation. RESTRICTED.

22. M. Becker, R. E. Bourdeau, T. R. Burnight, and W. F. Fry, "Upper Atmosphere Research Report No. 1, Part II", Office of Naval Research Laboratory, Report No. R-2956 (1 October 1946). CONFIDENTIAL.

23. F. P. Adler, "Measurement of the Conductivity of a Jet Flame", Journal of Applied Physics, Vol. 25 (July 1954).

24. E. S. Henning, "Effects of Ionized Exhaust Gases on Radar Tracking of Guided Missiles and Jet Aircraft", Radar Tracking of Guided Missiles Report No. 1, Air Material Command Technical Report, GS-USAF-Wright Field, No. 37 (January 1948). RESTRICTED.

25. F. M. Gager, "Propagation of Electromagnetic Waves Through Propellant Gases", Naval Research Laboratory Report No. NRL-R-3197 (6 November 1947). CONFIDENTIAL.

26. F. M. Gager, E. N. Zettle, H. M. Bryant, and F. E. Boyd, "S-Band Propagation with Acid-Aniline Flame Barriers", Naval Research Laboratory Report No. R-3209 (5 December 1947). CONFIDENTIAL.

27. H. M. Bryant and D. L. Frye, "Transparency of an Acid-Aniline Flame to S-Band Radiation", Naval Research Laboratory Report No. R-3690 (23 June 1950). CONFIDENTIAL.

28. F. M. Gager, H. H. Grimm, R. C. Peck, and G. D. Morehouse, "Incidental Flame Modulation of S-Band Continuous Wave Radiation", Naval Research Laboratory Report No. R-3261 (19 March 1948). CONFIDENTIAL.

29. R. H. Morrison, "S-Band Attenuation in an Oxygen-Alcohol Rocket Motor", Electronics Laboratory, General Electric Company Report No. R-49A0535 (June 1950). CONFIDENTIAL.

30. "S-Band Attenuation and Its Suppression in an Acid-Aniline Rocket Motor Flame", Boeing Aircraft Company Document No. D-9534 (18 February 1949). SECRET.

31. W. W. Balwanz, "Multifrequency Attenuation Measurements Through Propellant Gases - Part I", Naval Research Laboratory Report No. R-4229 (21 January 1954). CONFIDENTIAL.

32. W. W. Balwanz and E. W. Ward, "Interaction Between Electromagnetic Waves and Flames: Part I - The Effect of Altitude on Rocket-Motor Flame Geometry", Naval Research Laboratory, Special Research Branch, Radio Division III, Report No. 4232 (30 October 1953). CONFIDENTIAL.

33. "Radar Back Scattering Cross-Sections", Microwave Radiation Company, Inc., Report No. 102-1 (29 March 1954). SECRET.

34. W. Sichak, "Missile Detection - Final Report", Federal Telecommunications Laboratories, Inc., Contract W 36-039-sc-32119, ATI 42811 (August 1948). SECRET.

35. E. G. Fubini and W. A. Fails, "Methods of Measurement of Radar Cross-Section", Airborne Instrument Laboratories, Mineola, New York (January 1949).

36. H. Scharfman, "Antenna-Scattering Measurements by Modulation of the Scatterer", Proceedings of the I. R. E., Vol. 42, No. 5 (May 1954).

37. K. M. Siegel, M. E. Anderson, R. R. Bonkowski, and W. C. Orthwein, "Studies in Radar Cross-Sections XII: Summary of Radar Cross-Section Studies Under Project MIRO", Willow Run Research Center, University of Michigan, Report No. UMM-127 (December 1953). SECRET.

38. M. J. Ehrlich, "Measurements of Back Scattering Cross-Section of Cone Cylinder Model with Fins", Precision Engineering Company (since changed to Microwave Radiation Company, Inc.), University of Michigan Purchase Order No. 992163 (16 March 1953).

39. M. J. Ehrlich, "Measurement of the Back Scattering Cross-Section of the WRRC Model with V-2 Fins", Precision Engineering Company (since changed to Microwave Radiation Company, Inc.) Report No. 101 (September 1953). SECRET.

40. K. M. Siegel and J. M. Wolf, "Studies in Radar Cross-Sections XIII: Description of a Dynamic Measurement Program", Willow Run Research Center, University of Michigan, Report No. UMM-128 (May 1954). CONFIDENTIAL.

41. J. E. Rausch, et al, "Back Scattering Coefficient Patterns of Rocket Shells for 20 Mc", Ohio State University Research Foundation Report No. 302-15, ATI-49022 (15 August 1948). CONFIDENTIAL.

42. J. E. Rausch, "Back Scattering Coefficient Patterns of Rocket Shells for 50 Mc", Ohio State University Research Foundation Report No. 302-16, ATI-48939 (25 August 1948). CONFIDENTIAL.

43. J. E. Rausch, "Back Scattering Coefficient Patterns of Rocket Shells for 100 Mc", Ohio State University Research Foundation Report No. 302-17 (6 September 1948). CONFIDENTIAL.

44. J. E. Rausch, "Back Scattering Coefficient Patterns of Rocket Shells for 300 Mc", Ohio State University Research Foundation Report No. 302-18 ATI-40573 (15 September 1948). CONFIDENTIAL.

45. J. E. Rausch, "Echo Patterns of Rocket Shells for 600 Mc", Ohio State University Research Foundation Report No. 302-20, ATI-42137 (15 October 1948). CONFIDENTIAL.

46. J. E. Rausch, "Echo Patterns of Rocket Shells for 1200 Mc", Ohio State University Research Foundation Report No. 302-23, ATI-49037 (10 November 1948). CONFIDENTIAL.

47. W. E. Rife, "Progress Report, November 1, 1948 to December 31, 1948: Determination of Echoing Area Characteristics of Various Objects", Ohio State University Research Foundation Report No. 302-25, ATI-68314 (1 January 1949). CONFIDENTIAL.

48. W. E. Rife, "Quarterly Report: Determination of Back Scattering Coefficients (Echoing Area Characteristics) of Various Objects", Ohio State University Research Foundation Report No. 302-10, ATI-28341 (1 May 1948). CONFIDENTIAL.

49. "Echo Patterns of Tanks and Missiles", Ohio State University Research Foundation, Report 302-26 (ATI-71401), (January 1949). CONFIDENTIAL.

50. "Radar System Analysis Comparative-Performance Study of Pulse, F-M and Doppler Techniques for Ground-Based Long Range Search and M.T.I. Radar Systems", Sperry Gyroscope Company, Report Sperry - 5223-1109, ATI-52865 (June 1948). SECRET.

51. E. H. Kennard, Kinetic Theory of Gases, McGraw Hill Book Co., Inc., New York (1938).

52. J. S. Hay, J. T. Pinson, and P. E. V. Prince, "The Equivalent Echoing Area of a Rocket Missile Near Head-on Aspect", Radar Research and Development Establishment, R.R.D.E. Report No. 370 (August 1952). CONFIDENTIAL.

53. "Missile Echoing Area", General Electric Company, Report No. 55408 - Thumper Project (17 June 1948). CONFIDENTIAL.

54. R. Spencer, "Back Scattering from Conducting Surfaces", Cambridge Research Laboratories, Report CRL-R-E5070 (1951).

55. F. C. MacDonald, "Measurements of Radar Area of a V-2 Rocket", Naval Research Laboratory, Report NRL-C-3460-52/48A, ATI-105502 (August 1948). CONFIDENTIAL.

56. B. Baker and E. Copson, "The Mathematical Theory of Huygens' Principle", Oxford, at the Clarendon Press (1950).

57. K. Siegel, H. Alperin, R. Bonkowski, J. Crispin, A. Maffett, C. Schensted, and I. Schensted, "Studies in Radar Cross-Sections VIII - Theoretical Cross-Sections as a Function of Separation Angle Between Transmitter and Receiver at Small Wavelengths", Willow Run Research Center, University of Michigan, Report UMM-115 (October 1953).

58. L. Felsen, "Plane Wave Scattering by Small-Angle Cones, Air Force Cambridge Research Center, Report R-362-54 (February 1954).

59. W. Grannemann, C. Horton, and R. Watson, "Diffraction of Electromagnetic Waves by a Metallic Wedge of Acute Dihedral Angle", Austin, Texas Meeting of the American Physical Society, Paper No. J-10 (February 1954).

60. C. Schensted, J. Crispin, and K. Siegel, "Studies in Radar Cross-Sections XV - Radar Cross-Sections of B-47 and B-52 Aircraft", Willow Run Research Center, University of Michigan, Report 2260-1-T (August 1954). CONFIDENTIAL.

61. W. Hansen and L. Schiff, "Theoretical Study of Electromagnetic Waves Scattered from Shaped Metal Surfaces", Stanford University, Microwave Laboratory, Quarterly Report No. 3, ATI-104410 (May 1943).

62. C. Sletten, "Electromagnetic Scattering from Wedges and Cones", Cambridge Research Center, Report CRC-E5090 (July 1952).

63. K. Siegel, "Bistatic Early Warning Radars", Symposium on the Low-Altitude Target Problem, Panel on Guidance and Control Committee on Guided Missiles (6-8 January 1953). SECRET.

64. K. Siegel, B. Gere, I. Marx, and F. Sleator, "Studies in Radar Cross-Sections XI - The Numerical Determination of the Radar Cross-Section of a Prolate Spheroid", Willow Run Research Center, University of Michigan, Report UMM-126 (December 1953).

65. J. Van Vleck, F. Bloch, and M. Hammermesh, "Theory of Radar Reflections from Wires or Thin Metallic Strips", Journal of Applied Physics, Vol. 18, p. 274 (1947).

66. "Interim Engineering Report on Research and Development of Advanced Radar Confusion Techniques", December 1, 1953 to February 28, 1954, Standard Rolling Mills, Inc., Report No. 3-6 (20 March 1954). SECRET.

67. W. Franz and K. Depperman, "Theory of Diffraction by a Cylinder As Affected by the Surface Wave", Annalan der Physik, 10, p. 361 (1952).

68. D. Kerr, Propagation of Short Radio Waves, MIT Radiation Laboratory Series, Vol. 13, McGraw Hill Book Co., Inc., New York (1951).

69. K. Siegel, J. Crispin and R. Kleinman, "Studies in Radar Cross Sections VII - Summary of Radar Cross-Section Studies Under Project Wizard", Willow Run Research Center, University of Michigan Report UMM-108 (November 1952) SECRET

70. L. Loeb, The Kinetic Theory of Gases, McGraw Hill Book Co., New York (1934). (Section 81).

DISTRIBUTION

Distribution in accordance with Guided Missiles Technical Information Distribution List MML 200/5 No. 5, Report to Parts A and B; Abstract to Part C.

he exhaust, in addition to discussions of the cross-section of the missile itself.

Two missile types are discussed in considerable detail, the Atlas type intercontinental ballistic missile and the V-2 missile. The experimental data on Atlas and Atlas type missiles obtained by the Microwave Radiation Company and the Evans Signal Laboratory are compared with each other and with the theoretically computed valued obtained at the Willow Run Research Center. Detailed descriptions of the experimental procedures employed are included as well as an analysis of experimental techniques. In the discussion of V-2 type missiles a complete presentation of static V-2 type model experiments is given and compared with the dynamic experimental data recently obtained by the Willow Run Research Center at the Holloman Air Force Base (this dynamic experiment is described in UMM-128). These experimental data are then compared with each other and with theoretical computations.

SECRET

SECRET

he exhaust, in addition to discussions of the cross-section of the missile itself.

Two missile types are discussed in considerable detail, the Atlas type intercontinental ballistic missile and the V-2 missile. The experimental data on Atlas and Atlas type missiles obtained by the Microwave Radiation Company and the Evans Signal Laboratory are compared with each other and with the theoretically computed valued obtained at the Willow Run Research Center. Detailed descriptions of the experimental procedures employed are included as well as an analysis of experimental techniques. In the discussion of V-2 type missiles a complete presentation of static V-2 type model experiments is given and compared with the dynamic experimental data recently obtained by the Willow Run Research Center at the Holloman Air Force Base (this dynamic experiment is described in UMM-128). These experimental data are then compared with each other and with theoretical computations.

SECRET

SECRET

he exhaust, in addition to discussions of the cross-section of the missile itself.

Two missile types are discussed in considerable detail, the Atlas type intercontinental ballistic missile and the V-2 missile. The experimental data on Atlas and Atlas type missiles obtained by the Microwave Radiation Company and the Evans Signal Laboratory are compared with each other and with the theoretically computed valued obtained at the Willow Run Research Center. Detailed descriptions of the experimental procedures employed are included as well as an analysis of experimental techniques. In the discussion of V-2 type missiles a complete presentation of static V-2 type model experiments is given and compared with the dynamic experimental data recently obtained by the Willow Run Research Center at the Holloman Air Force Base (this dynamic experiment is described in UMM-128). These experimental data are then compared with each other and with theoretical computations.

SECRET

UMM-134

University of Michigan, Willow Run Research Center
Willow Run Airport, Ypsilanti, Michigan
Project MX-794, "Studies in Radar Cross-Sections--XIV; Radar Cross-Section of a Ballistic Missile", by K. M. Siegel, M. L. Barasch, J. W. Crispin, I. V. Schensted, W. C. Orthwein, and H. Weil. September 1954, 270 pages including graphs, charts and diagrams. SECRET

A coverage of the state of the art of the measurement and the computation of radar cross-sections of ballistic missiles is presented. This coverage includes the radar cross-section of shock fronts (indicated to be negligible), the radar cross-sections of ionization clouds not associated with flames (important at very high Mach numbers), and a short discussion of the contribution to cross-section from

Report: Distribution in accordance with Guided Missile Technical Information Distribution List MML 200/5 No. 5, Parts A and B.

Abstract: Distribution in accordance with Guided Missile Technical Information Distribution List MML 200/5 No. 5, Part C.

[redacted]

1. Guided Missiles
2. Radar Cross-Section
3. Air Defense
I. USAF Contract No. W-33(038)-ac-14222

SECRET

UMM-134

University of Michigan, Willow Run Research Center
Willow Run Airport, Ypsilanti, Michigan
Project MX-794, "Studies in Radar Cross-Sections--XIV; Radar Cross-Section of a Ballistic Missile", by K. M. Siegel, M. L. Barasch, J. W. Crispin, I. V. Schensted, W. C. Orthwein, and H. Weil. September 1954, 270 pages including graphs, charts and diagrams. SECRET

A coverage of the state of the art of the measurement and the computation of radar cross-sections of ballistic missiles is presented. This coverage includes the radar cross-section of shock fronts (indicated to be negligible), the radar cross-sections of ionization clouds not associated with flames (important at very high Mach numbers), and a short discussion of the contribution to cross-section from

Report: Distribution in accordance with Guided Missile Technical Information Distribution List MML 200/5 No. 5, Parts A and B.

Abstract: Distribution in accordance with Guided Missile Technical Information Distribution List MML 200/5 No. 5, Part C.

SECRET

1. Guided Missiles
2. Radar Cross-Section
3. Air Defense
I. USAF Contract No. W-33(038)-ac-14222

SECRET

UMM-134

University of Michigan, Willow Run Research Center
Willow Run Airport, Ypsilanti, Michigan
Project MX-794, "Studies in Radar Cross-Sections--XIV; Radar Cross-Section of a Ballistic Missile", by K. M. Siegel, M. L. Barasch, J. W. Crispin, I. V. Schensted, W. C. Orthwein, and H. Weil. September 1954, 270 pages including graphs, charts and diagrams. SECRET

A coverage of the state of the art of the measurement and the computation of radar cross-sections of ballistic missiles is presented. This coverage includes the radar cross-section of shock fronts (indicated to be negligible), the radar cross-sections of ionization clouds not associated with flames (important at very high Mach numbers), and a short discussion of the contribution to cross-section from

Report: Distribution in accordance with Guided Missile Technical Information Distribution List MML 200/5 No. 5, Parts A and B.

Abstract: Distribution in accordance with Guided Missile Technical Information Distribution List MML 200/5 No. 5, Part C.

SECRET

1. Guided Missiles
2. Radar Cross-Section
3. Air Defense
I. USAF Contract No. W-33(038)-ac-14222

UMM-134

University of Michigan, Willow Run Research Center
Willow Run Airport, Ypsilanti, Michigan
Project MX-794, "Studies in Radar Cross-Sections--XIV; Radar Cross-Section of a Ballistic Missile", by K. M. Siegel, M. L. Barasch, J. W. Crispin, I. V. Schensted, W. C. Orthwein, and H. Weil. September 1954, 270 pages including graphs, charts and diagrams. SECRET

A coverage of the state of the art of the measurement and the computation of radar cross-sections of ballistic missiles is presented. This coverage includes the radar cross-section of shock fronts (indicated to be negligible), the radar cross-sections of ionization clouds not associated with flames (important at very high Mach numbers), and a short discussion of the contribution to cross-section from

Report: Distribution in accordance with Guided Missile Technical Information Distribution List MML 200/5 No. 5, Parts A and B.

Abstract: Distribution in accordance with Guided Missile Technical Information Distribution List MML 200/5 No. 5, Part C.